Title

Boundary Control of Freeway Traffic Congestion

Author

Yu, Huan

Publication Date

2019

UNIVERSITY OF CALIFORNIA SAN DIEGO

Boundary Control of Freeway Traffic Congestion

A dissertation submitted in partial satisfaction of the
requirements for the degree
Doctor of Philosophy

in

Engineering Sciences (Aerospace Engineering)

by

Huan Yu

Committee in charge:

Professor Miroslav Krstic, Chair
Professor Nikolay A. Atanasov
Professor Henrik I. Christensen
Professor Jorge Cortes
Professor William M. McEneaney

2019

The dissertation of Huan Yu is approved, and it is acceptable in quality and form for publication on microfilm and electronically:

Chair

University of California San Diego

2019

DEDICATION

To my mother,

Xiao Li.

TABLE OF CONTENTS

LIST OF FIGURES

LIST OF TABLES

ACKNOWLEDGEMENTS

I would like to say thanks and express my sincere gratitude to many people for their support and love along the way that helps me to reach this point in my academic career.

First of all, I would like to thank my advisor Professor Miroslav Krstic for his continuous guidance and tremendous support throughout my PhD. If it was not for his brilliant ideas and encouragement, this interdisciplinary work would not be established in the first place. Along the way, he gave me freedom and unconditional help to explore various intriguing related topics and granted me opportunities to meet and collaborate with many talented researchers from control and traffic communities in seminars, workshops and conferences etc. I am enabled to grow and learn in such a supportive and collaborative environment that benefits my Ph.D. studies in a deep and comprehensive way. I am constantly motivated and amazed by his passion for research and education, his wealth of knowledge, his around-the-clock readiness to help and his strict standards in conducting research and in writing. I am also grateful for his advise for my career development. He is not only one of the most wise people I have ever met, but a role model I have always looked up to and maybe one day I could live up to some of his countless achievements in my future endeavors.

I would like to thank my committee members, Professor Miroslav Krstic, Professor Nikolay Atanasov, Professor Henrik Christensen, Professor Jorge Cortes, and Professor William McEneaney for devoting their expertise and limited time to this work.

I would like to thank my collaborators, Rafael Vazquez, Tiago Roux Oliveira, Shumon Koga, Mamadou Diagne, Liguo Zhang, Alexandre Bayen, Scott Moura, Saehong Park, Mark Burkhardt. Without your insights and knowledge, this work could not be so rewarding. I would like to thank Professor Bayen for having me for half a year as a visiting graduate researcher in his lab at University of California, Berkeley. I was enabled to explore various new topics and got to know many talented graduate students there. I owe my thanks to Professor Moura for his advise in academic career and insightful comments in our collaborated work. I would like to thank the graduate student Saehong Park at Berkeley for his concrete contributions to our work and the visiting graduate student Mark Burkhardt from Germany for his meticulousness and perseverance in achieving a high quality work under my guidance.

I would like to thank my labmates, Shumon Koga, Stephen Chen, Leobardo Camacho, Mostafa Bagheri, Imoleayo Abel, Drew Steves, Alan Williams, Cenk Demir, Mohammad Al Suwaidan, Azad Ghaffari, Shuxia Tang, Ji Wang, Libin Wang, Wuquan Li. I feel lucky to stay in such a friendly and chilled lab that enables me to maintain high productivity and more importantly, my sanity in this journey. Thanks for all the fruitful discussions and good coffee we had in the lab and all the jokes and fun we had during lunch and trip. You are the best colleagues and the most precious friends I have in my PhD. I would also like to thank my fellow graduate students in our control group, Yifu Zhang, Zhichao Li, Pio Ong, Erfan Nozari, Parth Paristoh, Aaron Ma, Priyank Srivastava, Dan Li, Yilong Chen, Yangsheng Hu, Daniele Cavaglieri, Pooriya Beyhaghi, whose talent and kindness has inspired me.

I would like to thank my fellow friends at UCSD, Lan Luo, Yue Zhang, Yuanjie Jiang, Qingqing Yang, Chendi Jiang, Nanzhi Zang, Yuesong Shi, Yewei Zheng, Changfu Li, Shu Zhang, Jiuyuan Nie, Dan Li, Zhongqi Jia, Wenbo Zhang, Haowei Jiang, Yang Wang, Yanzeng Zhang, Shengye Wang, Jianyu Cheng and many other dear friends for brightening my life during this journey and making San Diego feel like a home. My thanks also go to my old friends in China, Weilu Luo, Xue Hua, Zijin Qin, Hua Dong, Yuqi Zhao, Qiuyue Luo, Yuan yuan, Si Chen who makes my hometown not feeling so far away.

I owe my thanks to Lusia Veksler, Patrick Mallon, Linda McKamey, Melissa Kumler, Joana Halnez for their kind help in handling my funding and other graduate student affairs.

Last but not the least, I would like to thank my family for their support. Most importantly, I would like to thank my mom not only for her unconditional and selfless love throughout my life, but also for her encouragement and support for my decision of pursuing a PhD here in U.S., even if it means I am thousands miles away from her. This dissertation would have never been written if it was not for her understanding and belief in me. With that, I dedicate this work to my mom and another special one, my father. I know he would be proud if he was still with us.

This dissertation includes reprints and adaptations of the following papers.

Chapter 2 contains reprints and adaptations of the following paper: H. Yu and M. Krstic, "Traffic congestion control of Aw-Rascle-Zhang model," *Automatica*, vol. 100, pp. 38-51, 2019. The dissertation author is the primary investigator and author of this paper.

Chapter 3 contains reprints and adaptations of the following paper: H. Yu and M. Krstic, "Output Feedback Control of Two-lane Traffic Congestion," *Automatica*, under review. The dissertation author is the primary investigator and author of this paper.

Chapter 4 contains reprints and adaptations of the following paper: M. Burkhardt, H. Yu and M. Krstic, "Traffic Congestion Control of Two-Class Aw-Rascle Model," *Automatica*, under review. The dissertation author is the primary investigator and author of this paper.

Chapter 5 contains reprints and adaptations of the following paper: H. Yu, M. Diagne, L. Zhang, and M. Krstic, "Bilateral boundary control of moving shockwave in LWR model of congested traffic," *IEEE Transactions on Automatic Control*, under review. The dissertation author is the primary investigator and author of this paper.

Chapter 6 contains reprints and adaptations of the following paper: H. Yu, S. Koga, T. R. Oliveira, and M. Krstic, "Extremum seeking for traffic congestion control with a downstream bottleneck," *IEEE Transactions on Control Systems Technology*, under review. The dissertation author is the primary investigator and author of this paper.

Chapter 7 contains reprints and adaptations of the following paper: H. Yu, Q. Gan, A. M. Bayen, and M. Krstic, "PDE Traffic Observer Validated on Freeway Data," *IEEE Transactions on Control Systems Technology*, under review. The dissertation author is the primary investigator and author of this paper.

VITA

2013	B. S. in Aerospace Engineering, Northwestern Polytechnical University, China
2015	M. S. in Engineering Sciences (Aerospace Engineering), University of California San Diego
2018	Visiting Student Researcher, Institute of Transportation Studies, University of California at Berkeley
2019	Ph. D. in Engineering Sciences (Aerospace Engineering), University of California San Diego

PUBLICATIONS

Journal Articles

1. H. Yu and M. Krstic, “Traffic congestion control of Aw-Rascle-Zhang model,” *Automatica*, vol. 100, pp. 38-51, 2019.
2. H. Yu, M. Diagne, L.-G. Zhang, and M. Krstic, “Bilateral boundary control of moving schockwave in LWR model of congested traffic,” *IEEE Transactions on Automatic Control*, under review.
3. H. Yu, S. Koga, T. R. Oliveira, and M. Krstic, “Extremum seeking for traffic congestion control with a downstream bottleneck,” *IEEE Transactions on Control Systems Technology*, under review.
4. H. Yu and M. Krstic, “Output Feedback Control of Two-lane Traffic Congestion,” *Automatica*, under review.
5. M. Burkhardt, H. Yu and M. Krstic, “Traffic Congestion Control of Two-Class Aw-Rascle Model,” *Automatica*, under review.
6. H. Yu, Q. Gan, A. M. Bayen and M. Krstic, “PDE Traffic Observer Validated on Freeway Data,” *IEEE Transactions on Control Systems Technology*, under review.
7. H. Yu, R. Vazquez and M. Krstic, “Adaptive Output Feedback Control of Flow-induced Vibrations of a Membrane at High Mach Numbers,” *AIAA Journal*, under review.

Conference Proceedings

1. H. Yu, R. Vazquez and M. Krstic, “Adaptive Output Feedback for Hyperbolic PDE Pairs with Non-local Coupling,” *In2017 American Control Conference (ACC)*, pp. 487-492, Seattle, WA, 2017.

2. H. Yu, R. Vazquez and M. Krstic, “Adaptive Output Feedback Control of Flow-induced Vibrations of a Membrane at High Mach Numbers,” *In 2017 IEEE 56th Annual Conference on Decision and Control (CDC)*, pp. 670-675, Melbourne, Australia, 2017.
3. H. Yu and M. Krstic, “Traffic congestion control on Aw-Rascle-Zhang model: Full-state feedback,” *In 2018 Annual American Control Conference (ACC)*, pp. 943-948 , Milwaekee, WI, 2018.
4. H. Yu and M. Krstic, “Adaptive Output Feedback for Aw-Rascle-Zhang Traffic Model in Congested Regime,” *In 2018 Annual American Control Conference (ACC)*, pp. 3281-3286, Milwaekee, WI, 2018.
5. H. Yu, S. Koga and M. Krstic, “Stabilization of Traffic Flow With a Leading Autonomous Vehicle,” *In ASME 2018 Dynamic Systems and Control Conference*, pp. V002T22A006-V002T22A006, Atlanta, GA, 2018.
6. H. Yu and M. Krstic, “Varying Speed Limit Control of Aw-Rascle-Zhang Traffic Model,” *In 2018 21st International Conference on Intelligent Transportation Systems (ITSC)*, pp. 1846-1851, Maui, HI, 2018.
7. H. Yu and M. Krstic, “Traffic Congestion Control on Two-lane Aw-Rascle-Zhang Model,” *In 2018 IEEE Conference on Decision and Control (CDC)*, pp. 2144-2149, Miami, FL.
8. H. Yu, A. M. Bayen and M. Krstic, “Boundary Observer for Congested Freeway Traffic State Estimation via Aw-Rascle-Zhang model,” *In 2019 Control of Systems Governed by Partial Differential Equations-3rd CPDE*, to appear, Oaxaca, Mexico.
9. H. Yu, S. Park, S. Moura, A. M. Bayen and M. Krstic. “Reinforcement Learning vs. Backstepping Control of Stop-and-Go Traffic,” *In 2019 IEEE Conference on Decision and Control (CDC)*, Nice, France, 2019.
10. H. Yu, M. Diagne, L. Zhang, and M. Krstic, “Bilateral Boundary Control of Moving Traffic Bottleneck,” *In 2019 Joint Conference of the 8th IFAC Symposium on Mechatronic Systems and the 11th IFAC Symposium on Nonlinear Control Systems*, Vienna, Austria, 2019.

ABSTRACT OF THE DISSERTATION

Boundary Control of Freeway Traffic Congestion

by

Huan Yu

Doctor of Philosophy in Engineering Sciences (Aerospace Engineering)

University of California San Diego, 2019

Professor Miroslav Krstic, Chair

This dissertation develops a systematic model-based approach for the boundary control and estimation of freeway traffic congestion problem. Three topics of traffic congestion on a freeway segment are studied and include stop-and-go traffic oscillations, moving traffic shockwave, and downstream traffic bottleneck, which are governed by different partial differential equation (PDE) models and require the advancement and application of three PDE control techniques.

To supress stop-and-go oscillations, we introduce the macroscopic Aw-Rascle-Zhang traffic model, consisting of second-order nonlinear hyperbolic PDEs that govern dynamics of traffic density and velocity. The hetero-directional propagations of information in congested traffic generate the instabilities, motivating us to the stabilization problem for a coupled 2×2

hyperbolic system. Using the backstepping method, a full-state feedback control is designed for ramp metering at outlet to actuate the outgoing traffic flow. We design boundary observer for state estimation and combine it with the full state feedback control to construct an output feedback controller. The observer design is validated with traffic field data. Under model parameter uncertainties, adaptive control design is proposed with on-line parameter estimation. Furthermore, we develop output feedback boundary control for two types of 4×4 nonlinear hyperbolic PDEs which arise from two-lane and two-class traffic congestion. Stabilization of two-lane traffic involves regulation of the lane-changing interactions with lane-specific varying speed limits while stabilization of two-class traffic tackles the heterogeneity of vehicles and drivers.

A moving traffic shockwave, caused by changes of local road situations, segregates light traffic upstream and heavy traffic downstream. This density discontinuity travels upstream. As a result, drivers caught in the shockwave experience transitions from free to congested traffic. The interface position is governed by an ordinary differential equation (ODE) dependent on the density of the PDE states, described with Lighthill-Whitham-Richards model. For the coupled PDE-ODE system, the predictor feedback design is applied to compensate the state-dependent input delays. We design bilateral boundary controllers to drive the moving shockwave front to a desirable setpoint position, hindering the upstream propagation of the traffic congestion.

Traffic on a freeway segment with capacity drop at outlet causes a downstream bottleneck. Traffic congestion forms because the traffic at the outlet overflows its capacity. Therefore the incoming flow of the segment needs to be regulated so that the outgoing traffic at the bottleneck area is discharged with its maximum flow rate. Since the traffic dynamics of the bottleneck is hard to model, we apply extremum seeking control, a model free approach for real-time optimization, to obtain the optimal input density at the inlet. The predictor feedback design is combined with the extremum seeking to compensate the delay effect of traffic state of the segment. The maximum flow rate is achieved at the bottleneck by regulating its upstream density at the inlet.

Chapter 1

Introduction

This dissertation considers three topics of traffic congestion on a freeway segment include: stop-and-go traffic oscillations, moving traffic shockwave and downstream traffic bottleneck, which present as distinct PDE models and require the advancement and application of different PDE control techniques respectively. The PDE systems to be investigated in this dissertation are coupled hyperbolic PDEs, coupled PDEs-ODE, PDE with unknown nonlinear map for optimization. The following sections provide a through introduction to these three topics and control techniques that are employed to achieve varied control objectives.

1.1 Freeway traffic congestion

1.1.1 Stop-and-go traffic oscillations

The stop-and-go traffic is a common phenomenon appearing on congested freeway, causing increase consumptions of fuel and unsafe driving conditions. The oscillations can form with no apparent road change and therefore sometimes are referred as phantom traffic jam. It is of great importance if we can reduce this kind of traffic congestion. The traffic instabilities, also known as "jamiton", [32] [44] [96] are well represented by ARZ model [8] [123], which consists of second-order, nonlinear hyperbolic PDEs of traffic density and velocity.

The traffic congestion on freeway has been investigated intensively with different levels of traffic model. Macroscopic modeling of traffic dynamics with PDE has been proposed, including first-order model LWR [81] [94], second-order PW model [92] [114] and second-order ARZ model. The first-order LWR model fails to model stop-and-go traffic, which does not obey the density-velocity relation in equilibrium. This is caused by delay of drivers' response. To improve the LWR model, PW model developed a velocity equation to allow deviations from the density-velocity equilibrium. The PW model, consisting of the momentum equation and conservation law, are nonlinear second-order PDEs. It is shown in [27] [82] that disturbances in PW model travel faster than traffic velocity. As a result, vehicle on freeway is influenced from both behind and front, indicating that traffic flow is isotropic. However, [123] pointed out that traffic flow is anisotropic since drivers mostly respond to the traffic in front of them. To deal with this, Aw-Rascle [8] and Zhang [123] proposed a new velocity equation to address the non-static relation. Combining these two models together by proper definition and choice of coefficients, the ARZ model is used to describe the dynamics of stop-and-go traffic oscillations. When we consider multi-lane traffic with lane changing behaviors between lanes and multi-class traffic with heterogeneous vehicle and driver types on road, stop-and-go instabilities become more crucial to suppress.

To stabilize the oscillations of stop-and-go traffic, we propose boundary control strategies. Boundary control through ramp metering and varying speed limits are widely and effectively used nowadays in freeway traffic management. In developing boundary feedback control through ramp metering and varying speed limits, many recent efforts [18] [65] [117] [118] [119] [120] [121] [126] focus on ARZ model, due to its simplicity and realism. In [18], spectral analysis is applied to the linearized ARZ model and a parameter comparable to Froude number is proposed to classify different regimes in traffic flow. The boundary control and measurement are designed based on the spectral analysis. [124] investigates the local stability of a positive hyperbolic system with application to the ARZ model and [66] provides a feedback in-domain control law using varying speed limits. The control strategy developed in [18][124] both needed coordination of ramp metering and varying speed limits. The previously cited results [124] considered the homogeneous ARZ model, neglecting the relaxation term which reflects adaptation of driver's behavior to traffic conditions [45]. The relaxation term is kept in the ARZ model and therefore the inhomogeneous ARZ model is considered which preserves more potential to yield a realistic prediction. More importantly, only the inhomogeneous ARZ model considering the delay of driver's response is able to describe the instabilities of uniform states in stop-and-go traffic problem. At the same time, only ramp metering control is implemented which is more applicable in practice. Furthermore, the adaptive control problem is solved. The stabilization of ARZ model is achieved without knowing some boundary parameters and relaxation time.

The ARZ model treats multi-lane freeway traffic cumulatively as a single lane by assuming averaged velocity and density over cross section of all lanes. The individual dynamics of each lane and inter-lane interactions are neglected. However, distinct density and velocity equilibrium exist in multi-lane problems. The differences of velocities and densities give rise to lane-changing interactions and further lead to traffic congestion [82]. To address the phenomenon, a number of macroscopic multi-lane models [58] [60] [86] [69] [70] have been developed from microscopic, then kinetic to macroscopic descriptions. In this paper, we adopt the multi-lane ARZ traffic model proposed by [69] [60] to describe a two-lane freeway traffic with lane-changing between the two lanes. Lane interactions appear as interchanging source terms in the system, leading to more involved couplings and a higher order of PDEs. The complexity of the multi-lane model is greatly increased compared to the one-lane problem. This dissertation will introduce control design for the multi-lane congestion problem.

The heterogeneity in drivers and vehicles is exhibited in the ARZ model but has not been addressed from the control perspective. Macroscopic multi-class models were proposed after the ARZ model, including the first order models [20] [25] [46] [62] [88] [89] [107] [115].

The extended LWR model, introduced by [115], is the first macroscopic multi-class extension. Instead of adjusting their velocity only depending on the density of their own class, vehicles are affected by the densities of all other classes. Thus, the assumed speed-density relationship is formulated with respect to the sum of all densities, the total density. Furthermore, the n-populations model [20] extends this idea of coupling regarding the average length of the vehicle classes by denoting the speed-density relationship in dependence of the mean free space between the vehicles. In [46] and [88], a phenomenon called creeping is introduced. This behavior occurs in reality and corresponds to the scenario where one vehicle class, for instance trucks, are jammed and stopped due to congestion and a second vehicle class, for instance motorcycles, still moves in the gap between the trucks. In addition to first-order macroscopic multi-class models, second-order multi-class models are introduced in [23] [55] [61] [87] [103] and [104]. While first-order models assume that the velocities of all vehicles equal to their equilibrium velocities at every time, second-order models provide PDEs describing the velocity dynamics for each class. In this dissertation, we consider a macroscopic multi-class model [87] for the case of two different classes, yielding four coupled nonlinear hyperbolic PDEs. The two-class AR traffic model assumes that the vehicles adjust their speeds according to a measure called area occupancy [4] [6], which takes vehicle sizes into account.

1.1.2 Moving traffic shockwave

Consider in freeway traffic, there is a moving shockwave consisting of light traffic upstream of the shockwave and heavy traffic downstream. The shockwave conserves traffic flow at the interface of discontinuity and is caused by local changes of road situations like uphill and downhill gradients, curves, change of speed limits. The upstream propagation of the moving shockwave causes more and more vehicles entering into the congested traffic. The abrupt transition from free to congested traffic at the moving interface leads to unsafe driving conditions. We aim to halt the upstream propagation and drive the moving interface to a desirable location where the traffic congestion could be discharged by traffic management infrastructures on freeways.

Traffic discontinuity can be caused by various kinds of inhomogeneity of freeway or vehicles. Some studies consider it as a moving traffic flux constraint [33] [109] due to a reduction of road capacity. Slow moving vehicles, also known as moving bottlenecks, are represented in [21] [78] [120] with ODEs governing the velocity of slow vehicles. Moving bottleneck problem are out of the scope of this work and relevant to the controllability problem with boundary actuation. We consider the situation where road capacity is conserved but shockwaves form due to uphills, downhills, and curves of the road. Higher density traffic appears downstream of the shockwave front and the front of density discontinuity keeps moving upstream, driven by the flux discontinuity. The upstream propagation of the moving shockwave causes traffic congestion forming up on a freeway.

We adopt the seminal LWR model to describe the traffic dynamics of the moving shockwave problem. The LWR model is a first-order, hyperbolic macroscopic PDE model of traffic density. It is simple yet very powerful to describe the formation, dissipation and propagation of traffic shockwaves on a freeway. The moving shockwave consists of upstream, downstream traffic and a moving interface. The upstream and downstream traffic densities are governed by LWR PDE models and the interface position is governed by Rankine-Hugoniot jump condition, leading to a density state-dependent nonlinear ODE. Therefore, we are dealing with a PDE-ODE coupled system, where ODE state is dependent on PDE states at the moving interface. The traffic flow is actuated at both boundaries of a freeway segment and can be realized with ramp-metering. The control objective is to drive the moving interface to certain location and traffic states to steady values through bilateral boundary controls.

1.1.3 Downstream traffic bottleneck

When there are uphills, curvature or lane-drop further downstream on freeway, a bottleneck with lower capacity could appear. Traffic congestion then forms upstream of the bottleneck if there is no traffic regulation. Ramp metering and VSL have been proved to be very effective in freeway traffic management system. Boundary control of traffic in presence of downstream bottleneck is studied in this work.

The first local ramp metering strategy that was proposed based on feedback control theory is ALINEA developed by [91], and later on an adaptive strategy was employed by AD-ALINEA when downstream occupancy is uncertain [99]. The traffic flow entering the freeway is controlled from ramp metering on-ramps so that the downstream mainline traffic flow is maximized locally or the optimal freeway network traffic is achieved coordinately. The ALINEA algorithm uses real-time measurement of downstream occupancy and its set point value to calculate their difference, and then the control input is designed via the integration of the errors over time. In the presence of a downstream bottleneck, Proportional-Integrator (PI) ALINEA was developed by [113] to improve performance of the closed-loop system. A comparative study by [64] is conducted in comparison with ALINEA. PI-ALINEA is proposed as an extension to ALINEA by measuring the downstream bottleneck occupancy and feeding it back to the local ramp-metering. In [113], the stability of the closed-loop system with PI-ALINEA, a discretized ordinary differential equation (ODE) system, is proved with Lyapunov analysis. Simulation demonstrated that PI-ALINEA improved significantly than ALINEA in the case of distant downstream bottleneck.

Control of lane-drop bottleneck by VSL was explored by [63]. Authors approximated LWR model with the discretized ODE link queue model. A Proportional-Integrator-Derivative (PID) controller is employed for VSL control strategy. Modeling lane-drop traffic with macroscopic LWR PDE was firstly investigated by [16]. The traffic dynamics on a stretch of freeway upstream of the bottleneck area is governed by LWR model. The predictor feedback control law is designed for the ramp metering at the inlet of the freeway so that the density at bottleneck area is regulated to a desired equilibrium. This work assumes the prior knowledge of the optimal density that could maximize the discharging flow at the bottleneck area. However, the density and traffic flow relation at bottleneck area is usually hard to obtain or estimate, especially when the bottleneck is caused by a random accident and the traffic needs to be regulated immediately.

We consider a freeway segment with bottleneck located at the outlet where the road capacity drops. The traffic dynamics of the freeway segment is described with LWR model. The density-flow relationship at the bottleneck area is described with a nonlinear map at the outlet where the optimal density is unknown.

1.2 PDE model and control algorithms

1.2.1 PDE backstepping control

The key idea of our control design is applying backstepping method to ARZ model which is a coupled hyperbolic PDE system. Theoretical results on boundary control design for PDEs using backstepping method have been developed for 2×2 coupled hyperbolic systems in [3] [31] [34] [35] [108] [116]. Feedback boundary control design for a general class of hyperbolic PDEs using backstepping method are studied in [1] [2] [3] [7] [31] [41] [36] [80] [121]. In [41], stabilization of a $n+1$ counter convecting hyperbolic PDEs is achieved with a single boundary. [80] presents a solution to output feedback of a fully general case of heterodirectional $n+m$ first-order linear coupled hyperbolic PDEs. Actuation of all the m PDEs from the same boundary is required to stabilize the system in finite time. A shorter convergence time is further obtained in [7] by modifying the target system structure. We adopt and enhance the existing methodology to fit the ARZ model. This is an essential step for boundary control of freeway traffic in its PDE formulation. We develop full-state feedback boundary control law, boundary observer based on [108]. Furthermore, we develop adaptive output feedback and enhanced the design based on [116]. The problem of unknown parameter coupling with boundary measurement is addressed which is absent in the previous literature.

The main contribution of our work on control of one-lane ARZ model: this is the first result on boundary feedback control of inhomogeneous ARZ model. We address the traffic dynamics with ARZ PDE model from control perspectives, explore the general framework for stabilization problem of stop-and-go traffic and develop boundary feedback control design including both nonadaptive and adaptive designs. Motivated by the ARZ PDE model, our work yields theoretical advance relative to previous results on adaptive control design for hyperbolic systems. Most importantly, this result paves the way for addressing the traffic problem with PDE boundary control, as one of its most important application.

The contribution of our work on control of two-lane ARZ model: we solve the control problem of multi-lane traffic PDE model. The dynamics of two-lane traffic are studied from control perspectives. Theoretical result of output feedback control of the general class of heterodirectional linear hyperbolic PDE systems is developed in [7] [80], but has never been applied in traffic application. Being the first work to adopt the methodology, our result opens the door for solving related multi-lane traffic problems with PDE control techniques. Furthermore, we advance the theoretical results in [7] [80] by proposing a collocated boundary observer and controller design. The output feedback controllers in both papers are constructed with full-state feedback controllers and an anti-collocated observer. In implementation, collocated boundary observer and controllers are more practically applicable. We bridge this gap by developing a observer with sensing at outlet, which is also a more challenging problem in the design for the system of this paper.

The contribution of our work on control of two-class ARZ model: this work presents boundary control design for traffic congestion consisting of two different vehicle classes. On one hand, this work contributes to traffic modeling in the sense of deducing a macroscopic multi-class traffic model in its characteristic form and investigating the obtained characteristic speeds. On the other hand, a connection between the theoretical control design method backstepping and an up-to-date extension of the AR traffic model for two classes is created by designing a full-state feedback controller and output feedback controller.

1.2.2 Predictor feedback control

Boundary control of PDE with state-dependent ODE systems has been intensively studied over the past few years. Backstepping control design method is used in solving these problems. In parabolic PDE-ODE system, a recently studied one is the thermo-dynamical model known as Stefan problem with application to control of screw extruder for 3D Printing [72] and arctic sea ice temperature estimation [71]. The state-dependency of the ODE governs the moving interface and makes the PDE-ODE system nonlinear. [73] presents a backstepping-based control design.

In hyperbolic PDE-ODE system, the widely studied problem considers the ODE system with time-varying or state-dependent input delays. Many recent theoretical results have been developed for time-varying input delay in [11] and state-dependent input delays for nonlinear ODE in [12] [13] [38]. [14] and [106] studied multi-inputs constant and time-varying delays to nonlinear ODE system. But the multiple state-dependent input delays have not been discussed before and this dissertation will address this problem which arise from the moving traffic shockwave. In order to compensate the time-varying or state-dependent delays, the predictor feedback approach is employed. The predictor feedback laws use the future values of the state so that when the control signal reaches the state of the plant with delays compensated.

For application of the ODE system with the hyperbolic-type input delays, [22] develops boundary control piston position in inviscid gas and [37] develops the control of a mass balance in screw extrusion process. Other applications include vibration suppression of mining cable elevator [110], control of Saint-Venant equation with hydraulic jumps [10]. However, the application of the methodology in traffic problem has never been discussed before.

The contribution of our work on control of moving traffic shockwave: this is the first theoretical result on control of two PDE state-dependent input delays to ODE. Predictor-based state feedback design approach is adopted following [38] [106]. In fact, [106] shows a predictor feedback design for multiple constant delayed inputs to linear time-invariant systems while [38] considers a single implicitly defined state-dependent input delay to nonlinear time-invariant systems alternatively written as a PDE-ODE cascade system. In this work, we firstly present the predictor feedback design for two PDE states dependent input delays to ODE and address control problem of traffic moving shockwave.

1.2.3 Extremum Seeking control

Extremum Seeking (ES) control is a non-model based, real-time optimization tool emerging in 1990's. ES control is applicable to deal with nonlinearity in control problem or in the optimization problem with a local minimum or maximum. Its performance and analytical framework was further advanced and established after the publication of the theoretical work by [75] proving the convergence of cost function to a neighborhood of the optimal value by means of averaging analysis and singular perturbation. Many recent efforts include [5] [19] [47] [49] [50] [51] [54] [74] [75] [84] [90] [93] [95] [101] [102] [111].

ES approach relies on a small periodic excitation, usually sinusoidal to disturb the parameters being tuned and the effect of the parameters is then quantified by the output of a nonlinear map. The search of the optimal value is therefore generated. Despite the large number of previous work on ES control, authors in [90] firstly considered the problem of ES control in the presence of delays. The proposed method is based on the predictor-based feedback for delay compensation of [90]. Using backstepping transformation and averaging in infinite dimensional systems in [56], the stability analysis is rigorously obtained. The averaging based approach is employed due to the need to estimate the unknown second-order derivative of nonlinear map.

We consider a freeway segment with bottleneck located at the outlet where the road capacity drops. The traffic dynamics of the freeway segment is described with LWR model. The dynamics at the bottleneck area is described with a nonlinear map at the outlet where the optimal density is unknown. We apply ES control in order to find the unknown optimal density at the bottleneck. Since the control is actuated from the upstream freeway of the bottleneck, the delay effect of the traffic dynamics is compensated in designing ES control. The optimal density input at inlet of the freeway segment is achieved by estimating the unknown nonlinear map at the outlet.

Our contribution lies in the following aspects: this is the first work on control of traffic governed by LWR PDE model in the presence of unknown downstream bottleneck. ES control with delay compensation is firstly adapted to this traffic problem. The traffic dynamics is represented with linearized LWR model in the theoretical analysis, but the simulation is conducted on the nonlinear LWR model and ES control design is validated for the nonlinear system.

1.3 Thesis overview

The reminder of the dissertation is outlined below:

Chapter 2 develops boundary feedback control laws to reduce stop-and-go oscillations in congested traffic. The traffic dynamics is describe with the one-lane ARZ model and a coupled 2×2 nonlinear hyperbolic PDE system is considered. Nonadaptive and adaptive output feedback control are proposed to achieve exponential stability in L^2 sense and finite time convergence to uniform steady states.

Chapter 3 develops output feedback boundary control to mitigate traffic congestion of a unidirectional two-lane freeway segment. The macroscopic traffic dynamics are described by the two-lane ARZ model respectively for both the fast and slow lanes. Lane-changing interactions between the two lanes lead to exchanging source terms between the two pairs second-order PDEs. Therefore, we are dealing with 4×4 nonlinear coupled hyperbolic PDEs. Two full-state feedback boundary control laws are developed and a collocated boundary observer is designed for state estimation with sensing of densities at the outlet. Output feedback boundary controllers are obtained by combining the collocated observer and full-state feedback controllers. The finite time convergence to equilibrium is achieved for both the controllers and observer designs.

Chapter 4 develops boundary feedback control laws in order to damp out traffic oscillations in the congested regime of two-class Aw-Rascle (AR) traffic model. The macroscopic second-order two-class AR traffic model consists of 4×4 nonlinear coupled hyperbolic PDEs. The concept of area occupancy is proposed to express the traffic pressure and equilibrium speed relationship yielding a coupling between the two classes of vehicles. Each vehicle class is characterized by its own vehicle size and driver's behavior. Output feedback controller is designed for ramp metering at outlet to achieve finite time convergence of the density and velocity perturbations to zeros.

Chapter 5 develops backstepping state feedback control to stabilize a moving shockwave in a freeway segment under bilateral boundary actuations of traffic flow. Boundary control design in this chapter brings the moving shockwave front to a static setpoint position, hindering the upstream propagation of traffic congestion. The traffic dynamics are described with LWR model, leading to a system of two first-order PDEs. Each PDE represents the traffic density of a spatial domain and the segregating moving interface is governed by an ODE. For the PDE-ODE coupled system. The control objective is to stabilize both the PDE states of traffic density and the ODE state of moving shock position to setpoint values. We design predictor feedback controllers to cooperatively compensate state-dependent input delays to the ODE and show local stability of the closed-loop system in H^1 norm.

Chapter 6 develops boundary control for freeway traffic with a downstream bottleneck. If the incoming traffic flow remains unchanged, traffic congestion forms upstream of the bottleneck due to outgoing traffic overflowing its capacity. Therefore,incoming flow at the inlet of the freeway segment is controlled so that the optimal density could be achieved to maximize the outgoing flow and not to surpass the capacity at outlet. Traffic densities on the freeway segment are described with LWR macroscopic PDE model. We use ES Control with delay compensation for LWR PDE.

Chapter 7 develops boundary observer for estimation of congested freeway traffic states based on ARZ PDE model. Numerical simulations are conducted to validate the boundary observer design for estimation of the nonlinear ARZ model. In data validation, we calibrate model parameters of the ARZ model and then use vehicle trajectory data to test the performance of the observer design.

Chapter 2

One-Lane Traffic Congestion Control

We develop boundary feedback control laws to reduce stop-and-go oscillations in congested traffic. The macroscopic traffic dynamics are governed by ARZ model, consisting of second-order nonlinear PDEs. A criterion to distinguish free and congested regimes for the ARZ traffic model leads to the study of hetero-directional hyperbolic PDE model of congested traffic regime. To stabilize the oscillations of traffic density and speed in a freeway segment, a boundary input through ramp metering is considered. We discuss the stabilization problem for freeway segments respectively, upstream and downstream of the ramp. For the more challenging upstream control problem, our full-state feedback control law employs a backstepping transformation. Both collocated and anti-collocated boundary observers are designed. The exponential stability in L^2 sense and finite time convergence to equilibrium are achieved and validated with simulation. In the absence of relaxation time and boundary parameters' knowledge, we propose adaptive output feedback control design. Control is applied at outlet and the measurement is taken from inlet of the freeway segment. We use the backstepping method to obtain an observer canonical form in which unknown parameters multiply with measured output. A parametric model based on this form is derived and gradient-based parameter estimators are designed. An explicit state observer involving the delayed values of the input and the output is introduced for state estimation. Using the parameter and state estimates, we develop an adaptive output feedback control law which achieves convergence to the steady regulation in the L^2 sense.

This chapter is organized as follows: Section 2.1 presents linearized ARZ model and free and congested regime. Section 2.2 proposes a general freeway traffic control model through ramp-metering. Sections 2.3-2.4 provide boundary control design for downstream of the ramp metering traffic and full-state feedback control law and observers for upstream of the ramp metering traffic. Section 2.5 gives adaptive output feedback design for the upstream of ramp metering problem. Both the nonadaptive control design and adaptive design are validated with simulation in Section 2.6. Section 2.8 summarizes results and discuss future work of this paper.

2.1 Aw-Rascle-Zhang model

We consider the Aw-Rascle-Zhang model with a relaxation term and linearize it around steady states. The Aw-Rascle model is

$$\partial_t \rho + \partial_x(\rho v) = 0, \tag{2.1}$$

$$\partial_t v + (v - \rho p'(\rho))\partial_x v = \frac{V(\rho) - v}{\tau}. \tag{2.2}$$

The state variable $\rho(x,t)$ is the traffic density and $v(x,t)$ is the traffic speed, $V(\rho)$ is the equilibrium traffic speed profile and τ is the relaxation time related to driving behavior. The variable $p(\rho)$ is defined as the traffic pressure, an increasing function of density

$$p(\rho) = \rho^{\gamma}, \tag{2.3}$$

and $\gamma \in \mathbb{R}_+$.

The Zhang model is given by

$$\partial_t \rho + \partial_x(\rho v) = 0, \tag{2.4}$$

$$\partial_t v + \left(v + \rho V'(\rho)\right)\partial_x v = 0. \tag{2.5}$$

Combining these two models together, we have the Aw-Rascle-Zhang model in (ρ, v) given in (2.1), (2.2), and the conditions $p'(\rho) = -V'(\rho)$ and $p(0) = 0$ need to be satisfied so that the Aw-Rascle model and the Zhang model are consistent. Thus it holds that

$$p(\rho) = v_f - V(\rho), \tag{2.6}$$

where v_f is the free flow velocity. Since $V(\rho_m) = 0$ and ρ_m is the maximum density, $p(\rho) = \rho^\gamma$ is rescaled as

$$p(\rho) = v_f \left(\frac{\rho}{\rho_m}\right)^\gamma. \tag{2.7}$$

The equilibrium velocity-density relationship $V(\rho)$ is given in the form of Greenshield's model [52],

$$V(\rho) = v_f - p(\rho) = v_f \left(1 - \left(\frac{\rho}{\rho_m}\right)^\gamma\right). \tag{2.8}$$

2.1.1 Linearized ARZ model

The traffic density is the number of vehicles per unit length. The traffic flux is defined as the number of vehicles per unit time which cross a given point on the road, which is a more reasonable physical variable to control by ramp metering. Therefore, we rewrite the ARZ model in traffic flux and velocity (q, v),

$$q_t + v q_x = \frac{q(\gamma p - v)}{v} v_x + \frac{q(v_f - p - v)}{\tau v}, \tag{2.9}$$

$$v_t - (\gamma p - v) v_x = \frac{v_f - p - v}{\tau}, \tag{2.10}$$

where the traffic flow flux q is defined as

$$q = \rho v. \tag{2.11}$$

The traffic pressure $p(\rho)$ and flux q are related by

$$p = \frac{v_f}{\rho_m^{\gamma}} \left(\frac{q}{v}\right)^{\gamma}. \tag{2.12}$$

There is no explicit solution to the nonlinear hyperbolic (q,v)-system in (2.9), (2.10). To better understand the dynamics of the ARZ traffic model, we linearize the model around steady states ($q^\star$, $v^\star$). The small deviations from the nominal profile are defined as

$$\tilde{q}(x,t) = q(x,t) - q^\star, \tag{2.13}$$

$$\tilde{v}(x,t) = v(x,t) - v^\star, \tag{2.14}$$

where $x \in [0,L]$, $t \in [0,\infty)$.

We consider the traffic dynamics of a segment of freeway and L is the length of freeway segment. For inlet boundary at $x = 0$, we consider a constant traffic flux $q^\star$ entering the domain which can be realized by implementing a mainline flux metering at the inlet,

$$q(0,t) = q^\star. \tag{2.15}$$

For outlet, we assume to implement a mainline density metering so that the following condition holds,

$$\rho(L,t) = \rho^{\star}. \tag{2.16}$$

Applying this assumption to the outlet boundary $x = L$ of considered freeway section and we obtain a boundary condition for (q,v)-system in (2.9), (2.10),

$$v(L,t) = \frac{1}{\rho^{\star}} q(L,t). \tag{2.17}$$

The linearized ARZ model is describes with the following $(\tilde{q},\tilde{v})$-system,

$$\tilde{q}_t + v^{\star}\tilde{q}_x - \frac{q^{\star}(\gamma p^{\star} - v^{\star})}{v^{\star}}\tilde{v}_x = -\frac{q^{\star}}{\tau}\left(\frac{1}{v^{\star}} - \frac{1}{\gamma p^{\star}}\right)\tilde{v} - \frac{\gamma p^{\star}}{\tau v^{\star}}\tilde{q}, \tag{2.18}$$

$$\tilde{v}_t - (\gamma p^{\star} - v^{\star})\tilde{v}_x = \frac{\gamma p^{\star} - v^{\star}}{\tau v^{\star}}\tilde{v} - \frac{\gamma p^{\star}}{\tau q^{\star}}\tilde{q}, \tag{2.19}$$

with the linearized boundary conditions

$$\tilde{q}(0,t) = 0, \tag{2.20}$$

$$\tilde{v}(L,t) = \frac{1}{\rho^{\star}}\tilde{q}(L,t). \tag{2.21}$$

where $p^{\star} = p(q^{\star}, v^{\star})$, according to (2.12).

2.1.2 Free/congested regime analysis

According to the relation between $p^{\star}$ and $v^{\star}$ in (2.6), the following holds

$$v^{\star} - \gamma p^{\star} = v^{\star} - \gamma(v_f - v^{\star}) = (1+\gamma)v^{\star} - \gamma v_f. \tag{2.22}$$

For free-flow regime, $\gamma p^\star < v^\star$ implies $v^\star > \frac{\gamma}{\gamma+1} v_f$. For congested regime, $\gamma p^\star > v^\star$ implies $v^\star < \frac{\gamma}{\gamma+1} v_f$. Therefore, $v^\star = \frac{\gamma}{\gamma+1} v_f$ is the critical velocity to distinguish the free regime and the congested regime of traffic flow.

- Free-flow regime : $\rho^\star < \frac{\rho_m}{(1+\gamma)^{1/\gamma}} \Leftrightarrow \; v^\star > \frac{\gamma}{\gamma+1} v_f$

  In the free-flow regime, both the disturbances of traffic flux and velocity travel downstream, at respective speeds $v^\star$ and $v^\star - \gamma p^\star$. The linearized ARZ model in free-regime is a homo-directional hyperbolic PDEs.

- Congested regime : $\rho^\star > \frac{\rho_m}{(1+\gamma)^{1/\gamma}} \Leftrightarrow \; v^\star < \frac{\gamma}{\gamma+1} v_f$

  In the congested regime, the disturbances of the traffic flow flux are carried downstream by the vehicles that generated them. The disturbances of the traffic speed travel upstream at a speed of $\gamma p^\star - v^\star$. Therefore, we are dealing with a hetero-directional coupled hyperbolic system, given that $v^\star - \gamma p^\star < 0$ and $v^\star > 0$ in the congested regime. The disturbances force vehicles into deceleration-acceleration cycles, leading to the traffic oscillations, known as the stop-and-go traffic. This kind of instability in traffic causes unsafe driving conditions, extra fuel consumptions and eventually evolves into a bumper-to-bumper jam.

- Bumper-to-bumper traffic jam : $\rho^\star = \rho_m \Leftrightarrow \; v^\star = 0$

  The traffic becomes bumper-to-bumper jammed when the traffic density reaches its maximum and traffic speed equals to 0.

In this paper, we focus on control design for the congested regime

$$\rho_m > \rho^\star > \frac{\rho_m}{(1+\gamma)^{1/\gamma}} \Leftrightarrow \; 0 < v^\star < \frac{\gamma}{1+\gamma} v_f. \tag{2.23}$$

We choose the steady states $(\rho^\star, v^\star)$ satisfying above inequalities but not too close to bounds so that small disturbances will not exceed them.

2.2 Boundary Control Model

Before we apply boundary control to the linearized ARZ model in $(\tilde{q},\tilde{v})$, we represent the system in Riemann coordinates and then map it to a decoupled first-order 2×2 hyperbolic system in $(\bar{w},\bar{v})$. We propose two different control strategies for the hyperbolic $(\bar{w},\bar{v})$-system through ramp metering control.

We define new variables $(w,\bar{v})$ in Riemann coordinates,

$$w = \tilde{q} - q^\star\left(\frac{1}{v^\star} - \frac{1}{\gamma p^\star}\right)\tilde{v}, \tag{2.24}$$

$$\bar{v} = \frac{q^\star}{\gamma p^\star}\tilde{v}, \tag{2.25}$$

We obtain

$$w_t(x,t) + v^\star w_x(x,t) = -\frac{1}{\tau}w, \tag{2.26}$$

$$\bar{v}_t(x,t) - (\gamma p^\star - v^\star)\bar{v}_x(x,t) = -\frac{1}{\tau}w, \tag{2.27}$$

$$w(0,t) = -\frac{\gamma p^\star - v^\star}{v^\star}\bar{v}(0,t), \tag{2.28}$$

$$\bar{v}(L,t) = w(L,t). \tag{2.29}$$

In order to decouple (2.26) and (2.29), we introduce a scaled state as follows:

$$\bar{w}(x,t) = \exp\left(\frac{x}{\tau v^\star}\right)w(x,t). \tag{2.30}$$

The $(w,\bar{v})$-system is then transformed to a first-order 2×2 hyperbolic system

$$\bar{w}_t(x,t) =-v^\star \bar{w}_x(x,t), \tag{2.31}$$

$$\bar{v}_t(x,t) =(\gamma p^\star - v^\star)\bar{v}_x(x,t) + c(x)\bar{w}(x,t), \tag{2.32}$$

$$\bar{w}(0,t) =-k_0\bar{v}(0,t), \tag{2.33}$$

$$\bar{v}(L,t) =\kappa\bar{w}(L,t). \tag{2.34}$$

where

$$c(x) =-\frac{1}{\tau}\exp\left(-\frac{x}{\tau v^\star}\right), \tag{2.35}$$

$$k_0 =\frac{\gamma p^\star - v^\star}{v^\star}, \tag{2.36}$$

$$\kappa =\exp\left(\frac{-L}{\tau v^\star}\right). \tag{2.37}$$

The spatially varying coefficient $c(x)$ is a strictly increasing function and is bounded by

$$-\frac{1}{\tau} \leq c(x) \leq -\frac{\kappa}{\tau}. \tag{2.38}$$

The following relations for boundary values are obtained from (2.24)-(2.25),

$$\tilde{q}(0,t) =\bar{w}(0,t) + k_0\bar{v}(0,t), \tag{2.39}$$

$$\tilde{q}(L,t) =\kappa\bar{w}(L,t) + k_0\bar{v}(L,t), \tag{2.40}$$

The applicable boundary control inputs could be traffic flow flux at either the inlet or at the outlet of a freeway section. We summarize the transformation from the linearized ARZ model in $(\tilde{q},\tilde{v})$-system to $(\bar{w},\bar{v})$-system,

$$\begin{aligned}\bar{w}(x,t) =& \exp\left(\frac{x}{\tau v^{\star}}\right)\left(\tilde{q}(x,t)-\rho_1\tilde{v}(x,t)\right), && (2.41)\\ \bar{v}(x,t) =& \rho_2\tilde{v}(\xi,t). && (2.42)\end{aligned}$$

And the inverse transformation is given by

$$\begin{aligned}\tilde{q}(x,t) =& \exp\left(-\frac{x}{\tau v^{\star}}\right)\bar{w}(x,t)+k_0\bar{v}(x,t), && (2.43)\\ \tilde{v}(x,t) =& \frac{1}{\rho_2}\bar{v}(\xi,t). && (2.44)\end{aligned}$$

where the constant, positive coefficients are defined as follows:

$$\rho_1 = q^{\star}\left(\frac{1}{v^{\star}}-\frac{1}{\gamma p^{\star}}\right), \quad \rho_2 = \frac{q^{\star}}{\gamma p^{\star}}. \tag{2.45}$$

Therefore, we can study the stability of $(\tilde{q},\tilde{v})$-system through $(\bar{w},\bar{v})$-system due to their equivalence. The control laws we obtain later for the $(\bar{w},\bar{v})$-system guarantee the equivalent stability properties of the $(\tilde{q},\tilde{v})$-system.

2.2.1 UORM/DORM ramp metering control

Considering a ramp metering is installed at freeway on-ramp to reduce the oscillations in the congested traffic, we propose two different control design based on the domain we aim to control with the ramp metering.

If we consider controlling the traffic downstream of the ramp metering (DORM) in the domain $\mathscr{D}$, the ramp metering is located at the inlet of the domain $\mathscr{D}$ and $U_{\text{in}}(t)$ is the control law to be designed. The DORM controller $U_{\text{in}}(t)$ is applied with $\tilde{q}(0,t)$.

In the case that we control the traffic upstream of the ramp metering (UORM) in the

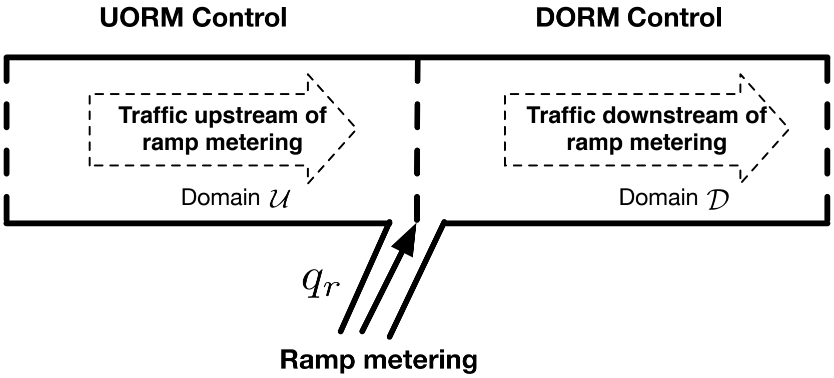

Figure 2.1: A freeway segment controlled by ramp-metering.

domain $\mathscr{U}$, the controller $U_{\text{out}}(t)$ is located at the outlet of domain $\mathscr{U}$. The UORM controller $U_{\text{out}}(t)$ is applied with $\tilde{q}(L,t)$.

DORM control

We define a ramp metering boundary control input $U_{\text{in}}(t)$ at the inlet of $\mathscr{D}$,

$$U_{\text{in}}(t) = q_r(t) = \tilde{q}(0,t), \tag{2.46}$$

$$\tilde{q}(L,t) = \rho^\star \tilde{v}(L,t). \tag{2.47}$$

Note that the DORM controller $U_{\text{in}}(t)$ is applied with the traffic flow flux variation at the inlet of domain $\mathscr{D}$. The other boundary condition does not change. We need to implement a density metering at mainline outlet so that a constant density is enforced.

Substituting (2.46) into (2.39), we obtain the controlled boundary. The DORM control model is given by $(\bar{w},\bar{v})$-system in (2.31), (2.32) with controlled boundary at the inlet in (2.50),

$$\bar{w}_t(x,t) = -v^\star \bar{w}_x(x,t), \tag{2.48}$$

$$\bar{v}_t(x,t) = (\gamma p^\star - v^\star)\bar{v}_x(x,t) + c(x)\bar{w}(x,t), \tag{2.49}$$

$$\bar{w}(0,t) = -k_0\bar{v}(0,t) + U_{\text{in}}(t), \tag{2.50}$$

$$\bar{v}(L,t) = \kappa\bar{w}(L,t). \tag{2.51}$$

UORM control

We consider a constant traffic flux entering the domain $\mathscr{U}$ and the control input $U_{\text{out}}(t)$ is implemented with the ramp metering at the outlet of the domain. For inlet, we need to implement a flux metering at mainline so that a constant flux is enforced. The UORM control input $U_{\text{out}}(t)$ and $\tilde{q}(0,t)$ are defined as

$$U_{\text{out}}(t) = q_r(t), \tag{2.52}$$

$$\tilde{q}(0,t) = 0. \tag{2.53}$$

The total traffic flow flux variation at the outlet of domain $\mathscr{U}$ includes the traffic flow flux variation from the mainline and from the ramp.

$$\tilde{q}(L^+,t) = \tilde{q}(L^-,t) + q_r(t). \tag{2.54}$$

The mainline flow flux variation $\tilde{q}(L^-,t)$ in the domain is given by (2.40). The flow flux variation $\tilde{q}(L^+,t)$ of the downstream of domain $\mathscr{U}$ is given by (2.21). Substituting (2.40) and (2.21) into (2.54), we obtain the UORM control model with controlled boundary at the outlet in (2.58).

$$\bar{w}_t(x,t) = -v^\star\bar{w}_x(x,t), \tag{2.55}$$

$$\bar{v}_t(x,t) = (\gamma p^\star - v^\star)\bar{v}_x(x,t) + c(x)\bar{w}(x,t), \tag{2.56}$$

$$\bar{w}(0,t) = -k_0\bar{v}(0,t), \tag{2.57}$$

$$\bar{v}(L,t) = \kappa\bar{w}(L,t) + U_{\text{out}}(t). \tag{2.58}$$

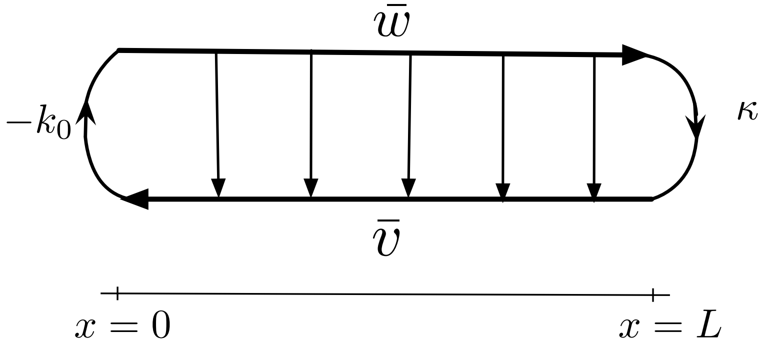

Figure 2.2: Diagram of control model with zero input.

2.2.2 Spectrum analysis of control models with zero input

In order to explore the traffic dynamics in the open loop-system, we consider the zero input for DORM or UORM control design

$$q_r(t) = 0, \tag{2.59}$$

$$U_{\text{in}}(t) = 0 \tag{2.60}$$

$$U_{\text{out}}(t) = 0. \tag{2.61}$$

According to boundary conditions in (2.50), (2.51) or (2.57), (2.58), we have the following zero input system that holds for both control models

$$\bar{w}_t(x,t) = - v^{\star}\bar{w}_x(x,t), \tag{2.62}$$

$$\bar{v}_t(x,t) = (\gamma p^{\star} - v^{\star})\bar{v}_x(x,t) + c(x)\bar{w}(x,t), \tag{2.63}$$

$$\bar{w}(0,t) = - k_0\bar{v}(0,t), \tag{2.64}$$

$$\bar{v}(L,t) = \kappa\bar{w}(L,t), \tag{2.65}$$

where $x \in [0,L]$ and $t > 0$. The diagram is shown in Fig. 2.2. The above zero-input system is equivalent to the open-loop $(\tilde{q},\tilde{v})$-system in (2.18)-(7.78).

In order to analyze the spectrum of the system with zero input in (2.62)-(2.65), we transform the first-order 2×2 hyperbolic system to a second-order wave equation.

$$\begin{aligned} y_{tt}(x,t) =& v^\star(\gamma p^\star - v^\star) y_{xx}(x,t) - (2v^\star - \gamma p^\star) y_{xt}(x,t) \\ & - \frac{1}{\tau} y_t(x,t) + \frac{\gamma p^\star - v^\star}{\tau} y_x(x,t), \end{aligned} \tag{2.66}$$

$$y_t(0,t) = 0, \tag{2.67}$$

$$y_x(L,t) = 0. \tag{2.68}$$

The new variable $y(x,t)$ satisfies the following relations,

$$\begin{aligned} w(x,t) =& y_t(x,t) - (\gamma p^\star - v^\star) y_x(x,t), \\ \bar{v}(x,t) =& y_t(x,t) + v^\star y_x(x,t). \end{aligned} \tag{2.69}$$

The term y_{xt} is a structural damping, of which effect is fully addressed in [26]. The term y_t is also a damping term and the longer reaction time τ will cause the weaker damping effect of y_t in the domain.

The wave equation is written in the vector form,

$$\frac{\partial}{\partial t} \begin{pmatrix} y \\ y_t \end{pmatrix} = A \begin{pmatrix} y \\ y_t \end{pmatrix}, \tag{2.70}$$

where the operator matrix A is given by

$$A = \begin{pmatrix} y_t \\ -\frac{1}{\tau} y_t - (2v^\star - \gamma p^\star) y_{xt} + \frac{\gamma p^\star - v^\star}{\tau} y_x + v^\star(\gamma p^\star - v^\star) y_{xx} \end{pmatrix}.$$

The eigenvalues of A are obtained by solving the following equations,

$$\begin{aligned} \lambda y =& y_t, \\ \lambda^2 y =& -(2v^\star - \gamma p^\star)\lambda y_x - \frac{\lambda}{\tau} + \frac{\gamma p^\star - v^\star}{\tau} y_x + v^\star(\gamma p^\star - v^\star) y_{xx}. \end{aligned} \tag{2.71}$$

We take Fourier transform with respect to the spatial variable $x \in [0, L]$. We map $y(x,t) \to \hat{y}(n,t)$, $n \in \mathbb{Z}$,

$$y(x) = \sum_{n=1}^{\infty} \hat{y}_n \exp\left(\frac{inx}{L}\right). \tag{2.72}$$

The nth Fourier coefficient is defined as

$$\hat{y}_n = \int_0^L y(x) \exp\left(\frac{-inx}{L}\right) dx, \tag{2.73}$$

the transformation yields

$$\hat{y}_x = \frac{inx}{L} \hat{y}, \quad \hat{y}_{xx} = \frac{-n^2}{L^2} \hat{y}. \tag{2.74}$$

Substituting $\hat{y}_x$ and $\hat{y}_{xx}$ into (2.72), the kth pair of eigenvalues satisfy the following quadratic equation:

$$0 = \lambda^2 + \left(\frac{2v^\star - \gamma p^\star}{L} ni + \frac{1}{\tau}\right)\lambda + \frac{v^\star(\gamma p^\star - v^\star)}{L^2} n^2 - \frac{\gamma p^\star - v^\star}{\tau L} ni. \tag{2.75}$$

The nth pair of eigenvalues are obtained by solving the quadratic equation,

$$\lambda_{1,2} = \frac{-\frac{1}{\tau} - \frac{(2v^\star - \gamma p^\star)}{L} n\mathrm{i} \pm \left(\frac{1}{\tau} + \frac{\gamma p^\star}{L} n\mathrm{i}\right)}{2}. \tag{2.76}$$

Thus there are two sets of eigenvalues in the left half plane,

$$\lambda_1 = \frac{\gamma p^\star - v^\star}{L} n\mathrm{i}, \quad \lambda_2 = -\frac{1}{\tau} - \frac{v^\star}{L} n\mathrm{i}. \tag{2.77}$$

The eigenvalue λ_1 only contains the imaginary part. The longer of the relaxation time τ, the smaller of the negative real part in the eigenvalue λ_2. As $\tau \to \infty$ and $n \to \infty$,

$$\lambda_1 \to \mathrm{Im}(+\infty), \tag{2.78}$$

$$\lambda_2 \to \mathrm{Im}(-\infty). \tag{2.79}$$

According to the above spectral analysis, two sets of eigenvalues locate along the imaginary axis. The system is marginal stable and there are persistent oscillations in the domain of the zero input system in (2.62)-(2.65). Therefore, it is meaningful to propose control design for the system.

2.3 DORM control design

The DORM control problem is given by

$$\bar{w}_t(x,t) = -v^\star \bar{w}_x(x,t), \tag{2.80}$$

$$\bar{v}_t(x,t) = (\gamma p^\star - v^\star)\bar{v}_x(x,t) + c(x)\bar{w}(x,t), \tag{2.81}$$

$$\bar{w}(0,t) = -k_0 \bar{v}(0,t) + U_{\mathrm{in}}(t), \tag{2.82}$$

$$\bar{v}(L,t) = \kappa \bar{w}(L,t), \tag{2.83}$$

where $x \in \mathscr{D} \triangleq [0,L]$ and $t > 0$. The diagram of DORM control model is shown in Fig. 2.3.

If we choose the DORM controller as

$$U_{\mathrm{in}}(t) = k_0 \bar{v}(0,t), \tag{2.84}$$

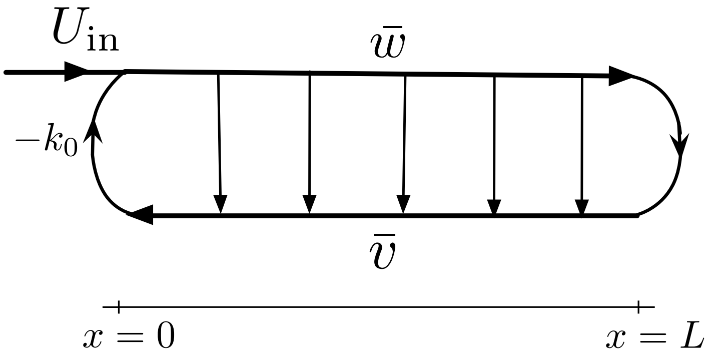

Figure 2.3: Time response of DORM control model.

we get $\bar{w}(0,t) = 0$. The explicit solution to the above $(\bar{w},\bar{v})$-system with the DORM control law (2.84) is

$$\bar{w}(x,t) = \begin{cases} \bar{w}(x - v^\star t, 0), & t < \frac{x}{v^\star}, \\ \bar{w}\left(0, t - \frac{x}{v^\star}\right), & t \geq \frac{x}{v^\star}, \end{cases} \tag{2.85}$$

and for $t \geq \frac{x}{v^\star}$,

$$\bar{w}(x,t) \equiv 0. \tag{2.86}$$

Solving for $\bar{v}(x,t)$, we have

$$\bar{v}(x,t) = \begin{cases} \bar{v}(x + (\gamma p^\star - v^\star)t, 0) + \int_0^t c(x + (\gamma p^\star - v^\star)(t-s))\bar{w}(0,s)ds, & t < \frac{L-x}{\gamma p^\star - v^\star}, \\ \kappa \bar{w}\left(L, t - \frac{L-x}{\gamma p^\star - v^\star}\right) + \frac{1}{\gamma p^\star - v^\star}\int_x^L c(s)\bar{w}\left(0, t + \frac{x-s}{\gamma p^\star - v^\star}\right)ds, & t \geq \frac{L-x}{\gamma p^\star - v^\star}. \end{cases} \tag{2.87}$$

Thus for $t \geq t_f$, it holds that

$$\bar{v}(x,t) \equiv 0. \tag{2.88}$$

where

$$t_f = \frac{L}{v^\star} + \frac{L}{\gamma p^\star - v^\star}. \tag{2.89}$$

Substituting k_0 in (2.36) and $\bar{v}$ in (2.42), we get

$$U_{\text{in}}(t) = \rho_1 \tilde{v}(0,t). \tag{2.90}$$

The DORM boundary controller $U_{\text{in}}(t)$ is obtained by the measurement of $\tilde{v}(0,t)$. To show the exponential stability of the system in the L^2 sense, we construct the following Lyapunov functions

$$V_1(t) = \frac{1}{2v^\star} \int_0^L e^{-x} \bar{w}^2(x,t) dx, \tag{2.91}$$

$$V_2(t) = \frac{1}{2(\gamma p^\star - v^\star)} \int_0^L e^{x} \bar{v}^2(x,t) dx, \tag{2.92}$$

and differentiate the Lyapunov functions in time. We obtain the following inequalities using Cauchy-Schwarz Inequality and Young's Inequality,

$$\begin{aligned} \dot{V}_1 \leq & -e^{-L}(\bar{w}^2(L) + ||\bar{w}||^2), \\ \dot{V}_2 \leq & e^{L}\bar{v}^2(L) - \bar{v}^2(0) - ||\bar{v}||^2 + \frac{1}{\gamma p^\star - v^\star} \int_0^L e^{x} \bar{v}(x) c(x) \bar{w}(x) dx. \end{aligned} \tag{2.93}$$

According to the boundedness of $c(x)$ in (7.34), we have

$$|c(x)| \leq C_0 = \frac{1}{\tau} \tag{2.94}$$

Then it holds that

$$\dot{V}_2 \leq e^{L} \kappa^2 \bar{w}^2(L) + \frac{1}{2d_1(\gamma p^\star - v^\star)} ||\bar{w}||^2 - \left(1 - \frac{d_1 C_0^2 e^{2L}}{2(\gamma p^\star - v^\star)}\right) ||\bar{v}||^2, \tag{2.95}$$

where d_1 is a positive constant and we choose $d_1 < \frac{2\tau^2(\gamma p^\star - v^\star)}{e^{2L}}$. Consider the following Lyapunov function

$$V = d_2 V_1 + V_2, \tag{2.96}$$

where $d_2 = \max\left(e^{2L}\kappa^2, \frac{e^{2L}}{2d_1(\gamma p^\star - v^\star)}\right)$, it holds that

$$\dot{V} \leq -d_0 V, \tag{2.97}$$

where $d_0 = \min\left(\frac{d_2}{e^L} - \frac{1}{2d_1(\gamma p^\star - v^\star)}, 1 - \frac{d_1 C_0^2 e^{2L}}{2(\gamma p^\star - v^\star)}\right)$. The exponential stability of the system (2.80)-(2.83) with the DORM boundary controller (2.84) is shown above. From the explicit solution of the system, it holds for $t \geq t_f$,

$$\bar{w}(x,t) \equiv 0, \quad \bar{v}(x,t) \equiv 0. \tag{2.98}$$

We summarize above result in the following Theorem.

Theorem 2.1. *Consider system* (2.80)-(2.83) *with inital conditions* $\bar{w}_0, \bar{v}_0 \in L^2[0,L]$ *and the control law* (2.84). *The equilibrium* $\bar{w} \equiv \bar{v} \equiv 0$ *is exponentially stable in the* L^2 *sense and the equilibrium is reached in finite time* $t = t_f$ *given in* (2.89).

2.4 UORM control designs

For UORM control design, we have

$$\bar{w}_t(x,t) = -v^\star \bar{w}_x(x,t), \tag{2.99}$$

$$\bar{v}_t(x,t) = (\gamma p^\star - v^\star)\bar{v}_x(x,t) + c(x)\bar{w}(x,t), \tag{2.100}$$

$$\bar{w}(0,t) = -k_0 \bar{v}(0,t), \tag{2.101}$$

$$\bar{v}(L,t) = \kappa \bar{w}(L,t) + U_{\text{out}}(t), \tag{2.102}$$

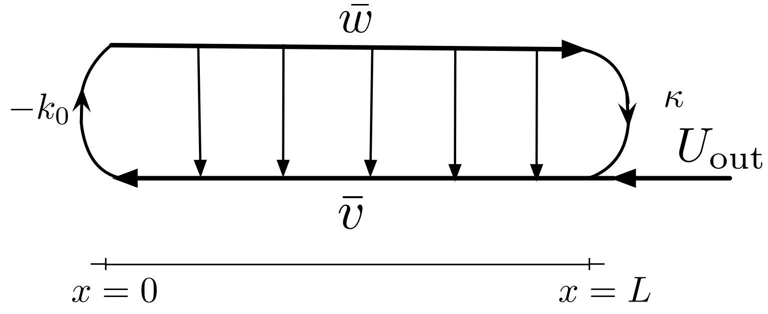

Figure 2.4: Time response of UORM control model.

where $x \in \mathscr{U} \triangleq [0,L]$ and $t>0$. The diagram of the UORM control model is shown in Fig.4.

2.4.1 UORM full-state feedback control design

Using the following backstepping transformation, we transform the system of UORM control design (2.99)-(2.102) into the target system,

$$\alpha(x,t) =\bar{w}(x,t), \tag{2.103}$$

$$\beta(x,t) =\bar{v}(x,t)-\int_0^x M(x-\xi)\bar{v}(\xi,t)d\xi-\int_0^x K(x,\xi)\bar{w}(\xi,t)d\xi. \tag{2.104}$$

For boundary conditions, we have $\bar{w}(0,t)=\alpha(0,t)$ and $\bar{v}(0,t)=\beta(0,t)$. The target system is given by

$$\alpha_t(x,t) =-v^\star\alpha_x(x,t), \tag{2.105}$$

$$\beta_t(x,t) =(\gamma p^\star-v^\star)\beta_x(x,t), \tag{2.106}$$

$$\alpha(0,t) =-k_0\beta(0,t), \tag{2.107}$$

$$\beta(L,t) =0. \tag{2.108}$$

To obtain the target system, we take time derivative and spatial derivative on (2.104). The following kernel equations and boundary condition need to be satisfied,

$$(\gamma p^\star - v^\star)K_x - v^\star K_\xi = c(\xi)K(x-\xi,0), \tag{2.109}$$

$$K(x,x) = -\frac{c(x)}{\gamma p^\star}, \tag{2.110}$$

where $K(x,\xi)$ evolves in the triangular domain $\mathscr{X} = \{(x,\xi) : 0 \le \xi \le x \le L\}$ and $M(x)$ is defined as

$$M(x) = -K(x,0). \tag{2.111}$$

The well-posedness of the kernel equations (2.109)-(2.111) and the boundedness of kernel variables are obtained following the same steps of the proof in the Appendix of [108]. Therefore, invertibility of the backstepping transformation in (2.103), (2.104) is established and we can study the target system for stability of the plant.

The UORM full-state feedback controller is chosen as

$$U_{\text{out}}(t) = -\kappa\bar{w}(L,t) + \int_0^L M(L-\xi)\bar{v}(\xi,t)d\xi + \int_0^L K(L,\xi)\bar{w}(\xi,t)d\xi, \tag{2.112}$$

so that $\beta(L,t) = 0$ is satisfied. One can easily find the explicit solution to the target system (2.105)-(2.108) and obtain that

$$\alpha(x,t) \equiv \beta(x,t) \equiv 0, \tag{2.113}$$

after $t_f = t_\alpha + t_\beta = \frac{L}{v^\star} + \frac{L}{\gamma p^\star - v^\star}$. Thus α and β go to zeros in finite time $t = t_f$. It is straightforward to prove that the α, β system is L^2 exponentially stable. Due to the invertibility of the transformation, $(\bar{w}, \bar{v})$-system is also L^2 exponentially stable.

Theorem 2.2. *Consider system* (2.99)-(2.102) *with inital conditions* $\bar{w}_0, \bar{v}_0 \in L^2[0,L]$ *and the control law* (2.112) *where the kernels* $K(x,\xi)$ *and* $M(x)$ *are obtained by solving* (2.109)-(2.111). *The equilibrium* $\bar{w} \equiv \bar{v} \equiv 0$ *is exponentially stable in the* L^2 *sense and the equilibrium is reached in finite time* $t = t_f$ *given in* (2.89).

Transforming $\bar{w}$ and $\bar{v}$ in (2.112) to $\tilde{q}$ and $\tilde{v}$ using the inverse transformation in (2.43)-(2.44), we get the control law in $(\tilde{q}, \tilde{v})$ as

$$\begin{aligned} U_{\text{out}}(t) = & -\tilde{q}(L,t) + \rho_1 \tilde{v}(L,t) + \rho_1 \int_0^L M(L-\xi)\tilde{v}(\xi,t)d\xi \\ & - \kappa \int_0^L K(L,\xi)\exp\left(\frac{\xi}{\tau v^\star}\right)\tilde{v}(\xi,t)d\xi \\ & + k_0 \int_0^L K(L,\xi)\exp\left(\frac{\xi}{\tau v^\star}\right)\tilde{q}(\xi,t)d\xi. \end{aligned} \tag{2.114}$$

Due to the invertibility of transformation (2.41)-(2.44) between $(\bar{w}, \bar{v})$ and $(\tilde{q}, \tilde{v})$, the $(\tilde{q}, \tilde{v})$-system is exponentially stable and converges to zero in the finite time. Therefore, the (q, v) system is exponentially stable and converges to $(q^\star, v^\star)$ in the finite time t_f.

To obtain $U_{\text{out}}(t)$, we need to take measurement of $\tilde{v}$ and $\tilde{q}$ in the domain $\mathscr{U}$, which might be realized by traffic camera and fleet GPS data. However, we propose the boundary observer design, considering the difficulties and costs to implement sensors along the freeway. We introduce two boundary observers; one is located at the same boundary with the full-state feedback controller and the other one is anti-collocated with the controller.

2.4.2 UORM anti-collocated boundary observer design

We define the following anti-collocated boundary measurement

$$Y_a(t) = \bar{v}(0,t). \tag{2.115}$$

According to (2.42), we obtain $\bar{v}(0,t) = \rho_2 \tilde{v}(0,t)$, by the measurement of $\tilde{v}(0,t)$. Then we design an observer by constructing the following system,

$$\hat{w}_t(x,t) = - v^\star \hat{w}_x(x,t), \tag{2.116}$$

$$\hat{v}_t(x,t) = (\gamma p^\star - v^\star)\hat{v}_x(x,t) + c(x)\hat{w}(x,t), \tag{2.117}$$

$$\hat{w}(0,t) = - k_0 Y_a(t), \tag{2.118}$$

$$\hat{v}(L,t) = \kappa \hat{w}(L,t) + U_{\mathrm{out}}(t), \tag{2.119}$$

where $\hat{w}$ and $\hat{v}$ are the estimates of state variables $\bar{w}$ and $\bar{v}$. The error system is obtained by subtracting the above estimates from (2.99)-(2.102),

$$\check{w}_t(x,t) = - v^\star \check{w}_x(x,t), \tag{2.120}$$

$$\check{v}_t(x,t) = (\gamma p^\star - v^\star) + c(x)\check{w}(x,t), \tag{2.121}$$

$$\check{w}(0,t) = 0, \tag{2.122}$$

$$\check{v}(L,t) = \kappa \check{w}(L,t), \tag{2.123}$$

where $\check{w} = \bar{w} - \hat{w}$ and $\check{v} = \bar{v} - \hat{v}$. The error system is same as (2.80)-(2.83) with (2.90). According to Theorem 1, the error system is exponentially stable in the L^2 sense and converges to zeros in finite time t_f.

Theorem 2.3. *Consider system* (2.120)-(2.123) *with initial conditions* $\check{w}_0, \check{v}_0 \in L^2[0,L]$. *The equilibrium* $\check{w} \equiv \check{v} \equiv 0$ *is exponentially stable in the* L^2 *sense, which implies that* $||\bar{w}(\cdot,t) - \hat{w}(\cdot,t)|| \to 0$ *and* $||\bar{v}(\cdot,t) - \hat{v}(\cdot,t)|| \to 0$. *The convergence to* 0 *is reached in finite time* $t = t_f$.

2.4.3 UORM collocated boundary observer design

We define a collocated boundary measurement

$$Y_c(t) = \bar{w}(L,t). \tag{2.124}$$

We obtain $\bar{w}(L,t) = (\tilde{q}(L,t) - \rho_1 \tilde{v}(L,t))/\kappa$, by the measurement of $\tilde{q}(L,t)$ and $\tilde{v}(L,t)$. Then we design a collocated boundary observer to estimate $\bar{w}(x,t)$ and $\bar{v}(x,t)$ by constructing the system

$$\hat{w}_t(x,t) = -v^\star \hat{w}_x(x,t) + r(x)(\bar{w}(L,t) - \hat{w}(L,t)), \tag{2.125}$$

$$\begin{aligned}\hat{v}_t(x,t) =& (\gamma p^\star - v^\star)\hat{v}_x(x,t) + c(x)\hat{w}(x,t) \\ &+ s(x)(\bar{w}(L,t) - \hat{w}(L,t)),\end{aligned} \tag{2.126}$$

$$\hat{w}(0,t) = -k_0 \hat{v}(0,t), \tag{2.127}$$

$$\hat{v}(L,t) = \kappa Y_c(t) + U_{\mathrm{out}}(t), \tag{2.128}$$

where $\hat{w}$ and $\hat{v}$ are the estimates of the state variables $\bar{w}$ and $\bar{v}$. The term $r(x)$ and $s(x)$ are output injection gains to be designed. The error system is obtained by subtracting the estimates from (2.99)-(2.102),

$$\check{w}_t(x,t) = -v^\star \check{w}_x(x,t) - r(x)\check{w}(L,t), \tag{2.129}$$

$$\begin{aligned}\check{v}_t(x,t) =& (\gamma p^\star - v^\star)\check{v}_x(x,t) + c(x)\check{w}(x,t) \\ &- s(x)\check{w}(L,t),\end{aligned} \tag{2.130}$$

$$\check{w}(0,t) = -k_0 \check{v}(0,t), \tag{2.131}$$

$$\check{v}(L,t) = 0, \tag{2.132}$$

where $\check{w} = \bar{w} - \hat{w}$ and $\check{v} = \bar{v} - \hat{v}$. We need to find the output injection gain $r(x)$ and $s(x)$ that guarantee the error system decays to zero. Using backstepping transformation, we transform the error system (2.129)-(2.132) into the following system

$$\check{\lambda}_t(x,t) = -v^\star \check{\lambda}_x(x,t), \tag{2.133}$$

$$\check{\nu}_t(x,t) = (\gamma p^\star - v^\star)\check{\nu}_x(x,t), \tag{2.134}$$

$$\check{\lambda}(0,t) = -k_0\check{\nu}(0,t), \tag{2.135}$$

$$\check{\nu}(L,t) = 0. \tag{2.136}$$

The backstepping transformation is

$$\check{\lambda}(x,t) = \check{w}(x,t) - \int_x^L \check{K}(L+x-\xi)\check{w}(\xi,t)d\xi, \tag{2.137}$$

$$\check{\nu}(x,t) = \check{v}(x,t) - \int_x^L \check{M}(v^\star x + (\gamma p^\star - v^\star)\xi)\check{w}(\xi,t)d\xi, \tag{2.138}$$

where the kernel $\check{L}$ is given by

$$\check{M}(x) = -\frac{1}{\gamma p^\star} c\left(\frac{x}{\gamma p^\star}\right). \tag{2.139}$$

For boundary condition (2.135) to hold, the kernels $\check{K}$ and $\check{M}$ satisfy the relation

$$\check{K}(L-\xi) = \check{M}((\gamma p^\star - v^\star)\xi). \tag{2.140}$$

the kernel $\check{K}$ is then obtained

$$\check{K}(x) = -\frac{1}{\gamma p^\star} c\left(\frac{\gamma p^\star - v^\star}{\gamma p^\star}(L-x)\right), \tag{2.141}$$

and

$$|\check{K}(x)| \leq \frac{1}{\gamma p^\star \tau}, \tag{2.142}$$

according to the boundedness of $c(x)$ in (2.94). The output injection gain $r(x)$ and $s(x)$ are

$$r(x) = v^\star \check{K}(x) = -\frac{v^\star}{\gamma p^\star} c\left(\frac{\gamma p^\star - v^\star}{\gamma p^\star}(L-x)\right), \tag{2.143}$$

$$\begin{aligned} s(x) =& -v^\star \check{M}(v^\star x + (\gamma p^\star - v^\star)L) \\ =& \frac{v^\star}{\gamma p^\star} c\left(\frac{v^\star}{\gamma p^\star} x - \frac{\gamma p^\star - v^\star}{\gamma p^\star} L\right). \end{aligned} \tag{2.144}$$

The backstepping transformation is invertible. Therefore, we study the stability of the error system through the target system (2.133)-(2.136). It is straightforward to prove the exponential stability of error system in the L^2 sense and finite-time convergence.

Theorem 2.4. *Consider system* (2.129)-(2.132) *with inital conditions* $\check{w}_0, \check{v}_0 \in L^2[0,L]$. *The equilibrium* $\check{w} \equiv \check{v} \equiv 0$ *is exponentially stable in the* L^2 *sense. It holds that* $||\bar{w}(\cdot,t) - \hat{w}(\cdot,t)|| \to 0$ *and* $||\bar{v}(\cdot,t) - \hat{v}(\cdot,t)|| \to 0$ *and the convergence to equilibrium is reached in finite time* $t = t_f$.

We design an anti-collocated boundary observer and a collocated boundary observer. Both of them achieve the exponential stability of estimation errors in the L^2 sense and finite-time convergence to 0. In comparison, the collocated boundary observer needs two spatially varying output injection gain, but could be easier to install in practice since it is located at the same boundary with UORM controller $U_{\text{out}}(t)$.

2.4.4 UORM output feedback control design

Combining the state feedback controller and the boundary observers, we have the output feedback controller

$$\begin{aligned} U_{\text{out}}(t) =& -\kappa \hat{w}(L,t) + \int_0^L M(L-\xi)\hat{v}(\xi,t)d\xi \\ &+ \int_0^L K(L,\xi)\hat{w}(\xi,t)d\xi, \end{aligned} \tag{2.145}$$

where $\hat{w}$ and $\hat{v}$ can be obtained from the anti-collocated boundary observer in (2.116)-(2.119) with measurement $Y_a(t) = \bar{v}(0,t)$ or from the collocated boundary observer in (2.129)-(2.132) with measurement $Y_c(t) = \bar{w}(L,t)$ and observer gains given in (2.143), (2.144). The following theorem summarizes the results from Theorem 2 to Theorem 4.

Theorem 2.5. *Consider system* (2.99)-(2.102) *with inital conditions* $\hat{w}_0, \hat{v}_0 \in L^2[0,L]$ *and with output feed control law* (2.145)*, where the kernels* $K(x,\xi)$*,* $M(x)$ *are obtained by solving* (2.109)-(2.111)*. The equilibrium* $\bar{w} \equiv \bar{v} \equiv \hat{w} \equiv \hat{v} \equiv 0$ *is exponentially stable in the* L^2 *sense.*

2.5 Adaptive UORM control design

The previous feedback control designs are based on the knowledge of parameters in the system. However, the relaxation time τ is hard to measure in practice and are affected by many factors. In addition, coefficient γ in the pressure-density relation reflects the aggressiveness of drivers' behavior and relates to road situation. Due to the change of road at inlet or outlet with on-ramp, values of γ are different for in-domain and boundaries. We consider γ to be unknown at boundaries but a known coefficient within the domain $\mathscr{U}$. According to (2.36), k_0 is considered as an unknown constant parameter at boundary. The adaptive control law that is proposed in this section can also be used as an alternative non-adaptive output feedback control design if parameters are given.

Consider the following hyperbolic system with adaptive control input $U(t)$,

$$\bar{w}_t(x,t) = - v^\star \bar{w}_x(x,t), \tag{2.146}$$

$$\bar{v}_t(x,t) = (\gamma p^\star - v^\star)\bar{v}_x(x,t) + c(x)\bar{w}(x,t), \tag{2.147}$$

$$\bar{w}(0,t) = - k_0 \bar{v}(0,t), \tag{2.148}$$

$$\bar{v}(L,t) = \kappa \bar{w}(L,t) + U(t), \tag{2.149}$$

with the measurement $Y(t)$ at the inlet and by (2.25),

$$Y(t) = \bar{v}(0,t), \tag{2.150}$$

$$\bar{v}(0,t) = \rho_2 Y(t), \tag{2.151}$$

where $x \in \mathscr{U} \triangleq [0,L]$ and $t > 0$. The coefficients k_0, ρ_2 and $\kappa = \exp\left(\frac{-L}{\tau v^\star}\right)$ are unknown constant boundary parameters and $c(x) = -\frac{1}{\tau}\exp\left(-\frac{x}{\tau v^\star}\right)$ is unknown spatially-varying parameter, since τ is unknown. The steady states $p^\star$, $q^\star$ and $v^\star$ are known.

2.5.1 Scaling the states

First we scale $\bar{w}$ with unknown constant κ and $\bar{v}$ with unknown constant k_2 for the convenience of the parameter estimation,

$$\omega(x,t) = \frac{\kappa}{\rho_2}\bar{w}(x,t), \tag{2.152}$$

$$\tilde{v}(x,t) = \frac{1}{\rho_2}\bar{v}(x,t), \tag{2.153}$$

and the system is mapped into

$$\omega_t(x,t) = -v^\star \omega_x(x,t), \tag{2.154}$$

$$\tilde{v}_t(x,t) = (\gamma p^\star - v^\star)\tilde{v}_x(x,t) + \bar{c}(x)\omega(x,t), \tag{2.155}$$

$$\omega(0,t) = -\kappa k_0 \tilde{v}(0,t), \tag{2.156}$$

$$\tilde{v}(L,t) = \omega(L,t) + \frac{1}{\rho_2}U(t), \tag{2.157}$$

where the unknown parameters are defined as

$$\bar{c}(x) = \frac{c(x)}{\kappa}, \quad r_0 = -\kappa k_0, \quad r_1 = \frac{1}{\rho_2}, \tag{2.158}$$

with measurement $\tilde{v}(0,t) = Y(t)$. The scaling of $\bar{w}$ and $\bar{v}$ reduces the number of couplings between unknown coefficients and state variables.

2.5.2 Observer canonical form

In order to decouple the $(\omega, \bar{v})$-system in domain, we use the following backstepping transformation.

$$\alpha(x,t) = \omega(x,t) - \int_0^x \bar{M}(x-\xi)\omega(\xi,t)d\xi, \tag{2.159}$$

$$\beta(x,t) = \tilde{v}(x,t) - \int_0^x \bar{K}(v^\star x + (\gamma p^\star - v^\star)\xi)\omega(\xi,t)d\xi. \tag{2.160}$$

We transform the $(\omega, \bar{v})$-system into an observer canonical form,

$$\alpha_t(x,t) = -v^\star \alpha_x(x,t) + \theta_1(x)Y(t), \tag{2.161}$$

$$\beta_t(x,t) = (\gamma p^\star - v^\star)\beta_x(x,t) + \theta_2(x)Y(t) \tag{2.162}$$

$$\alpha(0,t) = r_0\beta(0,t), \tag{2.163}$$

$$\beta(L,t) = \alpha(L,t) + r_1 U(t), \tag{2.164}$$

where $\theta_1(x) = -v^\star r_0 \bar{M}(x)$ and $\theta_2(x) = -v^\star r_0 \bar{K}(v^\star x)$. The measurement is

$$\alpha(0,t) = r_0 Y(t), \tag{2.165}$$

$$\beta(0,t) = Y(t). \tag{2.166}$$

To obtain the target system, we take the time and spatial derivatives on both sides of (2.159), (2.160). The kernels are

$$\bar{M}(x) = -\frac{1}{\gamma p^\star}\bar{c}\left(L - \frac{\gamma p^\star - v^\star}{\gamma p^\star}x\right), \tag{2.167}$$

$$\bar{K}(x) = -\frac{1}{\gamma p^\star}\bar{c}\left(\frac{x}{\gamma p^\star}\right), \tag{2.168}$$

and new spatial parameters are

$$\theta_1(x) = \frac{r_0 v^\star}{\gamma p^\star}\bar{c}\left(L - \frac{\gamma p^\star - v^\star}{\gamma p^\star}x\right), \tag{2.169}$$

$$\theta_2(x) = \frac{r_0 v^\star}{\gamma p^\star}\bar{c}\left(\frac{v^\star}{\gamma p^\star}x\right). \tag{2.170}$$

Remark 2.6. For $\forall x \in [0, L]$, the following holds for $\Theta \triangleq \frac{\gamma p^\star - v^\star}{\gamma p^\star \tau}$,

$$|\theta_1(x)| \leq \Theta, \tag{2.171}$$

$$|\theta_2(x)| \leq \Theta. \tag{2.172}$$

2.5.3 Parametric model and parameter estimation

We can easily find the input/output relation for the observer canonical form by solving the system (2.161)-(2.164) directly,

$$\alpha(x,t) = \begin{cases} \alpha(x - v^\star t, 0) + \int_0^t \theta_1(x - v^\star(t-s))Y(s)ds, & t < \frac{x}{v^\star}, \\ \alpha\left(0, t - \frac{x}{v^\star}\right) + \frac{1}{v^\star}\int_0^x \theta_1(s)Y\left(t - \frac{x-s}{v^\star}\right)ds, & t \geq \frac{x}{v^\star}. \end{cases} \tag{2.173}$$

Substituting into $\alpha(0,t) = r_0 Y(t)$ and therefore we find, for $t \geq \frac{x}{v^\star}$:

$$\alpha(x,t) = r_0 Y\left(t - \frac{x}{v^\star}\right) + \frac{1}{v^\star}\int_0^x \theta_1(s)Y\left(t - \frac{x-s}{v^\star}\right)ds. \tag{2.174}$$

Thus we can obtain $\alpha(L,t)$ by the knowledge of $Y(t)$ from $t - \frac{L}{v^\star}$ to t,

$$\alpha(L,t) = r_0 Y\left(t - \frac{L}{v^\star}\right) + \frac{1}{v^\star}\int_0^L \theta_1(s)Y\left(t - \frac{L-s}{v^\star}\right)ds. \tag{2.175}$$

Given $\beta(L,t) = \alpha(L,t) + r_1 U(t)$, we solve for $\beta(x,t)$,

$$\beta(x,t) = \begin{cases} \beta(x+(\gamma p^\star - v^\star)t, 0) + \int_0^t \theta_2(x+(\gamma p^\star - v^\star)(t-s))Y(s)ds, & t < \frac{L-x}{\gamma p^\star - v^\star}, \\ \beta\left(L, t - \frac{L-x}{\gamma p^\star - v^\star}\right) + \frac{1}{\gamma p^\star - v^\star}\int_x^L \theta_2(s)Y\left(t - \frac{s-x}{\gamma p^\star - v^\star}\right)ds, & t \geq \frac{L-x}{\gamma p^\star - v^\star}. \end{cases} \tag{2.176}$$

We now find for $t \geq \frac{L-x}{\gamma p^\star - v^\star}$:

$$\begin{aligned} \beta(x,t) =& \beta\left(L, t - \frac{L-x}{\gamma p^\star - v^\star}\right) \\ &+ \frac{1}{\gamma p^\star - v^\star}\int_x^L \theta_2(s)Y\left(t - \frac{s-x}{\gamma p^\star - v^\star}\right)ds, \end{aligned} \tag{2.177}$$

thus for $t \geq \frac{L}{\gamma p^\star - v^\star}$, we have

$$\begin{aligned} \beta(0,t) =& \alpha\left(L, t - \frac{L}{\gamma p^\star - v^\star}\right) + r_1 U\left(t - \frac{L}{\gamma p^\star - v^\star}\right) \\ &+ \frac{1}{\gamma p^\star - v^\star}\int_0^L \theta_2(s)Y\left(t - \frac{s}{\gamma p^\star - v^\star}\right)ds. \end{aligned} \tag{2.178}$$

By substituting $\alpha(L,t)$ in $Y(t)$, we obtain the input/output parametric model,

$$\begin{aligned} Y(t) =& r_1 U\left(t - \frac{L}{\gamma p^\star - v^\star}\right) + r_0 Y\left(t - \frac{L}{v^\star} - \frac{L}{\gamma p^\star - v^\star}\right) \\ &+ \int_{t - \frac{L}{v^\star} - \frac{L}{\gamma p^\star - v^\star}}^{t - \frac{L}{\gamma p^\star - v^\star}} \theta_1\left(v^\star(s-t) + \frac{\gamma p^\star}{\gamma p^\star - v^\star}L\right)Y(s)ds \\ &- \int_{t - \frac{L}{\gamma p^\star - v^\star}}^{t} \theta_2\left((\gamma p^\star - v^\star)(t-s)\right)Y(s)ds + \varepsilon(t), \end{aligned} \tag{2.179}$$

where $\varepsilon(t)$ is defined as the error of the parametric model. The value of $\varepsilon(t)$ is abitrary for $t \in [0, \frac{L}{v^\star} + \frac{L}{\gamma p^\star - v^\star}]$, depending on the initial values of $\alpha(x,0), \beta(x,0)$ and $\varepsilon(t) = 0$ for $t \in [\frac{L}{v^\star} + \frac{L}{\gamma p^\star - v^\star}, \infty)$. We use this input/output parametric model to estimate the unknown spatially-varying parameters $\theta_1(x)$, $\theta_2(x)$ and unknown constant boundary parameter r_0.

The following update laws are based on the gradient algoritheorem with normalization and projection,

$$\begin{aligned}
\partial_t \hat{\theta}_1(x) =& \operatorname{Proj}\left(\tau_1(x,t), \hat{\theta}_1(x,t)\right), & (2.180)\\
\partial_t \hat{\theta}_2(x) =& \operatorname{Proj}\left(\tau_2(x,t), \hat{\theta}_2(x,t)\right), & (2.181)\\
\partial_t \hat{r}_0 =& \frac{\gamma_3}{\sigma(t)} Y\left(t - \frac{L}{v^\star} - \frac{L}{\gamma p^\star - v^\star}\right)\tilde{\beta}(0,t), & (2.182)\\
\partial_t \hat{r}_1 =& \frac{\gamma_4}{\sigma(t)} U\left(t - \frac{L}{\gamma p^\star - v^\star}\right)\tilde{\beta}(0,t), & (2.183)
\end{aligned}$$

where $\gamma_1(x)$, $\gamma_2(x)$, γ_3 and γ_4 are positive adaptation gains and

$$\begin{aligned}
\tau_1(x,t) =& \frac{\gamma_1(x) Y\left(t - \frac{L-x}{v^\star} - \frac{L}{\gamma p^\star - v^\star}\right)}{\sigma(t) v^\star}\tilde{\beta}(0,t), & (2.184)\\
\tau_2(x,t) =& \frac{\gamma_2(x) Y\left(t - \frac{x}{\gamma p^\star - v^\star}\right)}{\sigma(t)(\gamma p^\star - v^\star)}\tilde{\beta}(0,t). & (2.185)
\end{aligned}$$

The normalization is given by

$$\begin{aligned}
\sigma(t) =& 1 + Y^2\left(t - \frac{L}{v^\star} - \frac{L}{\gamma p^\star - v^\star}\right) + U^2\left(t - \frac{L}{\gamma p^\star - v^\star}\right)\\
& + \int_{t - \frac{L}{v^\star} - \frac{L}{\gamma p^\star - v^\star}}^{t} Y^2(s) ds. & (2.186)
\end{aligned}$$

The adaptive estimation error $\tilde{\beta}(0,t)$ of parameter estimates $\hat{\theta}_1(x)$, $\hat{\theta}_2(x)$, $\hat{r}_0$ and $\hat{r}_1$ are obtained from the input/output parametric model as follows,

$$\begin{aligned}
\tilde{\beta}(0,t) =& \beta(0,t) - \hat{\beta}(0,t)\\
=& Y(t) - \hat{r}_1 U\left(t - \frac{L}{\gamma p^\star - v^\star}\right)\\
& - \hat{r}_0 Y\left(t - \frac{L}{v^\star} - \frac{L}{\gamma p^\star - v^\star}\right)\\
& + \int_{t - \frac{L}{v^\star} - \frac{L}{\gamma p^\star - v^\star}}^{t - \frac{L}{\gamma p^\star - v^\star}} \hat{\theta}_1\left(v^\star(s-t) + \frac{\gamma p^\star}{\gamma p^\star - v^\star} L\right) Y(s) ds
\end{aligned}$$

$$-\int_{t-\frac{L}{\gamma p^\star - v^\star}}^{t} \hat{\theta}_2\left((\gamma p^\star - v^\star)(t-s)\right)Y(s)ds - \varepsilon(t). \tag{2.187}$$

The projection operator is given by

$$\mathrm{Proj}(\tau_i, \hat{\theta}_i) = \begin{cases} \tau_i, & |\hat{\theta}_i| < \Theta \quad \text{or} \quad \hat{\theta}_i\tau_i \leq 0, \\ 0, & |\hat{\theta}_i| = \Theta \quad \text{and} \quad \hat{\theta}_i\tau_i > 0. \end{cases} \tag{2.188}$$

Denote the parameter estimation errors as

$$\tilde{\theta}_i(x,t) = \theta_i(x) - \hat{\theta}_i(x,t), \quad i = 1,2 \tag{2.189}$$

$$\tilde{r}_j(t) = r_j - \hat{r}_j(t), \qquad j = 0,1. \tag{2.190}$$

Lemma 2.7. *The update laws* (2.180)-(2.182) *guarantee that:*

$$|\hat{\theta}_1(x)| \leq \Theta, |\hat{\theta}_2(x)| \leq \Theta, \tag{2.191}$$

$$||\widetilde{\theta}_1||, ||\widetilde{\theta}_2||, \widetilde{r}_0, \widetilde{r}_1 \in \mathscr{L}_\infty, \tag{2.192}$$

$$||\partial_t\hat{\theta}_1||, ||\partial_t\hat{\theta}_2||, \partial_t\hat{r}_0, \partial_t\hat{r}_1, \frac{\tilde{\beta}(0,t)}{\sqrt{\sigma(t)}} \in \mathscr{L}_2 \cap \mathscr{L}_\infty. \tag{2.193}$$

By constructing Lyapunov function for the adaptive estimation errors $\tilde{\theta}_i$ and $\tilde{r}_j$, it is straightforward to prove the above lemma. The detailed proof is omitted here. The projection in (2.188) guarantees that $\theta_1(x)$, $\theta_2(x)$ are pointwise bounded not only L^2 bounded, as shown in (2.191).

2.5.4 Filter-based observer design

We introduce the adaptive state estimates based on the input and output filters,

$$\hat{\alpha}(x,t) = \hat{r}_0\phi_1(x,t) + \frac{1}{v^\star}\int_0^x \hat{\theta}_1(\xi)\phi_1(x-\xi,t)d\xi, \tag{2.194}$$

$$\hat{\beta}(x,t) =\hat{\psi}(x,t)+\frac{1}{\gamma p^\star - v^\star}\int_x^L \hat{\theta}_2(\xi)\phi_2(L+x-\xi,t)d\xi. \tag{2.195}$$

We represent the signal $\hat{\beta}(L,t)$, the output $Y(t)$ with the following transport PDEs. The filter for $\hat{\beta}(L,t)$ is

$$\hat{\psi}_t(x,t) =(\gamma p^\star - v^\star)\hat{\psi}_x(x,t), \tag{2.196}$$

$$\hat{\psi}(L,t) =\hat{\beta}(L,t), \tag{2.197}$$

$$\hat{\psi}(x,0) =\hat{\psi}_0(x), \tag{2.198}$$

where $\hat{\beta}(L,t) = \hat{r}_1 U(t) + \hat{\alpha}(L,t)$. The signal $\hat{\alpha}(L,t)$ is obtained from (2.175) with updated parameters $\hat{\theta}_1(x,t)$ and $\hat{r}_1(t)$,

$$\hat{\alpha}(L,t) =\hat{r}_0 Y\left(t-\frac{L}{v^\star}\right)+\frac{1}{v^\star}\int_0^L \hat{\theta}_1(s)Y\left(t-\frac{L-s}{v^\star}\right)ds. \tag{2.199}$$

The filters for $Y(t)$ are

$$\partial_t\phi_1(x,t) =-v^\star\partial_x\phi_1(x,t), \tag{2.200}$$

$$\phi_1(0,t) =Y(t), \tag{2.201}$$

$$\phi_1(x,0) =\phi_{10}(x), \tag{2.202}$$

and

$$\partial_t\phi_2(x,t) =(\gamma p^\star - v^\star)\partial_x\phi_2(x,t), \tag{2.203}$$

$$\phi_2(L,t) =Y(t), \tag{2.204}$$

$$\phi_2(x,0) =\phi_{20}(x), \tag{2.205}$$

where $x \in [0,L]$, and $\hat{\psi}_0, \phi_{10}, \phi_{20}$ are arbitrary initial conditions verifying boundary conditions. The explicit solutions to the above PDE filters for $t > \max\left(\frac{L}{v^\star}, \frac{L}{\gamma p^\star - v^\star}\right)$ are given by

$$\hat{\psi}(x,t) = \hat{r}_1 U\left(t - \frac{L-x}{\gamma p^\star - v^\star}\right) + \hat{\alpha}\left(L, t - \frac{L-x}{\gamma p^\star - v^\star}\right), \tag{2.206}$$

$$\phi_1(x,t) = Y\left(t - \frac{x}{v^\star}\right), \tag{2.207}$$

$$\phi_2(x,t) = Y\left(t - \frac{L-x}{\gamma p^\star - v^\star}\right). \tag{2.208}$$

The adaptive estimates $\hat{\alpha}(x,t)$ and $\hat{\beta}(x,t)$ verify that

$$\begin{aligned}\hat{\alpha}_t = & - v^\star \hat{\alpha}_x + \hat{\theta}_1(x) Y(t) + \hat{r}_{0t} \phi_1(x,t) \\ & + \frac{1}{v^\star} \int_0^x \partial_t \hat{\theta}_1(\xi) \phi_1(x-\xi, t) d\xi,\end{aligned} \tag{2.209}$$

$$\begin{aligned}\hat{\beta}_t = & (\gamma p^\star - v^\star) \hat{\beta}_x + \hat{\theta}_2(x) Y(t) \\ & + \frac{1}{\gamma p^\star - v^\star} \int_x^L \partial_t \hat{\theta}_2(\xi) \phi_2(L + x - \xi, t) d\xi,\end{aligned} \tag{2.210}$$

with boundary conditions

$$\hat{\alpha}(0,t) = \hat{r}_0 \phi_1(0,t) = \hat{r}_0 Y(t), \tag{2.211}$$

$$\hat{\beta}(L,t) = \hat{\psi}(L,t) = \hat{r}_1 U(t) + \hat{\alpha}(L,t). \tag{2.212}$$

Denote the adaptive observer errors as

$$\tilde{\alpha} = \alpha - \hat{\alpha}, \quad \tilde{\beta} = \beta - \hat{\beta}, \tag{2.213}$$

The error system is governed by

$$\tilde{\alpha}_t = - v^\star \tilde{\alpha}_x + \tilde{\theta}_1(x) Y(t) - \hat{r}_{0t} \phi_1(x,t)$$

$$-\frac{1}{v^\star}\int_0^x \partial_t\hat{\theta}_1(\xi)\phi_1(x-\xi,t)d\xi, \tag{2.214}$$

$$\begin{aligned}\tilde{\beta}_t =&(\gamma p^\star - v^\star)\tilde{\beta}_x + \tilde{\theta}_2(x)Y(t)\\ &-\frac{1}{\gamma p^\star - v^\star}\int_x^L \partial_t\hat{\theta}_2(\xi)\phi_2(L+x-\xi,t)d\xi,\end{aligned} \tag{2.215}$$

with boundary conditions

$$\tilde{\alpha}(0,t) =\tilde{r}_0 Y(t), \tag{2.216}$$

$$\tilde{\beta}(L,t) =\tilde{r}_1 U(t) + \tilde{\alpha}(L,t). \tag{2.217}$$

2.5.5 Adaptive output feedback control design

To obtain the adaptive control law, we apply the backstepping transformation to the adaptive state estimate $\hat{\beta}$. The transformed state is given by

$$\eta(x) = \hat{\beta}(x) - \frac{1}{\gamma p^\star - v^\star}\int_0^x \hat{K}_2(x-\xi)\hat{\beta}(\xi)d\xi \triangleq \mathscr{F}[\hat{\beta}](x), \tag{2.218}$$

where $\hat{K}_2$ is obtained by solving online the following Volterra equation,

$$\hat{K}_2(x) = -\hat{\theta}_2(x) + \frac{1}{\gamma p^\star - v^\star}\int_0^x \hat{K}_2(x-\xi)\hat{\theta}_2(\xi)d\xi. \tag{2.219}$$

Note that $\hat{K}_2(x)$ and $\hat{\theta}_2(x)$ are functions of time. The inverse transformation is then given by

$$\begin{aligned}\hat{\beta}(x) =&\eta(x) - \frac{1}{\gamma p^\star - v^\star}\int_0^x \hat{\theta}_2(x-\xi)\hat{\eta}(\xi)d\xi\\ \triangleq&\hat{\eta} - \frac{1}{\gamma p^\star - v^\star}\hat{\theta}_2 * \hat{\eta}.\end{aligned} \tag{2.220}$$

With a lengthy but straightforward calculation, we obtain that

$$\begin{aligned}\eta_t =&(\gamma p^\star - v^\star)\eta_x - \hat{K}_2(x)\tilde{\beta}(0) + \eta * \mathscr{F}[\partial_t \hat{\theta}_2](x)\\&+\frac{1}{\gamma p^\star - v^\star}\left(\int_x^L \partial_t \hat{\theta}_2(\xi)\phi_2(L+x-\xi,t)d\xi\right), \qquad (2.221)\\ \eta(L) =&0, \qquad (2.222)\end{aligned}$$

and the adaptive control law is derived from (2.222).

We summarize the transformation and inverse transformation between the original system $(\bar{w}, \bar{v}, \hat{\psi}, \phi_1, \phi_2)$ and the final target system $(\tilde{\alpha}, \tilde{\beta}, \hat{\zeta}, \hat{\eta}, \phi_1, \phi_2)$ as:

$$\begin{aligned}\phi_1 =&\phi_1, &(2.223)\\ \phi_2 =&\phi_2, &(2.224)\\ \hat{\alpha} =&\mathscr{T}_\alpha[\phi_1], &(2.225)\\ \eta =&(\mathscr{I}-\mathscr{F})[\hat{\psi}+\mathscr{T}_\beta[\phi_2]], &(2.226)\\ \tilde{\beta} =&(\mathscr{I}-\mathscr{G})[\bar{v}/k_2]-(\hat{\psi}+\mathscr{T}_\beta[\phi_2]), &(2.227)\\ \tilde{\alpha} =&(\mathscr{I}-\mathscr{G})[-\kappa\bar{w}]-\mathscr{T}_\alpha[\phi_1], &(2.228)\end{aligned}$$

and we can obtain the original states from the inverse transformation as:

$$\begin{aligned}\phi_1 =&\phi_1, &(2.229)\\ \phi_2 =&\phi_2, &(2.230)\\ \hat{\psi} =&\eta - \frac{1}{v^\star}\hat{\theta}_2 * \eta - \mathscr{T}_\beta[\phi_2], &(2.231)\\ \bar{w} =&-\frac{1}{\kappa}(\mathscr{I}-\mathscr{G})^{-1}[\tilde{\alpha}+\hat{\alpha}], &(2.232)\\ \bar{v} =&k_2(\mathscr{I}-\mathscr{G})^{-1}[\tilde{\beta}+\hat{\psi}+\mathscr{T}_\beta[\phi_2]]. &(2.233)\end{aligned}$$

Due to the invertibility of the above transformation, we can obtain the stability of the original system $(\bar{w}, \bar{v}, \hat{\psi}, \phi_1, \phi_2)$ by studying the system in the equivalent variables $(\tilde{\alpha}, \tilde{\beta}, \hat{\alpha}, \eta, \phi_1, \phi_2)$. The target system $(\tilde{\alpha}, \tilde{\beta}, \hat{\alpha}, \eta, \phi_1, \phi_2)$ are governed by the following PDEs,

$$\begin{aligned}
\tilde{\alpha}_t =& -v^\star \tilde{\alpha}_x + \tilde{\theta}_1(x)Y(t) - \hat{r}_{0t}\phi_1(x,t) \\
& - \frac{1}{v^\star}\int_0^x \partial_t \hat{\theta}_1(\xi)\phi_1(x-\xi,t)d\xi, && (2.234) \\
\tilde{\alpha}(0,t) =& \tilde{r}_0 Y(t), && (2.235) \\
\tilde{\beta}_t =& (\gamma p^\star - v^\star)\tilde{\beta}_x + \tilde{\theta}_2(x)Y(t) \\
& - \frac{1}{\gamma p^\star - v^\star}\int_x^L \partial_t \hat{\theta}_2(\xi)\phi_2(L+x-\xi,t)d\xi, && (2.236) \\
\tilde{\beta}(L,t) =& \tilde{\alpha}(L,t) + \tilde{r}_1 U(t), && (2.237) \\
\hat{\alpha}_t =& -v^\star \hat{\alpha}_x + \hat{\theta}_1(x)Y(t) + \hat{r}_{0t}\phi_1(x,t) \\
& + \frac{1}{v^\star}\int_0^x \partial_t \hat{\theta}_1(\xi)\phi_1(x-\xi,t)d\xi, && (2.238) \\
\hat{\alpha}(0,t) =& \hat{r}_0 Y(t), && (2.239) \\
\eta_t =& (\gamma p^\star - v^\star)\eta_x - \hat{K}_2(x)\tilde{\beta}(0) + \eta * \mathscr{F}[\partial_t \hat{\theta}_2](x) \\
& + \frac{1}{\gamma p^\star - v^\star}\mathscr{F}\left[\int_x^L \partial_t \hat{\theta}_2(\xi)\phi_2(L+x-\xi,t)d\xi\right], && (2.240) \\
\eta(L,t) =& 0, && (2.241) \\
\partial_t \phi_2(x,t) =& (\gamma p^\star - v^\star)\partial_x \phi_2(x,t), && (2.242) \\
\phi_2(L,t) =& Y(t), && (2.243) \\
\partial_t \phi_1(x,t) =& -v^\star \partial_x \phi_1(x,t), && (2.244) \\
\phi_1(0,t) =& Y(t). && (2.245)
\end{aligned}$$

Note that $Y(t) = \eta(0) + \tilde{\beta}(0)$. According to backstepping transformation (2.218), we can obtain from (2.241) that

$$\hat{\beta}(L,t) = \int_0^L \hat{K}_2(L-\xi)\hat{\beta}(\xi,t)d\xi. \tag{2.246}$$

Substituting $\hat{\beta}(L,t) = \hat{r}_1 U(t) + \hat{\alpha}(L,t)$, we have

$$U(t) = \frac{1}{\hat{r}_1}\int_0^L \hat{K}_2(L-\xi)\hat{\beta}(\xi,t)d\xi - \frac{1}{\hat{r}_1}\hat{\alpha}(L,t). \tag{2.247}$$

Using the adaptive estimates $\hat{\beta}(x,t)$ in (2.195) and $\hat{\alpha}(L,t)$ in (2.199), the adaptive controller is then obtained in an explicit integral form, consisting delayed values of input and output,

$$\begin{aligned}
U(t) =& \frac{1}{\hat{r}_1}\int_{t-\frac{L}{\gamma p^\star - v^\star}}^{t} \hat{K}_2\left(v^\star(t-\xi)\right)U(\xi)d\xi \\
&- \frac{\hat{r}_0}{\hat{r}_1}\hat{Y}\left(t-\frac{L}{v^\star}\right) - \frac{1}{\hat{r}_1}\int_{t-\frac{L}{v^\star}}^{t} m_1(\xi)Y(\xi)d\xi \\
&+ \frac{\hat{r}_0}{\hat{r}_1}\int_{t-\frac{L}{v^\star}-\frac{L}{\gamma p^\star - v^\star}}^{t-\frac{L}{v^\star}} m_2(\xi)Y(\xi)d\xi \\
&+ \frac{1}{\hat{r}_1}\int_{t-\frac{L}{\gamma p^\star - v^\star}}^{t} m_3(\xi)\int_{\xi-\frac{L}{v^\star}}^{\xi} m_4(\mu)Y(\mu)d\mu d\xi \\
&+ \frac{1}{\hat{r}_1}\int_{t-\frac{L}{\gamma p^\star - v^\star}}^{t} m_5(\xi)Y(\xi)d\xi,
\end{aligned} \tag{2.248}$$

where m_i are denoted as

$$m_1(\xi) = \hat{\theta}_1(L - v^\star(t-\xi)), \tag{2.249}$$

$$m_2(\xi) = \hat{K}_2\left((\gamma p^\star - v^\star)\left(t-\xi-\frac{L}{v^\star}\right)\right), \tag{2.250}$$

$$m_3(\xi) = \hat{K}_2\left((\gamma p^\star - v^\star)(t-\xi)\right), \tag{2.251}$$

$$m_4(\mu) = \hat{\theta}_1\left(L - v^\star(\xi-\mu)\right), \tag{2.252}$$

$$m_5(\xi) = \int_{(\gamma p^\star - v^\star)(t-\xi)}^{L} \hat{K}_2(\mu)\hat{\theta}_2((\gamma p^\star - v^\star)(t-\xi)+L-\mu)d\mu. \tag{2.253}$$

The parameter estimates $\hat{\theta}_1(x,t)$, $\hat{\theta}_2(x,t)$, $\hat{r}_0$ and $\hat{r}_1$ are generated from the update laws. We can obtain $\hat{K}_2(x,t)$ by solving online the Volterra equation in (2.219). The Lyapunov stability proof is shown in Appendix, which is derived from modifications of the proof in [116]. The key idea in proving the stability of $(\tilde{\alpha},\tilde{\beta},\hat{\alpha},\eta,\phi_1,\phi_2)$-system is to take advantage of the cascade structure of the system. Due to the invertibility between $(\tilde{q},\tilde{v})$-system and $(\bar{w},\bar{v})$-system, we arrive our main theorem for adaptive control design.

Theorem 2.8. *Consider the plant* (2.146)-(2.149) *with the adaptive control law* (2.248) *and update laws* (2.180)-(2.182). *For any initial conditions* $\hat{\theta}_1(\cdot,0),\hat{\theta}_2(\cdot,0),r_0(0),r_1(0)\in\mathscr{C}^1[0,L]$, $\bar{w}_0,\bar{v}_0,\phi_{10},\phi_{20},\hat{\psi}_0$ *that verify boundary conditions, the solution* $(\bar{w},\bar{v},\phi_1,\phi_2,$
$\hat{\psi},\hat{\theta}_1,\hat{\theta}_2,\hat{r}_0,\hat{r}_1)$ *is bounded for* $t\geq 0$ *and for* $\forall x\in[0,L]$ *it verifies that as* $t\to\infty$,

$$||\bar{w}(x,t)||\to 0, ||\bar{v}(x,t)||\to 0, \tag{2.254}$$

$$||\tilde{q}(x,t)||\to 0, ||\tilde{v}(x,t)||\to 0. \tag{2.255}$$

The proof of Theorem 2.8 is completed by the following sections of Lyapunov stability analysis.

2.6 Lyapunov stability analysis

2.6.1 L_2 boundedness

The boundedness of $\hat{\theta}_2$ is given by Lemma 2.7. Using (2.219) and Gronwall's inequality, we establish a bound on $\hat{K}_2$,

$$|\hat{K}_2(x)|\leq \Theta e^{\frac{\Theta}{\gamma p^\star-\nu^\star}}\triangleq K_2. \tag{2.256}$$

To prove the L_2 boundedness of system in (2.234)-(2.245), we construct the following Lyapunov functions:

$$V_1 = \frac{1}{2}\int_0^L e^{-x}\tilde{\alpha}^2(x)dx, \quad V_2 = \frac{1}{2}\int_0^L e^{x}\tilde{\beta}^2(x)dx, \tag{2.257}$$

$$V_3 = \frac{1}{2}\int_0^L e^{-x}\hat{\alpha}^2(x)dx, \quad V_4 = \frac{1}{2}\int_0^L e^{x}\eta^2(x)dx, \tag{2.258}$$

$$V_5 = \frac{1}{2}\int_0^L e^{x}\phi_1^2(x)dx \quad V_6 = \frac{1}{2}\int_0^L e^{x}\phi_2^2(x)dx. \tag{2.259}$$

Then we get

$$\begin{aligned} \dot{V}_1 \leq & -\frac{v^\star}{2e^L}\tilde{\alpha}^2(L) - \frac{1}{2}\left(\frac{v^\star}{e^L} - \frac{c_1}{v^\star} - c_2\right)||\tilde{\alpha}||^2 \\ & + \left(v^\star \tilde{r}_0^2 + ||\tilde{\theta}_1||^2\right)\hat{\eta}(0)^2 + l_1||\phi_1||^2 + l_2, \end{aligned} \tag{2.260}$$

$$\tag{2.261}$$

$$\begin{aligned} \dot{V}_2 \leq & e^L(\gamma p^\star - v^\star)\tilde{\alpha}^2(L) \\ & - \frac{1}{2}\left(\gamma p^\star - v^\star - \frac{e^L c_3}{2(\gamma p^\star - v^\star)} - e^L c_4\right)||\tilde{\beta}||^2 \\ & + \frac{e^L}{2c_4}||\tilde{\theta}_2||^2\hat{\eta}(0)^2 + l_3||\phi_2||^2 + l_4 + l_5, \end{aligned} \tag{2.262}$$

$$\begin{aligned} \dot{V}_3 \leq & -\frac{v^\star}{2e^L}\hat{\alpha}^2(L) - \frac{1}{2}\left(\frac{v^\star}{e^L} - \frac{c_5}{v^\star} - c_6\right)||\hat{\alpha}||^2 \\ & + \left(v^\star \hat{r}_0^2 + \frac{1}{2c_6}||\hat{\theta}_1||^2\right)\hat{\eta}(0)^2 + l_6||\phi_1||^2 + l_7, \end{aligned} \tag{2.263}$$

$$\begin{aligned} \dot{V}_4 \leq & -\frac{1}{2}\left(\gamma p^\star - v^\star - \frac{e^L c_7}{2(\gamma p^\star - v^\star)} - e^L c_8 - c_9\right)||\eta||^2 \\ & - \left(\frac{\gamma p^\star - v^\star}{2} + \frac{e^L K_2^2}{2c_8}\right)\eta^2(0) + l_8||\phi_2||^2 + l_9||\eta||^2 + l_{10}, \end{aligned} \tag{2.264}$$

$$\dot{V}_5 \leq -\frac{\gamma p^\star - v^\star}{2}||\phi_2||^2 + e^L(\gamma p^\star - v^\star)\hat{\eta}(0)^2 + l_{11}, \tag{2.265}$$

$$\dot{V}_6 \leq -\frac{v^\star}{2e^L}||\phi_1||^2 + v^\star\hat{\eta}(0)^2 + l_{12}, \tag{2.266}$$

where $l_i(t)$ are integrable, nonnegative function of time by applying Lemma 2.7. And $l_i(t)$ are denoted as

$$\begin{aligned}
l_1 =& \partial_t \hat{r}_0^2 + \frac{1}{2v^\star c_1}||\partial_t \hat{\theta}_1||^2,\ l_2 = \left(v^\star \tilde{r}_0^2 + \frac{1}{2c_2}||\tilde{\theta}_1||^2\right)\tilde{\beta}(0)^2, && (2.267)\\
l_3 =& \frac{e^L||\partial_t \hat{\theta}_2||^2}{4c_2(\gamma p^\star - v^\star)},\ l_4 = \left(e^L||\tilde{\theta}_2||^2 - \frac{\gamma p^\star - v^\star}{2}\right)\tilde{\beta}(0)^2, && (2.268)\\
l_5 =& e^L(\gamma p^\star - v^\star)\tilde{r}_1^2 U(t)^2,\ l_6 = \frac{1}{2v^\star c_5}||\partial_t \hat{\theta}_1||^2 + \hat{r}_0^2, && (2.269)\\
l_7 =& \left(v^\star \hat{r}_0^2 + \frac{1}{2c_6}||\hat{\theta}_1||^2\right)\tilde{\beta}(0)^2,\ l_8 = \frac{e^L(1+K_2^2)||\partial_t \hat{\theta}_2||^2}{4c_7(\gamma p^\star - v^\star)}, && (2.270)\\
l_9 =& \frac{2(1+K_2^2)}{c_9}||\partial_t \hat{\theta}_2||^2,\ l_{10} = \frac{e^L K_2^2}{2c_8}\tilde{\beta}^2(0), && (2.271)\\
l_{11} =& e^L(\gamma p^\star - v^\star)\tilde{\beta}(0)^2,\ l_{12} = v^\star \tilde{\beta}(0)^2, && (2.272)
\end{aligned}$$

and c_i are positive constants chosen as

$$\begin{aligned}
c_1 =& \frac{v^{\star 2}}{2e^L},\ c_2 = \frac{v^\star}{4e^L},\ c_3 = \frac{(\gamma p^\star)^2}{e^L}, && (2.273)\\
c_4 =& \frac{(\gamma p^\star - v^\star)}{4e^L},\ c_5 = \frac{v^{\star 2}}{2e^L},\ c_6 = \frac{v^\star}{4e^L}, && (2.274)\\
c_7 =& \frac{(\gamma p^\star)^2}{e^L},\ c_8 = \frac{(\gamma p^\star - v^\star)}{4e^L},\ c_9 = \frac{(\gamma p^\star - v^\star)}{8}. && (2.275)
\end{aligned}$$

Consider the following Lyapunov function $V = g_1V_1 + V_2 + V_3 + g_2V_4 + V_5 + V_6$, and g_1 and g_2 are positive constants defined as

$$\begin{aligned}
g_1 =& 2e^{2L}\frac{\gamma p^\star - v^\star}{v^\star}, && (2.276)\\
g_2 =& \frac{2(\gamma p^\star - v^\star)}{(\gamma p^\star - v^\star)^2 + 4e^{2L}K_2^2}\left(\frac{2e^{2L}(\gamma p^\star - v^\star)}{v^\star}\left(v^\star \tilde{r}_0^2 + ||\tilde{\theta}_1||^2\right)\right.\\
&\left. + \frac{2e^{2L}}{\gamma p^\star - v^\star}||\tilde{\theta}_2||^2 + \left(v^\star + \frac{2e^L}{v^\star}\right)\Theta^2 + e^L\gamma p^\star - e^L v^\star + v^\star\right), && (2.277)
\end{aligned}$$

we have

$$\dot{V} \leq -g_0 V + lV + l, \tag{2.278}$$

where g_0 is a positive constant defined as

$$g_0 = \min\left(\frac{v^\star}{4}, \frac{\gamma p^\star - v^\star}{8}\right), \tag{2.279}$$

and l is the linear combination of l_i and therefore is also integrable, nonnegative function of time. Since $\frac{1}{2e^L}||\tilde{\alpha}||^2 \leq V_1 \leq \frac{1}{2}||\tilde{\alpha}||^2$,$\frac{1}{2}||\tilde{\beta}||^2 \leq V_2 \leq \frac{e^L}{2}||\tilde{\beta}||^2$, $\frac{1}{2e^L}||\hat{\alpha}||^2 \leq V_3 \leq \frac{1}{2}||\hat{\alpha}||^2$, $\frac{1}{2}||\eta||^2 \leq V_4 \leq \frac{e^L}{2}||\eta||^2$, $\frac{1}{2e^L}||\phi_1||^2 \leq V_5 \leq \frac{1}{2}||\phi_1||^2$ and $\frac{1}{2}||\phi_2||^2 \leq V_6 \leq \frac{e^L}{2}||\phi_2||^2$. Then V is bounded and integrable (Lemma D.3. in [100]), and the following holds that

$$||\tilde{\alpha}||, ||\tilde{\beta}||, ||\hat{\alpha}||, ||\eta||, ||\phi_1||, ||\phi_2|| \in \mathscr{L}_2 \cap \mathscr{L}_\infty. \tag{2.280}$$

Then with the inverse transformation (2.231)-(2.233) from the final target system $(\tilde{\alpha}, \tilde{\beta}, \hat{\alpha}, \hat{\eta}, \phi_1, \phi_2)$ to $(\bar{w}, \bar{v}, \hat{\psi}, \phi_1, \phi_2)$-system, we have

$$||\bar{w}||, ||\bar{v}|| \in \mathscr{L}_2 \cap \mathscr{L}_\infty. \tag{2.281}$$

Finally, from the inverse transformation (7.65)-(7.66) from $(\bar{w}, \bar{v})$-system to $(\tilde{q}, \tilde{v})$-system, we get

$$||\tilde{q}||, ||\tilde{v}|| \in \mathscr{L}_2 \cap \mathscr{L}_\infty. \tag{2.282}$$

2.6.2 Convergence

The above Lyapunov proof shows that $\dot{V}$ is bounded from above and V is positive and integrable. According to Lemma D.2. in [100], we have

$$||\bar{w}(x,t)|| \to 0, \ ||\bar{v}(x,t)|| \to 0. \tag{2.283}$$

The inverse transformation (2.43)-(2.44) from $(\bar{w}, \bar{v})$-system to $(\tilde{q}, \tilde{v})$-system gives that

$$||\tilde{q}(x,t)|| \to 0, \ ||\tilde{v}(x,t)|| \to 0. \tag{2.284}$$

$\square$

2.7 Simulation

We take $\gamma = 1$. The length of freeway section is chosen to be $L = 1$ km. The free speed is $v_f = 40$ m/s and the maximum density is $\rho_m = 150$ vehicles/km. The steady states $(\rho^\star, v^\star)$ are chosen as $(120 \text{ vehicles/km}, 10 \text{ m/s})$ which is in the congested regime. The relaxation time $\tau = 60$ s. We use sinusoid initial conditions.

The Fig. 2.5 shows that in the open-loop system the density and velocity are slightly damped and keeps oscillating. In Fig. 2.6, the closed-loop system with DORM control is stabilized and converges to the steady states in the finite time about 2.5 min. The closed-loop system with UORM full-state feedback control in Fig. 2.7 is stabilized and converges to the reference and the finite convergence time is $t_f = L/v^\star + L/(\gamma p^\star - v^\star) = 150$ s $= 2.5$ min. The evolution of ramp metering control input is plotted with red color at outlet $x = 1000$ m. We see the control input oscillates around every half minute, which is reasonable in application. The Fig. 2.8 shows that the closed-loop system with UORM output feedback control (collocated observer) is stabilized and converges to the steady states in about 5 min since it takes the collocated observer

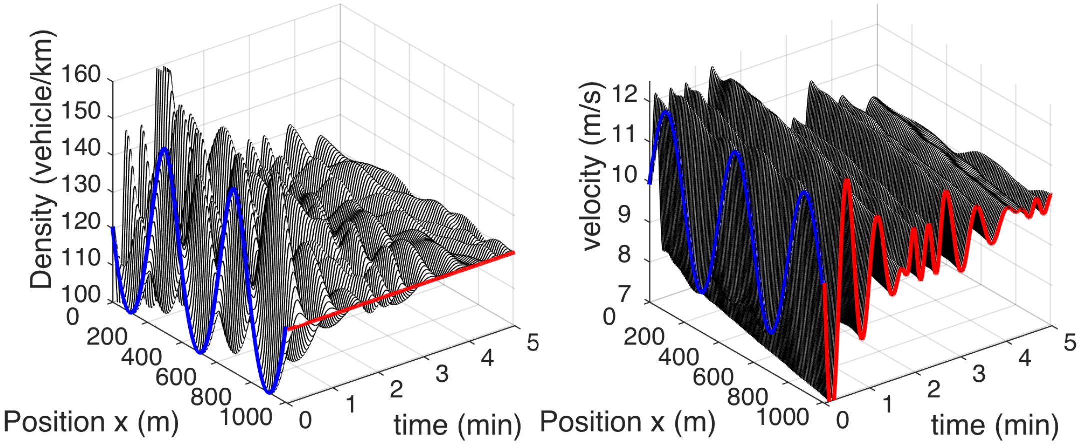

Figure 2.5: Open-loop system of the ARZ model.

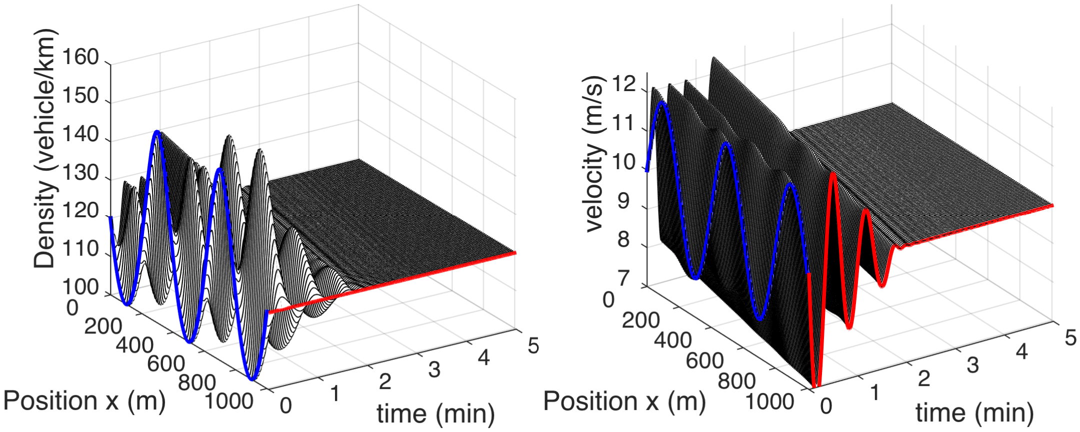

Figure 2.6: Closed-loop system with DORM control.

2.5 min to estimate state variables and another 2.5 min for state feedback control to converge to the steady states.

In the adaptive simulation, we choose $\tau = 100\,\mathrm{s}$. The open-loop system is more oscillated than that of the non-adaptive case. It takes longer time to stabilize with adaptive output feedback control law. In Fig. 2.9, we can see that the open-loop system is unstable. The adaptive output feedback result is shown in Fig. 2.10 The estimation of parameters in the system are given in Fig. 2.11 and Fig. 2.12 The blue lines in Fig. 2.12. represents the true values of the constant

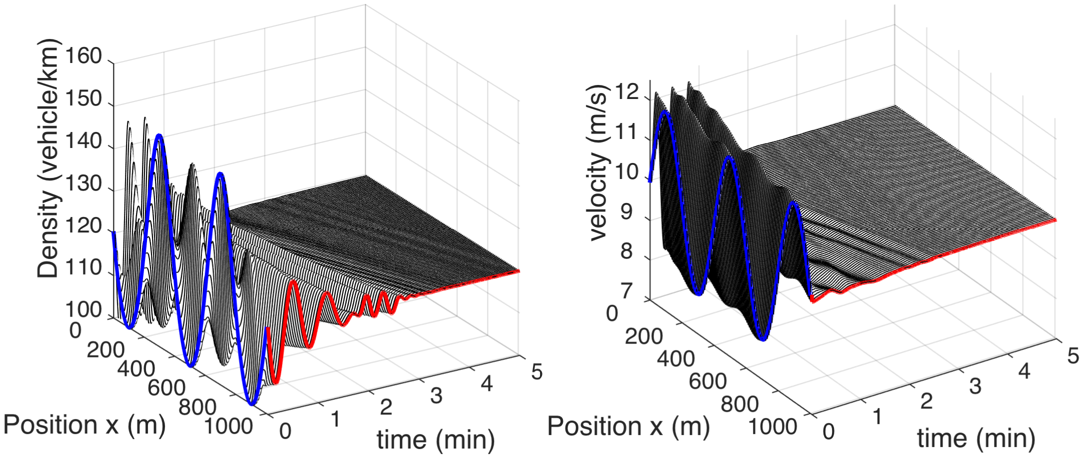

Figure 2.7: Closed-loop system with UORM full-state feedback.

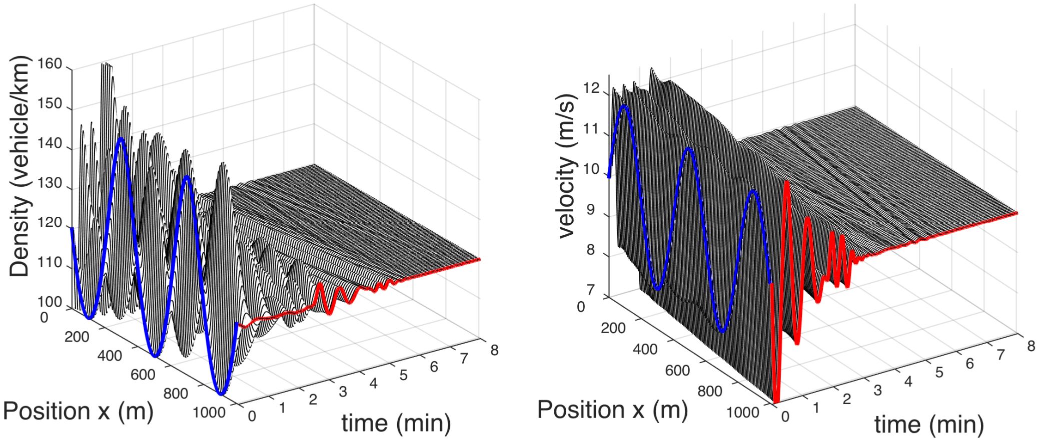

Figure 2.8: Closed-loop system with UORM output feedback.

parameters. The parameter estimates do not necessarily converge to the true values, due to the local property of gradient methods.

2.8 Conclusion

This chapter addresses the boundary feedback control problem of ARZ traffic model with relaxation term. To stabilize the oscillations of congested traffic regime, two control designs are

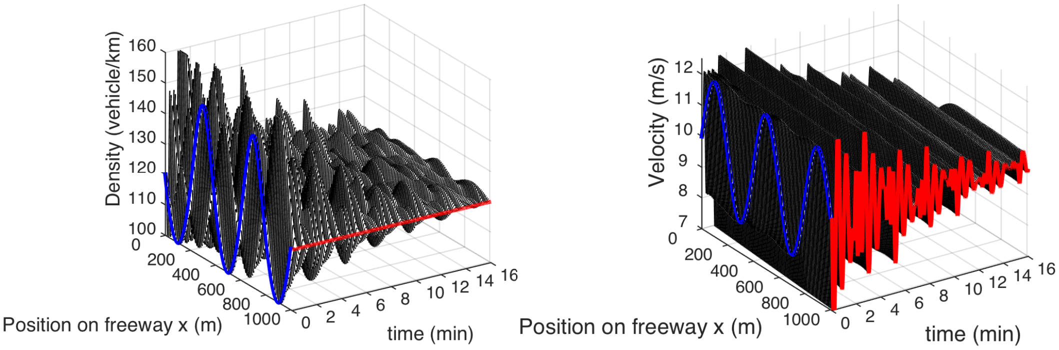

Figure 2.9: Open-loop system without adaptive UORM output feedback.

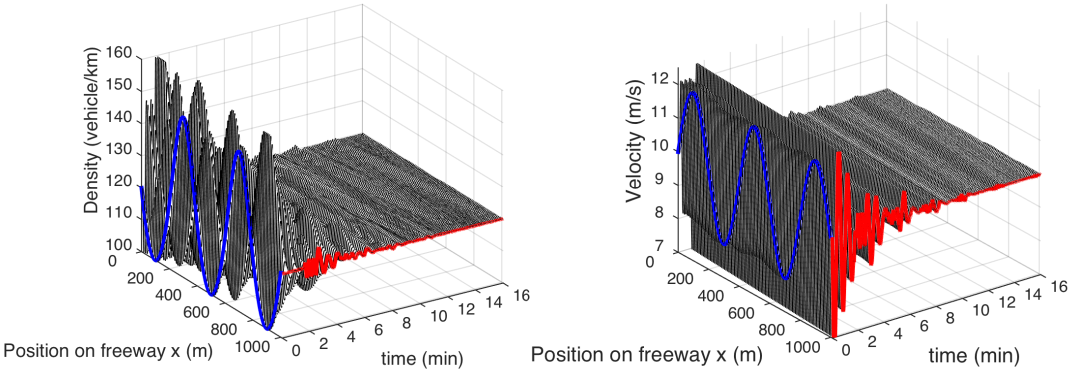

Figure 2.10: Closed-loop system with adaptive UORM output feedback.

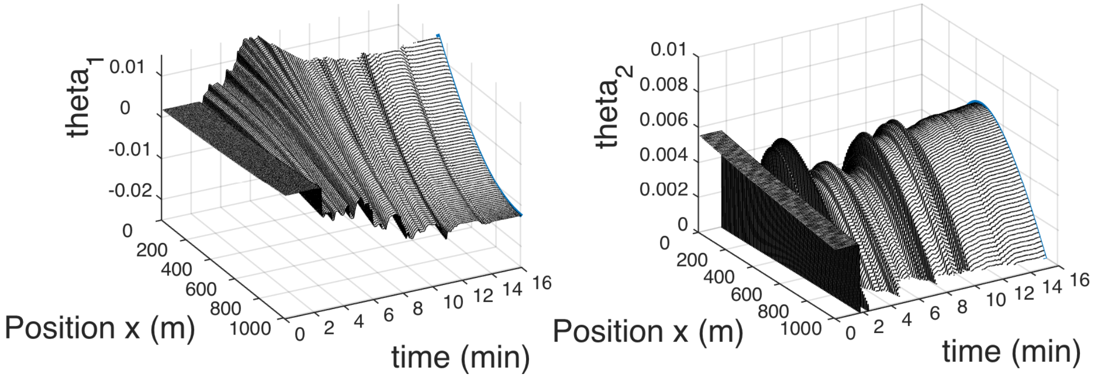

Figure 2.11: Estimates of spatially-varying parameters.

introduced for the second-order coupled hyperbolic system. The key idea in the DORM control design is to cancel the forward coupling in the system. In the harder case, UORM control design

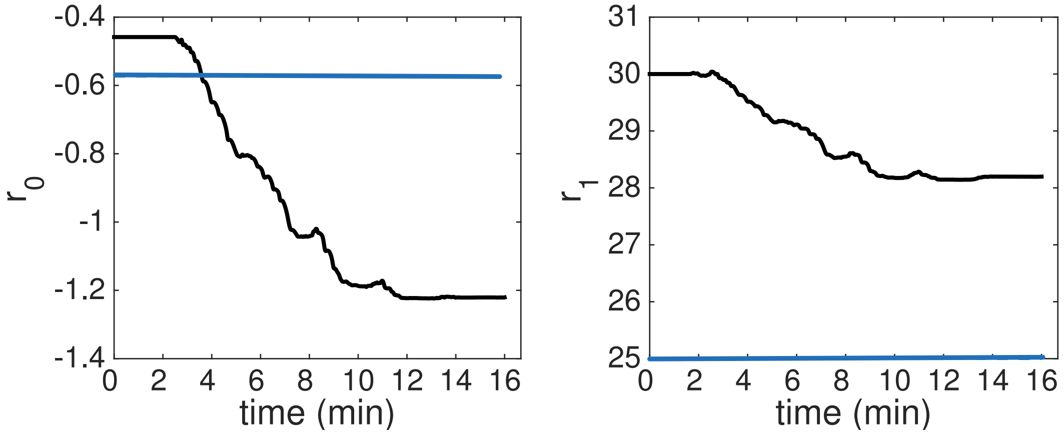

Figure 2.12: Estimates of constant parameters.

uses backstepping method to cancel the coupling at outlet and thus achieves exponential stability and finite time convergence to the steady states. In the absence of parameters knowledge, we solve adaptive boundary control problem of linearized ARZ model using backstepping method, gradient-based update laws and a filter-based approach. The main step is to develop upstream of ramp metering control approach and transform the hetero-directional coupled hyperbolic system to the observer canonical form that is suitable for adaptive design. It is of interest to explore adaptive control design for this problem without over-parameterization and more research is needed to be done on the property of relaxation time in the ARZ model. An useful extension is to consider the effect of changing lanes and autonomous vehicles in traffic model.

Chapter 2 contains reprints and adaptations of the following paper: H. Yu and M. Krstic, “Traffic congestion control of Aw-Rascle-Zhang model,” *Automatica*, vol. 100, pp. 38-51, 2019. The dissertation author is the primary investigator and author of this paper.

Chapter 3

Two-Lane Traffic Congestion Control

We develop output feedback boundary control to mitigate traffic congestion of a unidirectional two-lane freeway segment. The macroscopic traffic dynamics are described by the ARZ model respectively for both the fast and slow lanes. The traffic density and velocity of each of the two lanes are governed by coupled 2×2 nonlinear hyperbolic PDEs. Lane-changing interactions between the two lanes lead to exchanging source terms between the two pairs second-order PDEs. Therefore, we are dealing with 4×4 nonlinear coupled hyperbolic PDEs. Based on driver's preference for the slow and fast lanes, a reference system of lane-specific uniform steady states in congested traffic is chosen. To stabilize traffic densities and velocities of both lanes to the steady states, two distinct VSLs are applied at outlet boundary, controlling the traffic velocity of each lane. Using backstepping transformation, we map the coupled heterodirectional hyperbolic PDE system into a cascade target system, in which traffic oscillations are damped out through actuation of the velocities at the downstream boundary. Two full-state feedback boundary control laws are developed. We also design a collocated boundary observer for state estimation with sensing of densities at the outlet. Output feedback boundary controllers are obtained by combining the collocated observer and full-state feedback controllers. The finite time convergence to equilibrium is achieved for both the controllers and observer designs. Numerical

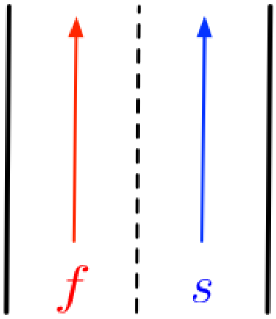

Figure 3.1: A unidirectional freeway segment of the fast and slow lanes.

simulations validate our design in two different traffic scenarios.

In this problem, a two-lane ARZ model of a freeway segment presents heterodirectional $2+2$ coupled nonlinear hyperbolic PDEs, governing the traffic densities and velocities of the fast and slow lanes. We aim to stabilize the oscillations in the two-lane traffic using the PDE backstepping method, based on the stabilization results in [80]. Actuation of traffic velocities at the outlet boundary are realized by two VSLs.

The chapter is organized as follows: in Section 3.1 we introduce the two-lane ARZ traffic model. We derive lane-specific uniform steady states according to the drivers' overall preference for the lanes and then linearize the nonlinear system around the steady states. In Section 3.2 backstepping transformation is derived for the linearized model in Riemann coordinates. We present full-state feedback control laws to actuate outlet boundary velocities. In Section 3.3, we design collocated boundary observers and then obtain output feedback control laws. In Section 3.4, control design in two different traffic scenarios are discussed and tested with numerical simulation.

3.1 Two-lane traffic ARZ PDE model

The two-lane traffic on unidirectional roads is described with the following two-lane traffic ARZ model by [60] [69]. The diagram in Fig. 3.1 is shown with the faster lane on the left and slower lane on the right. The two-lane traffic ARZ model is given by

$$\begin{aligned}
\partial_t \rho_f + \partial_x(\rho_f v_f) =& \frac{1}{T_s}\rho_s - \frac{1}{T_f}\rho_f, && (3.1)\\
\partial_t(\rho_f v_f) + \partial_x(\rho_f v_f^2) - (\gamma p_f)\partial_x v_f =& \frac{1}{T_s}\rho_s v_s - \frac{1}{T_f}\rho_f v_f \\
&+ \frac{\rho_f(V(\rho_f) - v_f)}{T_f^e}, && (3.2)\\
\partial_t \rho_s + \partial_x(\rho_s v_s) =& \frac{1}{T_f}\rho_f - \frac{1}{T_s}\rho_s, && (3.3)\\
\partial_t(\rho_s v_s) + \partial_x(\rho_s v_s^2) - (\gamma p_s)\partial_x v_s =& \frac{1}{T_f}\rho_f v_f - \frac{1}{T_s}\rho_s v_s \\
&+ \frac{\rho_s(V(\rho_s) - v_s)}{T_s^e}. && (3.4)
\end{aligned}$$

The traffic density $\rho_i(x,t)$ and velocity $v_i(x,t)$ $(i = f,s)$ are defined in $x \in [0,L]$, $t \in [0,\infty)$, where L is the length of the freeway segment. The above nonlinear hyperbolic PDEs consist of two subsystems of second-order nonlinear hyperbolic PDEs, each describing one-lane traffic dynamics. Lane-changing interactions and drivers' behavior adapting to the traffic appear as source terms on the right hand side of PDEs.

The variable $p_i(\rho_i)$ is defined as the traffic density pressure

$$p_i(\rho_i) = v_m \left(\frac{\rho_i}{\rho_m}\right)^{\gamma}, \tag{3.5}$$

which is an increasing function of density ρ_i. v_m is the maximum traffic velocity, ρ_m is the maximum traffic density and the constant coefficient $\gamma \in \mathbb{R}_+$ reflects the aggressiveness of drivers on road. The parameter T_i^e is defined as relaxation time that reflects driver's behavior adapting to the traffic equilibrium velocity in the lane i. The parameter T_i describes the driver's preference for remaining in lane i, which relates to the both lanes' density and velocity. We consider them to be constant coefficients in this paper.

The equilibrium velocity-density relationship $V(\rho)$ is given in the form of the Greenshield's model,

$$V(\rho_i) = v_m \left(1 - \left(\frac{\rho_i}{\rho_m}\right)^{\gamma}\right). \tag{3.6}$$

We choose the Greenshield's model for $V(\rho)$ due to its simplicity but the control design presented later is not limited by this choice. Note that the equilibrium velocity-density model (3.6) is for cumulative single lane traffic. Distinct velocity equilibrium does exist in each of the two lanes [70]. The lane-specific steady traffic velocities will be discussed in the following section.

3.1.1 Driver's preference for two lanes

We consider to linearize the nonlinear hyperbolic system (ρ_i, v_i) around uniform steady states $(\rho_i^\star, v_i^\star)$. We obtain the following equations

$$\frac{1}{T_s}\rho_s^\star - \frac{1}{T_f}\rho_f^\star = 0, \tag{3.7}$$

$$\frac{1}{T_s}\rho_s^\star v_s^\star - \frac{1}{T_f}\rho_f^\star v_f^\star + \frac{\rho_f^\star(V(\rho_f^\star) - v_f^\star)}{T_f^e} = 0, \tag{3.8}$$

$$\frac{1}{T_f}\rho_f^\star v_f^\star - \frac{1}{T_s}\rho_s^\star v_s^\star + \frac{\rho_s^\star(V(\rho_s^\star) - v_s^\star)}{T_s^e} = 0. \tag{3.9}$$

The steady state density-velocity relations are defined based on (3.6). Thus the steady states $(\rho_f^\star, v_f^\star, \rho_s^\star, v_s^\star)$ need to satisfy

$$\rho_f^\star = \sigma \rho_s^\star, \tag{3.10}$$

$$v_f^\star = v_m \left(1 - r_f \left(\frac{\rho_f^\star}{\rho_m}\right)^{\gamma}\right), \tag{3.11}$$

$$v_s^\star = v_m \left(1 - r_s \left(\frac{\rho_s^\star}{\rho_m}\right)^{\gamma}\right), \tag{3.12}$$

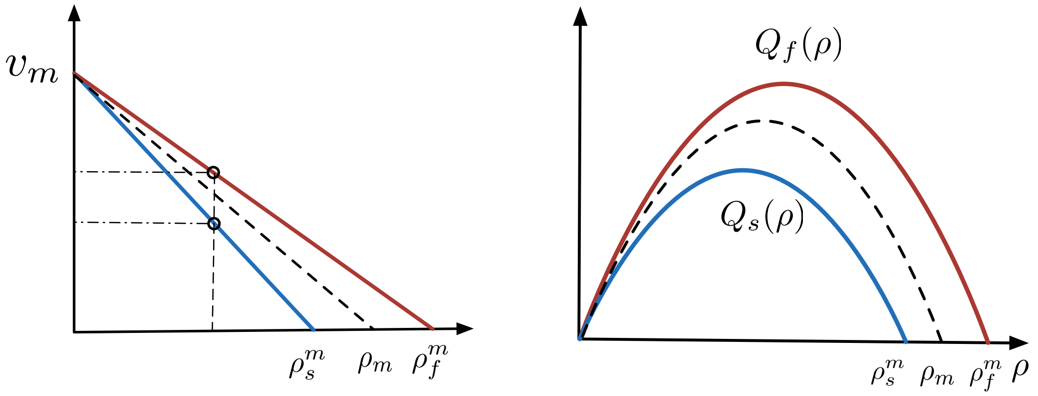

Figure 3.2: Steady states of one lane, fast and slow lane in equilibrium density and velocity relation and fundamental diagram.

where $v_f^\star$ and $v_s^\star$ differ from single-lane $V(\rho_i)$. The ratio coefficients r_f and r_s are defined as

$$r_f = \frac{1+\left(\frac{1}{\sigma}\right)^{\gamma}\frac{T_f^e}{T_f}+\frac{T_s^e}{T_s}}{1+\frac{T_f^e}{T_f}+\frac{T_s^e}{T_s}}, \tag{3.13}$$

$$r_s = \frac{1+\frac{T_f^e}{T_f}+\frac{T_s^e}{T_s}\left(\sigma\right)^{\gamma}}{1+\frac{T_f^e}{T_f}+\frac{T_s^e}{T_s}}. \tag{3.14}$$

The parameter σ defines driver's preference for the fast lane over slow lane according to (3.7), (3.10),

$$\sigma = \frac{T_f}{T_s}. \tag{3.15}$$

Compared with the single-lane Greenshield's model in (3.6), the relations of steady state traffic velocities $v_i^\star$ and densities $\rho_i^\star$ depend on the drivers lane-changing preference parameter σ.

Assuming that overall drivers prefer fast lane over slow lane, we use Fig. 3.2 $(\sigma > 1, \gamma = 1)$ to show the equilibrium velocity-density relation and fundamental diagram of the single-lane, the fast and slow lane. ρ_m represents the equivalent maximum density of the single-lane. The actual maximum density in the fast lane ρ_f^m and in the fast lane ρ_s^m are related to ρ_m by

$$\rho_f^m = \sqrt[\gamma]{r_f}\rho_m, \tag{3.16}$$

$$\rho_s^m = \sqrt[\gamma]{r_s}\rho_m. \tag{3.17}$$

- $\sigma > 1 \implies r_f < 1 < r_s$

If drivers prefer the fast lane, the decrease of velocity gets steeper in the slow lane and less steep in the fast lane. At the same density, the fast lane traffic is ”more tolerant to risk” of high density than in the single-lane case, and the slow lane traffic is ”less tolerant to risk” than in the single-lane case. As a result, the traffic flux of fast lane is higher than the slow lane at the same density in the fundamental diagram shown in Fig. 3.2.

- $\sigma < 1 \implies r_f > 1 > r_s$

Drivers prefer the slow lane. The decrease of velocity is steeper in the fast lane than that of slow lane at the same density. The slow lane is more tolerant to high density and the traffic flux is higher in the slow lane.

In general, the activities of lane changing segregate the drivers into the more ”risk-tolerant” ones in the fast lane and the more ”risk-averse” in the slow lane. The risk-tolerant drivers prefer to drive with a faster speed at the same density, compared with risk-averse drivers.

3.1.2 Linearized two-lane ARZ model

Before linearizing the nonlinear system (3.1)-(3.4) to steady states (3.10)-(3.12), we consider the following boundary conditions of (ρ_i, v_i)-system. We assume constant traffic flux entering from the inlet boundary $x = 0$ of the two lanes.

$$q_i^\star = \rho_i^\star v_i^\star. \tag{3.18}$$

Two VSLs implemented at the outlet $U_f(t)$ and $U_s(t)$ actuate the traffic velocity variations for the fast and slow lanes respectively.

$$\rho_f(0,t) = \frac{\rho_f^\star v_f^\star}{v_f(0,t)}, \tag{3.19}$$

$$v_f(L,t) = U_f(t) + v_f^\star, \tag{3.20}$$

$$\rho_s(0,t) = \frac{\rho_s^\star v_s^\star}{v_s(0,t)}, \tag{3.21}$$

$$v_s(L,t) = U_s(t) + v_s^\star, \tag{3.22}$$

Then we linearize the above nonlinear hyperbolic system $(\rho_f, v_f, \rho_s, v_s)$ around steady states $(\rho_f^\star, v_f^\star, \rho_s^\star, v_s^\star)$ that satisfy (3.10)-(3.12). The deviations from the steady states are defined as

$$\tilde{\rho}_f = \rho_f - \rho_f^\star, \quad \tilde{v}_f = v_f - v_f^\star, \tag{3.23}$$

$$\tilde{\rho}_s = \rho_s - \rho_s^\star, \quad \tilde{v}_s = v_s - v_s^\star. \tag{3.24}$$

The linearized hyperbolic system is obtained

$$\partial_t \tilde{\rho}_s + v_s^\star \partial_x \tilde{\rho}_s + \rho_s^\star \partial_x \tilde{v}_s = -\frac{1}{T_s}\tilde{\rho}_s + \frac{1}{T_f}\tilde{\rho}_f, \tag{3.25}$$

$$\partial_t \tilde{\rho}_f + v_f^\star \partial_x \tilde{\rho}_f + \rho_f^\star \partial_x \tilde{v}_f = \frac{1}{T_s}\tilde{\rho}_s - \frac{1}{T_f}\tilde{\rho}_f, \tag{3.26}$$

$$\begin{aligned} \partial_t \tilde{v}_s + (v_s^\star - \gamma p_s^\star)\partial_x \tilde{v}_s = & -\frac{1}{T_s}\frac{v_f^\star - v_s^\star}{\rho_s^\star}\tilde{\rho}_s + \frac{1}{T_f}\frac{v_f^\star - v_s^\star}{\rho_s^\star}\tilde{\rho}_f \\ & + \frac{1}{T_s}(\tilde{v}_f - \tilde{v}_s) + \frac{\tilde{\rho}_s V'(\rho_s^\star) - \tilde{v}_s}{T_s^e}, \end{aligned} \tag{3.27}$$

$$\begin{aligned} \partial_t \tilde{v}_f + (v_f^\star - \gamma p_f^\star)\partial_x \tilde{v}_f = & \frac{1}{T_s}\frac{v_s^\star - v_f^\star}{\rho_f^\star}\tilde{\rho}_s - \frac{1}{T_f}\frac{v_s^\star - v_f^\star}{\rho_f^\star}\tilde{\rho}_f \\ & + \frac{1}{T_f}(\tilde{v}_s - \tilde{v}_f) + \frac{\tilde{\rho}_f V'(\rho_f^\star) - \tilde{v}_f}{T_f^e}, \end{aligned} \tag{3.28}$$

with the linearized boundary conditions

$$\tilde{\rho}_s(0,t) = -\frac{\rho_s^\star}{v_s^\star}\tilde{v}_s(0,t), \tag{3.29}$$

$$\tilde{\rho}_f(0,t) = -\frac{\rho_f^\star}{v_f^\star}\tilde{v}_f(0,t), \tag{3.30}$$

$$\tilde{v}_s(L,t) = U_s(t), \tag{3.31}$$

$$\tilde{v}_f(L,t) = U_f(t). \tag{3.32}$$

In order to diagonalize the spatial derivatives on the left hand side of the equations, we write the above linearized hyperbolic system in the Riemann coordinates $(\tilde{w}_f, \tilde{v}_f, \tilde{w}_s, \tilde{v}_s)$ as

$$\tilde{w}_s = \frac{\gamma p_s^\star}{\rho_s^\star}\tilde{\rho}_s + \tilde{v}_s, \quad \tilde{v}_s = \tilde{v}_s, \tag{3.33}$$

$$\tilde{w}_f = \frac{\gamma p_f^\star}{\rho_f^\star}\tilde{\rho}_f + \tilde{v}_f, \quad \tilde{v}_f = \tilde{v}_f. \tag{3.34}$$

We consider the congested regime in [121] where steady state traffic density disturbances convect downstream and the velocity disturbances travel upstream. Therefore the following conditions hold for the characteristic speeds of $\tilde{v}_i$,

$$v_s^\star - \gamma p_s^\star < 0, \quad v_f^\star - \gamma p_f^\star < 0. \tag{3.35}$$

We obtain a coupled 4×4 first-order hetero-directional hyperbolic system in $(\tilde{w}_s, \tilde{w}_f, \tilde{v}_s, \tilde{v}_f)$,

$$\partial_t \tilde{w}_s + v_s^\star \partial_x \tilde{w}_s = a_{11}^{ww}\tilde{w}_s + a_{12}^{ww}\tilde{w}_f + a_{11}^{wv}\tilde{v}_s + a_{12}^{wv}\tilde{v}_f, \tag{3.36}$$

$$\partial_t \tilde{w}_f + v_f^\star \partial_x \tilde{w}_f = a_{21}^{ww}\tilde{w}_s + a_{22}^{ww}\tilde{w}_f + a_{21}^{wv}\tilde{v}_s + a_{22}^{wv}\tilde{v}_f, \tag{3.37}$$

$$\partial_t \tilde{v}_s - (\gamma p_s^\star - v_s^\star)\partial_x \tilde{v}_s = a_{11}^{vw}\tilde{w}_s + a_{12}^{vw}\tilde{w}_f + a_{11}^{vv}\tilde{v}_s + a_{12}^{vv}\tilde{v}_f, \tag{3.38}$$

$$\partial_t \tilde{v}_f - (\gamma p_f^\star - v_f^\star)\partial_x \tilde{v}_f = a_{21}^{vw}\tilde{w}_s + a_{22}^{vw}\tilde{w}_f + a_{21}^{vv}\tilde{v}_s + a_{22}^{vv}\tilde{v}_f, \tag{3.39}$$

$$\tilde{w}_s(0,t) = k_s \tilde{v}_s(0,t), \tag{3.40}$$

$$\tilde{w}_f(0,t) = k_f \tilde{v}_f(0,t), \tag{3.41}$$

$$\tilde{v}_s(L,t) = U_s(t), \tag{3.42}$$

$$\tilde{v}_f(L,t) = U_f(t), \tag{3.43}$$

where the constant boundary coefficients k_i are defined as

$$k_i = -\frac{\gamma p_i^\star - v_i^\star}{v_i^\star}, \tag{3.44}$$

and the constant parameter block matrix $\{A\}$ is denoted by

$$A = \begin{bmatrix} A^{ww} & A^{wv} \\ A^{vw} & A^{vv} \end{bmatrix}. \tag{3.45}$$

The elements of sub-matrices of $\{A\}$ are defined as,

$$a_{11}^{ww} = -\frac{1}{T_s^e} - \frac{1}{T_s}\frac{v_f^\star - v_s^\star + \gamma p_s^\star}{\gamma p_s^\star}, \quad a_{12}^{ww} = \frac{1}{T_s}\frac{v_f^\star - v_s^\star + \gamma p_s^\star}{\gamma p_f^\star}, \tag{3.46}$$

$$a_{21}^{ww} = \frac{1}{T_f}\frac{v_s^\star - v_f^\star + \gamma p_f^\star}{\gamma p_s^\star}, \quad a_{22}^{ww} = -\frac{1}{T_f^e} - \frac{1}{T_f}\frac{v_s^\star - v_f^\star + \gamma p_f^\star}{\gamma p_f^\star}, \tag{3.47}$$

$$a_{11}^{wv} = \frac{1}{T_s}\frac{v_f^\star - v_s^\star}{\gamma p_s^\star}, \quad a_{12}^{wv} = -\frac{1}{T_s}\frac{(\gamma p_s^\star - v_s^\star) - (\gamma p_f^\star - v_f^\star)}{\gamma p_f^\star}, \tag{3.48}$$

$$a_{21}^{wv} = -\frac{1}{T_f}\frac{(\gamma p_f^\star - v_f^\star) - (\gamma p_s^\star - v_s^\star)}{\gamma p_s^\star}, \quad a_{22}^{wv} = \frac{1}{T_f}\frac{v_s^\star - v_f^\star}{\gamma p_f^\star}, \tag{3.49}$$

$$a_{11}^{vw} = -\frac{1}{T_s^e} - \frac{1}{T_s}\frac{v_f^\star - v_s^\star}{\gamma p_s^\star}, \quad a_{12}^{vw} = \frac{1}{T_s}\frac{v_f^\star - v_s^\star}{\gamma p_f^\star}, \tag{3.50}$$

$$a_{21}^{vw} = \frac{1}{T_f}\frac{v_s^\star - v_f^\star}{\gamma p_s^\star}, \quad a_{22}^{vw} = -\frac{1}{T_f^e} - \frac{1}{T_f}\frac{v_s^\star - v_f^\star}{\gamma p_f^\star}, \tag{3.51}$$

$$a_{11}^{vv} = \frac{1}{T_s}\frac{v_f^\star - v_s^\star - \gamma p_s^\star}{\gamma p_s^\star}, \quad a_{12}^{vv} = -\frac{1}{T_s}\frac{v_f^\star - v_s^\star - \gamma p_f^\star}{\gamma p_f^\star}, \tag{3.52}$$

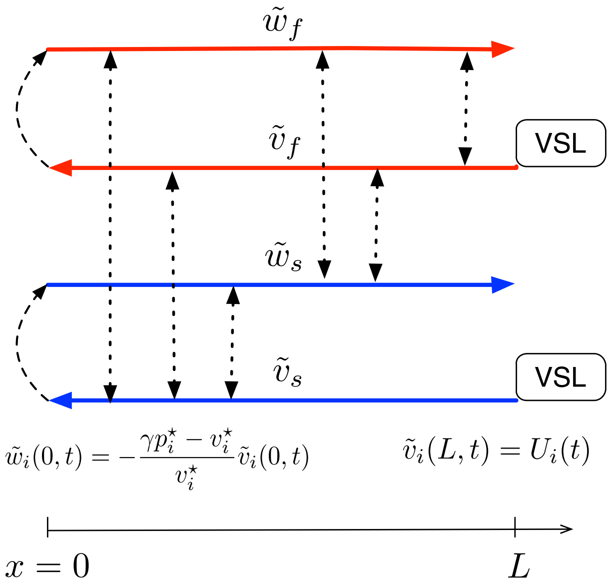

Figure 3.3: Flow diagram of linearized two-lane ARZ model.

$$a_{21}^{vv} = -\frac{1}{T_f}\frac{v_s^\star - v_f^\star - \gamma p_s^\star}{\gamma p_s^\star}, \quad a_{22}^{vv} = -\frac{1}{T_f}\frac{v_s^\star - v_f^\star - \gamma p_f^\star}{\gamma p_f^\star}. \tag{3.53}$$

The flow diagram of $(\tilde{w}_i, \tilde{v}_i)$-system is shown in Fig. 3.3. The 4×4 first-order hyperbolic system is composed of two coupled second-order heterodirectional hyperbolic systems. States $\tilde{w}_i$ convect downstream while states $\tilde{v}_i$ propagate upstream. We use two VSLs to damp out the oscillations to zero from the outlet.

3.2 Full-state feedback control design with VSLs

To apply the backstepping approach and to design boundary control for the system in (3.36)-(3.43), we scale the state variables $\tilde{v}_s$ and $\tilde{v}_f$ in space to cancel the diagonal terms in their equations. The Riemann variables $\tilde{w}_s$ and $\tilde{w}_f$ remain to be the same. The scaled variables $\bar{v}_s$ and $\bar{v}_f$ are defined as

$$\bar{v}_s = \exp\left(\frac{a_{11}^{vv}}{\mu_1}x\right)\tilde{v}_s, \tag{3.54}$$

$$\bar{v}_f = \exp\left(\frac{a_{22}^{vv}}{\mu_2}x\right)\tilde{v}_f. \tag{3.55}$$

Then we obtain the scaled system:

$$\partial_t\tilde{w}_s + v_s^\star\partial_x\tilde{w}_s = \bar{a}_{11}^{ww}\tilde{w}_s + \bar{a}_{12}^{ww}\tilde{w}_f + \bar{a}_{11}^{wv}(x)\bar{v}_s + \bar{a}_{12}^{wv}(x)\bar{v}_f, \tag{3.56}$$

$$\partial_t\tilde{w}_f + v_f^\star\partial_x\tilde{w}_f = \bar{a}_{21}^{ww}\tilde{w}_s + \bar{a}_{22}^{ww}\tilde{w}_f + \bar{a}_{21}^{wv}(x)\bar{v}_s + \bar{a}_{22}^{wv}(x)\bar{v}_f, \tag{3.57}$$

$$\partial_t\bar{v}_s - (\gamma p_s^\star - v_s^\star)\partial_x\bar{v}_s = \bar{a}_{11}^{vw}(x)\tilde{w}_s + \bar{a}_{12}^{vw}(x)\tilde{w}_f + \bar{a}_{12}^{vv}(x)\bar{v}_f, \tag{3.58}$$

$$\partial_t\bar{v}_f - (\gamma p_f^\star - v_f^\star)\partial_x\bar{v}_f = \bar{a}_{21}^{vw}(x)\tilde{w}_s + \bar{a}_{22}^{vw}(x)\tilde{w}_f + \bar{a}_{21}^{vv}(x)\bar{v}_s, \tag{3.59}$$

$$\tilde{w}_s(0,t) = k_s\bar{v}_s(0,t), \tag{3.60}$$

$$\tilde{w}_f(0,t) = k_f\bar{v}_f(0,t), \tag{3.61}$$

$$\bar{v}_s(L,t) = l_sU_s(t), \tag{3.62}$$

$$\bar{v}_f(L,t) = l_fU_f(t). \tag{3.63}$$

We denote the transports speeds as

$$\varepsilon_1 = v_s^\star, \tag{3.64}$$

$$\varepsilon_2 = v_f^\star, \tag{3.65}$$

$$\mu_1 = (\gamma p_s^\star - v_s^\star), \tag{3.66}$$

$$\mu_2 = (\gamma p_f^\star - v_f^\star). \tag{3.67}$$

Note that the steady velocity of the fast lane is larger than that of the slow lane, the constant transport speeds satisfy the following inequalities,

$$-\mu_1 < -\mu_2 < 0 < \varepsilon_1 < \varepsilon_2. \tag{3.68}$$

where the constant coefficients l_f and l_s are defined as

$$l_s = \exp\left(\frac{a_{11}^{vv}}{\mu_1}L\right), \tag{3.69}$$

$$l_f = \exp\left(\frac{a_{22}^{vv}}{\mu_2}L\right). \tag{3.70}$$

The new in-domain coefficient matrix $\{\bar{A}\}$ is given by

$$\bar{A} = \begin{bmatrix} \bar{A}^{ww} & \bar{A}^{wv} \\ \bar{A}^{vw} & \bar{A}^{vv} \end{bmatrix}, \tag{3.71}$$

where the sub-matrices are obtained as

$$\bar{A}^{ww} = A^{ww}, \tag{3.72}$$

$$\bar{A}^{wv}(x) = A^{wv} \begin{bmatrix} \exp\left(-\frac{a_{11}^{vv}}{\mu_1}x\right) & 0 \\ 0 & \exp\left(-\frac{a_{22}^{vv}}{\mu_2}x\right) \end{bmatrix}, \tag{3.73}$$

$$\bar{A}^{vw}(x) = A^{vw} \begin{bmatrix} \exp\left(\frac{a_{11}^{vv}}{\mu_1}x\right) & 0 \\ 0 & \exp\left(\frac{a_{22}^{vv}}{\mu_2}x\right) \end{bmatrix}, \tag{3.74}$$

$$\bar{A}^{vv}(x) = A^{vv} \begin{bmatrix} 0 & \exp\left(\frac{a_{22}^{vv}}{\mu_2}x - \frac{a_{11}^{vv}}{\mu_1}x\right) \\ \exp\left(\frac{a_{11}^{vv}}{\mu_1}x - \frac{a_{22}^{vv}}{\mu_2}x\right) & 0 \end{bmatrix}. \tag{3.75}$$

Among the transformed sub-matrices, the elements of $\{\bar{A}^{ww}\}$ are constant and the elements of $\{\bar{A}^{wv}(x)\}$, $\{\bar{A}^{vw}(x)\}$ and $\{\bar{A}^{vv}(x)\}$ are spatially-varying coefficients. We summarize the transformation between $(\tilde{w}_s, \tilde{w}_f, \bar{v}_s, \bar{v}_f)$ and $(\tilde{\rho}_s, \tilde{\rho}_f, \tilde{v}_s, \tilde{v}_f)$ from (3.33), (3.34) and (3.54), (3.55) as follows:

$$\tilde{\rho}_s = \frac{\rho_s^\star}{\gamma p_s^\star}\left(\tilde{w}_s - \exp\left(-\frac{a_{11}^{vv}}{\mu_1}x\right)\bar{v}_s\right), \tag{3.76}$$

$$\tilde{\rho}_f = \frac{\rho_f^\star}{\gamma p_f^\star}\left(\tilde{w}_f - \exp\left(-\frac{a_{22}^{vv}}{\mu_2}x\right)\bar{v}_s\right), \tag{3.77}$$

$$\tilde{v}_s = \exp\left(-\frac{a_{11}^{vv}}{\mu_1}x\right)\bar{v}_s, \tag{3.78}$$

$$\tilde{v}_f = \exp\left(-\frac{a_{22}^{vv}}{\mu_2}x\right)\bar{v}_f. \tag{3.79}$$

Then we introduce the backstepping transformation to the scaled $(\tilde{w}_i, \bar{v}_i)$-system in (3.56)-(3.63),

$$\begin{bmatrix} \alpha_s(x,t) \\ \alpha_f(x,t) \end{bmatrix} = \begin{bmatrix} \tilde{w}_s(x,t) \\ \tilde{w}_f(x,t) \end{bmatrix}, \tag{3.80}$$

$$\begin{aligned} \begin{bmatrix} \beta_s(x,t) \\ \beta_f(x,t) \end{bmatrix} = & \begin{bmatrix} \bar{v}_s(x,t) \\ \bar{v}_f(x,t) \end{bmatrix} - \int_0^x K(x,\xi) \begin{bmatrix} \tilde{w}_s(x,t) \\ \tilde{w}_f(x,t) \end{bmatrix} d\xi \\ & - \int_0^x L(x,\xi) \begin{bmatrix} \bar{v}_s(x,t) \\ \bar{v}_f(x,t) \end{bmatrix} d\xi, \end{aligned} \tag{3.81}$$

where the kernel matrices are denoted as

$$K = \begin{bmatrix} K_{11} & K_{12} \\ K_{21} & K_{22} \end{bmatrix}, \quad L = \begin{bmatrix} L_{11} & L_{12} \\ L_{21} & L_{22} \end{bmatrix}. \tag{3.82}$$

The kernel variables $\{K\}$ and $\{L\}$ evolve in the triangular domain $\mathscr{T} = \{(x,\xi) : 0 \le \xi \le x \le 1\}$. Taking derivative with respect to time and space on both sides of (3.80)-(3.81) along the solution of a target system given later, we obtain the following kernel equations. The kernels $\{K(x,\xi)\}$ and $\{L(x,\xi)\}$ are governed by

$$\mu_1 \partial_x K_{11} - \varepsilon_1 \partial_\xi K_{11} = \bar{a}_{11}^{ww} K_{11} + \bar{a}_{21}^{ww} K_{12} + \bar{a}_{11}^{vw} L_{11} + \bar{a}_{21}^{vw} L_{12}, \tag{3.83}$$

$$\mu_1 \partial_x K_{12} - \varepsilon_2 \partial_\xi K_{12} = \bar{a}_{12}^{ww} K_{11} + \bar{a}_{22}^{ww} K_{12} + \bar{a}_{12}^{vw} L_{11} + \bar{a}_{22}^{vw} L_{12}, \tag{3.84}$$

$$\mu_2 \partial_x K_{21} - \varepsilon_1 \partial_\xi K_{21} = \bar{a}_{11}^{ww} K_{21} + \bar{a}_{21}^{ww} K_{22} + \bar{a}_{11}^{vw} L_{21} + \bar{a}_{21}^{vw} L_{22}, \tag{3.85}$$

$$\mu_2\partial_x K_{22} - \varepsilon_2\partial_\xi K_{22} = \bar{a}^{ww}_{12}K_{21} + \bar{a}^{ww}_{22}K_{22} + \bar{a}^{vw}_{12}L_{21} + \bar{a}^{vw}_{22}L_{22}, \tag{3.86}$$

$$\mu_1\partial_x L_{11} + \mu_1\partial_\xi L_{11} = \bar{a}^{vv}_{21}L_{12} + \bar{a}^{vw}_{11}K_{11} + \bar{a}^{vw}_{21}K_{12}, \tag{3.87}$$

$$\mu_1\partial_x L_{12} + \mu_2\partial_\xi L_{12} = \bar{a}^{vv}_{12}L_{11} + \bar{a}^{vw}_{12}K_{11} + \bar{a}^{vw}_{22}K_{12}, \tag{3.88}$$

$$\mu_2\partial_x L_{21} + \mu_1\partial_\xi L_{21} = \bar{a}^{vv}_{21}L_{22} + \bar{a}^{vw}_{11}K_{21} + \bar{a}^{vw}_{21}K_{22}, \tag{3.89}$$

$$\mu_2\partial_x L_{22} + \mu_2\partial_\xi L_{22} = \bar{a}^{vv}_{12}L_{21} + \bar{a}^{vw}_{12}K_{21} + \bar{a}^{vw}_{22}K_{22}, \tag{3.90}$$

$$K_{11}(x,x) = -\frac{\bar{a}^{vw}_{11}(x)}{\varepsilon_1 + \mu_1}, \quad K_{12}(x,x) = -\frac{\bar{a}^{vw}_{12}(x)}{\varepsilon_2 + \mu_1}, \tag{3.91}$$

$$K_{21}(x,x) = -\frac{\bar{a}^{vw}_{21}(x)}{\varepsilon_1 + \mu_2}, \quad K_{22}(x,x) = -\frac{\bar{a}^{vw}_{22}(x)}{\varepsilon_2 + \mu_2}, \tag{3.92}$$

$$L_{11}(x,0) = \frac{\varepsilon_1 k_s}{\mu_1}K_{11}(x,0), \quad L_{12}(x,x) = -\frac{\bar{a}^{vv}_{12}(x)}{\mu_1 - \mu_2}, \tag{3.93}$$

$$L_{12}(x,0) = \frac{\varepsilon_2 k_f}{\mu_2}K_{12}(x,0), \quad L_{21}(x,x) = -\frac{\bar{a}^{vv}_{21}(x)}{\mu_2 - \mu_1}, \tag{3.94}$$

$$L_{21}(L,\xi) = 0, \quad L_{22}(x,0) = \frac{\varepsilon_2 k_f}{\mu_2}K_{22}(x,0). \tag{3.95}$$

The well-possedness of the kernel equations (3.83)-(3.95) is proved using the method of characteristics and the successive approximations following the result for a general class of kernel system in [80]. There exists a unique solution $K, L \in L^\infty(\mathscr{T})$. Therefore, we establish the invertibility of the backstepping transformation (3.80),(3.81) and can study the stability of the following target system due to its equivalence to the $(\tilde{w}_i, \bar{v}_i)$-system.

Note that we impose an artificial boundary condition $L_{21}(L,\xi)$ in (3.95) for the well-posedness of the kernel equations. This leads to one degree of freedom in backstepping transformation of the hyperbolic system as well as the following control design. The stabilization of the following target system is achieved with two controllers and the one degree of freedom enables the coordination between the two VSLs.

With the backstepping transformation and the above kernel equations, we map the $(\bar{w}_i, \bar{v}_i)$-

system to the cascade target system (α_i, β_i),

$$\begin{aligned}
\partial_t \alpha_s + v_s^\star \partial_x \alpha_s =& \bar{a}_{11}^{ww} \alpha_s + \bar{a}_{12}^{ww} \alpha_f + \bar{a}_{11}^{wv}(x) \beta_s + \bar{a}_{12}^{wv}(x) \beta_f \\
& + \int_0^x b_{11}(x,\xi) \alpha_s(\xi) d\xi + \int_0^x b_{12}(x,\xi) \alpha_f(\xi) d\xi \\
& + \int_0^x c_{11}(x,\xi) \beta_s(\xi) d\xi + \int_0^x c_{12}(x,\xi) \beta_f(\xi) d\xi, \qquad (3.96) \\
\partial_t \alpha_f + v_f^\star \partial_x \alpha_f =& \bar{a}_{21}^{ww} \alpha_s + \bar{a}_{22}^{ww} \alpha_f + \bar{a}_{21}^{wv}(x) \beta_s + \bar{a}_{22}^{wv}(x) \beta_f \\
& + \int_0^x b_{21}(x,\xi) \alpha_s(\xi) d\xi + \int_0^x b_{22}(x,\xi) \alpha_f(\xi) d\xi \\
& + \int_0^x c_{21}(x,\xi) \beta_s(\xi) d\xi + \int_0^x c_{22}(x,\xi) \beta_f(\xi) d\xi, \qquad (3.97) \\
\partial_t \beta_s - (\gamma p_s^\star - v_s^\star) \partial_x \beta_s =& 0, \qquad (3.98) \\
\partial_t \beta_f - (\gamma p_f^\star - v_f^\star) \partial_x \beta_f =& \theta(x) \beta_s(0,t), \qquad (3.99) \\
\alpha_f(0,t) =& k_f \beta_f(0,t), \qquad (3.100) \\
\alpha_s(0,t) =& k_s \beta_s(0,t), \qquad (3.101) \\
\beta_s(L,t) =& 0, \qquad (3.102) \\
\beta_f(L,t) =& 0, \qquad (3.103)
\end{aligned}$$

where the spatially varying parameter matrices $\{B\}$ and $\{C\}$ are denoted as

$$B = \begin{bmatrix} b_{11} & b_{12} \\ b_{21} & b_{22} \end{bmatrix}, \quad C = \begin{bmatrix} c_{11} & c_{12} \\ c_{21} & c_{22} \end{bmatrix}, \qquad (3.104)$$

and given by the following equations in the matrix form,

$$\begin{aligned}
B(x,\xi) =& \bar{A}^{wv} K(x,\xi) + \int_\xi^x B(x,s) K(s,\xi) d\xi, \qquad (3.105) \\
C(x,\xi) =& \bar{A}^{wv} L(x,\xi) + \int_\xi^x C(x,s) L(s,\xi) d\xi, \qquad (3.106)
\end{aligned}$$

and $\theta(x)$ is obtained from the kernel variables K_{21} and L_{21},

$$\theta(x) = -\varepsilon_1 k_s K_{21}(x,0) - \mu_1 L_{21}(x,0). \tag{3.107}$$

Considering the cascade structure of the target system, the following conclusion is arrived.

Lemma 3.1. *Consider the target system* (3.96)-(3.99) *and actuated boundary conditions* (3.96)-(3.103)*, the zero equilibrium*

$$\alpha_f(x,t) = \alpha_s(x,t) = \beta_f(x,t) = \beta_s(s,t) \equiv 0, \tag{3.108}$$

is reached in finite time $t = t_f$, where

$$t_f = \frac{L}{v_s^\star} + \frac{L}{\gamma p_f^\star - v_f^\star} + \frac{L}{\gamma p_s^\star - v_s^\star}. \tag{3.109}$$

Proof. By solving (3.99) and (3.103) directly, we obtain that after $t > \frac{L}{\gamma p_f^\star - v_f^\star}$,

$$\beta_f(x,t) \equiv 0. \tag{3.110}$$

Using the cascade structure of the target system in (3.98), we have after $t > \frac{L}{\gamma p_f^\star - v_f^\star} + \frac{L}{\gamma p_s^\star - v_s^\star}$,

$$\beta_s(s,t) \equiv 0. \tag{3.111}$$

Then after $t > \frac{L}{\gamma p_f^\star - v_f^\star} + \frac{L}{\gamma p_s^\star - v_s^\star} + \frac{L}{v_s^\star}$, we obtain that

$$\alpha_f(x,t) \equiv 0, \quad \alpha_s(x,t) \equiv 0, \tag{3.112}$$

which concludes the proof. $\square$

Boundary conditions (3.102),(3.103) and backstepping transformation (3.81) yield full-state feedback control laws given by $(\bar{w}_i, \bar{v}_i)$,

$$\begin{aligned}\begin{bmatrix} l_s U_s(t) \\ l_f U_f(t) \end{bmatrix} =& \int_0^L \begin{bmatrix} K_{11}(L,\xi) & K_{12}(L,\xi) \\ K_{21}(L,\xi) & K_{22}(L,\xi) \end{bmatrix} \begin{bmatrix} \bar{w}_s(x,t) \\ \bar{w}_f(x,t) \end{bmatrix} d\xi \\ &+ \int_0^L \begin{bmatrix} L_{11}(L,\xi) & L_{12}(L,\xi) \\ L_{21}(L,\xi) & L_{22}(L,\xi) \end{bmatrix} \begin{bmatrix} \bar{v}_s(x,t) \\ \bar{v}_f(x,t) \end{bmatrix} d\xi. \end{aligned} \tag{3.113}$$

Using the invertible transformation (3.76)-(3.79), we obtain the full-state feedback control laws given in traffic flow variables $(\rho_f, v_f, \rho_s, v_s)$ and the steady states $(\rho_f^\star, v_f^\star, \rho_s^\star, v_s^\star)$. We reach the main stabilization result of full-state feedback control design.

Theorem 3.2. *Consider the two-lane traffic ARZ model in* (3.1)-(3.4) *with boundary conditions* (3.19)-(3.22)*, initial conditions* $\rho_f(x,0), v_f(x,0), \rho_s(x,0), v_s(x,0) \in L^\infty([0,L])$ *and the following control laws*

$$\begin{aligned} U_s(t) =& \exp\left(-\frac{a_{11}^{vv}}{\mu_1} L\right) \int_0^L \frac{\gamma p_s^\star}{\rho_s^\star} K_{11}(L,\xi)\left(\rho_s(\xi,t) - \rho_s^\star\right) \\ &+ \frac{\gamma p_f^\star}{\rho_f^\star} K_{12}(L,\xi)\left(\rho_f(\xi,t) - \rho_f^\star\right) \\ &+ \left[K_{11}(L,\xi) + L_{11}(L,\xi) \exp\left(\frac{a_{11}^{vv}}{\mu_1}\xi\right)\right]\left(v_s(\xi,t) - v_s^\star\right) \\ &+ \left[K_{12}(L,\xi) + L_{12}(L,\xi) \exp\left(\frac{a_{22}^{vv}}{\mu_2}\xi\right)\right]\left(v_f(\xi,t) - v_f^\star\right) d\xi, \end{aligned} \tag{3.114}$$

$$\begin{aligned} U_f(t) =& \exp\left(-\frac{a_{22}^{vv}}{\mu_2} L\right) \int_0^L \frac{\gamma p_s^\star}{\rho_s^\star} K_{21}(L,\xi)\left(\rho_s(\xi,t) - \rho_s^\star\right) \\ &+ \frac{\gamma p_f^\star}{\rho_f^\star} K_{22}(L,\xi)\left(\rho_f(\xi,t) - \rho_f^\star\right) \\ &+ \left[K_{21}(L,\xi) + L_{21}(L,\xi) \exp\left(\frac{a_{11}^{vv}}{\mu_1}\xi\right)\right]\left(v_s(\xi,t) - v_s^\star\right) \\ &+ \left[K_{22}(L,\xi) + L_{22}(L,\xi) \exp\left(\frac{a_{22}^{vv}}{\mu_2}\xi\right)\right]\left(v_f(\xi,t) - v_f^\star\right) d\xi, \end{aligned} \tag{3.115}$$

where the kernels are obtained by solving (3.83)-(3.95). *The steady states* $(\rho_f^\star, v_f^\star, \rho_s^\star, v_s^\star)$ *are finite-time stable and the convergence is reached in* t_f *given in* (3.109).

Proof. Lemma 1 for the closed-loop target system in (3.96)-(3.103) with the existence of the backstepping transformation in (3.80),(3.81) yields the convergence of the states variables $(\tilde{w}_s,\tilde{w}_f, \bar{v}_s,\bar{v}_f)$ defined by (3.56)-(3.63) to zero for $t > t_f$. Given the transformation in (3.76)-(3.79), the finite-time convergence to zero is arrived for the linearized state variables $(\tilde{\rho}_s(x,t), \tilde{\rho}_f(x,t), \tilde{v}_s(x,t), \tilde{v}_f(x,t))$, which yields the convergence of the two-lane ARZ PDE model by $(\rho_s(x,t), \rho_f(x,t), v_s(x,t), v_f(x,t))$ to the steady states. □

3.3 Collocated observer design

In this section, we develop a collocated observer by taking measurement of density states at the outlet of the segment,

$$y_s(t) = \tilde{\rho}_s(L,t), \tag{3.116}$$

$$y_f(t) = \tilde{\rho}_f(L,t). \tag{3.117}$$

Using the state estimates obtained form the observer design and the full-state feedback control laws, we construct output feedback controllers.

Note that the anti-collocated observer can also be designed here by taking measurement of velocity states $\tilde{v}_s(0,t)$ and $\tilde{v}_f(0,t)$ at the inlet. The anti-collocated observer design is trivial in our case which presents as a copy of the $(\tilde{w}_f, \tilde{w}_s, \bar{v}_s, \bar{v}_f)$-system. More importantly, collocated observer design is practical in implementation along with the full-state feedback control design.

For state estimation of the scaled system in (3.56)-(3.63), we obtain the measurement of

$\tilde{w}_s(L,t)$ and $\tilde{w}_f(L,t)$ from (3.33),(3.34),

$$\begin{aligned} Y_s(t) =& \tilde{w}_s(L,t) = \frac{\gamma p_s^\star}{\rho_s^\star}\tilde{\rho}_s(L,t) + \tilde{v}_s(L,t), && (3.118)\\ Y_f(t) =& \tilde{w}_f(L,t) = \frac{\gamma p_f^\star}{\rho_f^\star}\tilde{\rho}_f(L,t) + \tilde{v}_f(L,t), && (3.119) \end{aligned}$$

thus the values of $Y_s(t)$ and $Y_f(t)$ are obtained from $y_s(t)$, $y_f(t)$ and control inputs $U_s(t)$, $U_f(t)$,

$$\begin{aligned} Y_s(t) =& \frac{\gamma p_s^\star}{\rho_s^\star} y_s(t) + U_s(t), && (3.120)\\ Y_f(t) =& \frac{\gamma p_f^\star}{\rho_f^\star} y_f(t) + U_f(t). && (3.121) \end{aligned}$$

The observer equations $(\hat{w}_f, \hat{w}_s, \hat{u}_s, \hat{u}_f)$ that estimate $(\tilde{w}_f, \tilde{w}_s, \bar{v}_s, \bar{v}_f)$ read as follows:

$$\begin{aligned} \partial_t \hat{w}_s + v_s^\star \partial_x \hat{w}_s =& \bar{a}_{11}^{ww}\hat{w}_s + \bar{a}_{12}^{ww}\hat{w}_f + \bar{a}_{11}^{wv}(x)\hat{u}_s + \bar{a}_{12}^{wv}(x)\hat{u}_f \\ & + p_{11}(x)\check{w}_s(L,t) + p_{12}(x)\check{w}_f(L,t), && (3.122)\\ \partial_t \hat{w}_f + v_f^\star \partial_x \hat{w}_f =& \bar{a}_{21}^{ww}\hat{w}_s + \bar{a}_{22}^{ww}\hat{w}_f + \bar{a}_{21}^{wv}(x)\hat{u}_s + \bar{a}_{22}^{wv}(x)\hat{u}_f \\ & + p_{21}(x)\check{w}_s(L,t) + p_{22}(x)\check{w}_f(L,t), && (3.123)\\ \partial_t \hat{u}_s - (\gamma p_s^\star - v_s^\star)\partial_x \hat{u}_s =& \bar{a}_{11}^{vw}(x)\hat{w}_s + \bar{a}_{12}^{vw}(x)\hat{w}_f + \bar{a}_{12}^{vv}(x)\hat{u}_f \\ & + q_{11}(x)\check{w}_s(L,t) + q_{12}(x)\check{w}_f(L,t), && (3.124)\\ \partial_t \hat{u}_f - (\gamma p_f^\star - v_f^\star)\partial_x \hat{u}_f =& \bar{a}_{21}^{vw}(x)\hat{w}_s + \bar{a}_{22}^{vw}(x)\hat{w}_f + \bar{a}_{21}^{vv}(x)\hat{u}_s \\ & + q_{21}(x)\check{w}_s(L,t) + q_{22}(x)\check{w}_f(L,t), && (3.125)\\ \hat{w}_s(0,t) =& k_s\hat{u}_s(0,t), && (3.126)\\ \hat{w}_f(0,t) =& k_f\hat{u}_f(0,t), && (3.127)\\ \hat{u}_s(L,t) =& l_s U_s(t), && (3.128)\\ \hat{u}_f(L,t) =& l_f U_f(t). && (3.129) \end{aligned}$$

The output injections in (3.122)-(3.125) are defined as

$$\check{w}_s(L,t) = \tilde{w}_s(L,t) - \hat{w}_s(L,t), \tag{3.130}$$

$$\check{w}_f(L,t) = \tilde{w}_f(L,t) - \hat{w}_f(L,t). \tag{3.131}$$

The observer output injection gains matrices $\{P\}$ and $\{Q\}$ are denoted as

$$P = \begin{bmatrix} p_{11} & p_{12} \\ p_{21} & p_{22} \end{bmatrix}, \quad Q = \begin{bmatrix} q_{11} & q_{12} \\ q_{21} & q_{22} \end{bmatrix}. \tag{3.132}$$

The output injection gains are to be designed so that the output injection terms can drive the estimation error system of the observer to converge to zero in finite-time.

The estimation errors are defined as

$$\check{w}_s = \tilde{w}_s - \hat{w}_s, \quad \check{v}_s = \bar{v}_s - \hat{u}_s, \tag{3.133}$$

$$\check{w}_f = \tilde{w}_f - \hat{w}_f, \quad \check{v}_f = \bar{v}_f - \hat{u}_f. \tag{3.134}$$

The error system $(\check{w}_s, \check{w}_f, \check{v}_f, \check{v}_s)$ of the observer is given by subtracting (3.122)-(3.129) from (3.56)-(3.63),

$$\begin{aligned} \partial_t \check{w}_s + v_s^\star \partial_x \check{w}_s = &\bar{a}^{ww}_{11} \check{w}_s + \bar{a}^{ww}_{12} \check{w}_f + \bar{a}^{wv}_{11}(x) \check{v}_s + \bar{a}^{wv}_{12}(x) \check{v}_f \\ &- p_{11}(x) \check{w}_s(L,t) - p_{12}(x) \check{w}_f(L,t), \end{aligned} \tag{3.135}$$

$$\begin{aligned} \partial_t \check{w}_f + v_f^\star \partial_x \check{w}_f = &\bar{a}^{ww}_{21} \check{w}_s + \bar{a}^{ww}_{22} \check{w}_f + \bar{a}^{wv}_{21}(x) \check{v}_s + \bar{a}^{wv}_{22}(x) \check{v}_f, \\ &- p_{21}(x) \check{w}_s(L,t) - p_{22}(x) \check{w}_f(L,t), \end{aligned} \tag{3.136}$$

$$\begin{aligned} \partial_t \check{v}_s - (\gamma p_s^\star - v_s^\star) \partial_x \check{v}_s = &\bar{a}^{vw}_{11}(x) \check{w}_s + \bar{a}^{vw}_{12}(x) \check{w}_f + \bar{a}^{vv}_{12}(x) \check{v}_f \\ &- q_{11}(x) \check{w}_s(L,t) - q_{12}(x) \check{w}_f(L,t), \end{aligned} \tag{3.137}$$

$$\begin{aligned}\partial_t \check{v}_f - (\gamma p_f^\star - v_f^\star)\partial_x \check{v}_f =& \bar{a}_{21}^{vw}(x)\check{w}_s + \bar{a}_{22}^{vw}(x)\check{w}_f + \bar{a}_{21}^{vv}(x)\check{v}_s,\\ &- q_{21}(x)\check{w}_s(L,t) - q_{22}(x)\check{w}_f(L,t),\end{aligned} \tag{3.138}$$

$$\check{w}_s(0,t) = k_s\check{v}_s(0,t), \tag{3.139}$$

$$\check{w}_f(0,t) = k_f\check{v}_f(0,t), \tag{3.140}$$

$$\check{v}_s(L,t) = 0, \tag{3.141}$$

$$\check{v}_f(L,t) = 0, \tag{3.142}$$

We apply the backstepping transformation to the error system given by

$$\begin{bmatrix}\check{w}_s(x,t)\\ \check{w}_f(x,t)\end{bmatrix} = \begin{bmatrix}\check{\alpha}_s(x,t)\\ \check{\alpha}_f(x,t)\end{bmatrix} + \int_x^L M(x,\xi)\begin{bmatrix}\check{\alpha}_s(\xi,t)\\ \check{\alpha}_f(\xi,t)\end{bmatrix} d\xi, \tag{3.143}$$

$$\begin{bmatrix}\check{v}_s(x,t)\\ \check{v}_f(x,t)\end{bmatrix} = \begin{bmatrix}\check{\beta}_s(x,t)\\ \check{\beta}_f(x,t)\end{bmatrix} + \int_x^L N(x,\xi)\begin{bmatrix}\check{\alpha}_s(\xi,t)\\ \check{\alpha}_f(\xi,t)\end{bmatrix} d\xi, \tag{3.144}$$

where the kernel matrices $\{M\}$, $\{N\}$ are denoted as

$$M = \begin{bmatrix}M_{11} & M_{12}\\ M_{21} & M_{22}\end{bmatrix}, \quad N = \begin{bmatrix}N_{11} & N_{12}\\ N_{21} & N_{22}\end{bmatrix}. \tag{3.145}$$

The kernels $\{M\}$, $\{N\}$ evolve in the triangular domain $\mathscr{T} = \{(x,\xi) : 0 \leq x \leq \xi \leq L\}$ and are defined later. We map the error system in (3.135)-(3.142) into the following cascade target system

$$\begin{aligned}\partial_t \check{\alpha}_s + v_s^\star \partial_x \check{\alpha}_s =& \bar{a}_{11}^{ww}\check{\alpha}_s + \bar{a}_{11}^{wv}(x)\check{\beta}_s + \bar{a}_{12}^{wv}(x)\check{\beta}_f\\ &+ \int_x^L d_{11}(x,\xi)\check{\beta}_s(\xi)d\xi + \int_x^L d_{12}(x,\xi)\check{\beta}_f(\xi)d\xi,\end{aligned} \tag{3.146}$$

$$\partial_t \check{\alpha}_f + v_f^\star \partial_x \check{\alpha}_f = \bar{a}_{22}^{ww}\check{\alpha}_f + \bar{a}_{21}^{wv}(x)\check{\beta}_s + \bar{a}_{22}^{wv}(x)\check{\beta}_f$$

$$+\int_x^L d_{21}(x,\xi)\check{\beta}_s(\xi)d\xi+\int_x^L d_{22}(x,\xi)\check{\beta}_f(\xi)d\xi, \tag{3.147}$$

$$\begin{aligned}\partial_t\check{\beta}_s-(\gamma p_s^\star-v_s^\star)\partial_x\check{\beta}_s =&\bar{a}_{12}^{vv}(x)\check{\beta}_f\\ &+\int_x^L f_{11}(x,\xi)\check{\beta}_s(\xi)d\xi+\int_x^L f_{12}(x,\xi)\check{\beta}_f(\xi)d\xi,\end{aligned} \tag{3.148}$$

$$\begin{aligned}\partial_t\check{\beta}_f-(\gamma p_f^\star-v_f^\star)\partial_x\check{\beta}_f =&\bar{a}_{21}^{vv}(x)\check{\beta}_s\\ &+\int_x^L f_{21}(x,\xi)\check{\beta}_s(\xi)d\xi+\int_x^L f_{22}(x,\xi)\check{\beta}_f(\xi)d\xi,\end{aligned} \tag{3.149}$$

$$\check{\alpha}_s(0,t) =k_s\check{\beta}_s(0,t), \tag{3.150}$$

$$\check{\alpha}_f(0,t) =k_f\check{\beta}_f(0,t)-\int_0^L \lambda(x)\check{\alpha}_s(x,t)d\xi, \tag{3.151}$$

$$\check{\beta}_s(L,t) =0, \tag{3.152}$$

$$\check{\beta}_f(L,t) =0, \tag{3.153}$$

where the coefficient matrices $\{D\}$ and $\{F\}$ are denoted as

$$D=\begin{bmatrix} d_{11} & d_{12}\\ d_{21} & d_{22}\end{bmatrix}, \quad F=\begin{bmatrix} f_{11} & f_{12}\\ f_{21} & f_{22}\end{bmatrix}. \tag{3.154}$$

and given by

$$D(x,\xi)=-M(x,\xi)\bar{A}^{wv}+\int_\xi^x M(x,s)D(s,\xi)d\xi, \tag{3.155}$$

$$F(x,\xi)=-N(x,\xi)\bar{A}^{ww}+\int_\xi^x N(x,s)F(s,\xi)d\xi. \tag{3.156}$$

The spatially varying coefficient $\lambda(x)$ is obtained from the kernel variables

$$\lambda(x)=M_{21}(0,x)-k_fN_{21}(0,x). \tag{3.157}$$

Lemma 3.3. *Consider the target system* (3.146)-(3.149) *with the boundary conditions* (3.150)-

(3.153). *The zero equilibrium is reached in finite time $t = t_o$, where*

$$t_o = \frac{L}{v_s^\star} + \frac{L}{v_f^\star} + \frac{L}{\gamma p_f^\star - v_f^\star}. \tag{3.158}$$

Proof. Noting the cascade structure of $\check{\alpha}_s$, $\check{\alpha}_f$ and $\check{\beta}_s$, $\check{\beta}_f$ system, $\check{\beta}$ variables appear as the right hand source terms in $\check{\alpha}$ equations and through the inlet boundaries. The integral of variable $\check{\alpha}_s$ enters the boundary condition of $\check{\alpha}_f$. Therefore we solve the target system explicitly by recursion. The $\check{\beta}$-system is independent of the $\check{\alpha}$ system. Given the boundary conditions in (3.152), (3.153), the explicit solutions hold for $\check{\beta}_s$ and $\check{\beta}_f$ after $t > \frac{1}{\gamma p_f^\star - v_f^\star}$,

$$\check{\beta}_s(x,t) \equiv 0, \quad \check{\beta}_f(x,t) \equiv 0. \tag{3.159}$$

When $t > \frac{1}{\gamma p_f^\star - v_f^\star}$, $\check{\alpha}$-system becomes

$$\partial_t \check{\alpha}_s + v_s^\star \partial_x \check{\alpha}_s = \bar{a}_{11}^{ww} \check{\alpha}_s, \tag{3.160}$$

$$\partial_t \check{\alpha}_f + v_f^\star \partial_x \check{\alpha}_f = \bar{a}_{22}^{ww} \check{\alpha}_f, \tag{3.161}$$

$$\check{\alpha}_s(0,t) = 0, \tag{3.162}$$

$$\check{\alpha}_f(0,t) = -\int_0^L \lambda(x) \check{\alpha}_s(x,t) d\xi. \tag{3.163}$$

After $t > \frac{1}{v_s^\star} + \frac{1}{\gamma p_f^\star - v_f^\star}$, we have $\check{\alpha}_s$ satisfies

$$\check{\alpha}_s(x,t) \equiv 0. \tag{3.164}$$

Then $\check{\alpha}_f(x,t) \equiv 0$ follows after another time period $\frac{1}{v_f^\star}$. Therefore, $\check{\alpha}$-system eventually identically vanishes for

$$t_o = \frac{1}{v_s^\star} + \frac{1}{v_f^\star} + \frac{1}{\gamma p_f^\star - v_f^\star}, \tag{3.165}$$

which concludes the proof. $\square$

Taking spatial and temporal derivatives of the backstepping transformation (3.143),(3.144) along the target system (3.146)-(3.153), then plugging into the error system (3.135)-(3.142), we obtain the kernel equations that govern the kernels $\{M(x,\xi)\}$ and $\{N(x,\xi)\}$,

$$\varepsilon_1\partial_x M_{11} + \varepsilon_1\partial_\xi M_{11} = -\bar{a}^{ww}_{12}M_{21} - \bar{a}^{wv}_{11}N_{11} - \bar{a}^{wv}_{12}N_{21}, \tag{3.166}$$

$$\varepsilon_1\partial_x M_{12} + \varepsilon_2\partial_\xi M_{12} = -\bar{a}^{ww}_{11}M_{12} - \bar{a}^{ww}_{12}M_{22} - \bar{a}^{wv}_{11}N_{12} - \bar{a}^{wv}_{12}N_{22}, \tag{3.167}$$

$$\varepsilon_2\partial_x M_{21} + \varepsilon_1\partial_\xi M_{21} = -\bar{a}^{ww}_{21}M_{11} - \bar{a}^{ww}_{22}M_{21} - \bar{a}^{wv}_{21}N_{11} - \bar{a}^{wv}_{22}N_{21}, \tag{3.168}$$

$$\varepsilon_2\partial_x M_{22} + \varepsilon_2\partial_\xi M_{22} = -\bar{a}^{ww}_{21}M_{12} - \bar{a}^{wv}_{21}N_{12} - \bar{a}^{wv}_{22}N_{22}, \tag{3.169}$$

$$\mu_1\partial_x N_{11} - \varepsilon_1\partial_\xi N_{11} = \bar{a}^{ww}_{11}N_{11} + \bar{a}^{vv}_{12}N_{21} + \bar{a}^{vw}_{11}M_{11} + \bar{a}^{vw}_{12}M_{21}, \tag{3.170}$$

$$\mu_1\partial_x N_{12} - \varepsilon_2\partial_\xi N_{12} = \bar{a}^{ww}_{22}N_{12} + \bar{a}^{vv}_{12}N_{22} + \bar{a}^{vw}_{11}M_{12} + \bar{a}^{vw}_{12}M_{22}, \tag{3.171}$$

$$\mu_2\partial_x N_{21} - \varepsilon_1\partial_\xi N_{21} = \bar{a}^{ww}_{11}N_{21} + \bar{a}^{vv}_{21}N_{11} + \bar{a}^{vw}_{21}M_{11} + \bar{a}^{vw}_{22}M_{21}, \tag{3.172}$$

$$\mu_2\partial_x N_{22} - \varepsilon_2\partial_\xi N_{22} = \bar{a}^{ww}_{22}N_{22} + \bar{a}^{vv}_{21}N_{12} + \bar{a}^{vw}_{21}M_{12} + \bar{a}^{vw}_{22}M_{22}, \tag{3.173}$$

$$N_{11}(x,x) = \frac{\bar{a}^{vw}_{11}(x)}{\varepsilon_1+\mu_1}, \quad N_{12}(x,x) = \frac{\bar{a}^{vw}_{12}(x)}{\varepsilon_2+\mu_1}, \tag{3.174}$$

$$N_{21}(x,x) = \frac{\bar{a}^{vw}_{21}(x)}{\varepsilon_1+\mu_2}, \quad N_{22}(x,x) = \frac{\bar{a}^{vw}_{22}(x)}{\varepsilon_2+\mu_2}, \tag{3.175}$$

$$M_{11}(0,\xi) = k_s N_{11}(0,\xi), \quad M_{22}(0,\xi) = k_f N_{22}(0,\xi), \tag{3.176}$$

$$M_{12}(0,\xi) = k_s N_{12}(0,\xi), \quad M_{21}(x,x) = -\frac{\bar{a}^{ww}_{21}}{\varepsilon_2-\varepsilon_1}, \tag{3.177}$$

$$M_{21}(x,L) = -\frac{\bar{a}^{ww}_{21}}{\varepsilon_2-\varepsilon_1}, \quad M_{12}(x,x) = -\frac{\bar{a}^{ww}_{12}}{\varepsilon_1-\varepsilon_2}. \tag{3.178}$$

Considering the following variables by defining

$$\bar{x} = L - x, \quad \bar{\xi} = L - \xi, \tag{3.179}$$

and new kernels $\bar{M}\left(\bar{x},\bar{\xi}\right)$ and $\bar{N}\left(\bar{x},\bar{\xi}\right)$

$$\bar{M}\left(\bar{x},\bar{\xi}\right) = M(L-\bar{x},L-\bar{\xi}) = M(x,\xi), \tag{3.180}$$

$$\bar{N}\left(\bar{x},\bar{\xi}\right) = N(L-\bar{x},L-\bar{\xi}) = N(x,\xi), \tag{3.181}$$

which are defined in the triangular domain $\mathscr{D} = \{(\bar{x},\bar{\xi}) : 0 \leq \bar{\xi} \leq \bar{x} \leq L\}$. We find that the following kernel equations obtained from (3.166) and (3.178) have the same structure with the controller kernel system in (3.83)-(3.95).

$$\varepsilon_1 \partial_{\bar{x}} \bar{M}_{11} + \varepsilon_1 \partial_{\bar{\xi}} \bar{M}_{11} = \bar{a}^{ww}_{12} \bar{M}_{21} + \bar{a}^{wv}_{11} \bar{N}_{11} + \bar{a}^{wv}_{12} \bar{N}_{21}, \tag{3.182}$$

$$\varepsilon_1 \partial_{\bar{x}} \bar{M}_{12} + \varepsilon_2 \partial_{\bar{\xi}} \bar{M}_{12} = \bar{a}^{ww}_{11} \bar{M}_{12} + \bar{a}^{ww}_{12} \bar{M}_{22} + \bar{a}^{wv}_{11} \bar{N}_{12} + \bar{a}^{wv}_{12} \bar{N}_{22}, \tag{3.183}$$

$$\varepsilon_2 \partial_{\bar{x}} \bar{M}_{21} + \varepsilon_1 \partial_{\bar{\xi}} \bar{M}_{21} = \bar{a}^{ww}_{21} \bar{M}_{11} + \bar{a}^{ww}_{22} \bar{M}_{21} + \bar{a}^{wv}_{21} \bar{N}_{11} + \bar{a}^{wv}_{22} \bar{N}_{21}, \tag{3.184}$$

$$\varepsilon_2 \partial_{\bar{x}} \bar{M}_{22} + \varepsilon_2 \partial_{\bar{\xi}} \bar{M}_{22} = \bar{a}^{ww}_{21} \bar{M}_{12} + \bar{a}^{wv}_{21} \bar{N}_{12} + \bar{a}^{wv}_{22} \bar{N}_{22}, \tag{3.185}$$

$$\mu_1 \partial_{\bar{x}} \bar{N}_{11} - \varepsilon_1 \partial_{\bar{\xi}} \bar{N}_{11} = -\bar{a}^{ww}_{11} \bar{N}_{11} - \bar{a}^{vv}_{12} \bar{N}_{21} - \bar{a}^{vw}_{11} \bar{M}_{11} - \bar{a}^{vw}_{12} \bar{M}_{21}, \tag{3.186}$$

$$\mu_1 \partial_{\bar{x}} \bar{N}_{12} - \varepsilon_2 \partial_{\bar{\xi}} \bar{N}_{12} = -\bar{a}^{ww}_{22} \bar{N}_{12} - \bar{a}^{vv}_{12} \bar{N}_{22} - \bar{a}^{vw}_{11} \bar{M}_{12} - \bar{a}^{vw}_{12} \bar{M}_{22}, \tag{3.187}$$

$$\mu_2 \partial_{\bar{x}} \bar{N}_{21} - \varepsilon_1 \partial_{\bar{\xi}} \bar{N}_{21} = -\bar{a}^{ww}_{11} \bar{N}_{21} - \bar{a}^{vv}_{21} \bar{N}_{11} - \bar{a}^{vw}_{21} \bar{M}_{11} - \bar{a}^{vw}_{22} \bar{M}_{21}, \tag{3.188}$$

$$\mu_2 \partial_{\bar{x}} \bar{N}_{22} - \varepsilon_2 \partial_{\bar{\xi}} N_{22} = -\bar{a}^{ww}_{22} \bar{N}_{22} - \bar{a}^{vv}_{21} \bar{N}_{12} - \bar{a}^{vw}_{21} \bar{M}_{12} - \bar{a}^{vw}_{22} \bar{M}_{22}, \tag{3.189}$$

$$\bar{N}_{11}(\bar{x},\bar{x}) = \frac{\bar{a}^{vw}_{11}(L-\bar{x})}{\varepsilon_1 + \mu_1}, \quad \bar{N}_{12}(\bar{x},\bar{x}) = \frac{\bar{a}^{vw}_{12}(L-\bar{x})}{\varepsilon_2 + \mu_1}, \tag{3.190}$$

$$\bar{N}_{21}(\bar{x},\bar{x}) = \frac{\bar{a}^{vw}_{21}(L-\bar{x})}{\varepsilon_1 + \mu_2}, \quad \bar{N}_{22}(\bar{x},\bar{x}) = \frac{\bar{a}^{vw}_{22}(L-\bar{x})}{\varepsilon_2 + \mu_2}, \tag{3.191}$$

$$\bar{M}_{11}(L,\bar{\xi}) = k_s \bar{N}_{11}(L,\bar{\xi}), \quad \bar{M}_{22}(L,\bar{\xi}) = k_f \bar{N}_{22}(L,\bar{\xi}), \tag{3.192}$$

$$\bar{M}_{12}(L,\bar{\xi}) = k_s \bar{N}_{12}(L,\bar{\xi}), \quad \bar{M}_{21}(\bar{x},\bar{x}) = -\frac{\bar{a}^{ww}_{21}}{\varepsilon_2 - \varepsilon_1}, \tag{3.193}$$

$$\bar{M}_{21}(\bar{x},0) = 0, \quad \bar{M}_{12}(\bar{x},\bar{x}) = -\frac{\bar{a}^{ww}_{12}}{\varepsilon_1 - \varepsilon_2}. \tag{3.194}$$

The well-posedness of the above kernel system is obtained following the same steps of the proof for (3.83)-(3.95). Therefore, there exists a unique solution $M,N \in L^\infty(\mathscr{T})$. The stability of target system (3.146)-(3.153) is equivalent to the error system (3.135)-(3.142). The artificial boundary condition $\bar{M}_{21}(\bar{x},0)$ in (3.95) is imposed for the well-posedness of the kernel equations.

The observer gains matrices $\{P(x)\}$ and $\{Q(x)\}$ are obtained from the kernel matrices

$$P(x) = M(x,L)\begin{bmatrix} v_s^\star & 0 \\ 0 & v_f^\star \end{bmatrix}, \tag{3.195}$$

$$Q(x) = N(x,L)\begin{bmatrix} v_s^\star & 0 \\ 0 & v_f^\star \end{bmatrix}. \tag{3.196}$$

Note that the states estimation of the original traffic flow variables $(\hat{\rho}_f, \hat{v}_f, \hat{\rho}_s, \hat{v}_s)$ are obtained by the invertible transformation given in the following,

$$\hat{\rho}_s = \rho_s^\star + \frac{\rho_s^\star}{\gamma p_s^\star}\left(\hat{w}_s - \exp\left(-\frac{a_{11}^{vv}}{\mu_1}x\right)\hat{u}_s\right), \tag{3.197}$$

$$\hat{\rho}_f = \rho_f^\star + \frac{\rho_f^\star}{\gamma p_f^\star}\left(\hat{w}_f - \exp\left(-\frac{a_{22}^{vv}}{\mu_2}x\right)\hat{u}_f\right), \tag{3.198}$$

$$\hat{v}_s = v_s^\star + \exp\left(-\frac{a_{11}^{vv}}{\mu_1}x\right)\hat{u}_s, \tag{3.199}$$

$$\hat{v}_f = v_f^\star + \exp\left(-\frac{a_{22}^{vv}}{\mu_2}x\right)\hat{u}_f. \tag{3.200}$$

Therefore, the state estimates $(\hat{w}_f, \hat{w}_s, \hat{u}_s, \hat{u}_f)$ can be transformed into the state estimates $(\hat{\rho}_f, \hat{v}_f,$ $\hat{\rho}_s, \hat{v}_s)$. The following conclusion is reached.

Theorem 3.4. *Consider the two-lane traffic ARZ model in* (3.1)-(3.4) *with boundary conditions* (3.19)-(3.22)*, initial conditions* $\rho_f(x,0), v_f(x,0), \rho_s(x,0), v_s(x,0) \in L^\infty([0,L])$*, state estimates* $(\hat{\rho}_s(x,t), \hat{\rho}_f(x,t), \hat{v}_s(x,t), \hat{v}_f(x,t))$ *are obtained from collocated observer design* (3.122)-(3.129) *for* $(\hat{w}_s, \hat{w}_f, \hat{v}_s, \hat{v}_f)$ *and the invertible transformation between them is given in* (3.197)-(3.200).

The output injection gains $\{P(x)\}$ *and* $\{Q(x)\}$ *are obtained in* (3.195), (3.196) *by solving the kernels* $\{M\}$ *and* $\{N\}$ *from* (3.166)-(3.178). *The finite-time convergence of estimation errors to zero equilibrium is reached in* t_o *given by* (3.158).

Proof. Lemma 3.3 with the existence of the backstepping transformation for the observer in (3.143), (3.144) yields the convergence of estimation errors $(\check{w}_s, \check{w}_f, \check{v}_s, \check{v}_f)$ defined by (3.135)-(3.142) to zero for $t > t_o$. Given the transformation in (3.197)-(3.200), the finite-time convergence to zero equilibrium is arrived for the estimation errors $(\tilde{\rho}_s(x,t), \tilde{\rho}_f(x,t), \tilde{v}_s(x,t), \tilde{v}_f(x,t))$. $\square$

3.4 Output feedback controller

The output feedback controllers are constructed by employing the states estimates in the full-state feedback laws which yield the finite-time stability of the closed-loop system to zero equilibrium. Combining the collocated observer design (3.122)-(3.129) and full-state feedback controllers (3.114),(3.115), we obtain the following output feedback controllers,

$$
\begin{aligned}
U_s(t) = & \exp\left(-\frac{a_{11}^{vv}}{\mu_1}L\right)\int_0^L \frac{\gamma p_s^\star}{\rho_s^\star} K_{11}(L,\xi)\left(\hat{\rho}_s(\xi,t) - \rho_s^\star\right) \\
& + \frac{\gamma p_f^\star}{\rho_f^\star} K_{12}(L,\xi)\left(\hat{\rho}_f(\xi,t) - \rho_f^\star\right) \\
& + \left[K_{11}(L,\xi) + L_{11}(L,\xi)\exp\left(\frac{a_{11}^{vv}}{\mu_1}\xi\right)\right]\left(\hat{v}_s(\xi,t) - v_s^\star\right) \\
& + \left[K_{12}(L,\xi) + L_{12}(L,\xi)\exp\left(\frac{a_{22}^{vv}}{\mu_2}\xi\right)\right]\left(\hat{v}_f(\xi,t) - v_f^\star\right)d\xi, \qquad (3.201) \\
U_f(t) = & \exp\left(-\frac{a_{22}^{vv}}{\mu_2}L\right)\int_0^L \frac{\gamma p_s^\star}{\rho_s^\star} K_{21}(L,\xi)\left(\hat{\rho}_s(\xi,t) - \rho_s^\star\right) \\
& + \frac{\gamma p_f^\star}{\rho_f^\star} K_{22}(L,\xi)\left(\hat{\rho}_f(\xi,t) - \rho_f^\star\right) \\
& + \left[K_{21}(L,\xi) + L_{21}(L,\xi)\exp\left(\frac{a_{11}^{vv}}{\mu_1}\xi\right)\right]\left(\hat{v}_s(\xi,t) - v_s^\star\right)
\end{aligned}
$$

$$+\left[K_{22}(L,\xi)+L_{22}(L,\xi)\exp\left(\frac{a_{22}^{vv}}{\mu_2}\xi\right)\right]\left(\hat{v}_f(\xi,t)-v_f^\star\right)d\xi, \tag{3.202}$$

where $(\hat{\rho}_f, \hat{\rho}_s, \hat{v}_s, \hat{v}_f)$ are obtained from $(\hat{w}_s, \hat{w}_f, \hat{v}_s, \hat{v}_f)$ using transformation in (3.197)-(3.200).

Theorem 3.5. *Consider the two-lane traffic ARZ model in* (3.1)-(3.4) *with boundary conditions* (3.19)-(3.22)*, initial conditions* $\rho_f(x,0), v_f(x,0), \rho_s(x,0), v_s(x,0) \in L^\infty([0,L])$ *and the output feedback laws in* (3.201),(3.202)*, where the kernels* $\{K\}$ *and* $\{L\}$ *are obtained by solving* (3.83)-(3.95) *and output injection gains obtained by solving the kernels* $\{M\}$ *and* $\{N\}$ *in* (3.166)-(3.173)*. The steady states* $(\rho_f^\star, v_f^\star, \rho_s^\star, v_s^\star)$ *are finite-time stable and the convergence is reached in* t_{out} *defined as*

$$t_{\text{out}} = t_o + t_f, \tag{3.203}$$

where t_o *is given in* (3.158) *and* t_f *in* (3.109).

Proof. Theorem 3.3 yields that state estimates $(\hat{\rho}_f, \hat{\rho}_s, \hat{v}_s, \hat{v}_f)$ converge to $(\rho_f, \rho_s, v_s, v_f)$ after $t = t_o$. Applying Theorem 3.2, one has that $(\rho_f, \rho_s, v_s, v_f)$ converge to $(\rho_f^\star, \rho_s^\star, v_s^\star, v_f^\star)$ after $t = t_f$. Therefore, after $t = t_o + t_f$, we have the convergence of state variables to steady states. □

3.5 Numerical simulation

To validate our control design including the full-state feedback controllers and the collocated boundary observer, we perform the numerical simulation for the two-lane ARZ model under two different secenrios of traffic congestion. For the first scenario, we consider the stop-and-go traffic appearing in the freeway segment of interest and therefore implement sinusoid initial conditions. For second scenario, we consider a single shock wave front for the initial state of traffic where the upstream vehicles are blocked by denser traffic downstream. This is a common phenomenon when slow moving vehicles block the road or changes of local road

Table 3.1: Model Parameter Table

Name	Slow lane	Fast lane	Unit
Freeway segment length L	1000	1000	m
Pressure exponent γ	0.8	0.8	1
Maximum density ρ_i^m	240	150	veh/km
Maximum velocity v_m	144	144	km/h
Steady state densities $\rho_i^\star$	180	80	veh/km
Steady state velocity $v_i^\star$	32	40	km/h
Relaxation time T_i^e	200	100	s
Driver's lane preference T_i	50	25	s

situations like hills and curves. Traffic bottleneck forms as a result. It follows the appearance of a moving shock wave consisting of high-density traffic downstream and relative low-density traffic upstream on the road.

The control design presented in the previous sections are tested and illustrated for both secenrios. The model parameters used in the numerical simulation are given in Table 3.1. Both the fast-lane and slow-lane are considered in the congested regime where the vehicles on the road are relatively dense so that the velocity disturbances propagate from the leading vehicle to the following vehicle. Steady states density $\rho_i^\star$ are chosen given the maximum density ρ_i^m and Maximum velocity v_m so that the traffic of both lanes are lightly congested. We consider the situation that in general drivers prefer the slow lane rather than the fast lane. T_f is smaller than T_s since drivers prefer remaining in the slow lane rather than changing to the fast lane. Therefore, higher density traffic appears in the slow lane and it can contain higher traffic flow. Steady state velocity $v_i^\star$ are obtained based on this parameter choice.

In the following figures, the evolution of the state variables are illustrated with surface plots. The initial conditions of the states are highlighted with color blue and the outlet boundary control inputs are highlighted with color red.

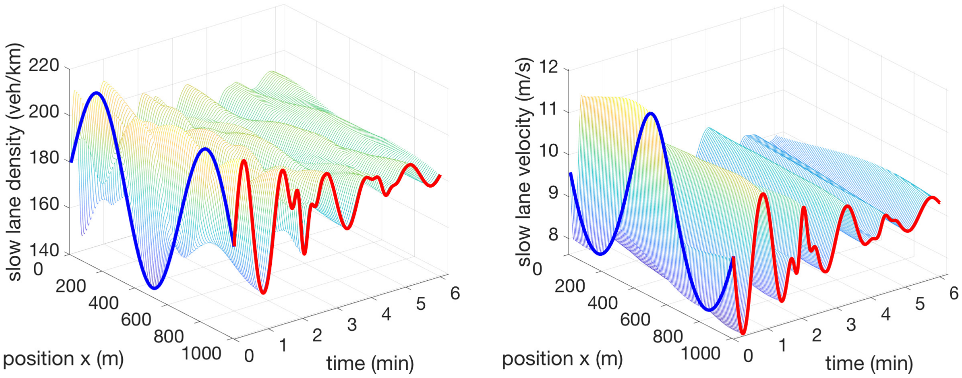

Figure 3.4: Scenario 1: density and velocity of slow lane traffic of open-loop system with sinusoid initial conditions.

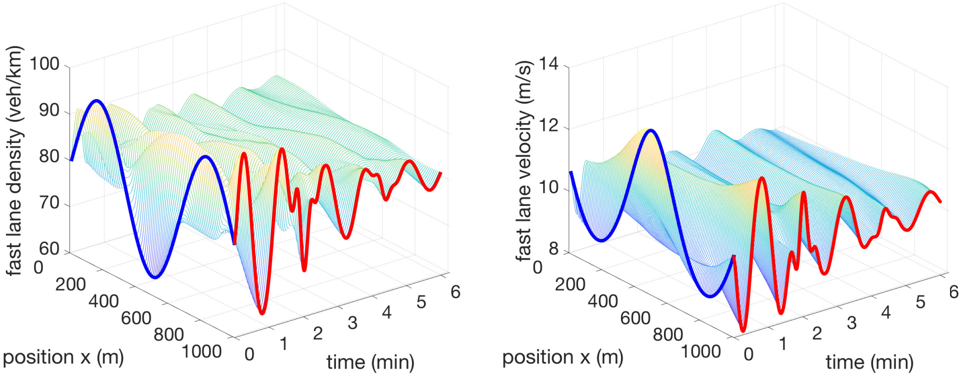

Figure 3.5: Scenario 1: density and velocity of fast lane traffic of open-loop system with sinusoid initial conditions.

3.5.1 Scenario 1: stop-and-go traffic

In this scenario, we consider the initial traffic states are oscillated around the equilibrium states and thus we implement sinusoid initial conditions for traffic density and velocity. The constant incoming flow and outgoing flow are considered for the open-loop simulation as shown in Fig. 3.4 and Fig. 3.5. For the steady state velocity, it takes around 100 s for both fast-lane and slow-lane vehicles to leave the considered freeway segment. But the oscillations sustain for more than 6 min.

The full state feedback stabilization results are shown in Fig. 3.6 and Fig. 3.7. The finite-

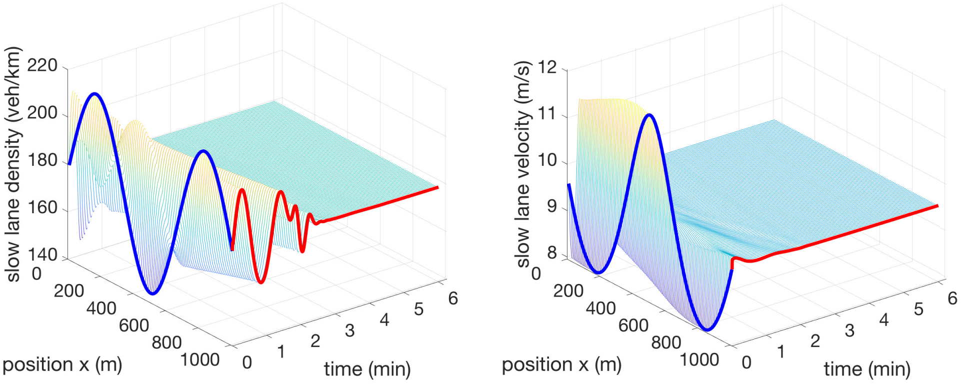

Figure 3.6: Scenario 1: density and velocity of slow lane traffic of closed-loop system with full-state feedback controllers.

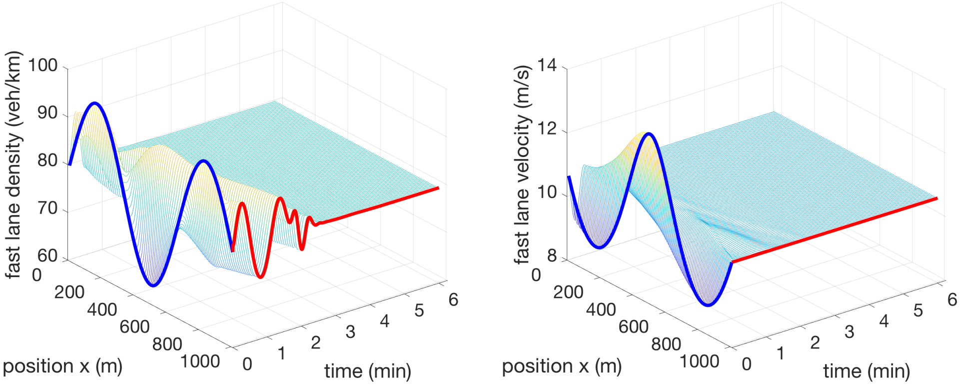

Figure 3.7: Scenario 1: density and velocity of fast lane traffic of closed-loop system with full-state feedback controllers.

time convergence of the density and velocity states to the steady states is achieved in $t_f = 260$ s.

The simulation results of the collocated observer design is shown in Fig. 3.8 and Fig. 3.9. The estimation errors are plotted in Fig. 3.10 and Fig. 3.11. Here we choose open-loop system to validate observer design since the oscillations are not damped out to zero by control design and therefore estimation result could be illustrated better in this case. Without knowledge of the initial state of the system, we implement uniform steady state value for initial conditions, highlighted with blue lines. From Fig. 3.10 and Fig. 3.11, we can see that after $t_o = 310$ s, the estimation errors converge to zero, indicating that the state estimates in Fig. 3.8 and Fig. 3.9

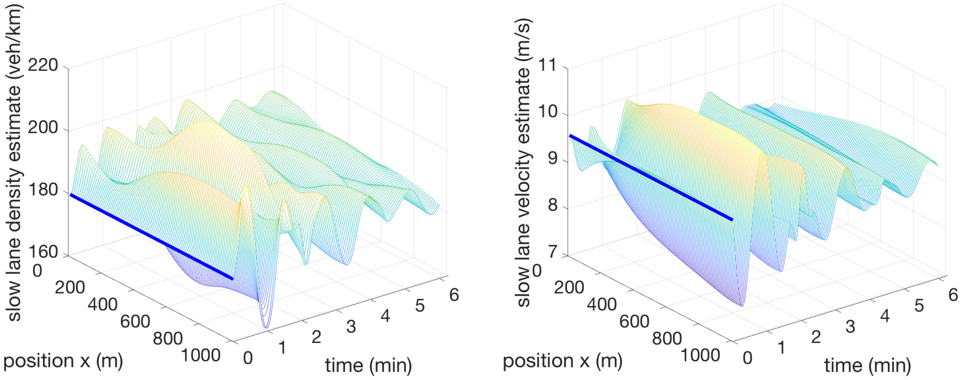

Figure 3.8: Scenario 1: density and velocity estimates of slow lane traffic of open-loop system with sinusoid initial conditions.

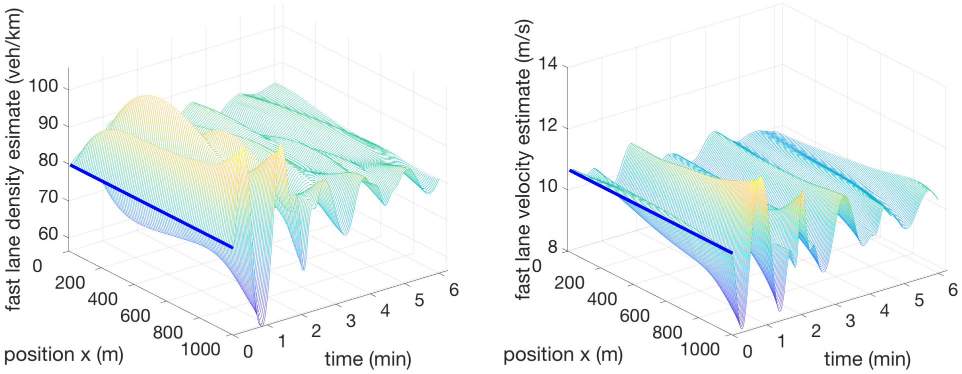

Figure 3.9: Scenario 1: density and velocity estimates of fast lane traffic of open-loop system with sinusoid initial conditions.

converge to the open-loop simulation of the states in Fig. 3.4 and Fig. 3.5.

Combining the observer design and the full-state feedback controllers, we derive the output feedback controllers and then simulate the closed-loop system in Fig. 3.12 and Fig. 3.13. The finite convergence time of the closed-loop with output feedback controllers are $t = t_o + t_f =$ 570s. It is shown in the figures that the states converge to the steady state values before 10 min.

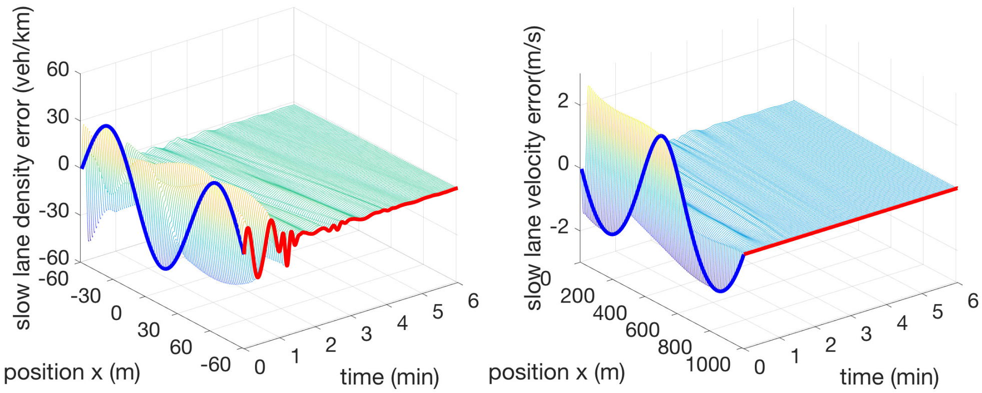

Figure 3.10: Scenario 1: density and velocity estimation errors of slow lane traffic of closed-loop system with full-state feedback controllers.

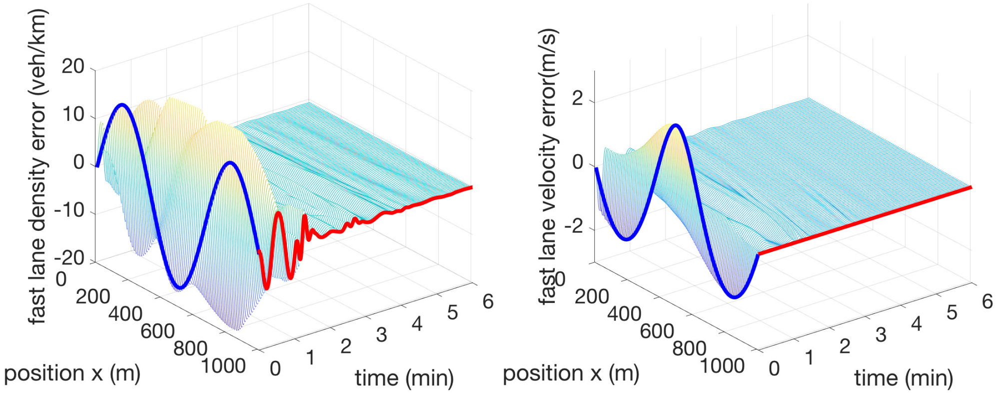

Figure 3.11: Scenario 1: density and velocity estimation errors of fast lane traffic of open-loop system with full-state feedback controllers.

3.5.2 Scenario 2: traffic bottleneck

Consider in Scenario 2 that there are some local changes of road situations like uphill and downhill gradients, curves downstream of the freeway segment. Therefore, traffic bottleneck forms from the downstream. We implement a shockwave front shape of the initial conditions for the slow-lane where traffic densities close to the outlet of the segment are denser and light densities traffic is blocked at the upstream. As a result, the traffic velocity is faster near the inlet while the velocity become slower near the outlet. On the other hand, we consider for the fast-lane that there is traffic flow of high density entering from the inlet. In general, drivers prefer the

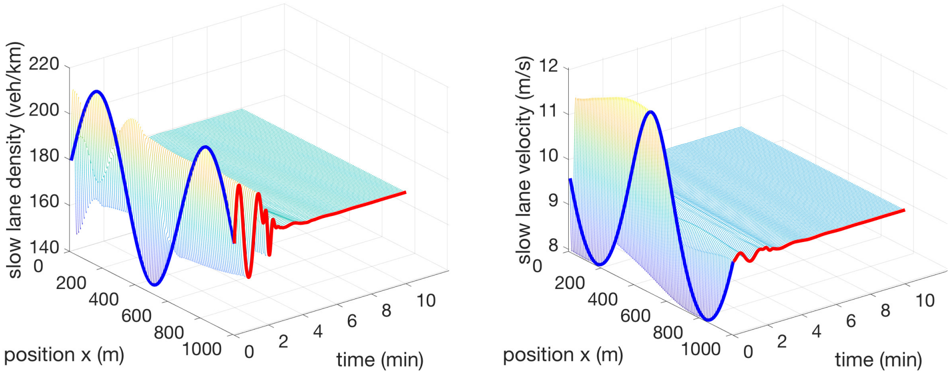

Figure 3.12: Scenario 1: density and velocity of slow lane closed-loop system with output feedback controllers.

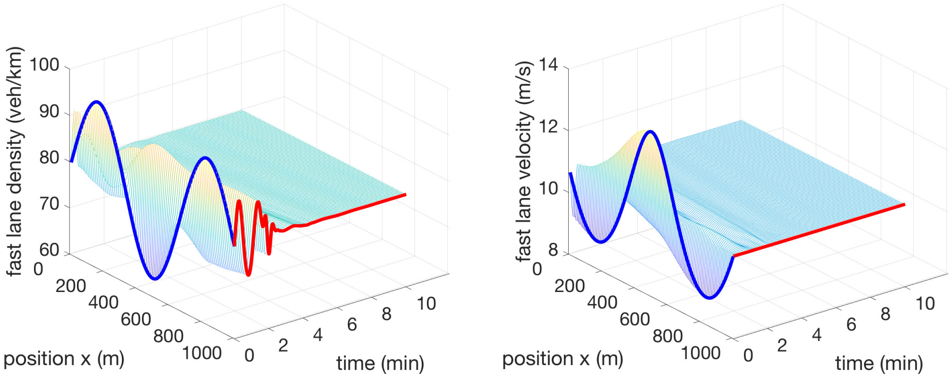

Figure 3.13: Scenario 1: density and velocity of fast lane closed-loop system with output feedback controllers.

slow lane and the relative light traffic flow close to the inlet will trigger the lane-changing from the fast lane to slow lane close to the inlet. This worsens the traffic congestion on the slow lane since the traffic bottleneck appears in the downstream of slow lane.

In the open-loop simulation shown by Fig. 3.14 and Fig. 3.15, soft shock wave initial traffic states result in the stop-and-go traffic on the freeway segment. Here we omit the state estimation results by collocated observer which has been demonstrated in Scenario 1. The simulation result of the output feedback control applied to Scenario 2 is given with Fig. 3.16 and Fig. 3.17. We can see that the oscillated traffic congestion of 1km in Fig. 3.14 and Fig. 3.15 is damped out in a fast manner for around 4 min.

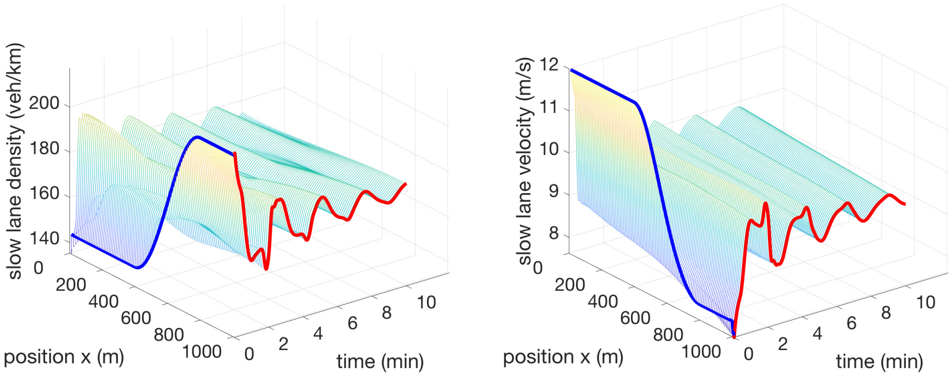

Figure 3.14: Scenario 2: density and velocity of slow lane traffic of open-loop system with shockwave initial conditions.

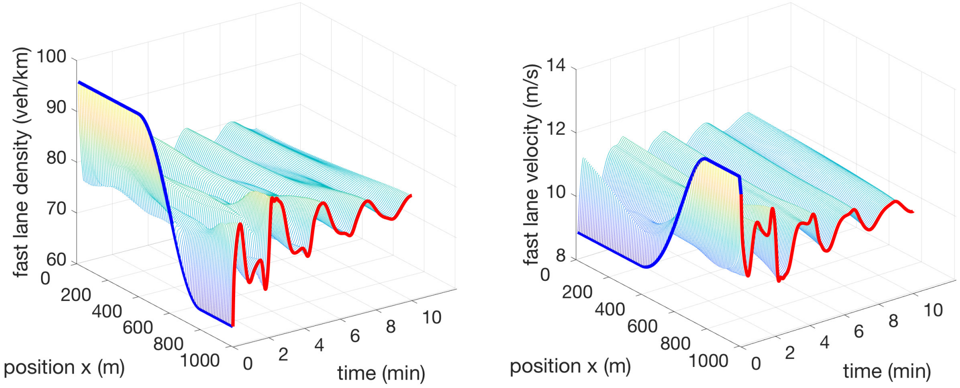

Figure 3.15: Scenario 2: density and velocity of fast lane traffic of open-loop system with shockwave initial conditions.

With the numerical simulation of the two-lane ARZ model with lane changing in two different secenrios, we demonstrate that the full-state feedback controllers, the collocated observer and the output feedback controllers achieve the finite-time convergence of the state variations from the steady states and estimation errors to zero.

3.6 Conclusion

This chapter solves the output feedback stabilization of a two-lane traffic congestion problem with lane-changing. Using coordinate transformation and backstepping method, the

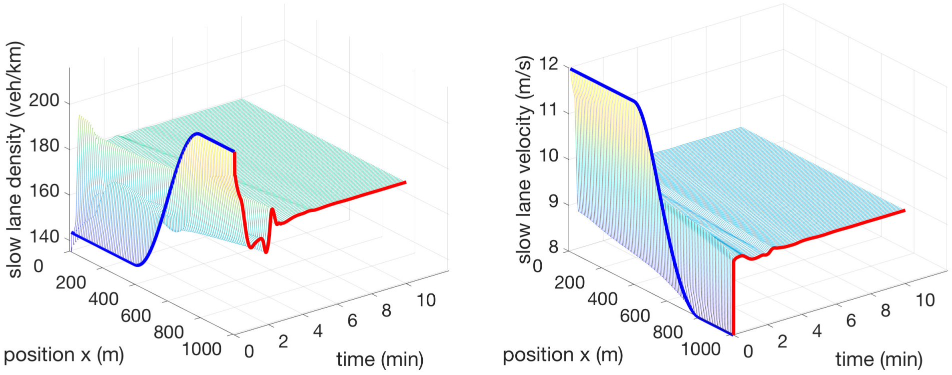

Figure 3.16: Scenario 2: density and velocity of slow lane closed-loop system with output feedback controllers.

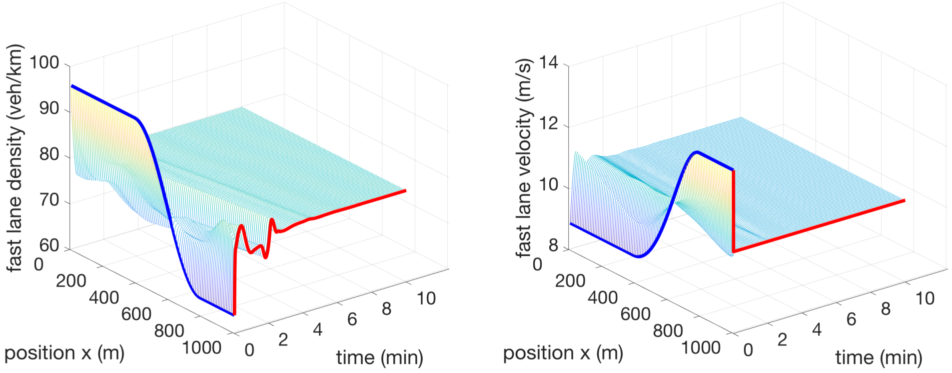

Figure 3.17: Scenario 2: density and velocity of fast lane closed-loop system with output feedback controllers.

linearized first-order coupled 4×4 coupled hyperbolic PDE system is transformed into a cascade target system. The finite-time convergence to the steady states is achieved with two VSLs control inputs actuating velocities at the outlet. By taking measurement of density variations at the outlet, a collocated observer design is proposed for state estimation, which is theoretically novel and practically sound. This result paves the way for applying PDE backstepping techniques for multi-lane traffic with inter-lane activities. There are concerns on modeling the lane-changing as density exchanging source terms. However, the control design and the methodology proposed in this paper should not be limited by possible modifications on these terms.

Chapter 3 contains reprints and adaptations of the following paper: H. Yu and M. Krstic, “Output Feedback Control of Two-lane Traffic Congestion,” *Automatica*, under review. The dissertation author is the primary investigator and author of this paper.

Chapter 4

Two-Class Traffic Congestion Control

This chapter considers the control problem of freeway traffic with heterogeneous vehicle sizes and drivers' behavior. The overall challenge addressed is the stabilization problem of the traffic oscillations in the congested regime while distinguishing two different vehicle classes. We develop boundary feedback control laws in order to damp out traffic oscillations in the congested regime of the linearized two-class Aw-Rascle (AR) traffic model. The macroscopic second-order two-class AR traffic model consists of four hyperbolic PDEs describing the dynamics of densities and velocities on freeway. The concept of area occupancy is used to express the traffic pressure and equilibrium speed relationship yielding a coupling between the two classes of vehicles. Each vehicle class is characterized by its own vehicle size and driver's behavior. The considered equilibrium profiles of the model represent evenly distributed traffic with constant densities and velocities of both classes along the investigated track section. After linearizing the model equations around those equilibrium profiles, it is observed that in the congested traffic one of the four characteristic speeds is negative, whereas the remaining three are positive. Backstepping control design is employed to stabilize the 4×4 heterodirectional hyperbolic PDEs. The control input actuates the traffic flow at outlet of the investigated track section and is realized by a ramp metering. A full-state feedback is designed to achieve finite time convergence of the density and velocity perturbations to the equilibrium at zero. This result is then combined with an anti-collocated observer design in order to construct an output feedback control law that damps out stop-and-go waves in finite time by measuring the velocities and densities of both vehicle classes at the inlet of the investigated track section.

This chapter is structured as follows: Section 4.1 introduces the two-class AR traffic model, the parameters characterizing the two classes and where they occur as well as the assumed boundary conditions. Section 4.2 includes the preparation of the linearized model for the control design and the formulation of the control design model. Furthermore, the full-state feedback controller result is presented in section 4.3 and the following section 4.4 presents the output feedback controller design. Section 4.6 verifies the performance of the presented controllers with simulation results.

4.1 Two-class AR traffic model

The extended AR model for heterogeneous traffic in [87] is presented in consideration of the two classes. This two-class AR traffic model is given by

$$\partial_t \rho_1 + \partial_x(\rho_1 v_1) = 0, \tag{4.1}$$

$$\partial_t(v_1 + p_1(AO)) + v_1 \partial_x(v_1 + p_1(AO)) = \frac{V_{e,1}(AO) - v_1}{\tau_1}, \tag{4.2}$$

$$\partial_t \rho_2 + \partial_x(\rho_2 v_2) = 0, \tag{4.3}$$

$$\partial_t(v_2 + p_2(AO)) + v_2 \partial_x(v_2 + p_2(AO)) = \frac{V_{e,2}(AO) - v_2}{\tau_2}, \tag{4.4}$$

where each vehicle class is described by traffic density $\rho_i(x,t)$ and velocity $v_i(x,t)$ with $(x,t) \in [0,L] \times [0,\infty)$. The parameter L is the length of the investigated track section. The traffic density $\rho_i(x,t)$ is defined as vehicles per unit length. The higher the traffic density, the more crowded is the traffic of class i vehicles at a specific spatial point. In addition, the velocity $v_i(x,t)$ describes the velocity of class i vehicles at a specified spatial point along the investigated track section. The traffic density $\rho_1(x,t)$ and velocity $v_1(x,t)$ correspond to the first vehicle class and the traffic density $\rho_2(x,t)$ and velocity $v_2(x,t)$ correspond to the second vehicle class. The non-zero terms on the right hand side represent the adaption of the vehicles to their desired velocities, where τ_i is the adaptation time.

The variable $AO(\rho_1,\rho_2)$ describes the area occupancy, based on the definition introduced in [6]. In [87], the expression for the area occupancy is simplified to

$$AO(\rho_1,\rho_2) = \frac{a_1 L \rho_1 + a_2 L \rho_2}{WL}, \tag{4.5}$$

where a_i is the occupied surface per vehicle class i and W the width of the investigated track. Assuming that the traffic densities are $\rho_1(x,t)$ and $\rho_2(x,t)$ along the entire considered highway section, the area occupancy $AO(\rho_1,\rho_2)$ is the percentage of occupied road space by *any* class. It holds that $0 \leq AO \leq 1$. The area occupancy depends on both densities since the occupied road surface is influenced by the vehicles of both classes.

The traffic pressure function $p_i(AO)$ is formulated as

$$p_i(AO) = V_i \left(\frac{AO(\rho_1,\rho_2)}{\overline{AO}_i} \right)^{\gamma_i}, \tag{4.6}$$

where V_i corresponds to the free-flow velocity, $\gamma_i > 1$ to the traffic pressure exponent and $0 < \overline{AO}_i \leq 1$ to the maximum area occupancy. The traffic pressure $p_i(AO)$ is the experienced traffic pressure by class i vehicles and depends on the area occupancy. The higher the area occupancy, the higher the experienced traffic pressure. For instance, if a vehicle suddenly decelerates, then the following vehicle experiences a high traffic pressure forcing another deceleration. Thereby, the free-flow velocity V_i represents the desired velocity of a driver, if no other vehicles of any class are present. The pressure exponent γ_i is a parameter that models the experience of the traffic pressure. Higher traffic pressure exponents lead to less experienced pressure. However, the maximum experienced pressure remains the same and is given by the free-flow velocity. The maximum area occupancy $\overline{AO}_i$ describes the percentage of occupied road surface for which the corresponding vehicle class is jammed. To obtain physically meaningful results, $0 < \overline{AO} \leq 1$ holds. For instance, $\overline{AO}_2 = 0.8$ means that if 80% of the highway are covered by vehicles of *any* class, then the class 2 vehicles are jammed and therefore their desired velocity is zero. Finally, the equilibrium speed-*AO* relationship is

$$V_{e,i}(AO) = V_i \left(1 - \left(\frac{AO(\rho_1, \rho_2)}{\overline{AO}_i}\right)^{\gamma_i}\right), \tag{4.7}$$

according to the model of Greenshield [52], and represents the desired velocity of the class i vehicles. It depends on the area occupancy since a very crowded road implies a lower desired speed in contrast to a nearly empty road. If the area occupancy is at the maximum $\overline{AO}_i$, then the corresponding equilibrium speed-*AO* relationship value is $V_{e,i}(\overline{AO}_i) = 0$. In order to show the qualitative behavior of the traffic pressure function (4.6) and the equilibrium speed-*AO* relationship (4.7), both functions are plotted in Figure 4.1 using an example parameter set. It is illustrated, that a more crowded highway, corresponding to a higher area occupancy, implies a higher experienced traffic pressure and a lower equilibrium speed.

4.1.1 Linearized two-class AR traffic model

The two-class AR traffic model (4.1) to (4.4) is linearized around a constant equilibrium state $(\rho_1^*, v_1^*, \rho_2^*, v_2^*)$. Inserting this constant state in (4.1) to (4.4) yields the conditions

$$v_1^*(\rho_1^*, \rho_2^*) = V_{e,1}(AO(\rho_1^*, \rho_2^*)), \tag{4.8}$$

$$v_2^*(\rho_1^*, \rho_2^*) = V_{e,2}(AO(\rho_1^*, \rho_2^*)). \tag{4.9}$$

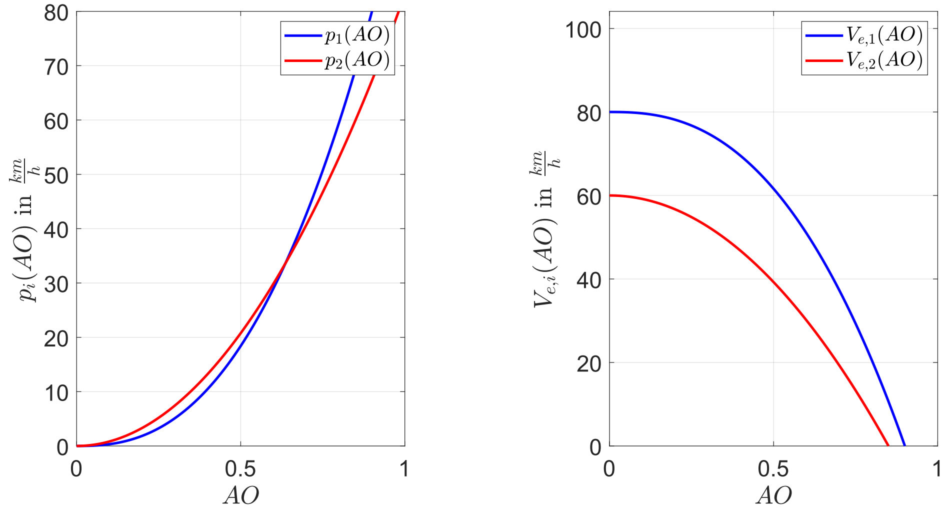

Figure 4.1: Traffic pressure functions $p_1(AO)$ and $p_2(AO)$ (left) and equilibrium speed-AO relationships $V_{e,1}(AO)$ and $V_{e,2}(AO)$ (right) for the example parameter set $\gamma_1 = 2.5$, $V_1 = 80\,\mathrm{km/h}$, $\overline{AO} = 0.9$ for class 1 and $\gamma_2 = 2$, $V_2 = 60\,\mathrm{km/h}$, $\overline{AO}_2 = 0.85$ for class 2.

Thus, the equilibrium velocities are determined by the equilibrium densities ρ_1^* and ρ_2^*. The perturbations of the distributed variables $\rho_i(x,t)$ and $v_i(x,t)$ are defined as

$$\tilde{\rho}_i(x,t) = \rho_i(x,t) - \rho_i^*, \tag{4.10}$$

$$\tilde{v}_i(x,t) = v_i(x,t) - v_i^*, \tag{4.11}$$

for each class i and the linearized model equations are given by

$$J_t \begin{bmatrix} \tilde{\rho}_{1t} \\ \tilde{v}_{1t} \\ \tilde{\rho}_{2t} \\ \tilde{v}_{2t} \end{bmatrix} + J_x \begin{bmatrix} \tilde{\rho}_{1x} \\ \tilde{v}_{1x} \\ \tilde{\rho}_{2x} \\ \tilde{v}_{2x} \end{bmatrix} + J \begin{bmatrix} \tilde{\rho}_{1} \\ \tilde{v}_{1} \\ \tilde{\rho}_{2} \\ \tilde{v}_{2} \end{bmatrix} = \begin{bmatrix} 0 \\ 0 \\ 0 \\ 0 \end{bmatrix}, \tag{4.12}$$

where the introduced Jacobian matrices are

$$J_t = \begin{bmatrix} 1 & 0 & 0 & 0 \\ \beta_{11} & 1 & \beta_{12} & 0 \\ 0 & 0 & 1 & 0 \\ \beta_{21} & 0 & \beta_{22} & 1 \end{bmatrix}, \tag{4.13}$$

$$J_x = \begin{bmatrix} v_1^* & \rho_1^* & 0 & 0 \\ v_1^*\beta_{11} & v_1^* & v_1^*\beta_{12} & 0 \\ 0 & 0 & v_2^* & \rho_2^* \\ v_2^*\beta_{21} & 0 & v_2^*\beta_{22} & v_2^* \end{bmatrix}, \tag{4.14}$$

$$J = \begin{bmatrix} 0 & 0 & 0 & 0 \\ \frac{1}{\tau_1}\beta_{11} & \frac{1}{\tau_1} & \frac{1}{\tau_1}\beta_{12} & 0 \\ 0 & 0 & 0 & 0 \\ \frac{1}{\tau_2}\beta_{21} & 0 & \frac{1}{\tau_2}\beta_{22} & \frac{1}{\tau_2} \end{bmatrix}, \tag{4.15}$$

and the abbreviations

$$\beta_{ij}(\rho_1^*, \rho_2^*) = \left. \frac{\partial p_i(AO(\rho_1, \rho_2))}{\partial \rho_j} \right|_{\rho_1 = \rho_1^*, \rho_2 = \rho_2^*} \tag{4.16}$$

are introduced with $i, j = 1, 2$. The abbreviations $\beta_{ij}(\rho_1^*, \rho_2^*)$ represent the derivative of the class i traffic pressure function with respect to class j traffic density. The boundary conditions are assumed to be

$$\rho_1(0,t) = \rho_1^*, \tag{4.17}$$

$$\rho_2(0,t) = \rho_2^*, \tag{4.18}$$

$$q_1(0,t) + q_2(0,t) = q_1^* + q_2^*, \tag{4.19}$$

$$q_1(L,t) + q_2(L,t) = q_1^* + q_2^*, \tag{4.20}$$

where (4.19) and (4.20) assume that the same total traffic flow enters and leaves the track section which is given by the sum of the class 1 and class 2 equilibrium flows q_1^* and q_2^*. The traffic flow of class i is defined as

$$q_i(x,t) = \rho_i(x,t)v_i(x,t). \tag{4.21}$$

Boundary conditions (4.17) and (4.18) indicate that the traffic densities of the incoming traffic flow are equivalent to the equilibrium densities. Thus, not only the entering traffic flow is constant, in fact the densities of both classes in this traffic flow are assumed to be constant. The linearization of the introduced boundary conditions (4.17) to (4.20) is

$$0 = \tilde{\rho}_1(0,t), \tag{4.22}$$

$$0 = \tilde{\rho}_2(0,t), \tag{4.23}$$

$$0 = v_1^*\tilde{\rho}_1(0,t) + \rho_1^*\tilde{v}_1(0,t) + v_2^*\tilde{\rho}_2(0,t) + \rho_2^*\tilde{v}_2(0,t), \tag{4.24}$$

$$0 = v_1^*\tilde{\rho}_1(L,t) + \rho_1^*\tilde{v}_1(L,t) + v_2^*\tilde{\rho}_2(L,t) + \rho_2^*\tilde{v}_2(L,t). \tag{4.25}$$

4.1.2 Free/congested regime analysis

In general, two different regimes of traffic are distinguished: the free-flow regime and the congested regime. The free-flow regime is characterized by the fact that the total information of the system travels downstream along with the vehicles. In that case, the model equations correspond to four homodirectional hyperbolic PDEs. On the other hand, a partial upstream propagation of information characterizes the traffic flow in the congested regime. The corresponding heterodirectional behavior causes the formation of the stop-and-go traffic. Therefore, it is reasonable to investigate which choices of equilibrium densities and parameters lead to heterodirectional information propagation. Therefore, the characteristic speeds are computed and their signs are considered in the following. First, the linearized model equations (4.12) need to be decoupled in time leading to

$$\begin{bmatrix} \tilde{\rho}_{1t} \\ \tilde{v}_{1t} \\ \tilde{\rho}_{2t} \\ \tilde{v}_{2t} \end{bmatrix} + \tilde{J}_x \begin{bmatrix} \tilde{\rho}_{1x} \\ \tilde{v}_{1x} \\ \tilde{\rho}_{2x} \\ \tilde{v}_{2x} \end{bmatrix} = \tilde{J} \begin{bmatrix} \tilde{\rho}_{1} \\ \tilde{v}_{1} \\ \tilde{\rho}_{2} \\ \tilde{v}_{2} \end{bmatrix} \tag{4.26}$$

with the new Jacobian matrices

$$\tilde{J}_x = \begin{bmatrix} v_1^* & \rho_1^* & 0 & 0 \\ 0 & v_1^* - \beta_{11}\rho_1^* & \beta_{12}(v_1^* - v_2^*) & -\beta_{12}\rho_2^* \\ 0 & 0 & v_2^* & \rho_2^* \\ \beta_{21}(v_2^* - v_1^*) & -\beta_{21}\rho_1^* & 0 & v_2^* - \beta_{22}\rho_2^* \end{bmatrix}$$

and

$$\tilde{J} = \begin{bmatrix} 0 & 0 & 0 & 0 \\ -\frac{1}{\tau_1}\beta_{11} & -\frac{1}{\tau_1} & -\frac{1}{\tau_1}\beta_{12} & 0 \\ 0 & 0 & 0 & 0 \\ -\frac{1}{\tau_2}\beta_{21} & 0 & -\frac{1}{\tau_2}\beta_{22} & -\frac{1}{\tau_2} \end{bmatrix}. \tag{4.27}$$

The characteristic speeds are given by the eigenvalues of $\tilde{J}_x$ which are

$$\lambda_1 = v_1^*(\rho_1^*, \rho_2^*), \tag{4.28}$$

$$\lambda_2 = v_2^*(\rho_1^*, \rho_2^*), \tag{4.29}$$

$$\begin{aligned}\lambda_3 =& \frac{v_1^*(\rho_1^*, \rho_2^*) + v_2^*(\rho_1^*, \rho_2^*) - \alpha_1(\rho_1^*, \rho_2^*) - \alpha_2(\rho_1^*, \rho_2^*)}{2} \\ &+ \frac{\Delta(\rho_1^*, \rho_2^*)}{2},\end{aligned} \tag{4.30}$$

$$\begin{aligned}\lambda_4 =& \frac{v_1^*(\rho_1^*, \rho_2^*) + v_2^*(\rho_1^*, \rho_2^*) - \alpha_1(\rho_1^*, \rho_2^*) - \alpha_2(\rho_1^*, \rho_2^*)}{2} \\ &- \frac{\Delta(\rho_1^*, \rho_2^*)}{2},\end{aligned} \tag{4.31}$$

where

$$\Delta(\rho_1^*, \rho_2^*) = \sqrt{\left(\alpha_2 \rho_2^* - \alpha_1 \rho_1^* + v_1^* - v_2^*\right)^2 + 4\alpha_1 \alpha_2 \rho_1^* \rho_2^*} \tag{4.32}$$

and

$$\alpha_i(\rho_1^*, \rho_2^*) = \beta_{ii}(\rho_1^*, \rho_2^*) = \left. \frac{\partial p_i(AO(\rho_1, \rho_2))}{\partial \rho_i} \right|_{\rho_1 = \rho_1^*, \rho_2 = \rho_2^*}. \tag{4.33}$$

For model validity, the equilibrium velocities of both vehicle classes are chosen to be positive, i.e. $v_1^* > 0$ and $v_2^* > 0$ and all vehicles travel downstream. Thus, the first two characteristic speeds (4.28) and (4.29) are positive. In addition, it is shown in [127] that

$$\lambda_4 \leq \min\{\lambda_1, \lambda_2\} \leq \lambda_3 \leq \max\{\lambda_1, \lambda_2\} \tag{4.34}$$

holds. Because $\lambda_1 > 0$ and $\lambda_2 > 0$, (4.34) implies that λ_3 is positive as well. Hence, the only characteristic speed that may have a negative sign is λ_4. Therefore, traffic is defined to be in the free regime if the equilibrium densities and parameters satisfy

$$\lambda_1, \lambda_2, \lambda_3, \lambda_4 > 0 \tag{4.35}$$

and in the congested regime if they meet

$$\lambda_1, \lambda_2, \lambda_3 > 0, \quad \lambda_4 < 0. \tag{4.36}$$

While λ_1 and λ_2 correspond to the flow of class 1 vehicles and class 2 vehicles, λ_3 is related to the fact that the faster vehicle class overtakes the slower one. For that reason, it is reasonable to obtain $\lambda_1 = \lambda_2 = \lambda_3$, if $v_1^* = v_2^*$ is assumed.

According to the definitions in (4.35) and (4.36), the boundary between the two regimes is defined as $\lambda_4 = 0$. In case of the two-class AR traffic model, this boundary is a line which can be drawn in the ρ_1^*-ρ_2^*-plane. Compared to the single class consideration, the boundary is

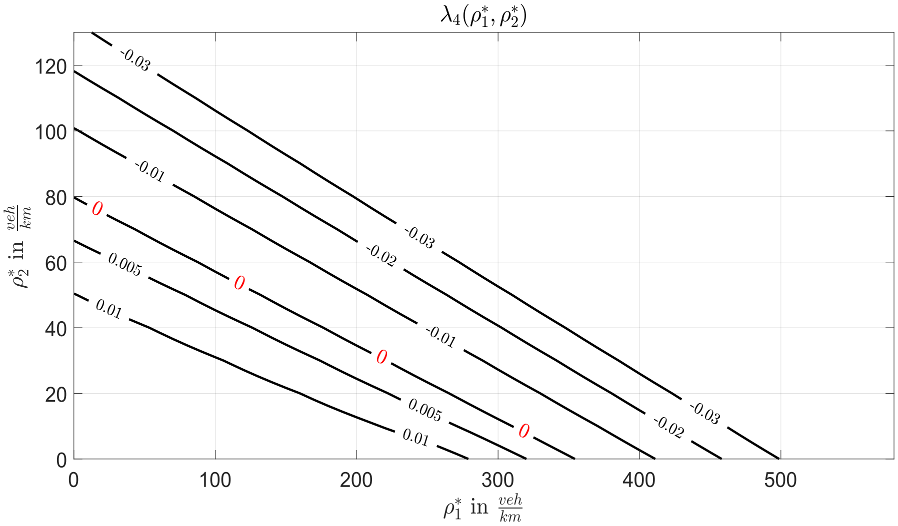

Figure 4.2: Contour plot of λ_4 for the parameter set $\gamma_1 = 2.5$, $V_1 = 80\,\mathrm{km/h}$, $\overline{AO} = 0.9$ for class 1 and $\gamma_2 = 2$, $V_2 = 60\,\mathrm{km/h}$, $\overline{AO}_2 = 0.85$ for class 2. The contour line $\lambda_4 = 0$ describes the boundary between the free-flow and congested regime.

equivalent to a single density which is the critical density. The numerically computed boundary between the two regimes is plotted as a contour plot for an example parameter set in Figure 4.2. The figure also indicates that small values for both equilibrium densities ρ_1^* and ρ_2^* correspond to a positive value of λ_4 and therefore homodirectional behavior. On the other hand, large values of densities lead to a negative value of λ_4 indicating heterodirectional behavior. Hence, smaller equilibrium densities correspond to free-flow regime and large equilibrium densities correspond to congested regime.

4.2 Boundary control design model

The control objective and the linearized two-class AR traffic model is introduced in this section. The preparation for control design is done using two transformations, the transformation to Riemann coordinates and a second transformation to further simplify the equations expressed in Riemann coordinates resulting in the control design model.

The overall goal is to damp out stop-and-go traffic in the congested regime and achieve convergence to the equilibrium states in a finite time. The ramp metering is considered to be installed at the outlet of the investigated track section regulating the traffic outflow. In this work, the ramp metering is used to damp out the introduced stop-and-go waves. Thus, the boundary condition (4.25) becomes

$$U(t) = v_1^* \tilde{\rho}_1(L,t) + \rho_1^* \tilde{v}_1(L,t) + v_2^* \tilde{\rho}_2(L,t) + \rho_2^* \tilde{v}_2(L,t). \tag{4.37}$$

Compared to the application of multi-phase flow in oil pipelines, [39], a ramp metering works as a valve at the end of the pipe to control the outgoing flow.

The system is transformed to Riemann coordinates to accomplish a decoupling of the spatial derivatives. The Riemann variables $(\bar{w}_1, \bar{w}_2, \bar{w}_3, \bar{w}_4)$ are defined in the new coordinates. The linear state transformation is given by

$$\begin{bmatrix} \bar{w}_1 \\ \bar{w}_2 \\ \bar{w}_3 \\ \bar{w}_4 \end{bmatrix} = V^{-1} \begin{bmatrix} \tilde{\rho}_1 \\ \tilde{v}_1 \\ \tilde{\rho}_2 \\ \tilde{v}_2 \end{bmatrix} \tag{4.38}$$

where the constant invertible transformation matrix V satisfies

$$\begin{bmatrix} \lambda_1 & 0 & 0 & 0 \\ 0 & \lambda_2 & 0 & 0 \\ 0 & 0 & \lambda_3 & 0 \\ 0 & 0 & 0 & \lambda_4 \end{bmatrix} = V^{-1} \tilde{J}_x V \tag{4.39}$$

and therefore diagonalizes the Jacobian $\tilde{J}_x$. The entries of V are denoted as

$$V = \left\{v_{ij}\right\}_{1\leq i\leq 4, 1\leq j\leq 4}. \tag{4.40}$$

The matrix V is straightforward to obtain and omitted due to its complexity and length. Inserting the transformation in (4.12) yields the model equations in Riemann coordinates

$$\begin{bmatrix} \bar{w}_{1t} \\ \bar{w}_{2t} \\ \bar{w}_{3t} \\ \bar{w}_{4t} \end{bmatrix} + \begin{bmatrix} \lambda_1 & 0 & 0 & 0 \\ 0 & \lambda_2 & 0 & 0 \\ 0 & 0 & \lambda_3 & 0 \\ 0 & 0 & 0 & \lambda_4 \end{bmatrix} \begin{bmatrix} \bar{w}_{1x} \\ \bar{w}_{2x} \\ \bar{w}_{3x} \\ \bar{w}_{4x} \end{bmatrix} = \hat{J} \begin{bmatrix} \bar{w}_1 \\ \bar{w}_2 \\ \bar{w}_3 \\ \bar{w}_4 \end{bmatrix}, \tag{4.41}$$

where

$$\hat{J} = V^{-1}\tilde{J}V \tag{4.42}$$

and the entries of the Jacobian $\hat{J}$ are denoted by

$$\hat{J} = \{\hat{J}_{ij}\}_{1\leq i\leq 4, 1\leq j\leq 4}. \tag{4.43}$$

Since the coefficient matrix of the spatial derivatives is now diagonal, a decoupling in spatial derivatives is achieved. The characteristic speeds (4.28) to (4.31) form the diagonal because they are the eigenvalues of $\tilde{J}_x$. In addition, the same transformation is applied to the boundary conditions (4.22), (4.23), (4.24) and (4.37) yielding

$$\begin{bmatrix} \bar{w}_1(0,t) \\ \bar{w}_2(0,t) \\ \bar{w}_3(0,t) \end{bmatrix} = \hat{Q}_0 \bar{w}_4(0,t), \tag{4.44}$$

$$\bar{w}_4(L,t) = \hat{R}_1 \begin{bmatrix} \bar{w}_1(L,t) \\ \bar{w}_2(L,t) \\ \bar{w}_3(L,t) \end{bmatrix} + \hat{U}(t). \tag{4.45}$$

The matrices are given by

$$\hat{Q}_0 = -\begin{bmatrix} v_{11} & v_{12} & v_{13} \\ v_{31} & v_{32} & v_{33} \\ \kappa_1 & \kappa_2 & \kappa_3 \end{bmatrix}^{-1} \begin{bmatrix} v_{14} \\ v_{34} \\ \kappa_4 \end{bmatrix}, \tag{4.46}$$

$$\hat{R}_1 = -\frac{1}{\kappa_4} \begin{bmatrix} \kappa_1 & \kappa_2 & \kappa_3 \end{bmatrix} \tag{4.47}$$

and are obtained by formulating the linearized boundary conditions in matrix form, inserting the transformation law to Riemann coordinates and decoupling afterwards. Besides, in (4.46) and (4.47), the abbreviations

$$\kappa_i = v_1^* v_{1i} + \rho_1^* v_{2i} + v_2^* v_{3i} + \rho_2^* v_{4i}, \quad i = 1,2,3,4, \tag{4.48}$$

are inserted. The input transformation, used in (4.45), is

$$\hat{U}(t) = \frac{1}{\kappa_4} U(t). \tag{4.49}$$

The next transformation achieves zero elements on the diagonal of $\hat{J}$ in (4.41) and sorts the positive characteristic speeds (4.28) to (4.30) in ascending order on the diagonal of the coefficient matrix of the spatial derivatives. We define an ascending order $\lambda_1 > \lambda_2$ without loss of generality, according to (4.34). It is assumed that class 1 vehicles represent small and fast average vehicles whereas class 2 describes big trucks which are large and slow. Thus, for the equilibrium velocities $v_1^* > v_2^*$ holds and therefore the ascending order of positive characteristic speeds is

$\lambda_2 < \lambda_3 < \lambda_1$. Hence, the transformation law

$$w_1 = e^{-\frac{\hat{J}_{22}}{v_2^*}x}\bar{w}_2, \tag{4.50}$$

$$w_2 = e^{-\frac{\hat{J}_{33}}{\lambda_3}x}\bar{w}_3, \tag{4.51}$$

$$w_3 = e^{-\frac{\hat{J}_{11}}{v_1^*}x}\bar{w}_1, \tag{4.52}$$

$$w_4 = e^{-\frac{\hat{J}_{44}}{\lambda_4}x}\bar{w}_4 \tag{4.53}$$

is applied to (4.41) yielding the transformed PDEs

$$\begin{bmatrix} w_{1t} \\ w_{2t} \\ w_{3t} \end{bmatrix} + \Lambda^+ \begin{bmatrix} w_{1x} \\ w_{2x} \\ w_{3x} \end{bmatrix} = \Sigma^{++}(x) \begin{bmatrix} w_1 \\ w_2 \\ w_3 \end{bmatrix} + \Sigma^{+-}(x) w_4, \tag{4.54}$$

$$w_{4t} - \Lambda^- w_{4x} = \Sigma^{-+}(x) \begin{bmatrix} w_1 \\ w_2 \\ w_3 \end{bmatrix}. \tag{4.55}$$

with

$$\Lambda^+ = \begin{bmatrix} v_2^* & 0 & 0 \\ 0 & \lambda_3 & 0 \\ 0 & 0 & v_1^* \end{bmatrix}, \tag{4.56}$$

$$\Lambda^- = -\lambda_4, \tag{4.57}$$

$$\Sigma^{++}(x) = \begin{bmatrix} 0 & \bar{J}_{12}(x) & \bar{J}_{13}(x) \\ \bar{J}_{21}(x) & 0 & \bar{J}_{23}(x) \\ \bar{J}_{31}(x) & \bar{J}_{32}(x) & 0 \end{bmatrix}, \tag{4.58}$$

$$\Sigma^{+-}(x) = \begin{bmatrix} \bar{J}_{14}(x) & \bar{J}_{24}(x) & \bar{J}_{34}(x) \end{bmatrix}^T, \tag{4.59}$$

$$\Sigma^{-+}(x) = \left[\begin{array}{ccc} \bar{J}_{41}(x) & \bar{J}_{42}(x) & \bar{J}_{43}(x) \end{array} \right]. \tag{4.60}$$

The abbreviations for the coefficients of the source term, $\bar{J}_{ij}(x),\ i,j = 1,2,3,4$, are:

$$\begin{aligned}
\bar{J}_{12}(x) &= \hat{J}_{23} e^{\left(\frac{\hat{J}_{33}}{\lambda_3} - \frac{\hat{J}_{22}}{v_2^*}\right)x}, \bar{J}_{13}(x) = \hat{J}_{21} e^{\left(\frac{\hat{J}_{11}}{v_1^*} - \frac{\hat{J}_{22}}{v_2^*}\right)x}, \\
\bar{J}_{14}(x) &= \hat{J}_{24} e^{\left(\frac{\hat{J}_{44}}{\lambda_4} - \frac{\hat{J}_{22}}{v_2^*}\right)x}, \bar{J}_{21}(x) = \hat{J}_{32} e^{\left(\frac{\hat{J}_{22}}{v_2^*} - \frac{\hat{J}_{33}}{\lambda_3}\right)x}, \\
\bar{J}_{23}(x) &= \hat{J}_{31} e^{\left(\frac{\hat{J}_{11}}{v_1^*} - \frac{\hat{J}_{33}}{\lambda_3}\right)x}, \bar{J}_{24}(x) = \hat{J}_{34} e^{\left(\frac{\hat{J}_{44}}{\lambda_4} - \frac{\hat{J}_{33}}{\lambda_3}\right)x}, \\
\bar{J}_{31}(x) &= \hat{J}_{12} e^{\left(\frac{\hat{J}_{22}}{v_2^*} - \frac{\hat{J}_{11}}{v_1^*}\right)x}, \bar{J}_{32}(x) = \hat{J}_{13} e^{\left(\frac{\hat{J}_{33}}{\lambda_3} - \frac{\hat{J}_{11}}{v_1^*}\right)x}, \\
\bar{J}_{34}(x) &= \hat{J}_{14} e^{\left(\frac{\hat{J}_{44}}{\lambda_4} - \frac{\hat{J}_{11}}{v_1^*}\right)x}, \bar{J}_{41}(x) = \hat{J}_{42} e^{\left(\frac{\hat{J}_{22}}{v_2^*} - \frac{\hat{J}_{44}}{\lambda_4}\right)x}, \\
\bar{J}_{42}(x) &= \hat{J}_{43} e^{\left(\frac{\hat{J}_{33}}{\lambda_3} - \frac{\hat{J}_{44}}{\lambda_4}\right)x}, \bar{J}_{43}(x) = \hat{J}_{41} e^{\left(\frac{\hat{J}_{11}}{v_1^*} - \frac{\hat{J}_{44}}{\lambda_4}\right)x}.
\end{aligned}$$

The diagonal elements of Λ^+ are sorted in an ascending order and the relations $\lambda_1 = v_1^*$, (4.28), and $\lambda_2 = v_2^*$, (4.29), are inserted. In addition, $\Sigma^{++}(x)$, $\Sigma^{+-}(x)$ and $\Sigma^{-+}(x)$ are depending on the spatial coordinate. Their entries $\bar{J}_{ij}(x)$ are bounded and either positive or negative on the whole domain, depending on the sign of the corresponding $\hat{J}_{ij}$. Applying the transformation (4.50) to (4.53) on the boundary conditions (4.44) and (4.45) yields

$$\begin{bmatrix} w_1(0,t) \\ w_2(0,t) \\ w_3(0,t) \end{bmatrix} = \bar{Q}_0 w_4(0,t), \tag{4.61}$$

$$w_4(L,t) = \bar{R}_1 \begin{bmatrix} w_1(L,t) \\ w_2(L,t) \\ w_3(L,t) \end{bmatrix} + \bar{U}(t) \tag{4.62}$$

with

$$\bar{Q}_0 = \begin{bmatrix} 0 & 0 & 1 \\ 1 & 0 & 0 \\ 0 & 1 & 0 \end{bmatrix}^{-1} \hat{Q}_0,$$

$$\bar{R}_1 = \hat{R}_1 \begin{bmatrix} 0 & 0 & e^{\left(\frac{\hat{f}_{11}}{v_1^*} - \frac{\hat{f}_{44}}{\lambda_4}\right)L} \\ e^{\left(\frac{\hat{f}_{22}}{v_2^*} - \frac{\hat{f}_{44}}{\lambda_4}\right)L} & 0 & 0 \\ 0 & e^{\left(\frac{\hat{f}_{33}}{\lambda_3} - \frac{\hat{f}_{44}}{\lambda_4}\right)L} & 0 \end{bmatrix}. \tag{4.63}$$

In addition, the input given in (4.62) is defined as

$$\bar{U}(t) = e^{-\frac{\hat{f}_{44}}{\lambda_4}L}\hat{U}(t). \tag{4.64}$$

All in all, the control design model is given by (4.54), (4.55), (4.61) and (4.62). In Figure 4.3, the qualitative behavior of the control design model is illustrated. According to the sign of the characteristic speeds, the propagation direction for each state $w_i(x,t)$ is drawn in Figure 4.3. It shows that the control input $\bar{U}(t)$ acts at the outlet of system, first propagating upstream and, after it is carried through the boundary condition at the inlet of the investigated track section, affecting downstream traffic. The summary of the two transformations is

$$\begin{bmatrix} w_1 \\ w_2 \\ w_3 \\ w_4 \end{bmatrix} = T^{-1}(x) \begin{bmatrix} \tilde{\rho}_1 \\ \tilde{v}_1 \\ \tilde{\rho}_2 \\ \tilde{v}_2 \end{bmatrix} \Leftrightarrow \begin{bmatrix} \tilde{\rho}_1 \\ \tilde{v}_1 \\ \tilde{\rho}_2 \\ \tilde{v}_2 \end{bmatrix} = T(x) \begin{bmatrix} w_1 \\ w_2 \\ w_3 \\ w_4 \end{bmatrix}, \tag{4.65}$$

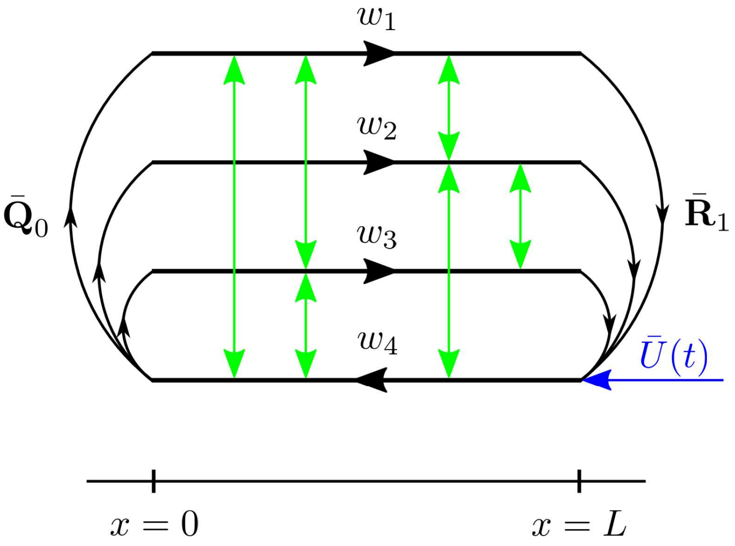

Figure 4.3: Schematic diagram of the control design model. The green arrow indicates the location where the control input acts on the system. The blue arrows represent the couplings between all four states.

where

$$T^{-1}(x) = \begin{bmatrix} 0 & e^{-\frac{\hat{f}_{22}}{v_2^*}x} & 0 & 0 \\ 0 & 0 & e^{-\frac{\hat{f}_{33}}{\lambda_3}x} & 0 \\ e^{-\frac{\hat{f}_{11}}{v_1^*}x} & 0 & 0 & 0 \\ 0 & 0 & 0 & e^{-\frac{\hat{f}_{44}}{\lambda_4}x} \end{bmatrix} V^{-1}, \tag{4.66}$$

$$T(x) = V \begin{bmatrix} 0 & 0 & e^{\frac{\hat{f}_{11}}{v_1^*}x} & 0 \\ e^{\frac{\hat{f}_{22}}{v_2^*}x} & 0 & 0 & 0 \\ 0 & e^{\frac{\hat{f}_{33}}{\lambda_3}x} & 0 & 0 \\ 0 & 0 & 0 & e^{\frac{\hat{f}_{44}}{\lambda_4}x} \end{bmatrix}. \tag{4.67}$$

The overall transformation law depends on the spatial coordinate. In addition, we have

$$\bar{U}(t) = e^{-\frac{\hat{\jmath}_{44}}{\lambda_4}L}\frac{1}{\kappa_4}U(t) \tag{4.68}$$

and the inversion is given by

$$U(t) = \kappa_4 e^{\frac{\hat{\jmath}_{44}}{\lambda_4}L}\bar{U}(t). \tag{4.69}$$

Since all transformations are invertible, the stability properties of the linearized model in density and velocity perturbations and the control design model are the same.

4.3 Full-state feedback control design

In the following, a full-state feedback control design for the system of four coupled hyperbolic PDEs given by (4.54) and (4.55) with boundary conditions (4.61) and (4.62) is carried out in order to achieve finite time convergence to zero for initial conditions $w_i(x,0) \in \mathscr{L}^\infty[0,L]$. The full-state feedback controller is designed by applying the backstepping control design in [80]. The general idea is to transform the coupled hyperbolic PDEs to a cascade target system. The control law is chosen such that the instabilities in the system are eliminated through the boundary conditions of the target system. The states of the target system are denoted as $(\alpha_1, \alpha_2, \alpha_3, \beta)$. The kernels of the backstepping transformation are denoted by $K(x,\xi)$ and $L_{11}(x,\xi)$. Then, the backstepping transformation is defined as

$$\alpha_1(x,t) = w_1(x,t), \tag{4.70}$$

$$\alpha_2(x,t) = w_2(x,t), \tag{4.71}$$

$$\alpha_3(x,t) = w_3(x,t), \tag{4.72}$$

$$\beta(x,t) = w_4(x,t) - \int_0^x \left(K(x,\xi) \begin{bmatrix} w_1(\xi,t) \\ w_2(\xi,t) \\ w_3(\xi,t) \end{bmatrix} + L_{11}(x,\xi) w_4(\xi,t) \right) d\xi, \tag{4.73}$$

where

$$K(x,\xi) = \begin{bmatrix} k_{11}(x,\xi) & k_{12}(x,\xi) & k_{13}(x,\xi) \end{bmatrix} \tag{4.74}$$

and $L_{11}(x,\xi)$ are defined on a triangular domain

$$\mathscr{T} = \{0 \le \xi \le x \le 1\}. \tag{4.75}$$

The introduced kernels $K(x,\xi)$ and $L_{11}(x,\xi)$ are unknown and will be determined later on. Furthermore, the choice of the target system is

$$\begin{aligned} \begin{bmatrix} \alpha_{1t} \\ \alpha_{2t} \\ \alpha_{3t} \end{bmatrix} = & -\Lambda^+ \begin{bmatrix} \alpha_{1x} \\ \alpha_{2x} \\ \alpha_{3x} \end{bmatrix} + \Sigma^{++}(x) \begin{bmatrix} \alpha_1 \\ \alpha_2 \\ \alpha_3 \end{bmatrix} \\ & + \Sigma^{+-}(x)\beta + \int_0^x C^+(x,\xi) \begin{bmatrix} \alpha_1(\xi,t) \\ \alpha_2(\xi,t) \\ \alpha_3(\xi,t) \end{bmatrix} d\xi \\ & + \int_0^x C^-(x,\xi)\beta(\xi,t) d\xi, \end{aligned} \tag{4.76}$$

$$\beta_t = \Lambda^- \beta_x. \tag{4.77}$$

The coefficients $C^{+}(x,\xi) \in \mathbb{R}^{3\times 3}$ and $C^{-}(x,\xi) \in \mathbb{R}^{3\times 1}$ are defined on the same triangular domain $\mathscr{T}$ and are determined later on. Besides, the boundary conditions of the target system are

$$\begin{bmatrix} \alpha_1(0,t) \\ \alpha_2(0,t) \\ \alpha_3(0,t) \end{bmatrix} = \bar{Q}_0 \beta(0,t), \tag{4.78}$$

$$\beta(L,t) = 0. \tag{4.79}$$

The target system (4.76) to (4.79) converges to its equilibrium at zero

$$\alpha_{e,i}(x) \equiv \beta_e(x) \equiv 0, \quad i = 1,2,3,\ t \geq 0,\ x \in [0,L] \tag{4.80}$$

in the finite time

$$t_F = \frac{L}{v_2^*} + \frac{L}{-\lambda_4}. \tag{4.81}$$

The proof is given in Lemma 3.1 in [80]. It remains to compute the kernels $K(x,\xi)$ and $L_{11}(x,\xi)$, coefficients $C^{+}(x,\xi)$ and $C^{-}(x,\xi)$ and the control input $\bar{U}(t)$ such that the transformation is completed and to show the existence of the kernels. Deriving (4.73) with respect to space and time, inserting the resulting derivatives and (4.61) in (4.77) yields the kernel equations that determine $K(x,\xi)$ and $L_{11}(x,\xi)$ after partial integration. The kernel equations are given by four coupled first order hyperbolic PDEs as well as four boundary conditions

$$\begin{aligned} -\Lambda^{-} K_x(x,\xi) + K_\xi(x,\xi)\Lambda^{+} = &-K(x,\xi)\Sigma^{++}(\xi) \\ &-L_{11}(x,\xi)\Sigma^{-+}(\xi), \end{aligned} \tag{4.82}$$

$$-\Lambda^{-} L_{11x}(x,\xi) - L_{11\xi}(x,\xi)\Lambda^{-} = -K(x,\xi)\Sigma^{+-}(\xi), \tag{4.83}$$

$$K(x,0)\Lambda^{+}\bar{Q}_0 - L_{11}(x,0)\Lambda^{-} = 0, \tag{4.84}$$

$$K(x,x)\Lambda^{+} + \Lambda^{-} K(x,x) = -\Sigma^{-+}(x). \tag{4.85}$$

Inserting expressions for Λ^-, $K(x,\xi)$, Λ^+, $\Sigma^{++}(\xi)$, $\Sigma^{-+}(\xi)$, $\Sigma^{+-}(\xi)$ and denoting the entries of $\bar{Q}_0 = \left\{\bar{Q}_{0i1}\right\}_{1\le i\le 3}$, the kernel equations in matrix form become

$$\lambda_4 \begin{bmatrix} k_{11x} \\ k_{12x} \\ k_{13x} \\ L_{11x} \end{bmatrix} + \begin{bmatrix} v_2^* & 0 & 0 & 0 \\ 0 & \lambda_3 & 0 & 0 \\ 0 & 0 & v_1^* & 0 \\ 0 & 0 & 0 & \lambda_4 \end{bmatrix} \begin{bmatrix} k_{11\xi} \\ k_{12\xi} \\ k_{13\xi} \\ L_{11\xi} \end{bmatrix} = \begin{bmatrix} 0 & -\bar{J}_{21}(\xi) & -\bar{J}_{31}(\xi) & -\bar{J}_{41}(\xi) \\ -\bar{J}_{12}(\xi) & 0 & -\bar{J}_{32}(\xi) & -\bar{J}_{42}(\xi) \\ -\bar{J}_{13}(\xi) & -\bar{J}_{23}(\xi) & 0 & -\bar{J}_{43}(\xi) \\ -\bar{J}_{14}(\xi) & -\bar{J}_{24}(\xi) & -\bar{J}_{34}(\xi) & 0 \end{bmatrix} \begin{bmatrix} k_{11} \\ k_{12} \\ k_{13} \\ L_{11} \end{bmatrix} \tag{4.86}$$

with boundary condition at $\xi = 0$,

$$\begin{bmatrix} \bar{Q}_{011}v_2^* & \bar{Q}_{021}\lambda_3 & \bar{Q}_{031}v_1^* & \lambda_4 \end{bmatrix} \begin{bmatrix} k_{11}(x,0) \\ k_{12}(x,0) \\ k_{13}(x,0) \\ L_{11}(x,0) \end{bmatrix} = 0, \tag{4.87}$$

and boundary conditions at $\xi = x$,

$$k_{11}(x,x) = \frac{\bar{J}_{41}(x)}{\lambda_4 - v_2^*}, \tag{4.88}$$

$$k_{12}(x,x) = \frac{\bar{J}_{42}(x)}{\lambda_4 - \lambda_3}, \tag{4.89}$$

$$k_{13}(x,x) = \frac{\bar{J}_{43}(x)}{\lambda_4 - v_1^*}. \tag{4.90}$$

As shown in Theorem 3.3 of [80], the kernel equations (4.82) to (4.85) are a well-posed system of equations and thus there exist unique solutions $K(x,\xi)$ and $L_{11}(x,\xi)$ in $L^\infty(\mathscr{T})$. Moreover, solving the equations (4.83) and (4.84) with the method of characteristics yields

$$\begin{aligned} L_{11}(x,\xi) =& -\frac{1}{\lambda_4}K(x-\xi,0)\Lambda^+\bar{Q}_0 \\ &+\int_0^{-\frac{\xi}{\lambda_4}} K(\lambda_4\nu+x,\lambda_4\nu+\xi)\Sigma^{+-}(\lambda_4\nu+\xi)d\nu. \end{aligned} \tag{4.91}$$

Inserting this result in the remaining PDEs (4.82) reduces the kernel equations to three coupled first order hyperbolic PDEs with three boundary conditions

$$\begin{aligned} 0 =& \lambda_4 K_x(x,\xi)+\Lambda^+K_\xi(x,\xi)+K(x,\xi)\Sigma^{++}(\xi) \\ &-\frac{1}{\lambda_4}K(x-\xi,0)\Lambda^+\bar{Q}_0\Sigma^{-+}(\xi) \\ &+\int_0^{-\frac{\xi}{\lambda_4}} K(\lambda_4\nu+x,\lambda_4\nu+\xi)\Sigma^{+-}(\lambda_4\nu+\xi)d\nu\Sigma^{-+}(\xi) \end{aligned} \tag{4.92}$$

$$0 = K(x,x)\Lambda^+ + \Lambda^-K(x,x)+\Sigma^{-+}(x) \tag{4.93}$$

Furthermore, deriving (4.70) to (4.72) with respect to space and time and inserting the obtained derivatives, (4.73) and (4.54) in (4.76) yields

$$C^-(x,\xi) = \Sigma^{+-}(x)L(x,\xi)+\int_\xi^x C^-(x,s)L(s,\xi)ds, \tag{4.94}$$

$$C^+(x,\xi) = \Sigma^{+-}(x)K(x,\xi)+\int_\xi^x C^-(x,s)K(s,\xi)ds. \tag{4.95}$$

Finally, inserting (4.62) and (4.79) in (4.73) evaluated at $x=L$ delivers

$$\bar{U}(t) = -\bar{R}_1\begin{bmatrix} w_1(L,t) \\ w_2(L,t) \\ w_3(L,t) \end{bmatrix} \int_0^L \left(K(L,\xi)\begin{bmatrix} w_1(\xi,t) \\ w_2(\xi,t) \\ w_3(\xi,t) \end{bmatrix} + L_{11}(L,\xi)w_4(\xi,t) \right) d\xi \tag{4.96}$$

and therefore determines the control input. Before the results of the controller design are summarized in a theorem, the control law is formulated in dependence of the original physical variables, i.e. the densities and velocities of both classes. For that reason, the transformation matrix $T^{-1}(x)$, (4.66), is separated in two parts

$$T^{-1}(x) = \begin{bmatrix} T_u^{-1}(x) \\ T_l^{-1}(x) \end{bmatrix}, \tag{4.97}$$

where $T_u^{-1}(x) \in \mathbb{R}^{3\times 4}$ and $T_l^{-1}(x) \in \mathbb{R}^{1\times 4}$. Hence, the states of the control design model can be formulated as

$$\begin{bmatrix} w_1(\xi,t) \\ w_2(\xi,t) \\ w_3(\xi,t) \end{bmatrix} = T_u^{-1}(\xi) \begin{bmatrix} \tilde{\rho}_1(\xi,t) \\ \tilde{v}_1(\xi,t) \\ \tilde{\rho}_2(\xi,t) \\ \tilde{v}_2(\xi,t) \end{bmatrix}, \tag{4.98}$$

$$w_4(L,t) = T_l^{-1}(\xi) \begin{bmatrix} \tilde{\rho}_1(\xi,t) \\ \tilde{v}_1(\xi,t) \\ \tilde{\rho}_2(\xi,t) \\ \tilde{v}_2(\xi,t) \end{bmatrix} \tag{4.99}$$

and the control law after applying the inverse input transformation (4.69) becomes

$$U(t) = -\,\kappa_4 e^{\frac{\hat{J}_{44}}{\lambda_4}L} \bar{R}_1 T_u^{-1}(L) \begin{bmatrix} \rho_1(L,t) - \rho_1^* \\ v_1(L,t) - v_1^* \\ \rho_2(L,t) - \rho_2^* \\ v_2(L,t) - v_2^* \end{bmatrix}$$

$$- \kappa_4 e^{\frac{\hat{J}_{44}}{\lambda_4}L} \int_0^L K(L,\xi) T_u^{-1}(\xi) \begin{bmatrix} \rho_1(\xi,t) - \rho_1^* \\ v_1(\xi,t) - v_1^* \\ \rho_2(\xi,t) - \rho_2^* \\ v_2(\xi,t) - v_2^* \end{bmatrix} d\xi$$

$$- \kappa_4 e^{\frac{\hat{J}_{44}}{\lambda_4}L} \int_0^L L_{11}(L,\xi) T_l^{-1}(\xi) \begin{bmatrix} \rho_1(\xi,t) - \rho_1^* \\ v_1(\xi,t) - v_1^* \\ \rho_2(\xi,t) - \rho_2^* \\ v_2(\xi,t) - v_2^* \end{bmatrix} d\xi \tag{4.100}$$

using the definitions of the perturbations (4.10) and (4.11). The result is now summarized in the following theorem.

Theorem 4.1. *Traffic density and velocity perturbations* $(\tilde{\rho}_1, \tilde{\rho}_2, \tilde{v}_1, \tilde{v}_2)$ *governed by the linearized two-class AR traffic model* (4.12)*, with the boundary conditions* (4.22) *to* (4.24) *and* (4.37) *as well as initial profiles*

$$\tilde{\rho}_1(x,0), \tilde{v}_1(x,0), \tilde{\rho}_2(x,0), \tilde{v}_2(x,0) \in \mathscr{L}^\infty([0,L]), \tag{4.101}$$

converge to the equilibrium at zero

$$\tilde{\rho}_{e,1}(x) \equiv \tilde{v}_{e,1}(x) \equiv \tilde{\rho}_{e,2}(x) \equiv \tilde{v}_{e,2}(x) \equiv 0 \tag{4.102}$$

in finite time t_F *given by* (4.81)*, if the control law* (4.100) *is applied. Thereby, the kernels* $K(x,\xi)$ *and* $L_{11}(x,\xi)$ *are obtained by solving the kernel equations* (4.92) *and* (4.93) *on the triangular domain* (4.75) *and using* (4.91) *afterwards.*

The full-state feedback law in (4.100) requires measurements of the densities and velocities of both classes at every spatial point. In practice, it is possible to measure the densities and velocities at every spatial point by installing traffic cameras, collecting GPS data or helicopter data recordings.

4.4 Anti-collocated boundary observer design

The installation of traffic cameras or the gain of GPS data in order to supply the full-state feedback control (4.100) with the required in-domain measurements is expensive. Therefore, a boundary observer design for full-state observation is proposed. In this work, an anti-collocated boundary observer is designed, i.e. the densities and velocities of both classes are measured at the opposite of the boundary where the control input acts. Therefore, it is assumed that only the traffic density and velocity of both classes at the inlet of the track section

$$y_1(t) = \rho_1(0,t), \tag{4.103}$$

$$y_2(t) = v_1(0,t), \tag{4.104}$$

$$y_3(t) = \rho_2(0,t), \tag{4.105}$$

$$y_4(t) = v_2(0,t) \tag{4.106}$$

are measured. In terms of the control design model coordinates, inserting the measurements in (4.65) yields that

$$\bar{y}(t) = w_4(0,t) \tag{4.107}$$

is known.

The observer states $(\hat{w}_1, \hat{w}_2, \hat{w}_3, \hat{w}_4)$ are estimates of the control design model states

(w_1, w_2, w_3, w_4). Thus, the observer equations become

$$\begin{aligned}\begin{bmatrix}\hat{w}_{1t}\\ \hat{w}_{2t}\\ \hat{w}_{3t}\end{bmatrix} =& -\Lambda^+\begin{bmatrix}\hat{w}_{1x}\\ \hat{w}_{2x}\\ \hat{w}_{3x}\end{bmatrix} + \Sigma^{++}(x)\begin{bmatrix}\hat{w}_1\\ \hat{w}_2\\ \hat{w}_3\end{bmatrix} + \Sigma^{+-}(x)\hat{w}_4\\ &- P^+(x)(\hat{w}_4(0,t) - w_4(0,t)) \end{aligned} \tag{4.108}$$

$$\begin{aligned}\hat{w}_{4t} =& \Lambda^- \hat{w}_{4x} + \Sigma^{-+}(x)\begin{bmatrix}\hat{w}_1\\ \hat{w}_2\\ \hat{w}_3\end{bmatrix}\\ &- P_{11}^-(x)(\hat{w}_4(0,t) - w_4(0,t))\end{aligned} \tag{4.109}$$

where the gains of the output injections $P^+(x)$ and $P_{11}^-(x)$ need to be designed. The boundary conditions of the observer are

$$\begin{bmatrix}\hat{w}_1(0,t)\\ \hat{w}_2(0,t)\\ \hat{w}_3(0,t)\end{bmatrix} = \bar{Q}_0 w_4(0,t), \tag{4.110}$$

$$\hat{w}_4(L,t) = \bar{R}_1\begin{bmatrix}\hat{w}_1(L,t)\\ \hat{w}_2(L,t)\\ \hat{w}_3(L,t)\end{bmatrix} + \bar{U}(t). \tag{4.111}$$

As a next step, the system describing the dynamic behavior of the error between the states and their estimations is formulated. The estimation errors are defined as

$$\tilde{w}_i(x,t) = \hat{w}_i(x,t) - w_i(x,t), \quad i = 1,2,3,4. \tag{4.112}$$

Subtracting the model equations of the control design model (4.54), (4.55), (4.61) and (4.62) from the observer equations (4.108), (4.109), (4.110) and (4.111) yields the following error system

$$\begin{aligned}
\begin{bmatrix} \tilde{w}_{1t} \\ \tilde{w}_{2t} \\ \tilde{w}_{3t} \end{bmatrix} =& -\Lambda^{+} \begin{bmatrix} \tilde{w}_{1x} \\ \tilde{w}_{2x} \\ \tilde{w}_{3x} \end{bmatrix} + \Sigma^{++}(x) \begin{bmatrix} \tilde{w}_{1} \\ \tilde{w}_{2} \\ \tilde{w}_{3} \end{bmatrix} \\
&+ \Sigma^{+-}(x)\tilde{w}_4 - P^{+}(x)\tilde{w}_4(0,t), \qquad (4.113) \\
\tilde{w}_{4t} =& \Lambda^{-}\tilde{w}_{4x} + \Sigma^{-+}(x) \begin{bmatrix} \tilde{w}_{1} \\ \tilde{w}_{2} \\ \tilde{w}_{3} \end{bmatrix} \\
&- P_{11}^{-}(x)\tilde{w}_4(0,t) \qquad (4.114)
\end{aligned}$$

with the boundary conditions

$$\begin{bmatrix} \tilde{w}_1(0,t) \\ \tilde{w}_2(0,t) \\ \tilde{w}_3(0,t) \end{bmatrix} = 0, \qquad (4.115)$$

$$\tilde{w}_4(L,t) = \bar{R}_1 \begin{bmatrix} \tilde{w}_1(L,t) \\ \tilde{w}_2(L,t) \\ \tilde{w}_3(L,t) \end{bmatrix}. \qquad (4.116)$$

Using the backstepping method, the output injection gains can be designed such that the error system converges to the equilibrium at zero in a finite time. Similar to the control design, a target system and a backstepping transformation are defined in the observer design as well. The output injections gains $P^{+}(x)$ and $P_{11}^{-}(x)$ are chosen such that the target converges to its equilibrium at zero in finite time. The state of the target system is denoted as $(\tilde{\alpha}_1, \tilde{\alpha}_2, \tilde{\alpha}_3, \tilde{\beta})$ and the kernels introduced in the backstepping transformation are $M(x,\xi)$ and $N_{11}(x,\xi)$. Thus, the backstepping transformation is given by

$$\begin{bmatrix} \tilde{w}_1(x,t) \\ \tilde{w}_2(x,t) \\ \tilde{w}_3(x,t) \end{bmatrix} = \begin{bmatrix} \tilde{\alpha}_1(x,t) \\ \tilde{\alpha}_2(x,t) \\ \tilde{\alpha}_3(x,t) \end{bmatrix} + \int_0^x M(x,\xi)\tilde{\beta}(\xi,t)d\xi, \tag{4.117}$$

$$\tilde{w}_4(x,t) = \tilde{\beta}(x,t) + \int_0^x N_{11}(x,\xi)\tilde{\beta}(\xi,t)d\xi \tag{4.118}$$

where

$$M(x,\xi) = \begin{bmatrix} m_{11}(x,\xi) & m_{21}(x,\xi) & m_{31}(x,\xi) \end{bmatrix}^T. \tag{4.119}$$

The kernels $M(x,\xi)$ and $N_{11}(x,\xi)$ are defined in the triangular domain (4.75). In addition, the target system is defined as

$$\begin{aligned} \begin{bmatrix} \tilde{\alpha}_{1t} \\ \tilde{\alpha}_{2t} \\ \tilde{\alpha}_{3t} \end{bmatrix} =& -\Lambda^+ \begin{bmatrix} \tilde{\alpha}_{1x} \\ \tilde{\alpha}_{2x} \\ \tilde{\alpha}_{3x} \end{bmatrix} + \Sigma^{++}(x) \begin{bmatrix} \tilde{\alpha}_1 \\ \tilde{\alpha}_2 \\ \tilde{\alpha}_3 \end{bmatrix} \\ &+ \int_0^x D^+(x,\xi) \begin{bmatrix} \tilde{\alpha}_1(\xi,t) \\ \tilde{\alpha}_2(\xi,t) \\ \tilde{\alpha}_3(\xi,t) \end{bmatrix} d\xi, \end{aligned} \tag{4.120}$$

$$\begin{aligned} \tilde{\beta}_t =& \Lambda^- \tilde{\beta}_x + \Sigma^{-+}(x) \begin{bmatrix} \tilde{\alpha}_1 \\ \tilde{\alpha}_2 \\ \tilde{\alpha}_3 \end{bmatrix} \\ &+ \int_0^x D^-(x,\xi) \begin{bmatrix} \tilde{\alpha}_1(\xi,t) \\ \tilde{\alpha}_2(\xi,t) \\ \tilde{\alpha}_3(\xi,t) \end{bmatrix} d\xi \end{aligned} \tag{4.121}$$

with the boundary conditions

$$\begin{bmatrix} \tilde{\alpha}_1(0,t) \\ \tilde{\alpha}_2(0,t) \\ \tilde{\alpha}_3(0,t) \end{bmatrix} = 0, \tag{4.122}$$

$$\tilde{\beta}(L,t) = \bar{R}_1 \begin{bmatrix} \tilde{\alpha}_1(L,t) \\ \tilde{\alpha}_2(L,t) \\ \tilde{\alpha}_3(L,t) \end{bmatrix}. \tag{4.123}$$

It can be shown that the target system converges in finite time t_F, given by (4.81). Besides, the coefficients $D^+(x,\xi) \in \mathbb{R}^{3\times 3}$ and $D^-(x,\xi) \in \mathbb{R}^{1\times 3}$ still need to be determined in the following.

The equations for the output injection gains $P^+(x)$ and $P^-(x)$, the kernels of the backstepping transformation $M(x,\xi)$ and $N_{11}(x,\xi)$ and the coefficients in the target system $D^+(x,\xi)$ and $D^-(x,\xi)$ need to be deduced in a next step. The kernel equations for $M(x,\xi)$ and $N_{11}(x,\xi)$ are

$$\begin{aligned} M_\xi(x,\xi)\Lambda^- - \Lambda^+ M_x(x,\xi) =& -\Sigma^{++}(x)M(x,\xi) \\ & -\Sigma^{+-}(x)N_{11}(x,\xi), & (4.124) \\ N_{11\xi}(x,\xi)\Lambda^- + \Lambda^- N_{11x}(x,\xi) =& -\Sigma^{-+}(x)M(x,\xi), & (4.125) \\ M(\xi,\xi)\Lambda^- + \Lambda^+ M(\xi,\xi) =& \Sigma^{+-}(\xi), & (4.126) \\ N_{11}(L,\xi) - \bar{R}_1 M(L,\xi) =& 0, & (4.127) \end{aligned}$$

where (4.124), (4.125) and (4.126) are obtained by inserting the transformation (4.117) and (4.118) as well as derivatives with respect to time and space of (4.117) and (4.118) in the PDEs of the error system (4.113) and (4.114), followed by partial integration and noticing that $\tilde{\beta}(0,t) = \tilde{w}(0,t)$. In addition, (4.127) is deduced by evaluating (4.118) at $x = L$, plugging in the boundary conditions at the outlet of error system and target system, (4.116) and (4.123), and inserting (4.117) evaluated at $x = L$ afterwards. Plugging in the expressions for Λ^+, $M(x,\xi)$, Λ^-, $\Sigma^{++}(x)$, $\Sigma^{+-}(x)$ and $\Sigma^{-+}(x)$, yields the kernel equations in matrix form:

$$\begin{aligned}
&\lambda_4 \begin{bmatrix} m_{11\xi}(x,\xi) \\ m_{21\xi}(x,\xi) \\ m_{31\xi}(x,\xi) \\ N_{11\xi}(x,\xi) \end{bmatrix} + \begin{bmatrix} v_2^* & 0 & 0 & 0 \\ 0 & \lambda_3 & 0 & 0 \\ 0 & 0 & v_1^* & 0 \\ 0 & 0 & 0 & \lambda_4 \end{bmatrix} \begin{bmatrix} m_{11x}(x,\xi) \\ m_{21x}(x,\xi) \\ m_{31x}(x,\xi) \\ N_{11x}(x,\xi) \end{bmatrix} \\
&= \begin{bmatrix} 0 & \bar{J}_{12}(x) & \bar{J}_{13}(x) & \bar{J}_{14}(x) \\ \bar{J}_{21}(x) & 0 & \bar{J}_{23}(x) & \bar{J}_{24}(x) \\ \bar{J}_{31}(x) & \bar{J}_{32}(x) & 0 & \bar{J}_{34}(x) \\ \bar{J}_{41}(x) & \bar{J}_{42}(x) & \bar{J}_{43}(x) & 0 \end{bmatrix} \begin{bmatrix} m_{11}(x,\xi) \\ m_{21}(x,\xi) \\ m_{31}(x,\xi) \\ N_{11}(x,\xi) \end{bmatrix}
\end{aligned} \tag{4.128}$$

with boundary conditions at $x = \xi$ and $x = L$:

$$m_{11}(\xi,\xi) = \frac{\bar{J}_{14}(\xi)}{v_2^* - \lambda_4}, \tag{4.129}$$

$$m_{21}(\xi,\xi) = \frac{\bar{J}_{24}(\xi)}{\lambda_3 - \lambda_4}, \tag{4.130}$$

$$m_{31}(\xi,\xi) = \frac{\bar{J}_{34}(\xi)}{v_1^* - \lambda_4}, \tag{4.131}$$

$$N_{11}(L,\xi) = \bar{R}_1 \begin{bmatrix} m_{11}(L,\xi) \\ m_{21}(L,\xi) \\ m_{31}(L,\xi) \end{bmatrix}. \tag{4.132}$$

It can be shown that the well-posedness of the kernel equations (4.124) to (4.127) is equivalent to the kernel equations (4.82) to (4.85). In fact, a transformation is introduced which achieves the exact same structure as the kernel equations which are developed during the full-state feedback design. Similar to the full-state feedback design, solving the PDE (4.125) and boundary condition (4.127) with the method of characteristics delivers the expression

$$\begin{aligned} N_{11}(x,\xi) =& \bar{R}_1 M(L, L-(x-\xi)) \\ &+ \int_0^{\frac{x-L}{\lambda_4}} \Sigma^{-+}(-\lambda_4\nu + x) M(-\lambda_4\nu + x, -\lambda_4\nu + \xi) d\nu, \end{aligned} \tag{4.133}$$

in dependence of $M(x,\xi)$. Inserting this result in (4.124) reduces the kernel equations to three PDEs and three boundary conditions

$$\begin{aligned} 0 =& -\Lambda^- M_\xi(x,\xi) + \Lambda^+ M_x(x,\xi) - \Sigma^{++}(x) M(x,\xi) \\ & - \Sigma^{+-}(x) \bar{R}_1 M(L, L-(x-\xi)) \\ & -\Sigma^{+-}(x) \int_0^{\frac{x-L}{\lambda_4}} \Sigma^{-+}(x-\lambda_4\nu) M(x-\lambda_4\nu, \xi-\lambda_4\nu) d\nu, \end{aligned} \tag{4.134}$$

$$0 = M(\xi,\xi)\Lambda^- + \Lambda^+ M(\xi,\xi) - \Sigma^{+-}(\xi) \tag{4.135}$$

Besides, the computation that yields the kernel equations (4.124) to (4.126) for $M(x,\xi)$ and $N_{11}(x,\xi)$ implies

$$D^+(x,\xi) = -M(x,\xi)\Sigma^{-+}(\xi) + \int_\xi^x M(x,s) D^-(s,\xi) ds, \tag{4.136}$$

$$\begin{aligned} D^-(x,\xi) =& -N_{11}(x,\xi)\Sigma^{-+}(\xi) \\ &+ \int_\xi^x N_{11}(x,s) D^-(s,\xi) ds, \end{aligned} \tag{4.137}$$

and

$$P^+(x) = -\lambda_4 M(x,0), \tag{4.138}$$

$$P^-_{11}(x) = -\lambda_4 N_{11}(x,0). \tag{4.139}$$

Since the kernels $M(x,\xi)$ and $N_{11}(x,\xi)$ are well-posed, (4.136) to (4.139) imply that the output injection gains as well as the target system coefficients are well-posed, too. Thus, the observer design is completed and is summarized in a theorem.

Theorem 4.2. *The error states* $(\tilde{w}_1, \tilde{w}_2, \tilde{w}_3, \tilde{w}_4)$ *between the observer* (4.108) *to* (4.111) *and control design model* (4.54) *to* (4.62) *are described by* (4.113) *to* (4.116)*. If the output injections gains* $P^+(x)$ *and* $P_{11}^-(x)$ *are chosen as* (4.138) *and* (4.139)*, where the kernel* $M(x,\xi)$ *is obtained by the well-posed equations* (4.134) *and* (4.135) *and* $N_{11}(x,\xi)$ *by* (4.133)*, and the initial error profiles are assumed to be*

$$\tilde{w}_i(x,0) \in \mathscr{L}^\infty([0,L]), \quad i = 1,2,3,4, \tag{4.140}$$

then the errors converge to the equilibrium at zero

$$\tilde{w}_{e,i}(x) \equiv 0, \quad i = 1,2,3,4 \tag{4.141}$$

in the finite time t_F *given by* (4.81).

The estimates of the observer $(\hat{w}_1, \hat{w}_2, \hat{w}_3, \hat{w}_4)$ can be transformed to the estimates of the density and velocity perturbations $(\hat{\tilde{\rho}}_1, \hat{\tilde{v}}_1, \hat{\tilde{\rho}}_2, \hat{\tilde{v}}_2)$ of both vehicle classes according to

$$\begin{bmatrix} \hat{\tilde{\rho}}_1 \\ \hat{\tilde{v}}_1 \\ \hat{\tilde{\rho}}_2 \\ \hat{\tilde{v}}_2 \end{bmatrix} = T(x) \begin{bmatrix} \hat{w}_1 \\ \hat{w}_2 \\ \hat{w}_3 \\ \hat{w}_4 \end{bmatrix}. \tag{4.142}$$

Furthermore, the estimates of the original state variables are obtained by

$$\hat{\rho}_i(x,t) = \hat{\tilde{\rho}}_i(x,t) + \rho_i^*, \tag{4.143}$$

$$\hat{v}_i(x,t) = \hat{\tilde{v}}_i(x,t) + v_i^* \tag{4.144}$$

with respect to the estimates of the densities and velocities $(\hat{\rho}_1, \hat{v}_1, \hat{\rho}_2, \hat{v}_2)$.

4.5 Output feedback control design

So far, a full-state feedback, that requires measurements of all states at every spatial point and damps out stop-and-go traffic, and an observer, that generates estimates of all states at every spatial point based on a measurement at the inlet of the track section, has been designed. Both results are combined resulting in an output feedback control. Therefore, the control law (4.100) is reformulated in terms of the generated estimates. This is done by replacing the densities and velocities by their estimates yielding the output feedback controller

$$\begin{aligned} U(t) = {} & -\kappa_4 e^{\frac{\hat{f}_{44}}{\lambda_4}L} \bar{R}_1 T_u^{-1}(L) \begin{bmatrix} \hat{\rho}_1(L,t) - \rho_1^* \\ \hat{v}_1(L,t) - v_1^* \\ \hat{\rho}_2(L,t) - \rho_2^* \\ \hat{v}_2(L,t) - v_2^* \end{bmatrix} \\ & - \kappa_4 e^{\frac{\hat{f}_{44}}{\lambda_4}L} \int_0^L K(L,\xi) T_u^{-1}(\xi) \begin{bmatrix} \hat{\rho}_1(\xi,t) - \rho_1^* \\ \hat{v}_1(\xi,t) - v_1^* \\ \hat{\rho}_2(\xi,t) - \rho_2^* \\ \hat{v}_2(\xi,t) - v_2^* \end{bmatrix} d\xi \\ & - \kappa_4 e^{\frac{\hat{f}_{44}}{\lambda_4}L} \int_0^L L_{11}(L,\xi) T_l^{-1}(\xi) \begin{bmatrix} \hat{\rho}_1(\xi,t) - \rho_1^* \\ \hat{v}_1(\xi,t) - v_1^* \\ \hat{\rho}_2(\xi,t) - \rho_2^* \\ \hat{v}_2(\xi,t) - v_2^* \end{bmatrix} d\xi \end{aligned} \tag{4.145}$$

where the estimates $(\hat{\rho}_1, \hat{v}_1, \hat{\rho}_2, \hat{v}_2)$ are obtained by transforming the states of the anti-collocated observer (4.108) to (4.111) according to (4.142), (4.143) and (4.144), the transformation matrices $T_u^{-1}(\cdot)$ and $T_l^{-1}(\cdot)$ are given by (4.97), the kernel $K(x,\xi)$ is the solutions of (4.92) and (4.93) and $L_{11}(x,\xi)$ is given by (4.91). Finally, the abbreviation κ_4 is introduced in (4.48). This combination of the results obtained by the first two theorems is summarized in a final third theorem.

Theorem 4.3. *The linearized two-class AR model is given by* (4.12) *with the assumptions* (4.22) *to* (4.24) *and* (4.37) *as boundary conditions. If the control law* (4.145) *is applied in* (4.37)*, where the estimates are generated by the anti-collocated observer* (4.108) *to* (4.111) *with the transformed control law* (4.68) *as input and transformation* (4.142)*,* (4.143) *and* (4.144) *afterwards, and the initial profiles satisfy*

$$\tilde{\rho}_1(x,0), \tilde{v}_1(x,0), \tilde{\rho}_2(x,0), \tilde{v}_2(x,0) \in \mathscr{L}^{\infty}([0,L]), \tag{4.146}$$

then the perturbations converge to the equilibrium at zero

$$\tilde{\rho}_{e,1}(x) \equiv \tilde{v}_{e,1}(x) \equiv \tilde{\rho}_{e,2}(x) \equiv \tilde{v}_{e,2}(x) \equiv 0 \tag{4.147}$$

in the finite time $2t_F$, where t_F is given by (4.81)*. The kernels $K(x,\xi)$ and $L_{11}(x,\xi)$ are obtained by solving the well-posed kernel equations* (4.92)*,* (4.93) *and using* (4.91) *and the observer gains are given by* (4.138) *and* (4.139)*, where the kernels $M(x,\xi)$ represents the solution of the well-posed system of equations* (4.134) *and* (4.135) *and $N_{11}(x,\xi)$ is given by* (4.133)*.*

The finite convergence time is twice as large as the time proposed in the previous theorems, because it requires t_F to obtain correct state estimates and afterwards the control needs another t_F to achieve convergence of the state variable to equilibrium state.

4.6 Numerical simulation

The performance of the full-state feedback and output feedback control is investigated by simulation. The linearized model equations (4.12) are approximated by using an upwind

Table 4.1: Simulation parameters.

Name	Symbol	Value	Unit
Relaxation time	τ_1	10	s
	τ_2	25	s
Pressure exponent	γ_1	2.5	1
	γ_2	2	1
Free-flow velocity	V_1	80	km/h
	V_2	60	km/h
Maximum *AO*	$\overline{AO}_1$	0.9	1
	$\overline{AO}_2$	0.85	1
Occupied surface per vehicle	a_1	10	m^2
	a_2	40	m^2
Equilibrium density	ρ_1^*	150	veh/h
	ρ_2^*	75	veh/h
Track width	W	6.5	m
Track length	L	1000	m
Amount of grid points	N	40	1

scheme. In order to achieve numerical stability, the grid sizes for the spatial coordinate and time are chosen such that the Courant-Friedrichs-Lewy condition,

$$\left|\frac{\lambda_i \Delta t}{\Delta x}\right| \leq 1, \quad i = 1,2,3,4, \tag{4.148}$$

is satisfied for all four characteristic speeds.

The assumed parameter values are stated in Table 4.1. In addition, the type of vehicles that are represented by the vehicle classes are denoted in Table 4.2. Typically, it holds that the larger the vehicle size the larger the relaxation time which is why $\tau_1 < \tau_2$. Since vehicle class 1 corresponds to smaller and faster average vehicles, the free-flow velocity V_1 is higher than V_2 and the highway needs to be occupied in a greater extent such that the average vehicles become jammed, i.e. $\overline{AO}_1 > A\bar{O}_2$. Furthermore, it is assumed that faster and smaller vehicles experience less traffic pressure for low *AO* values and therefore $\gamma_1 > \gamma_2$. Finally, the equilibrium densities are chosen such that the investigated traffic is in the congested regime. The equilibrium velocities are determined by the choice of the equilibrium densities and result in $v_1^* \approx 38\,\frac{\mathrm{km}}{\mathrm{h}}$ and $v_2^* \approx 20\,\frac{\mathrm{km}}{\mathrm{h}}$.

Table 4.2: Traffic classes with length and width of each vehicle.

Name	Class number	Length	Width
Average vehicle	1	5 m	2 m
Big trucks	2	10 m	4 m

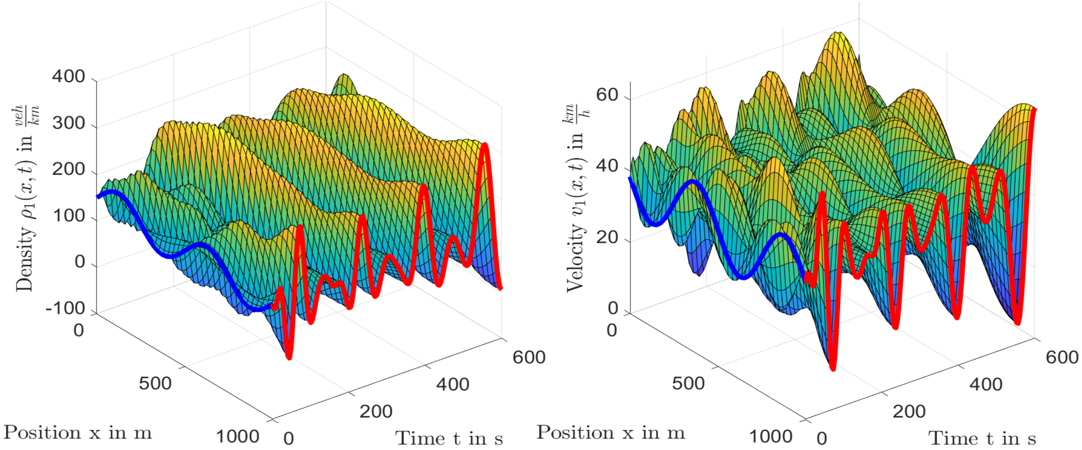

Figure 4.4: Traffic density and velocity of class 1 without control.

Although v_1^* and v_2^* seem to be low, the equilibrium velocities are realistic in case of congested traffic which is evenly distributed.

The initial profiles represent stop-and-go traffic with oscillations in density and velocity of sinusoidal shape. The mean value of the oscillations are the equilibrium values. At spatial points where the densities of both classes are increased, their velocities are decreased and thus the profiles

$$\rho_i(x,0) = \rho_i^* + \frac{\rho_i^*}{4} \sin\left(\frac{4\pi}{L}x\right), \quad i = 1,2, \tag{4.149}$$

$$v_i(x,0) = v_i^* - \frac{v_i^*}{4} \sin\left(\frac{4\pi}{L}x\right), \quad i = 1,2 \tag{4.150}$$

are assumed as initial profiles.

The simulation results of the open loop simulation are illustrated in Figure 4.4 for vehicle class 1 and in Figure 4.5 for vehicle class 2. In each figure, the left plot shows the density of

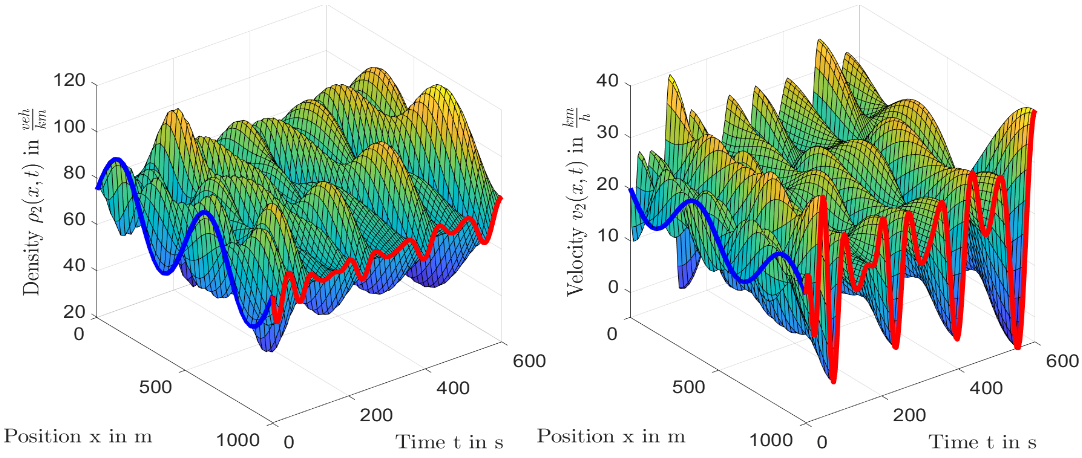

Figure 4.5: Traffic density and velocity of class 2 without control.

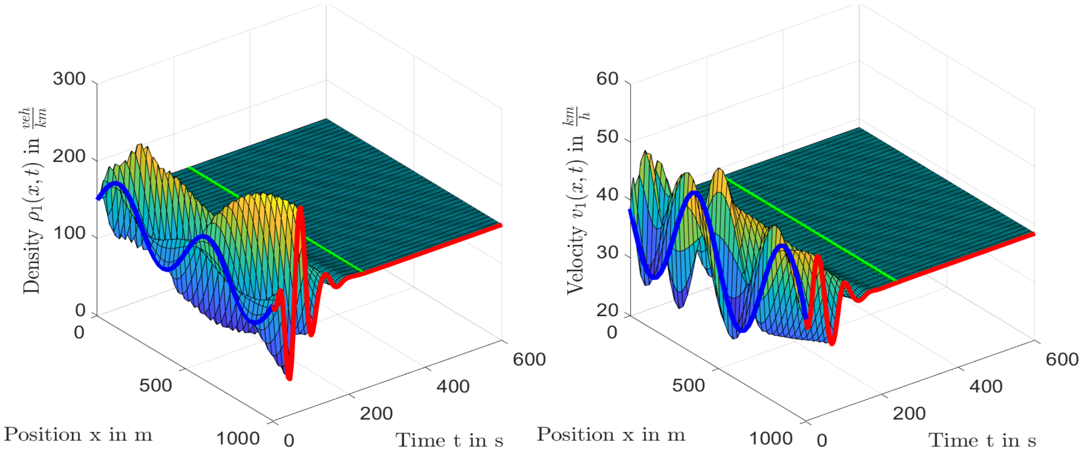

Figure 4.6: Traffic density and velocity of class 1 with full-state feedback control. The green line indicates t_F.

the corresponding vehicle class, whereas the plot on the right hand side illustrates the velocity. The values of the states at the outlet of the track section are marked with a red line, whereas the blue line emphasizes the initial profiles (4.149). The four plots indicate that the stop-and-go oscillations do not vanish without the influence of control. Next, the Figures 4.6 and 4.7 illustrate the simulation results for the same initial condition but with activated full-state feedback control. The green line marks the finite convergence time $t_F \approx 237\,\mathrm{s}$. Thus, it is easy to see that

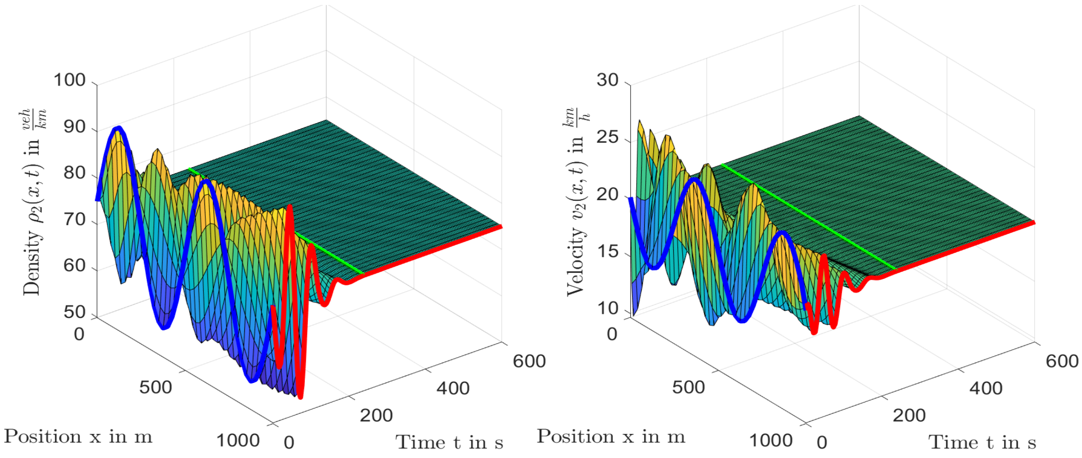

Figure 4.7: Traffic density and velocity of class 2 with full-state feedback control. The green line indicates t_F.

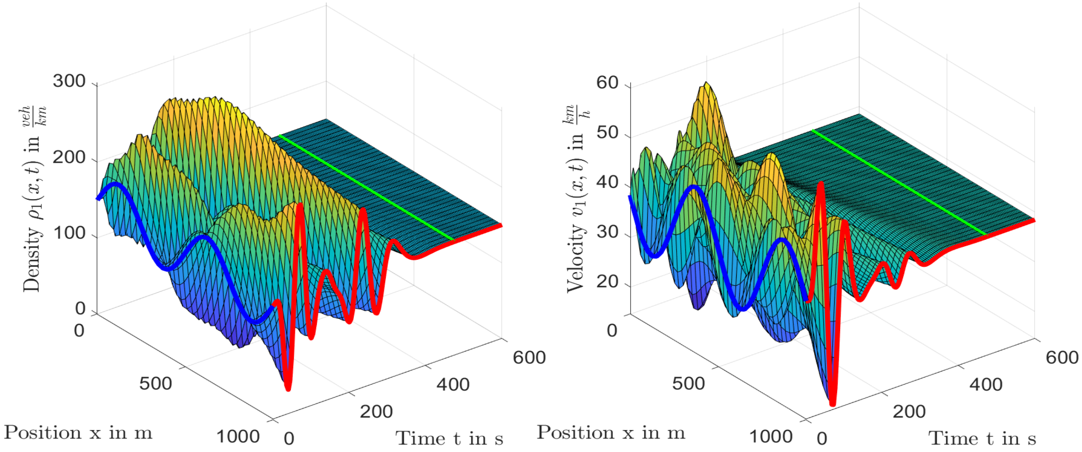

Figure 4.8: Traffic density and velocity of class 1 with output feedback control. The green line indicates $2t_F$.

the convergence to the constant equilibrium profile in t_F is achieved. Finally, Figure 4.8 and Figure 4.9 show the simulation results for the initial profiles using the designed output feedback control. Since the observer requires t_F to estimate the states without error and afterwards the controller needs t_F to achieve finite time convergence, the total finite convergence time is now $2t_F \approx 474\,\mathrm{s}$ and therefore green line is adjusted accordingly.

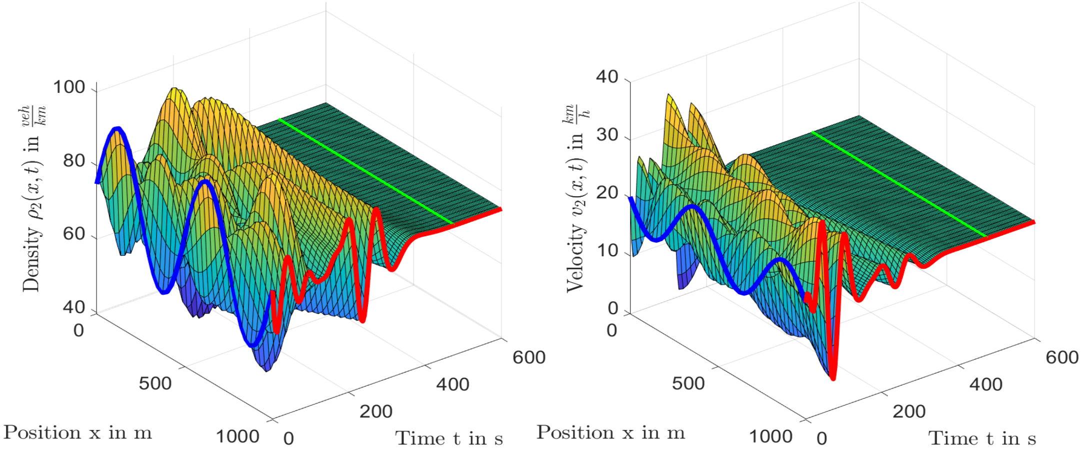

Figure 4.9: Traffic density and velocity of class 2 with output feedback control. The green line indiciates $2t_F$.

4.7 Conclusion

This chapter discusses ramp metering control for the linearized Two-Class Aw-Rascle Traffic model in order to damp out stop-and-go traffic in the congested regime upstream. The concept of area occupancy is used to model the coupling between the vehicle classes and is described by its own driving behavior and average vehicle size. The model equations consist out of four coupled hyperbolic PDEs whose characteristic speeds are analyzed in order to investigate whether a specific linearization point and parameter values represent a scenario of congested traffic. It is explained that only one of the characteristic speeds may have a negative sign causing information propagating upstream. The UORM control design model is deduced by applying two transformations to the linearized model equations resulting in a simplified representation of the model in Riemann coordinates. First, a full-state feedback controller is designed by using the backstepping technique. The controller achieves finite time damping of stop-and-go traffic. The uncollocated boundary observer is developed which generates estimates of the based on a measurement of the density and velocity of each class only at the inlet of the investigated track section. The full-state feedback and the observer are combined to an output feedback controller achieving the elimination of stop-and-go traffic only by the measurement at the inlet of the track section in finite time.

This work leads to some interesting topics that could be explored in future. First, it is typically preferred that the measurement for the observer is at the same spot where the control input acts on the system. Therefore, the design of the collocated observer is a result of great interest. In addition, the extended AR traffic model presented in [87] is formulated for n classes and there are results for $n+m$ heterodirectional behaving linear PDEs in the literature which enables the extension to more than two classes and hence even more realistic considerations. Especially the definition of the congestion boundary in case of three or more classes would be an interesting result. Finally, a combination of the results presented in this work with the results regarding two lanes [122] is of interest for further research.

Chapter 4 contains reprints and adaptations of the following paper: M. Burkhardt, H. Yu and M. Krstic, “Traffic Congestion Control of Two-Class Aw-Rascle Model,” *Automatica*, under review. The dissertation author is the primary investigator and author of this paper.

Chapter 5

Bilateral Control of Moving Traffic Shockwave

We develop backstepping state feedback control to stabilize a moving shockwave in a freeway segment under bilateral boundary actuations of traffic flow. A moving shockwave, consisting of light traffic upstream of the shockwave and heavy traffic downstream, is usually caused by changes of local road situations. The density discontinuity travels upstream and drivers caught in the shockwave experience transitions from free to congested traffic. Boundary control design in this paper brings the moving shockwave front to a static setpoint position, hindering the upstream propagation of traffic congestion. The traffic dynamics are described with LWR model, leading to a system of two first-order PDEs. Each represents the traffic density of a spatial domain segregated by the moving interface. By Rankine-Hugoniot condition, the interface position is driven by flux discontinuity and thus governed by a PDE state dependent ODE. For the PDE-ODE coupled system. the control objective is to stabilize both the PDE states of traffic density and the ODE state of moving shock position to setpoint values. Using delay representation and backstepping method, we design predictor feedback controllers to cooperatively compensate state-dependent input delays to the ODE. From Lyapunov stability analysis, we show local

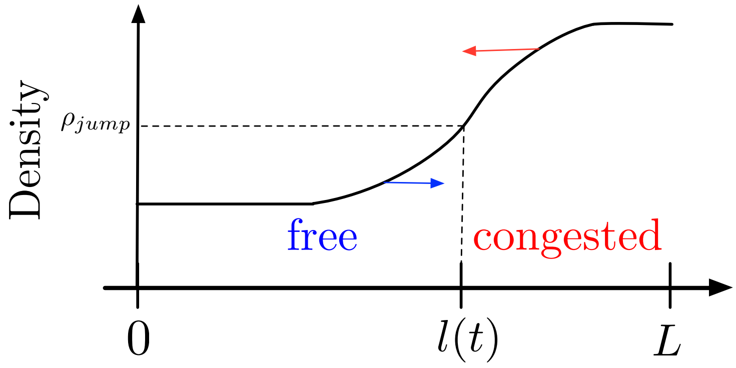

Figure 5.1: Traffic moving shockwave front on freeway, the arrows represent propagation directions of density variations. In LWR model, the propagation directions are given by the characteristic speeds of density $Q'(\rho)$.

stability of the closed-loop system in H^1 norm. The performance of controllers is demonstrated by numerical simulation.

The outline of this chapter: we introduce the LWR model in section to describe the moving shockwave problem. Then we linearized the coupled PDE-ODE model around steady states. The predictor state feedback control design follows and using Lyapunov analysis, we prove the local exponential stability of the closed-loop system. Model validity is guaranteed with the control design. In the end, the result is validated with numerical simulations.

5.1 LWR traffic model

The moving shockwave front is the head of a shockwave, segregating traffic on a segment of freeway into two different schemes. The upstream traffic of the shockwave front is in free regime and the downstream is in congested regime, as shown in Fig.1. The traffic densities are described with the first-order macroscopic LWR model.

In LWR model, traffic density $\rho(x,t)$ is governed by the following first-order nonlinear

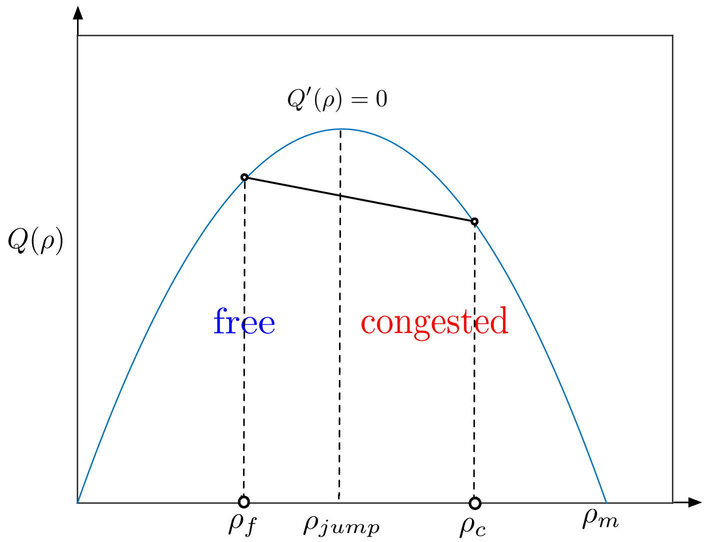

Figure 5.2: Fundamental digram of traffic density and traffic flux relation

hyperbolic PDE, where $x \in [0,L]$, $t \in [0,\infty)$,

$$\partial_t \rho + Q'(\rho)\partial_x \rho = 0, \tag{5.1}$$

where $Q(\rho)$ is a fundamental diagram which shows the relation of equilibrium density and traffic flux. The fundamental diagram $Q(\rho)$ is defined as $Q(\rho) = \rho V(\rho)$. The equilibrium velocity $V(\rho)$ is a decreasing function of density. We choose the following Greenshield's model for $V(\rho)$ in which velocity is a linear decreasing function of density.

$$V(\rho) = v_m \left(1 - \frac{\rho}{\rho_m}\right). \tag{5.2}$$

where v_m is the maximum speed, ρ_m is the maximum density. Greenshield's model $V(\rho)$ yields that the fundamental diagram $Q(\rho)$ is a quadratic map, shown in Fig. 5.2. The jump density ρ_{jump} segregates densities into two sections, the density smaller than ρ_{jump} is defined as free-regime while the density greater than ρ_{jump} is defined as congested regime.

In the LWR PDE (5.1), density variations propagate with the characteristic speed $Q'(\rho)$. The free regime with light traffic, equivalently, $\rho_{\mathrm{f}} < \rho_{\mathrm{jump}}$, has its density variations transported downstream with

$$Q'(\rho)|_{\rho=\rho_{\mathrm{f}}} = V(\rho_{\mathrm{f}}) + \rho_{\mathrm{f}} V'(\rho_{\mathrm{f}}) > 0, \tag{5.3}$$

while the congested regime with denser traffic, namely, $\rho_{\mathrm{c}} > \rho_{\mathrm{jump}}$ has its density variations transported upstream with

$$Q'(\rho)|_{\rho=\rho_{\mathrm{c}}} = V(\rho_{\mathrm{c}}) + \rho_{c} V'(\rho_{\mathrm{c}}) < 0. \tag{5.4}$$

As shown in figure Fig. 5.1, the moving shockwave considered here is the shock of a traffic wave which physically represents the discontinuity of density. The congested traffic density propagates upstream while the light traffic density propagates downstream. Therefore, the upstream front of the shockwave becomes steeper in propagation and eventually, the gradient $\partial_x \rho$ tends to be infinity [105]. In this context, drivers located in the upstream front of the shock will experience transition from free to congested traffic. The position of the shockwave front is later defined by an ODE according to Rankine-Hugoniot condition.

5.2 Moving shockwave model

The moving shockwave model consists of upstream, downstream traffic densities and a moving interface located at the density discontinuity spatial coordinate. The dynamics of the upstream free traffic, the downstream congested traffic and the position of the moving interface are presented below, respectively.

Define the traffic density of the congested regime as $\rho_{\mathrm{c}}(x,t)$ for $x \in [0, l(t)]$, $t \in [0, +\infty]$, and the free regime as $\rho_{\mathrm{f}}(x,t)$, for $x \in [l(t), L]$, $t \in [0, +\infty]$, the LWR model that describes the traffic is given by

$$\partial_t \rho_{\mathrm{f}} + \partial_x(\rho_{\mathrm{f}} v_{\mathrm{f}}) = 0, \quad x \in [0, l(t)] \tag{5.5}$$

$$\partial_t \rho_{\mathrm{c}} + \partial_x(\rho_{\mathrm{c}} v_{\mathrm{c}}) = 0, \quad x \in [l(t), L] \tag{5.6}$$

where $l(t) \in [0, L]$ is the location of moving interface. The density and velocity relation is given by Greenshield's model in (5.2), $(i = \mathrm{f}, \mathrm{c})$,

$$v_i(x,t) = V_i(\rho_i(x,t)) = v_m \left(1 - \frac{\rho_i(x,t)}{\rho_m}\right). \tag{5.7}$$

Due to the flux discontinuity at the moving boundary, a traveling vehicle leaves the free regime to enter the congested regime. Dynamics of moving interface $l(t)$ is derived under the Rankine-Hugoniot condition which guarantees that the mass of traffic flow is conserved at the moving interface. The upstream propagation of the shockwave front is driven by the flux discontinuity.

$$\dot{l}(t) = \frac{\rho_{\mathrm{c}}(l(t),t) v_{\mathrm{c}}(l(t),t) - \rho_{\mathrm{f}}(l(t),t) v_{\mathrm{f}}(l(t),t)}{\rho_{\mathrm{c}}(l(t),t) - \rho_{\mathrm{f}}(l(t),t)}, \tag{5.8}$$

where the initial position of the shockwave front $0 < l(0) < L$. The following inequalities for initial conditions of PDEs (5.5),(5.6) are assumed

$$\rho_{\mathrm{c}}(l(0),0) v_{\mathrm{c}}(l(0),0) < \rho_{\mathrm{f}}(l(0),0) v_{\mathrm{f}}(l(0),0), \tag{5.9}$$

$$\rho_{\mathrm{c}}(l(0),0) > \rho_{\mathrm{f}}(l(0),0). \tag{5.10}$$

Initially, the traffic downstream the interface is denser but with a smaller flux which lets less vehicles to pass through while the traffic upstream is light and let more vehicles to come in the segment. With the above assumptions to hold, we obtain from (5.8) that $\dot{l}(0) < 0$. The moving interface is traveling upstream and is driven by a flux difference induced by the density discontinuity.

Substituting density-velocity relation in (5.7) into (5.5),(5.6), and (5.8), we have two nonlinear PDEs and an ODE coupled system describing the dynamics of $\rho_{\mathrm{f}}(x,t)$, $\rho_{\mathrm{c}}(x,t)$ and $l(t)$ given by

$$\partial_t \rho_{\mathrm{f}}(x,t) = -v_m \partial_x \left(\rho_{\mathrm{f}}(x,t) - \frac{\rho_{\mathrm{f}}^2(x,t)}{\rho_m} \right), \tag{5.11}$$

$$\partial_t \rho_{\mathrm{c}}(x,t) = -v_m \partial_x \left(\rho_{\mathrm{c}}(x,t) - \frac{\rho_{\mathrm{c}}^2(x,t)}{\rho_m} \right), \tag{5.12}$$

$$\dot{l}(t) = v_m - \frac{v_m}{\rho_m} (\rho_{\mathrm{c}}(l(t),t) + \rho_{\mathrm{f}}(l(t),t)). \tag{5.13}$$

Remark 5.1. *For model validity, we assume that there exists a constant $L > 0$ such that the ODE state $l(t)$ satisfies*

$$0 < l(t) < L, \tag{5.14}$$

so that (5.11),(5.12)*, and* (5.13) *are well-defined for $x \in [0,L]$, $t \in [0,+\infty]$. We emphasize that the proposed control law needs to guarantee the above condition.*

Our control objective is to stabilize both free and congested regime traffic $\rho_i(x,t)$ to uniform steady states $\rho_i^\star$ and at the same time, the moving interface $l(t)$ to a desirable static setpoint $l^\star$. Therefore, the shockwave becomes standstill within the freeway segment instead of moving upstream.

We consider the following controlled boundary condition for the nonlinear coupled PDE-ODE system consisting of (5.11), (5.12), and (5.13)

$$\rho_{\mathrm{f}}(0,t) = U_{\mathrm{in}}(t) + \rho_{\mathrm{f}}^\star, \tag{5.15}$$

$$\rho_{\mathrm{c}}(L,t) = U_{\mathrm{out}}(t) + \rho_{\mathrm{c}}^\star, \tag{5.16}$$

where we control the incoming and outgoing density variations of the freeway segment $U_{\text{in}}(t)$ and $U_{\text{out}}(t)$. The control of density can be realized with on-ramp metering actuating the flux at both boundaries:

$$q_{\text{in}}(t) = Q(\rho_{\text{f}}(0,t)), \tag{5.17}$$

$$q_{\text{out}}(t) = Q(\rho_{\text{c}}(L,t)). \tag{5.18}$$

Now, we linearize the coupled PDE-ODE model $(\rho_{\text{f}}(x,t), \rho_{\text{c}}(x,t), l(t))$-system defined in (5.11),(5.12) and (5.13) around steady states and setpoint $(\rho_{\text{f}}^{\star}, \rho_{\text{c}}^{\star}, l^{\star})$. The constant equilibrium setpoint values are chosen so that the following conditions that ensure the model validity hold

$$0 < \rho_{\text{f}}^{\star} < \rho_{\text{jump}} < \rho_{\text{c}}^{\star} < \rho_m, \tag{5.19}$$

$$0 < l^{\star} < L. \tag{5.20}$$

At steady-state, the flux equilibrium needs to be achieved for both sides of the moving interface. Hence,

$$\rho_{\text{f}}^{\star} V(\rho_{\text{f}}^{\star}) = \rho_{\text{c}}^{\star} V(\rho_{\text{c}}^{\star}). \tag{5.21}$$

Using condition (5.21), the quadratic fundamental diagram yields that

$$\rho_{\text{f}}^{\star} + \rho_{\text{c}}^{\star} = \rho_m. \tag{5.22}$$

Define the state deviations from the system reference as

$$\tilde{\rho}_i(x,t) = \rho_i(x,t) - \rho_i^{\star}, \tag{5.23}$$

$$X(t) = l(t) - l^{\star}, \tag{5.24}$$

where $\dot{X}(t) = \dot{l}(t)$ is satisfied.

The linearized PDE-ODE model (5.11)-(5.13) with the boundary conditions (5.15) and (5.16) around the system reference $(\rho_{\mathrm{f}}^{\star}, \rho_{\mathrm{c}}^{\star}, l^{\star})$ is defined as the following $(\tilde{\rho}_{\mathrm{f}}(x,t), \tilde{\rho}_{\mathrm{c}}(x,t), X(t))$-system

$$\partial_t \tilde{\rho}_{\mathrm{f}}(x,t) = -u\partial_x \tilde{\rho}_{\mathrm{f}}(x,t), \quad x \in [0, l(t)] \tag{5.25}$$

$$\partial_t \tilde{\rho}_{\mathrm{c}}(x,t) = u\partial_x \tilde{\rho}_{\mathrm{c}}(x,t), \qquad x \in [l(t), L] \tag{5.26}$$

$$\tilde{\rho}_{\mathrm{f}}(0,t) = U_{\mathrm{in}}(t), \tag{5.27}$$

$$\tilde{\rho}_{\mathrm{c}}(L,t) = U_{\mathrm{out}}(t), \tag{5.28}$$

$$\dot{X}(t) = -b\left(\tilde{\rho}_{\mathrm{f}}(l(t),t) + \tilde{\rho}_{\mathrm{c}}(l(t),t)\right), \tag{5.29}$$

where the transport speed is defined as

$$u = v_m \left(1 - \frac{2\rho_{\mathrm{f}}^{\star}}{\rho_m}\right), \tag{5.30}$$

and satisfy $0 < u < v_m$. The constant coefficient b in ODE is defined as

$$b = \frac{v_m}{\rho_m} > 0. \tag{5.31}$$

The linearized model (5.25)-(5.29) is a PDE-ODE coupled system with bilateral boundary control inputs from inlet and outlet.

5.3 Predictor-based control design

In this section, we first introduce the equivalent delay system representation to the system (5.25)-(5.29). Then, a backstepping transformation is applied to obtain predictor-based state feedback controls to compensate the PDE state-dependent delays to the ODE.

5.3.1 Coupled PDE-ODE to delay system representation

The system (5.25)-(5.29) can be represented by an unstable ODE with two distinct state-dependent input delays. Introduce the following state-dependent delays for the two transport PDEs

$$D_{\mathrm{f}}(t) = \frac{l(t)}{u}, \tag{5.32}$$

$$D_{\mathrm{c}}(t) = \frac{L - l(t)}{u}, \tag{5.33}$$

where $l(t) = X(t) + l^{\star}$. The PDE states are represented by

$$\tilde{\rho}_{\mathrm{f}}(l(t), t) = U_{\mathrm{in}}(t - D_{\mathrm{f}}(t)), \tag{5.34}$$

$$\tilde{\rho}_{\mathrm{c}}(l(t), t) = U_{\mathrm{out}}(t - D_{\mathrm{c}}(t)), \tag{5.35}$$

where $U_{\mathrm{in}}(t)$ and $U_{\mathrm{out}}(t)$ are the boundary control inputs defined in (5.27) and (5.28). Substituting (5.34) and (5.35) into the ODE (5.29), the following state-dependent input delay system representation is derived

$$\dot{X}(t) = -b\left(U_{\mathrm{in}}(t - D_{\mathrm{f}}(X(t))) + U_{\mathrm{out}}(t - D_{\mathrm{c}}(X(t)))\right). \tag{5.36}$$

Remark 5.2. *If the position of the moving shock front is close to the inlet half segment such that $l(t) \in \left[0, \frac{L}{2}\right]$, it holds that $\forall t \in [0, \infty)$, $D_{\mathrm{f}}(t) \leq D_{\mathrm{c}}(t)$. As a result, delayed inlet control input $U_{\mathrm{in}}(t - D_{\mathrm{f}}(t))$ reaches the moving shock front faster than delayed outlet control input $U_{\mathrm{out}}(t - D_{\mathrm{c}}(t))$. If $l(t) \in \left[\frac{L}{2}, L\right]$, $\forall t \in [0, \infty)$, $D_{\mathrm{f}}(t) \geq D_{\mathrm{c}}(t)$ holds. Then $U_{\mathrm{out}}(t - D_{\mathrm{c}}(t))$ reaches the moving shock front faster than $U_{\mathrm{in}}(t - D_{\mathrm{f}}(t))$.*

We introduce a new coordinate z defined as

$$z = \begin{cases} \dfrac{l(t)-x}{u}, & x \in [0, l(t)], \\ \dfrac{x-l(t)}{u}, & x \in [l(t), L], \end{cases} \tag{5.37}$$

and new variables $\tilde{\rho}_{\rm f}(z,t)$ and $\tilde{\rho}_{\rm c}(z,t)$ defined in z-coordinate. The transformations between $\tilde{\rho}_{\rm f}(x,t), \tilde{\rho}_{\rm c}(x,t)$ and $\tilde{\rho}_{\rm f}(z,t), \tilde{\rho}_{\rm c}(z,t)$ are given by

$$\tilde{\rho}_{\rm f}(z,t) = \tilde{\rho}_{\rm f}(l(t)-uz,t), \quad z \in [0, D_{\rm f}(t)], \tag{5.38}$$

$$\tilde{\rho}_{\rm c}(z,t) = \tilde{\rho}_{\rm c}(l(t)+uz,t), \quad z \in [0, D_{\rm c}(t)], \tag{5.39}$$

and the associated inverse transformations of (5.38) and (5.39) are given by

$$\tilde{\rho}_{\rm f}(x,t) = \tilde{\rho}_{\rm f}\left(\frac{l(t)-x}{u}, t\right), \quad x \in [0, l(t)], \tag{5.40}$$

$$\tilde{\rho}_{\rm c}(x,t) = \tilde{\rho}_{\rm c}\left(\frac{x-l(t)}{u}, t\right), \quad x \in [l(t), L]. \tag{5.41}$$

Using (5.38) and (5.39), the original system (5.25)-(5.29) is rewritten in the new z-coordinate as

$$\partial_t \tilde{\rho}_{\rm f}(z,t) = \left(1 - \frac{\dot{l}(t)}{u}\right) \partial_z \tilde{\rho}_{\rm f}(z,t), \; z \in [0, D_{\rm f}(t)], \tag{5.42}$$

$$\partial_t \tilde{\rho}_{\rm c}(z,t) = \left(1 + \frac{\dot{l}(t)}{u}\right) \partial_z \tilde{\rho}_{\rm c}(z,t), \; z \in [0, D_{\rm c}(t)], \tag{5.43}$$

$$\tilde{\rho}_{\rm f}(D_{\rm f}(t),t) = U_{\rm in}(t), \tag{5.44}$$

$$\tilde{\rho}_{\rm c}(D_{\rm c}(t),t) = U_{\rm out}(t), \tag{5.45}$$

with the ODE given by

$$\dot{X}(t) = -b\left(\tilde{\rho}_{\rm f}(0,t) + \tilde{\rho}_{\rm c}(0,t)\right). \tag{5.46}$$

5.3.2 Predictor-based backstepping transformation

We consider the following backstepping transformation, motivated by the predictor-based transformation for delay representation $\rho_{\mathrm{f}}(z,t)$ and $\rho_{\mathrm{c}}(z,t)$ defined in (5.42)-(5.45),

$$\begin{aligned} w_{\mathrm{f}}(z,t) =& \tilde{\rho}_{\mathrm{f}}(z,t) - K_{\mathrm{f}}\left(X(t) - b\int_0^z \tilde{\rho}_{\mathrm{f}}(\xi,t)d\xi \right. \\ & \left. -b\int_0^{\min\{D_{\mathrm{c}}(t),z\}} \tilde{\rho}_{\mathrm{c}}(\xi,t)d\xi \right), \quad z \in [0, D_{\mathrm{f}}(t)], \end{aligned} \tag{5.47}$$

$$\begin{aligned} w_{\mathrm{c}}(z,t) =& \tilde{\rho}_{\mathrm{c}}(z,t) - K_{\mathrm{c}}\left(X(t) - b\int_0^z \tilde{\rho}_{\mathrm{c}}(\xi,t)d\xi \right. \\ & \left. -b\int_0^{\min\{D_{\mathrm{f}}(t),z\}} \tilde{\rho}_{\mathrm{f}}(\xi,t)d\xi \right), \quad z \in [0, D_{\mathrm{c}}(t)]. \end{aligned} \tag{5.48}$$

where $K_{\mathrm{f}}, K_{\mathrm{c}} > 0$ are positive constant gain kernels.

The above transformation in the original PDE state variables $\rho_{\mathrm{f}}(x,t)$ for $x \in [0, l(t)]$ and $\rho_{\mathrm{c}}(x,t)$ for $x \in [l(t), L]$, is given by

$$\begin{aligned} w_{\mathrm{f}}(x,t) =& \tilde{\rho}_{\mathrm{f}}(x,t) - K_{\mathrm{f}}\left(X(t) - \frac{b}{u}\int_x^{l(t)} \tilde{\rho}_{\mathrm{f}}(\xi,t)d\xi \right. \\ & \left. -\frac{b}{u}\int_{l(t)}^{\min\{L,2l(t)-x\}} \tilde{\rho}_{\mathrm{c}}(\xi,t)d\xi \right), \quad x \in [0, l(t)], \end{aligned} \tag{5.49}$$

$$\begin{aligned} w_{\mathrm{c}}(x,t) =& \tilde{\rho}_{\mathrm{c}}(x,t) - K_{\mathrm{c}}\left(X(t) - \frac{b}{u}\int_{l(t)}^{x} \tilde{\rho}_{\mathrm{c}}(\xi,t)d\xi \right. \\ & \left. -\frac{b}{u}\int_{\max\{0,2l(t)-x\}}^{l(t)} \tilde{\rho}_{\mathrm{f}}(\xi,t)d\xi \right), \quad x \in [l(t), L]. \end{aligned} \tag{5.50}$$

- For the case $D_{\mathrm{f}}(t) \le D_{\mathrm{c}}(t)$, it follows that $l(t) \in \left[0, \frac{L}{2}\right]$ and the following holds

$$x \in [0, l(t)] \implies \min\{L, 2l(t) - x\} = 2l(t) - x. \tag{5.51}$$

- For the case $D_{\mathrm{f}}(t) \geq D_{\mathrm{c}}(t)$, it follows that $l(t) \in \left[\frac{L}{2}, L\right]$, the following holds

$$x \in [l(t), L] \implies \max\{0, 2l(t)-x\} = 2l(t)-x. \tag{5.52}$$

Later on, two pairs of state feedback controllers are obtained respectively for $l(t) \in \left[0, \frac{L}{2}\right]$ and $l(t) \in \left[\frac{L}{2}, L\right]$. The inverse transformation of (5.49),(5.50) is given by

$$\begin{aligned}\tilde{\rho}_{\mathrm{f}}(x,t) =& w_{\mathrm{f}}(x,t) + K_{\mathrm{f}}\Bigg(X(t) - \frac{b}{u}\int_x^{l(t)} w_{\mathrm{f}}(\xi,t)d\xi \\ & - \frac{b}{u}\int_{l(t)}^{\min\{L,2l(t)-x\}} w_{\mathrm{c}}(\xi,t)d\xi\Bigg), \quad x \in [0, l(t)], \end{aligned}\tag{5.53}$$

$$\begin{aligned}\tilde{\rho}_{\mathrm{c}}(x,t) =& w_{\mathrm{c}}(x,t) + K_{c}\Bigg(X(t) - \frac{b}{u}\int_{l(t)}^{x} w_{\mathrm{c}}(\xi,t)d\xi \\ & - \frac{b}{u}\int_{\max\{0,2l(t)-x\}}^{l(t)} w_{\mathrm{f}}(\xi,t)d\xi\Bigg), \quad x \in [l(t), L]. \end{aligned}\tag{5.54}$$

Let us denote the above transformations as

$$\tilde{\rho}_{\mathrm{f}} = \mathscr{T}_{\mathrm{f}}[w_{\mathrm{f}}, w_{\mathrm{c}}], \tag{5.55}$$

$$\tilde{\rho}_{\mathrm{c}} = \mathscr{T}_{\mathrm{c}}[w_{\mathrm{f}}, w_{\mathrm{c}}]. \tag{5.56}$$

At the moving interface, we have

$$w_{\mathrm{f}}(l(t),t) = \tilde{\rho}_{\mathrm{f}}(l(t),t) - K_{\mathrm{f}}X(t), \tag{5.57}$$

$$w_{\mathrm{c}}(l(t),t) = \tilde{\rho}_{\mathrm{c}}(l(t),t) - K_{\mathrm{c}}X(t). \tag{5.58}$$

Taking temporal and spatial derivative on both sides of (5.49),(5.50) and substituting into the

PDE-ODE original system (5.25)-(5.29), we obtain target system by $w_{\mathrm{f}}(x,t)$ and $w_{\mathrm{c}}(x,t)$,

$$\partial_t w_{\mathrm{f}} + u\partial_x w_{\mathrm{f}} = \frac{K_{\mathrm{f}} b}{u}\dot{l}(t)(g(t) + 2\varepsilon_c(x,t)),\ x \in [0, l(t)], \tag{5.59}$$

$$\partial_t w_{\mathrm{c}} - u\partial_x w_{\mathrm{c}} = \frac{K_{\mathrm{c}} b}{u}\dot{l}(t)(g(t) - 2\varepsilon_{\mathrm{f}}(x,t)),\ x \in [l(t), L], \tag{5.60}$$

$$w_{\mathrm{f}}(0,t) = 0, \tag{5.61}$$

$$w_{\mathrm{c}}(L,t) = 0, \tag{5.62}$$

$$\dot{X}(t) = -aX(t) - b\left(w_{\mathrm{c}}(l(t),t) + w_{\mathrm{f}}(l(t),t)\right), \tag{5.63}$$

where the constant coefficient $a = b(K_{\mathrm{f}} + K_{\mathrm{c}}) > 0$ is obtained by substituting (5.57),(5.58) into (5.29), given $b, K_{\mathrm{f}}, K_{\mathrm{c}} > 0$. The time-varying term $g(t)$ is defined as

$$g(t) = (K_{\mathrm{f}} - K_{\mathrm{c}})X(t) + w_{\mathrm{f}}(l(t),t) - w_{\mathrm{c}}(l(t),t), \tag{5.64}$$

and the space and time-varying terms $\varepsilon_{\mathrm{c}}(x,t)$ and $\varepsilon_{\mathrm{f}}(x,t)$ are given by

$$\begin{aligned} \varepsilon_{\mathrm{c}}(x,t) &= \tilde{\rho}_{\mathrm{c}}(2l(t) - x, t) \\ &= \mathscr{T}_{\mathrm{c}}[w_{\mathrm{f}}, w_{\mathrm{c}}](2l(t) - x, t), \end{aligned} \tag{5.65}$$

$$\begin{aligned} \varepsilon_{\mathrm{f}}(x,t) &= \tilde{\rho}_{\mathrm{f}}(2l(t) - x, t) \\ &= \mathscr{T}_{\mathrm{f}}[w_{\mathrm{f}}, w_{\mathrm{c}}](2l(t) - x, t). \end{aligned} \tag{5.66}$$

We assume that densities outside freeway segment $[0, L]$ are at steady states, therefore $\tilde{\rho}_{\mathrm{c}}(2l(t) - x, t) = 0$ when $2l(t) - x > L$, and $\tilde{\rho}_{\mathrm{f}}(2l(t) - x, t) = 0$ when $2l(t) - x < 0$. Hence, the followings hold for $\varepsilon_{\mathrm{f}}(x,t)$ and $\varepsilon_{\mathrm{c}}(x,t)$,

$$\begin{cases} \varepsilon_{\mathrm{f}}(x,t) = 0, \quad l(t) \in [0, L/2] \text{ and } x \in [2l(t), L], \\ \varepsilon_{\mathrm{c}}(x,t) = 0, \quad l(t) \in [L/2, L] \text{ and } x \in [0, 2l(t) - L]. \end{cases} \tag{5.67}$$

Otherwise, $\varepsilon_{\rm f}(x,t)$ and $\varepsilon_{\rm c}(x,t)$ are given by expressions in (5.65) and (5.66). The bilateral state feedback boundary actuations for inlet and outlet of the segment are derived from (5.49),(5.50) and (5.61),(5.62) as

$$U_{\rm in}(t) = K_{\rm f}\left(X(t) - \frac{b}{u}\int_0^{l(t)} \tilde{\rho}_{\rm f}(\xi,t)d\xi - \frac{b}{u}\int_{l(t)}^{\min\{L,2l(t)\}} \tilde{\rho}_{\rm c}(\xi,t)d\xi\right), \tag{5.68}$$

$$U_{\rm out}(t) = K_{\rm c}\left(X(t) - \frac{b}{u}\int_{l(t)}^{L} \tilde{\rho}_{\rm c}(\xi,t)d\xi - \frac{b}{u}\int_{\max\{0,2l(t)-L\}}^{l(t)} \tilde{\rho}_{\rm f}(\xi,t)d\xi\right). \tag{5.69}$$

We obtain two pairs of controller designs for $l(t) \in \left[0,\frac{L}{2}\right]$ and $l(t) \in \left[\frac{L}{2},L\right]$, respectively. When $l(t) \in \left[0,\frac{L}{2}\right]$, it holds true that $\min\{L,2l(t)\} = 2l(t), \max\{0,2l(t)-L\} = 0$ and when $l(t) \in \left[\frac{L}{2},L\right]$ one gets $\min\{L,2l(t)\} = L, \max\{0,2l(t)-x\} = 2l(t)$.

In addition, when $l(t) = \frac{L}{2}$, controller integral forms become identical for $l(t) \in \left[0,\frac{L}{2}\right]$ and $l(t) \in \left[\frac{L}{2},L\right]$:

$$U_{\rm in}(t) = K_{\rm f}\left(X(t) - \frac{b}{u}\int_0^{\frac{L}{2}} \tilde{\rho}_{\rm f}(\xi,t)d\xi - \frac{b}{u}\int_{\frac{L}{2}}^{L} \tilde{\rho}_{\rm c}(\xi,t)d\xi\right), \tag{5.70}$$

$$U_{\rm out}(t) = K_{\rm c}\left(X(t) - \frac{b}{u}\int_0^{\frac{L}{2}} \tilde{\rho}_{\rm f}(\xi,t)d\xi - \frac{b}{u}\int_{\frac{L}{2}}^{L} \tilde{\rho}_{\rm c}(\xi,t)d\xi\right). \tag{5.71}$$

It is remarkable that the bilateral control input smoothly switches between the above control laws when the moving interface position passes through the middle of the freeway segment.

Due to the invertibility of the transformation in (5.49),(5.50), stability of the target system $(w_{\rm c}(x,t), w_{\rm f}(x,t), X(t))$ and stability the plant $(\tilde{\rho}_{\rm f}(x,t), \tilde{\rho}_{\rm c}(x,t), X(t))$ are equivalent. In the next section, we apply Lyapunov analysis to prove the stability of the target system. Define the H^1-norm $||f(\cdot,t)||_{H^1_{[a,b]}}$ as

$$||f(\cdot,t)||_{H^1_{[a,b]}} = \left(\int_a^b f^2(x,t) + f_x^2(x,t)dx\right)^{1/2}. \tag{5.72}$$

We now state the main result of the chapter.

Theorem 5.3. *Consider a closed-loop system consisting of the PDE-ODE system* (5.11)-(6.77) *and the bilateral full-state feedback control laws for inlet and outlet* (5.68),(5.69). *For any system reference* $(\rho_{\mathrm{f}}^{\star}, \rho_{\mathrm{c}}^{\star}, l^{\star})$ *which satisfies conditions* (5.19),(5.20) *and* (5.22) , *and for any given* $L > 0$, *there exist* $c > 0,\ \gamma > 0,\ \zeta > 0$ *such that if the initial conditions of the system* $(\rho_{\mathrm{f}}(x,0), \rho_{\mathrm{c}}(x,0), l(0))$ *satisfy* $Z(0) < \zeta$, *local exponential stability of the closed-loop system with bilateral control laws holds* $\forall t \in [0,\infty)$, *namely,*

$$Z(t) \leq c e^{-\gamma t} Z(0), \tag{5.73}$$

where $Z(t)$ *is defined as*

$$Z(t) = ||\rho_{\mathrm{f}}(x,t) - \rho_{\mathrm{f}}^{\star}||_{H^1_{[0,l(t)]}} + ||\rho_{\mathrm{c}}(x,t) - \rho_{\mathrm{c}}^{\star}||_{H^1_{[l(t),L]}} + |l(t) - l^{\star}|^2,$$

and condition (5.14) *is satisfied for model validity.*

5.4 Lyapunov stability analysis

In the proof, the local stability of the closed-loop system in the H^1 sense is shown with Lyapunov analysis and the following condition of model validity (5.14) is guaranteed by our control design. The proof of Theorem 5.3 is established through following steps: we firstly prove the local stability of the target system (5.59)-(5.63) for a given time interval $\forall t \in [0, t^{\star})$ under the assumption that condition (5.14) is satisfied. Then we prove that with initial conditions of states variables bounded, the local exponential stability of the above target system holds for $\forall t \in [0,\infty)$ with the assumption removed. This is achieved by comparison principle and contradiction proof in Lemma 5.6. In the end, the stability analysis of the target system leads to stability of the original PDE-ODE system in (5.11)-(6.77).

Let us define the Lyapunov functional

$$V(t) = V_1(t) + V_2(t) + \lambda V_3(t) + \lambda V_4(t) + V_5(t), \tag{5.74}$$

where $\lambda > 0$ with the component Lyapunov functions

$$\begin{aligned}
V_1(t) &= \int_0^{l(t)} e^{-x} w_{\mathrm{f}}^2(x,t)dx, && (5.75)\\
V_2(t) &= \int_{l(t)}^{L} e^{x-L} w_{\mathrm{c}}^2(x,t)dx, && (5.76)\\
V_3(t) &= \int_0^{l(t)} e^{-x} \partial_x w_{\mathrm{f}}^2(x,t)dx, && (5.77)\\
V_4(t) &= \int_{l(t)}^{L} e^{x-L} \partial_x w_{\mathrm{c}}^2(x,t)dx, && (5.78)\\
V_5(t) &= X(t)^2. && (5.79)
\end{aligned}$$

Lemma 5.4. *Assume* $\exists t^\star > 0$ *such that the condition in* (5.14) *is satisfied, then there exists* $\sigma > 0$ *such that the following holds* $\forall t \in [0, t^\star)$*,*

$$\dot{V}(t) \leq -\sigma V + \tau V^{3/2}. \tag{5.80}$$

Proof. Taking time derivative of the Lyapunov function (5.74) along the solution of the target system (5.59)-(5.63), we have

$$\begin{aligned}
\dot{V}_1(t) = &-u \int_0^{l(t)} e^{-x} w_{\mathrm{f}}^2(x,t)dx - (u - \dot{l}(t)) e^{-l(t)} w_{\mathrm{f}}^2(l(t),t)\\
&+ \frac{2K_{\mathrm{f}}b}{u} \dot{l}(t) g(t) \int_0^{l(t)} e^{-x} w_{\mathrm{f}}(x,t)dx\\
&+ \frac{4K_{\mathrm{f}}b}{u} \dot{l}(t) \int_0^{l(t)} e^{-x} \varepsilon_{\mathrm{c}}(x,t) w_{\mathrm{f}}(x,t)dx, && (5.81)\\
\dot{V}_2(t) = &-u \int_{l(t)}^{L} e^{x-L} w_{\mathrm{c}}^2(x,t)dx - (u + \dot{l}(t)) e^{l(t)-L} w_c^2(l(t),t)
\end{aligned}$$

$$
\begin{aligned}
&+\frac{2K_{\mathrm{c}}b}{u}\dot{l}(t)g(t)\int_{l(t)}^{L}e^{x-L}w_{\mathrm{c}}(x,t)dx\\
&-\frac{4K_{\mathrm{c}}b}{u}\dot{l}(t)\int_{l(t)}^{L}e^{x-L}\varepsilon_{\mathrm{f}}(x,t)w_{\mathrm{c}}(x,t)dx, \qquad (5.82)
\end{aligned}
$$

$$
\begin{aligned}
\dot{V}_3(t)=&-u\int_0^{l(t)}e^{-x}\partial_x w_f^2(x,t)dx\\
&-(u-\dot{l}(t))e^{-l(t)}\partial_x w_{\mathrm{f}}^2(l(t),t)+u\partial_x w_{\mathrm{f}}^2(0,t)\\
&+\frac{4K_{\mathrm{f}}b}{u}\dot{l}(t)\int_0^{l(t)}e^{-x}\partial_x\varepsilon_{\mathrm{c}}(x,t)\partial_x w_{\mathrm{f}}(x,t)dx, \qquad (5.83)\\
\dot{V}_4(t)=&-u\int_{l(t)}^{L}e^{x-L}\partial_x w_{\mathrm{c}}^2(x,t)dx\\
&-(u+\dot{l}(t))e^{l(t)-L}\partial_x w_{\mathrm{c}}^2(l(t),t)+u\partial_x w_{\mathrm{c}}^2(L,t)\\
&-\frac{4K_{\mathrm{c}}b}{u}\dot{l}(t)\int_{l(t)}^{L}e^{x-L}\partial_x\varepsilon_{\mathrm{c}}(x,t)\partial_x w_{\mathrm{c}}(x,t)dx, \qquad (5.84)\\
\dot{V}_5(t)=&-aX(t)^2-b\left(w_{\mathrm{c}}(l(t),t)+w_{\mathrm{f}}(l(t),t)\right)X(t). \qquad (5.85)
\end{aligned}
$$

By Agmon's inequality, the followings hold

$$
w_{\mathrm{f}}^2(l(t),t)\le||w_{\mathrm{f}}||_\infty^2\le 4||\partial_x w_{\mathrm{f}}||_2^2=4V_3, \qquad (5.86)
$$

$$
w_{\mathrm{c}}^2(l(t),t)\le||w_{\mathrm{c}}||_\infty^2\le 4||\partial_x w_{\mathrm{c}}||_2^2=4V_4. \qquad (5.87)
$$

Plugging the above inequalities into the ODE (5.63) yields that there exists $\delta>0$ such that

$$
\begin{aligned}
|\dot{l}(t)|&<a\sqrt{V_5}+b(\sqrt{V_3}+\sqrt{V_4})\\
&<\delta\sqrt{V}. \qquad (5.88)
\end{aligned}
$$

Using Young's inequality, Cauchy-Schwarz inequality for (5.64) and (5.86),(5.87), we have

$$
g(t)^2\le\mu_1V_3+\mu_2V_4+\mu_3V_5, \qquad (5.89)
$$

where $\mu_j > 0, j = 1,2,3$. By definition of $\varepsilon_{\mathrm{c}}(x,t)$ in (5.65), there exist $\eta_k > 0,\ k = 1,2,4$ such that

$$\int_0^{l(t)} \varepsilon_{\mathrm{c}}^2(x,t)dx \leq \eta_1 V_1 + \eta_2 V_2 + \eta_4 V_4. \tag{5.90}$$

It follows that

$$\begin{aligned}\dot{V}_1(t) \leq & -uV_1 + |\dot{l}(t)| w_{\mathrm{f}}^2(l(t),t) \\ & + \frac{2K_{\mathrm{f}}b}{u}|\dot{l}(t)| \left(g^2(t) + \int_0^{l(t)} w_{\mathrm{f}}^2(x,t)dx \right) \\ & + \frac{4K_{\mathrm{f}}b}{u}|\dot{l}(t)| \left(\int_0^{l(t)} \varepsilon_{\mathrm{c}}^2(x,t)dx + \int_0^{l(t)} w_{\mathrm{f}}^2(x,t)dx \right),\end{aligned} \tag{5.91}$$

Plugging (5.86) and (5.88)-(5.90) into the above inequality, there exists $\kappa_1 > 0$ such that

$$\dot{V}_1(t) \leq -uV_1 + \kappa_1 V^{3/2}, \tag{5.92}$$

Taking total time derivative of boundary condition (5.61) yields,

$$\partial_x w_{\mathrm{f}}(0,t) = \frac{K_{\mathrm{f}}b}{u^2}\dot{l}(t)(g(t) + 2\varepsilon_{\mathrm{c}}(0,t)), \tag{5.93}$$

Given definition of $\varepsilon_{\mathrm{c}}(x,t)$ in (5.65), there exist $\nu_0,\ \nu > 0$ such that

$$\varepsilon_{\mathrm{c}}(0,t) < \nu_0 V, \tag{5.94}$$

$$\int_0^{l(t)} \partial_x \varepsilon_{\mathrm{c}}^2(x,t) < \nu V. \tag{5.95}$$

Using Young's inequality and plugging (5.89) and (5.94) into (5.93), we obtain that there exists

$\theta > 0$ such that

$$\begin{aligned}\partial_x w_{\mathrm{f}}^2(0,t) \leq{}& \frac{K_{\mathrm{c}} b}{u^2} |\dot{l}(t)| \left(g^2(t) + 4\varepsilon_{\mathrm{c}}^2(0,t)\right) \\ <{}& \theta V^{3/2}, \end{aligned} \tag{5.96}$$

Plugging (5.86), (5.88), (5.95) and (5.96) into (5.83), we obtain that there exists $\kappa_3 > 0$ such that

$$\dot{V}_3(t) \leq -uV_3 + \kappa_3 V^{3/2}. \tag{5.97}$$

In the same fashion, we could obtain that there exist $\kappa_2, \kappa_4 > 0$ such that

$$\dot{V}_2(t) \leq -uV_2 + \kappa_2 V^{3/2}, \tag{5.98}$$

$$\dot{V}_4(t) \leq -uV_4 + \kappa_4 V^{3/2}, \tag{5.99}$$

For the last Lyapunov component, the following holds

$$\dot{V}_5(t) \leq -aV_5 + \frac{4b}{a} V_3 + \frac{4b}{a} V_4. \tag{5.100}$$

Using inequalities (5.92) and (5.97)-(5.100) into (5.74), it follows that

$$\begin{aligned}\dot{V}(t) \leq{}& -uV_1 - uV_2 - \left(\lambda u - \frac{4b}{a}\right) V_3 \\ & - \left(\lambda u - \frac{4b}{a}\right) V_4 - aV_5 + \tau V^{3/2}. \end{aligned} \tag{5.101}$$

where $\tau = \kappa_1 + \kappa_2 + \lambda\kappa_3 + \lambda\kappa_4 > 0$. We choose λ such that

$$\lambda > \frac{4b}{au}, \tag{5.102}$$

thus it holds that for $\sigma = \min\left\{u - \frac{4b}{\lambda a}, a\right\}$,

$$\dot{V}(t) \leq -\sigma V + \tau V^{3/2}. \tag{5.103}$$

□

Lemma 5.5. *According to* (5.80)*, for any* σ_0 *such that* $0 < \sigma_0 < \sigma$*, there exists* $\delta_0 > 0$ *such that for any* $V(0) < \delta_0$*,*

$$\tau|V^{3/2}| < (\sigma - \sigma_0)V \tag{5.104}$$

and,

$$\dot{V}(t) \leq -\sigma_0 V. \tag{5.105}$$

By comparison principle, the exponential stability is satisfied that $\forall t \in [0, t^\star)$*,*

$$V(t) \leq V(0)e^{-\sigma_0 t} < \delta_0. \tag{5.106}$$

Lemma 5.6. *If the initial conditions of the target system* $(w_{\mathrm{f}}(x,0), w_{\mathrm{c}}(x,0), X(0))$ *satisfy the following*

$$V(0) \leq \min\{\delta_0, \delta_1\}, \tag{5.107}$$

where the positive constant δ_1 *is defined as*

$$\delta_1 = \min\left\{(L - l^\star)^2, l^\star\right\}. \tag{5.108}$$

Then Lyapunov functional inequality (5.105) *and condition* (5.14) *hold for* $t \in [0, \infty)$.

Proof. We assume that there exists $t^\star > 0$ such that condition (5.14) is satisfied for $t \in [0, t^\star)$ but is violated at $t = t^\star$. Given (5.107) and by comparison principle, the following inequality holds

$$V(t^\star) \leq V(0) < \delta_1. \tag{5.109}$$

According to the definition of $V(t)$ in (5.74), we obtain that

$$X^2(t^\star) < V(t^\star). \tag{5.110}$$

Combining (5.108) and (5.109), we have

$$X^2(t^\star) < \delta_1 = \min\left\{(L - l^\star)^2, (l^\star)^2\right\}. \tag{5.111}$$

Since $l(t^\star) = X(t^\star) + l^\star$ and $0 < l^\star < L$, we obtain from (5.111) that

$$0 < l(t^\star) < L. \tag{5.112}$$

We conclude that (5.112) contradicts the assumption that (5.14) is violated at $t = t^\star$. Therefore, the condition (5.14) is guaranteed for $t \in [0, \infty)$ when the initial condition $V(0)$ satisfies (5.107). This completes the proof Lemma 5.6.

Due to invertibility of the transformation in (5.49),(5.50), we conclude that the system (5.25)-(5.29) with control laws (5.68),(5.69) is locally exponentially stable in the H^1 norm, which completes the proof of Theorem 5.3. □

5.5 Simulation

We simulate the previous control design considering a moving traffic shockwave in a 500-meter freeway segment. The initial condition of the traffic profile and the desirable target traffic

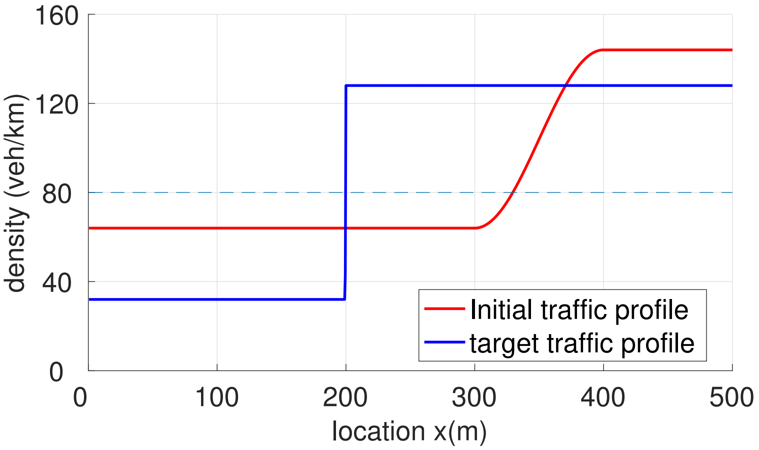

Figure 5.3: Traffic density profiles for initial condition with a soft shockwave and target system on freeway.

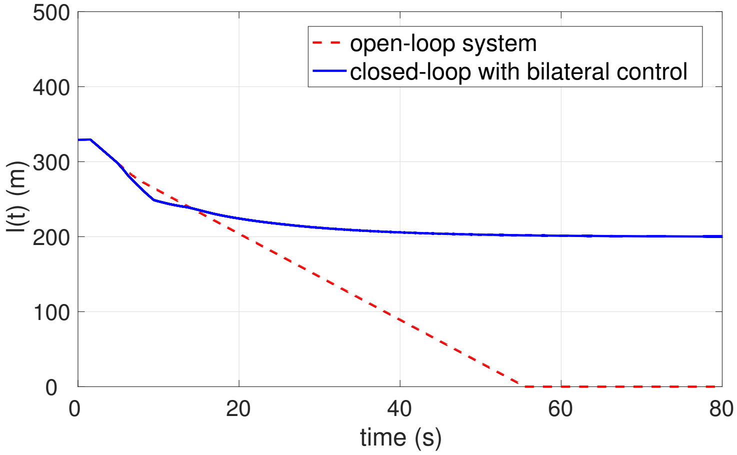

Figure 5.4: Evolution of the moving interface position $l(t)$ for open-loop system and for closed-loop system with bilateral boundary control.

profile $\rho_{\mathrm{f}}^{\star} = 32$ vehs/km, $\rho_{\mathrm{c}}^{\star} = 128$ vehs/km, $l^{\star} = 200$ m, $\rho_{\mathrm{jump}} = 80$ vehs/km are shown in Fig. 5.3, where the position of the shockwave front is initially located at 330-meter and the final setpoint location is at 200-meter. The initial position of the shockwave front is in the right-half plane of the segment while its final position is located at the left-half plane of the segment. The control objective is to regulate PDE states and ODE state from the initial profile to the reference profile.

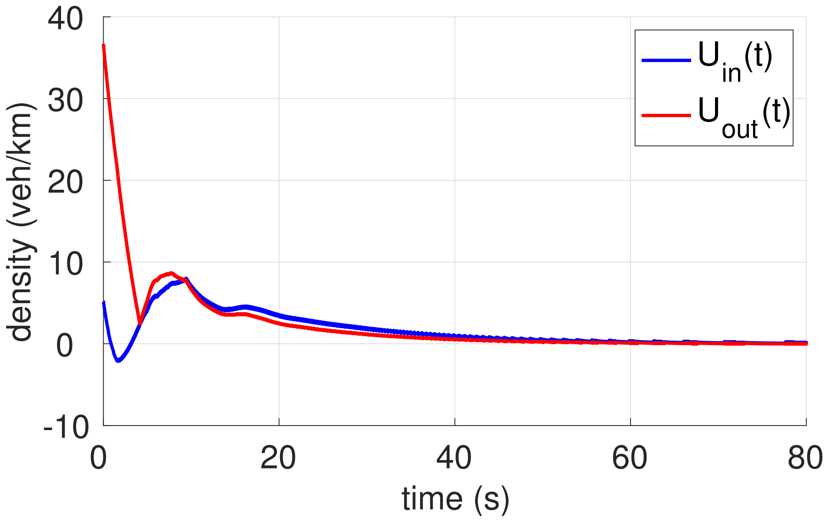

Figure 5.5: Evolution of bilateral control inputs over time.

In Fig. 5.4, after around 40*s*, the moving interface position stops at the setpoint location $l = 200$ m with bilateral control while in open-loop system it propagates upstream and travels out of the freeway segment before 1 min. In Fig. 5.5, one can observe that the bilateral control signals, the control inputs also converge to zeros after around 40*s*.

5.6 Conclusion

This chapter addresses boundary feedback control problem of moving shockwave in congested traffic described by an PDE-ODE system. To stabilize the coupled system to a desired setpoint, we use predictor-based backstepping method to transform the state-dependent PDE-ODE coupled system to a target system, where the PDE state-dependent input delays to ODE are compensated by the bilateral boundary control inputs to PDEs. Actuations of traffic densities at both boundaries are considered. The local exponential stability in H^1 norm is achieved and the model validity is guaranteed with the control designs. For future work, general theoretical results on multiple PDEs state-dependent input delays cascading to a nonlinear ODE is of authors' interest.

Chapter 5 contains reprints and adaptations of the following paper: H. Yu, M. Diagne, L.-G. Zhang, and M. Krstic, “Bilateral boundary control of moving schockwave in LWR model of congested traffic,” *IEEE Transactions on Automatic Control*, under review. The dissertation author is the primary investigator and author of this paper.

Chapter 6

Extremum Seeking Control of Downstream Traffic Bottleneck

We develop boundary control for freeway traffic with a downstream bottleneck. Traffic on a freeway segment with capacity drop at outlet of the segment is a common phenomenon leading to traffic bottleneck problem. The capacity drop can be caused by lane-drop, hills, tunnel, bridge or curvature on the road. If incoming traffic flow remains unchanged, traffic congestion forms upstream of the bottleneck due to outgoing traffic overflowing its capacity. Therefore, it is important for us to regulate the incoming traffic flow of the segment so that the outgoing traffic at the bottleneck can be discharged with the maximum flow rate. Traffic densities on the freeway segment are described with LWR macroscopic PDE model. To prevent the traffic congestion forming upstream of the bottleneck, incoming flow at the inlet of the freeway segment is controlled so that the optimal density could be achieved to maximize the outgoing flow and not to surpass the capacity at outlet. The density and traffic flow relation, described with fundamental diagram, is assumed to be unknown at the bottleneck area. We tackle this problem using ES Control with delay compensation for LWR PDE. ES control, a non-model based approach for real-time optimization, is adopted to find the optimal density for the unknown fundamental diagram. A predictor feedback control design is proposed to compensate the delay effect of traffic dynamics in the freeway segment. In the end, simulation results validate a desired performance of the controller on the nonlinear LWR model with an unknown fundamental diagram.

The outline of this chapter: we firstly introduce LWR PDE model for the freeway segment upstream of bottleneck and describe density-flow relation at bottleneck with a nonlinear map. For the linearized error system, we design a predictor feedback control law with delay compensation. Stability analysis is conducted for the closed-loop system using backstepping transformation and averaging approach. To illustrate our result, simulation is performed on the nonlinear LWR PDE model and a quadratic fundamental diagram is considered. The conclusion and discussion of future work are given in the end.

6.1 Downstream bottleneck problem

We consider a traffic problem on a freeway-segment with lane drop downstream of the segment. The freeway segment upstream of the bottleneck and the lane-drop area are shown in Fig. 6.1 which illustrates the clear Zone C and the bottleneck Zone B respectively. To prevent the traffic in Zone B overflowing its capacity and then causing congestion in the freeway segment, we aim to find out the optimal density ahead of Zone C that maximizes outgoing flux of Zone B given unknown density-flow relation. Traffic dynamics in Zone C is described with macroscopic traffic model for aggregated values of traffic density. The traffic dynamics in lane-drop Zone B is usually difficult to describe with mathematical model and thus assumes that the fundamental diagram is unknown.

Here we choose the first-order LWR model instead of more sophisticated second-order ARZ model for the following reasons. The second-order ARZ model consisting of two PDEs governs both the traffic density and velocity. The second-order ARZ PDE model was brought up to resolve the issue that equilibrium fundamental diagram are not suited for the congested

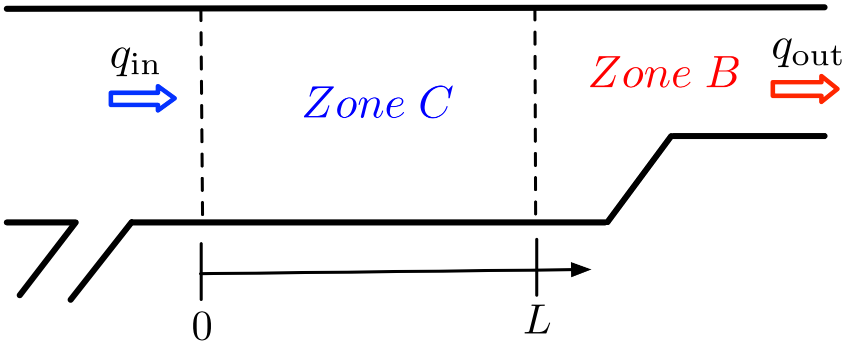

Figure 6.1: Traffic on a freeway segment with lane-drop.

regime. Traffic velocity could vary from the single-valued equilibrium function. In this problem, we consider the free regime for freeway segment to prevent the formation of traffic congestion in bottleneck area. LWR model therefore suit our needs.

We control traffic flow entering at the inlet of Zone C upstream of block Zone B. Traffic dynamics of Zone C is described with the first-order LWR model. Therefore, we design ES control for an unknown static map with actuation dynamics governed by a nonlinear hyperbolic PDE. The control objective is to find the optimal input density at inlet of Zone C that drives the measurable output flux of Zone B to its unknown optimal value of an unknown fundamental diagram.

The traffic dynamics in Zone C upstream of Zone B is described with the first-order, hyperbolic LWR model. Traffic density $\rho(x,t)$ in Zone C is governed by the following nonlinear hyperbolic PDE, where $x \in [0,L]$, $t \in [0,\infty)$,

$$\partial_t \rho + \partial_x(\rho V(\rho)) = 0, \tag{6.1}$$

where traffic velocity follows an equilibrium velocity-density relation $V(\rho)$. The fundamental diagram of traffic flow and density function $Q(\rho)$ is given by

$$Q(\rho) = \rho V(\rho). \tag{6.2}$$

There are different models to describe the flux and density relation. A basic and popular choice is Greenshield's model for $V(\rho)$ which is given by

$$V(\rho) = v_f \left(1 - \frac{\rho}{\rho_m}\right), \tag{6.3}$$

where $v_f \in \mathbb{R}^+$ is defined as maximum velocity and $\rho_m \in \mathbb{R}^+$ is maximum density for Zone C. Then the fundamental diagram of flow and density function $Q(\rho)$ is in a quadratic form of density,

$$Q(\rho) = -\frac{v_f}{\rho_m}\rho^2 + v_f \rho. \tag{6.4}$$

In practice, quadratic fundamental diagram does not provide a good fitting with real traffic density-flow data. The critical density usually happens at 20% of the maximum value of density. There are several other equilibrium model e.g. Greenberg model, Underwood model and diffusion model for which fundamental diagrams are nonlinear functions. According to Taylor expansion, second-order differentiable nonlinear function can be approximated as a quadratic function in the neighborhood of its extremum. The following assumption is made for the nonlinear fundamental diagram. The stability results derived in this paper holds locally for the general form of $Q(\rho)$ that satisfy the following assumption.

Assumption 6.1. *We assume the fundamental diagram $Q(\rho)$ is a $\mathscr{C}^2$ function, then $Q(\rho)$ can be decomposed at the critical density ρ_c as follows:*

$$Q(\rho) = q_c + \frac{Q''(\rho)}{2}(\rho(t) - \rho_c)^2, \tag{6.5}$$

where $q_c = Q(\rho_c)$ defined as the road capacity or maximum flow, with assumption that $Q''(\rho) < 0$ is satisfied.

When there is a bottleneck present downstream, the density at outlet of Zone C is $\rho(L,t)$

governed by PDE in (6.1) for $x \in [0,L]$, $t \in [0,\infty)$ and boundary condition at inlet in (6.6). The inlet boundary flow is,

$$q_{\text{in}}(t) = Q(\rho(0,t)). \tag{6.6}$$

The control objective is to design the traffic flow input $q_{\text{in}}(t)$ so that the outgoing flow in lane-drop area Zone B $q_{\text{out}}(t)$ is maximized.

The traffic dynamics in Zone B is described by an unknown fundamental diagram since density and traffic flow relation at the bottleneck area is hard to determine. Therefore, we assume that the equilibrium fundamental diagram for Zone B is an unknown quadratic map $Q_B(\rho)$, shown in Fig. 6.2. The measurement of traffic flow in Zone B, $q_{\text{out}}(t)$ is defined by $Q_B(\rho)$ with outlet density $\rho(L,t)$ at outlet,

$$q_{\text{out}}(t) = Q_B(\rho(L,t)). \tag{6.7}$$

Due to the lane-drop at outlet, maximum density and road capacity reduced at Zone B compared with Zone C. We consider that optimal density of Zone B is smaller than critical density $\rho^\star \in \mathbb{R}^+$ of Zone C. We aim to find out the critical outlet density $\rho^\star$ of Zone C that maximize $q_{\text{out}}(t)$ in Zone B,

$$q_{\text{out}}(t) = q^\star + \frac{H}{2}(\rho(L,t) - \rho^\star)^2, \tag{6.8}$$

where $q^\star \in \mathbb{R}^+$ is the unknown optimal output flow for Zone B and $H < 0$ is the unknown Hessian of the static map Q_B.

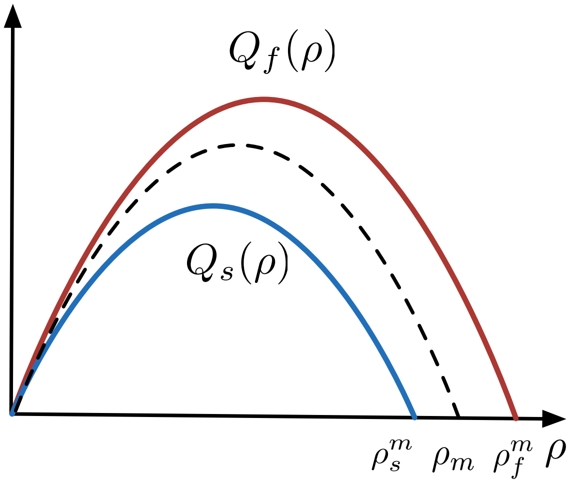

Figure 6.2: Quadratic fundamental diagram with distant bottleneck.

6.1.1 Linearized reference error system

We linearize the nonlinear LWR model around a constant reference density $\rho_r \in \mathbb{R}^+$, which is assumed to be close to the optimal density $\rho^\star$. Note that the reference density ρ_r is in the free regime of $Q(\rho)$ of Zone C thus is smaller than the critical density ρ_c and therefore the following is satisfied

$$\rho_r < \rho_c. \tag{6.9}$$

Here we do not specify fundamental diagram $Q(\rho)$ for Zone C but require assumption 6.1 to be satisfied. Define the reference error density as

$$\tilde{\rho}(x,t) = \rho(x,t) - \rho_r, \tag{6.10}$$

and reference flux q_r is

$$q_r = Q(\rho_r) > 0. \tag{6.11}$$

By the governing equation (6.1) together with (6.3), the linearized reference error model is derived as

$$\partial_t \tilde{\rho}(x,t) + u\partial_x \tilde{\rho}(x,t) = 0, \tag{6.12}$$

$$\tilde{\rho}(0,t) = \rho(0,t) - \rho_r, \tag{6.13}$$

where the constant transport speed u is given by

$$\begin{aligned} u =& Q'(\rho)|_{\rho=\rho_r} \\ =& V(\rho_r) + \rho_r V'(\rho)|_{\rho=\rho_r}. \end{aligned} \tag{6.14}$$

The equilibrium velocity-density relation $V(\rho)$ is a strictly decreasing function. The reference density ρ_r is in the left-half plane of the fundamental diagram $Q_c(\rho)$ which yields the following inequality for the propagation speed u,

$$u > 0. \tag{6.15}$$

According to (6.6) and (6.13), we define the input density as

$$\rho(t) = \rho(0,t), \tag{6.16}$$

and the linearized input at inlet is

$$\tilde{\rho}(t) = \rho(t) - \rho_r. \tag{6.17}$$

The linearized error dynamics in (6.12), (6.13) is a transport PDE with an explicit solution for $t > \frac{x}{u}$ and thus is represented with input density

$$\tilde{\rho}(x,t) = \tilde{\rho}\left(t - \frac{x}{u}\right), \tag{6.18}$$

The density variation at outlet is

$$\tilde{\rho}(L,t) = \tilde{\rho}\,(t - D)\,. \tag{6.19}$$

where the time delay D is defined as

$$D = \frac{L}{u}. \tag{6.20}$$

Therefore, the density at outlet is given by a delayed input density variation and the reference

$$\rho(L,t) = \rho_r + \tilde{\rho}(L,t). \tag{6.21}$$

Finally, substituting (6.19), (6.21) into the static map (6.8), we arrive at the following

$$\begin{aligned} q_{\text{out}}(t) =& q^\star + \frac{H}{2}(\tilde{\rho}\,(t-D) + \rho_r - \rho^\star)^2 \\ =& q^\star + \frac{H}{2}\left(\rho\,(t-D) - \rho^\star\right)^2. \end{aligned} \tag{6.22}$$

The control objective is to regulate the input $q_{\text{in}}(t)$ so that $\rho\,(t-D)$ reaches to an unknown optimal $\rho^\star$ and the maximum of the uncertain quadratic flux-density map $q_{\text{out}}(t)$ can be achieved. We can apply the method of extremum seeking for static map with delays developed in [90]. The extremum seeking control is designed for finding the extremum of the unknown map.

In practice, control of density at inlet can be realized with simultaneous operation of a

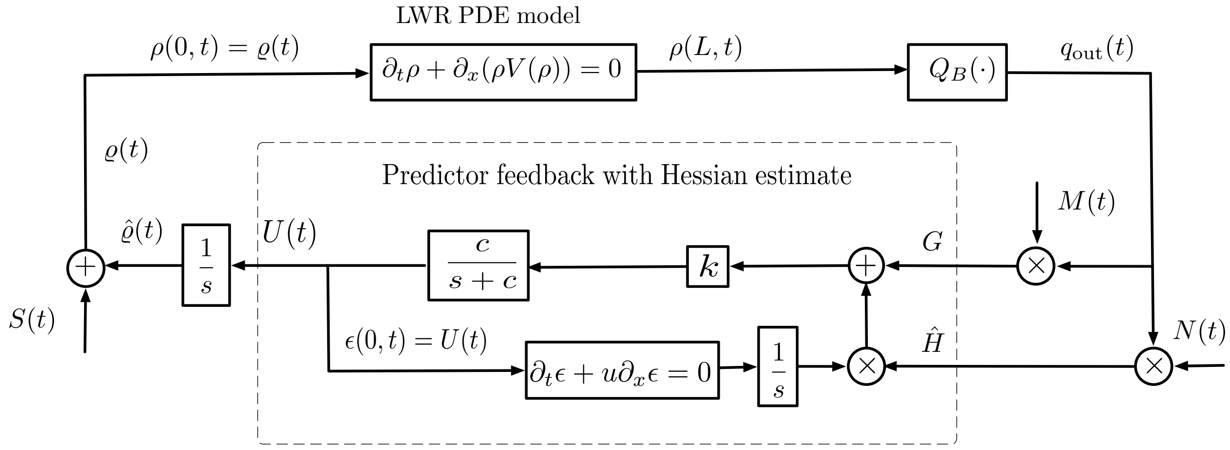

Figure 6.3: Block diagram for implementation of ES control design for nonlinear LWR PDE model.

ramp metering and a VSL at inlet. The controlled density is then given by

$$\rho(t)=\frac{q_{\text{in}}(t)}{v_c}. \tag{6.23}$$

where v_c is the speed limit implemented by VSL and $q_{\text{in}}(t)$ is actuated by a on-ramp metering upstream of the inlet. Note that the linearized model is valid at the optimal density $\rho^\star$ since the reference density is assumed to be chosen near the optimal value.

6.2 Online optimization by extremum seeking control

In this section, we present the design of extremum seeking control with delay by following analogously the procedure in [90]. The block diagram of the delay-compensated ES algorithm applied to LWR PDE model is depicted in Fig. 6.3.

Let $\hat{\rho}(t)$ be the estimate of $\rho^\star$, and $e(t)$ be the estimation error defined as

$$e(t)=\hat{\rho}(t)-\rho^\star. \tag{6.24}$$

From Fig. 6.3, the error dynamics can be written as

$$\dot{e}(t-D) = U(t-D). \tag{6.25}$$

First, we introduce the dither signals $(M(t), N(t))$ given by

$$M(t) = \frac{2}{a}\sin(\omega t), \tag{6.26}$$

$$N(t) = -\frac{8}{a^2}\cos(2\omega t), \tag{6.27}$$

where a and ω are amplitude and frequency of a slow periodic perturbation signal $a\sin(\omega t)$ introduced later. Using the dither signals, we calculate estimates of the gradient and Hessian of the cost function, denoted as $(G(t), \hat{H}(t))$,

$$G(t) = M(t)q_{\mathrm{out}}(t), \tag{6.28}$$

$$\hat{H}(t) = N(t)q_{\mathrm{out}}(t), \tag{6.29}$$

where $\hat{H}(t)$ is to estimate the unknown Hessian H. The averaging of $G(t)$ and $\hat{H}(t)$ yields that

$$G_{\mathrm{av}}(t) = He_{\mathrm{av}}(t-D), \tag{6.30}$$

$$\hat{H}_{\mathrm{av}} = (Nq_{\mathrm{out}})_{\mathrm{av}} = H. \tag{6.31}$$

Taking average of (6.25), we have

$$\dot{e}_{\mathrm{av}}(t-D) = U_{\mathrm{av}}(t-D), \tag{6.32}$$

where $U_{\mathrm{av}}(t)$ is the averaged value for $U(t)$ designed later. Substituting the above equation into

(6.30) gives that

$$\dot{G}_{\mathrm{av}}(t) = HU_{\mathrm{av}}(t-D). \tag{6.33}$$

The motivation for predictor feedback design is to compensate for the delay by feeding back future states in the equivalent averaged system $G_{av}(t+D)$. Given an arbitrary control gain $k > 0$, we aim to design

$$U_{\mathrm{av}}(t) = kG_{\mathrm{av}}(t+D), \quad \forall t \geq 0. \tag{6.34}$$

which requires knowledge of future states. Therefore we have the following by plugging (6.34) into (6.25),

$$\dot{e}_{\mathrm{av}}(t) = U_{\mathrm{av}}(t) = kHe_{\mathrm{av}}(t), \quad \forall t \geq D. \tag{6.35}$$

Reminding that $k > 0, H < 0$, the equilibrium of the average system $e_{\mathrm{av}}(t) = 0$ is exponentially stable.

Applying the variation of constants formula

$$G_{\mathrm{av}}(t+D) = G_{\mathrm{av}}(t) + \hat{H}_{\mathrm{av}}(t)\int_{t-D}^{t} U_{\mathrm{av}}(\tau)d\tau, \tag{6.36}$$

and from (6.34), one has:

$$U_{\mathrm{av}}(t) = k\left(G_{\mathrm{av}}(t) + \hat{H}_{\mathrm{av}}(t)\int_{t-D}^{t} U_{\mathrm{av}}(\tau)d\tau\right), \tag{6.37}$$

which represents the future state $G_{\mathrm{av}}(t+D)$ in (6.33) in terms of the average control signal $U_{\mathrm{av}}(\tau)$ for $\tau \in [t-D,t]$. The control input is infinite-dimensional due to its use of history over the past D time units.

For the stability analysis in which the averaging theorem for infinite dimensional systems is used, we employ a low-pass filter for the above basic predictor feedback controller and then derive an infinite dimensional and averaging based predictor feedback given by

$$U(t)=\mathscr{T}\left\{k\left(G(t)+\hat{H}(t)\int_{t-D}^{t}U(\tau)d\tau\right)\right\}, \tag{6.38}$$

where $k>0$ is an arbitrary control gain, the Hessian estimate $\hat{H}(t)$ is updated according to (6.29), satisfying average property in (6.31). $\mathscr{T}\{\}$ is the low pass filter operator defined by

$$\mathscr{T}\{\varphi(t)\}=\mathscr{L}^{-1}\left\{\frac{c}{s+c}\right\}*\varphi(t), \tag{6.39}$$

where $c\in\mathbb{R}^{+}$ is the corner frequency, $\mathscr{L}^{-1}$ is the inverse Laplace transformation, and $*$ is the convolution in time.

6.3 Stability analysis

This section is devoted to the proof of the main theorem for delay-compensated ES algorithm, following [90]. Although the results in [90] are oriented to multiple and distinct delays, the derivation for the case of single delay was omitted there and it will be completely detailed here as a further contribution.

Theorem 6.2. *Consider the closed-loop system in Fig. 6.3. There exits* $c_0>0$ *such that* $\forall c\geq c_0$*, there exists* $\omega_0(c_0)>0$ *such that* $\forall\omega>\omega_0$*, the closed-loop system has a unique exponentially stable periodic solution in period* $T=\frac{2\pi}{\omega}$*, denoted by* $e^{T}(t-D)$*,* $U^{T}(\tau)$*,* $\forall\tau\in[t-D,t]$*, satisfying* $\forall t>0$

$$\left(|e^{T}(t-D)|^{2}+|U^{T}(t)|^{2}+\int_{0}^{D}|U^{T}(\tau)|^{2}d\tau\right)^{\frac{1}{2}}\leq\mathscr{O}(1/\omega). \tag{6.40}$$

Furthermore,

$$\lim_{t\to+\infty} \sup |\rho(t) - \rho^\star| = \mathscr{O}(a + 1/\omega), \tag{6.41}$$

$$\lim_{t\to+\infty} \sup |q_{\text{out}}(t) - q^\star| = \mathscr{O}(a^2 + 1/\omega^2). \tag{6.42}$$

The proof of Theorem 6.2 is carried out in the following sections.

6.3.1 Closed-loop system

The estimate $\hat{\rho}(t)$ of the unknown optimal outgoing $\rho^\star$ is an integrator of the predictor-based feedback signal $U(t)$ as

$$\dot{\hat{\rho}}(t) = U(t), \tag{6.43}$$

and it follows that

$$\dot{e}(t-D) = U(t-D). \tag{6.44}$$

The input $\rho(t)$ to LWR PDE model is given by

$$\rho(t) = \hat{\rho}(t) + S(t), \tag{6.45}$$

where the dither signal $S(t)$ is the inverse operator of a delayed perturbation signal $a\sin(\omega t)$, described as

$$S(t) = a\sin(\omega(t+D)). \tag{6.46}$$

Substituting $S(t)$ into (6.45), we have

$$\rho(t) = \hat{\rho}(t) + a\sin\left(\omega(t+D)\right). \tag{6.47}$$

The delayed estimation error dynamics can be written as transport PDE system, $x \in [0, L]$

$$\dot{e}(t-D) = \varepsilon(L,t), \tag{6.48}$$

$$\partial_t \varepsilon(x,t) = -u\partial_x \varepsilon(x,t), \tag{6.49}$$

$$\varepsilon(0,t) = U(t). \tag{6.50}$$

where

$$\varepsilon(x,t) = U\left(t - \frac{x}{u}\right). \tag{6.51}$$

Combining (6.22), (6.24), and (6.46), the relation among the estimation error $e(t)$, the input density $\rho(t)$, and optimal outlet density $\rho^\star$ is given by

$$e(t) + a\sin(\omega t) = \rho(t) - \rho^\star, \tag{6.52}$$

Substituting the above relation into the output map in (6.22), we obtain the following equation

$$q_{\mathrm{out}}(t) = q^\star + \frac{H}{2}\left(e(t-D) + a\sin(\omega t)\right)^2. \tag{6.53}$$

Plugging $M(t)$ and $G(t)$ into (6.28) and (6.29) and representing the delayed input with PDE state $\varepsilon(x,t)$, we have

$$U(t) = \mathscr{T}\left\{k\left(G(t) + \hat{H}(t)\int_0^L \varepsilon(\tau,t)d\tau\right)\right\}, \tag{6.54}$$

$$G(t) = \frac{2}{a}\sin(\omega t)\, q_{\text{out}}(t), \tag{6.55}$$

$$\hat{H}(t) = -\frac{8}{a^2}\cos(2\omega t)\, q_{\text{out}}(t). \tag{6.56}$$

It yields

$$U(t) = \mathscr{T}\left\{ k q_{\text{out}}(t)\left(\frac{2}{a}\sin(\omega t) - \frac{8}{a^2}\cos(2\omega t)\int_0^L \varepsilon(\tau,t)d\tau\right)\right\}, \tag{6.57}$$

and by substituting q_{out} with (6.53) and combining with transport PDE in (6.48)-(6.50), we can write the closed-loop system as

$$\dot{e}(t-D) = \varepsilon(L,t), \tag{6.58}$$

$$\partial_t \varepsilon(x,t) = -u\partial_x \varepsilon(x,t), \tag{6.59}$$

$$\begin{aligned}\varepsilon(0,t) = \mathscr{T}\Bigg\{ k\left(q^\star + \frac{H}{2}\left(e(t-D) + a\sin(\omega t)\right)^2\right) \\ \left(\frac{2}{a}\sin(\omega t) - \frac{8}{a^2}\cos(2\omega t)\int_0^L \varepsilon(\tau,t)d\tau\right)\Bigg\}.\end{aligned} \tag{6.60}$$

6.3.2 Average system

Expanding (6.60) and taking average of the closed-loop system, we obtain average model by setting the averages of sine and cosine functions of $n\omega, (n = 1,2,3,4)$ to zeros. Note that the averaged controller satisfies

$$\dot{U}_{av}(t) + cU_{av}(t) = ck\left(G_{av}(t) + H\int_0^L \varepsilon_{\text{av}}(\tau,t)d\tau\right), \tag{6.61}$$

where $c > 0$ is the corner frequency of the low pass filter and $k > 0$ is the control gain. Denoting

$$\theta(t) = e(t-D), \tag{6.62}$$

the average system of (6.58)-(6.60) is rewritten by

$$\dot{\theta}_{\text{av}}(t) = \varepsilon_{\text{av}}(L,t), \tag{6.63}$$

$$\partial_t \varepsilon_{\text{av}}(x,t) = -u\partial_x \varepsilon_{\text{av}}(x,t), \tag{6.64}$$

$$\partial_t \varepsilon_{\text{av}}(0,t) = -c\varepsilon_{\text{av}}(0,t) + ckH\left(\theta_{\text{av}}(t) + \int_0^L \varepsilon_{\text{av}}(\tau,t)d\tau\right). \tag{6.65}$$

6.3.3 Backstepping transformation

We apply backstepping transformation for the averaged delay state

$$w(x,t) = \varepsilon_{\text{av}}(x,t) - kH\left[\theta_{\text{av}}(t) + \int_x^L \varepsilon_{\text{av}}(\tau,t)d\tau\right], \tag{6.66}$$

where $k > 0$ and $H < 0$. The average system (6.63)-(6.65) is mapped into the target system:

$$\dot{\theta}_{\text{av}}(t) = kH\theta_{\text{av}}(t) + w(L,t), \tag{6.67}$$

$$\partial_t w(x,t) = -u\partial_x w(x,t), \tag{6.68}$$

$$\begin{aligned}\partial_t w(0,t) &= -(c+kH)w(0,t) \\ &\quad -(kH)^2\left[e^{\frac{kHL}{u}}\theta_{\text{av}}(t) + \int_0^L e^{\frac{kH(L-\tau)}{u}} w(\tau,t)d\tau\right] .\end{aligned} \tag{6.69}$$

We explain how to derive (6.69) in detail. Combining (6.65) and (6.66), we have

$$w(0,t) = -\frac{1}{c}\partial_t \varepsilon_{\text{av}}(0,t). \tag{6.70}$$

Taking time derivative on (6.66) for $w(0,t)$, we obtain

$$\partial_t w(0,t) = \partial_t \varepsilon_{\text{av}}(0,t) - kH\varepsilon_{\text{av}}(0,t). \tag{6.71}$$

The inverse transformation is given by

$$\varepsilon_{\text{av}}(x,t) = w(x,t) + kH\left[e^{\frac{kH(L-x)}{u}}\theta_{\text{av}}(t)\int_x^L e^{\frac{kH(L-x+\tau)}{u}}\varepsilon_{\text{av}}(\tau,t)d\tau\right]. \tag{6.72}$$

Plugging (6.72) and (6.65) into (6.71), we obtain (6.69) in the target system.

6.3.4 Lyapunov stability analysis

Now consider the following Lyapunov functional for the target system

$$V(t) = \frac{a\theta_{\text{av}}^2(t)}{2} + \int_0^L e^{-x}w^2(x,t)dx + \frac{1}{2}w^2(0,t), \tag{6.73}$$

where the parameter $a > 0$ is chosen later. Taking time derivative of the Lyapunov function, we have

$$\begin{aligned}\dot{V}(t) =& akH\theta_{\text{av}}^2 + a\theta_{\text{av}}w(L,t) + \frac{u}{2}w^2(0,t) - \frac{ue^{-L}}{2}w^2(L,t)\\ &- \frac{u}{2}\int_0^L e^{-x}w^2(x,t)dx + w(0,t)w_t(0,t)\\ \leq& akH\theta_{\text{av}}^2 + \frac{a}{2b}\theta_{\text{av}}^2 + \left(\frac{ab - ue^{-L}}{2}\right)w^2(L,t)\\ &- \frac{u}{2}\int_0^L e^{-x}w^2(x,t)dx\\ &+ w(0,t)\left(w_t(0,t) + \frac{u}{2}w(0,t)\right)\end{aligned} \tag{6.74}$$

where the positive constant b satisfies the following,

$$b = \frac{ue^{-L}}{a}, \tag{6.75}$$

so that $ab - ue^{-L} = 0$. The positive constant a is chosen as

$$a = -ukHe^{-L}. \tag{6.76}$$

Substituting $w_t(0,t)$ by (6.69) and using Young's, Cauchy-Schwarz inequalities, the last term in (6.74) is bounded by

$$\begin{aligned}
& w(0,t)\left(w_t(0,t) + \frac{u}{2}w(0,t)\right) \\
\leq & -\left(c - \frac{u}{2} + kH\right) w^2(0,t) \\
& + \frac{e^L a^2}{4u}\theta_{\text{av}}^2(t) + \frac{ue^{-L}}{a^2}\left|(kH)^2 e^{\frac{kHL}{u}}\right|^2 w(0,t)^2 \\
& + \frac{ue^{-L}}{4}\|w(t)\|^2 + \frac{e^L}{u}\left\|(kH)^2 e^{\frac{kH(L-\tau)}{u}}\right\|^2 w(0,t)^2
\end{aligned} \tag{6.77}$$

Plugging (6.75)–(6.77) into (6.74), one can arrive at

$$\begin{aligned}
\dot{V}(t) \leq & -\frac{e^L a^2}{4u}\theta_{\text{av}}^2(t) - \frac{ue^{-L}}{4}\int_0^L w^2(x,t)dx \\
& -(c - c_0)w^2(0,t),
\end{aligned} \tag{6.78}$$

where c_0 is defined as

$$c_0 = \frac{u}{2} - kH + \frac{ue^{-L}}{a^2}\left|(kH)^2 e^{\frac{kHL}{u}}\right|^2 + \frac{e^L}{u}\left\|(kH)^2 e^{\frac{kH(L-\tau)}{u}}\right\|^2 \tag{6.79}$$

where $\tau \in [0,L]$. An upper bound for c_0 can be obtained from lower and upper bounds of the unknown Hessian H. Therefore, by choosing c such that $c > c^*$, we obtain

$$\dot{V}(t) \leq -\mu V(t), \tag{6.80}$$

for some $\mu > 0$. Thus, the closed-loop system is exponentially stable in the sense of the L^2 norm

$$\left(|\theta_{\mathrm{av}}(t)|^2 + \int_0^L w^2(x,t)dx + w^2(0,t)\right)^{1/2}. \tag{6.81}$$

By the invertibility of the transformation, we can see that there exist constants α_1 and α_2 such that the following inequality is obtained

$$\alpha_1 \Psi(t) \le V(t) \le \alpha_2 \Psi(t), \tag{6.82}$$

where $\Psi(t) \triangleq |\theta_{\mathrm{av}}(t)|^2 + \int_0^L \varepsilon_{\mathrm{av}}^2(x,t)dx + \varepsilon_{\mathrm{av}}^2(L,t)$, or equivalently,

$$\Psi(t) \triangleq |\theta_{\mathrm{av}}(t-D)|^2 + \int_{t-D}^t U_{\mathrm{av}}^2(\tau)d\tau + U_{\mathrm{av}}^2(t). \tag{6.83}$$

Hence, with (6.80), we get

$$\Psi(t) \le \frac{\alpha_2}{\alpha_1} e^{-\mu t} \Psi(0), \tag{6.84}$$

which completes the proof of exponential stability of the averaged system.

6.3.5 Averaging theorem

The closed-loop system is written as

$$\dot{e}(t-D) = U(t-D), \tag{6.85}$$

$$\dot{U}(t) = -cU(t) + c\left\{k\left(G(t) + \hat{H}(t)\int_{t-D}^t U(\tau)d\tau\right)\right\}. \tag{6.86}$$

Defining the state vector $z(t)$ as $z(t)=[e(t-D),U(t)]^T$, and noting that $\int_{t-D}^{t}U(\tau)d\tau=\int_{-D}^{0}U(t+\tau)d\tau$, we can write the dynamics of z as a functional differential equation described by

$$\dot{z}(t)=f(\omega t,z_t), \tag{6.87}$$

where $z_t(\tau)=z(t+\tau)$ for $-D\leq\tau\leq 0$. According to (6.84), the origin of the average closed-loop system with transport PDE is exponentially stable. Applying the averaging theorem for infinite dimensional systems developed in [56], for ω sufficiently large, (6.58)-(6.60) has a unique exponentially stable periodic solution around its equilibrium satisfying (6.40).

6.3.6 Asymptotic convergence to a neighborhood of the extremum

By using the change of variables (6.62) and then integrating both sides of (6.58) within the interval $[t,\sigma+D]$, we have:

$$\theta(\sigma+D)=\theta(t)+\int_{t}^{\sigma+D}\varepsilon(L,s)ds. \tag{6.88}$$

From (6.51), we can rewrite (6.88) in terms of U, namely

$$\theta(\sigma+D)=\theta(t)+\int_{t-D}^{\sigma}U(\tau)d\tau. \tag{6.89}$$

We define

$$\vartheta(\sigma)=\theta(\sigma+D), \quad \forall\sigma\in[t-D,t]. \tag{6.90}$$

Applying (6.89) to the above equation, we get

$$\vartheta(\sigma)=\vartheta(t-D)+\int_{t-D}^{\sigma}U(\tau)d\tau, \quad \forall\sigma\in[t-D,t]. \tag{6.91}$$

By applying the supremum norm in both sides of (6.91) and using Cauchy-Schwarz inequality, we have

$$\begin{aligned}
\sup_{t-D\leq\sigma\leq t}|\vartheta(\sigma)| &= \sup_{t-D\leq\sigma\leq t}|\vartheta(t-D)| + \sup_{t-D\leq\sigma\leq t}\left|\int_{t-D}^{\sigma}U(\tau)d\tau\right| \\
&\leq \sup_{t-D\leq\sigma\leq t}|\vartheta(t-D)| + \sup_{t-D\leq\sigma\leq t}\int_{t-D}^{t}|U(\tau)|d\tau \\
&\leq |\vartheta(t-D)| + \int_{t-D}^{t}|U(\tau)|d\tau \\
&\leq |\vartheta(t-D)| + \left(\int_{t-D}^{t}d\tau\right)^{1/2}\left(\int_{t-D}^{t}|U(\tau)|^2d\tau\right)^{1/2} \\
&\leq |\vartheta(t-D)| + \sqrt{D}\left(\int_{t-D}^{t}U^2(\tau)d\tau\right)^{1/2}. \qquad (6.92)
\end{aligned}$$

One can easily derive

$$|\vartheta(t-D)| \leq \left(|\vartheta(t-D)|^2 + \int_{t-D}^{t}U^2(\tau)d\tau\right)^{1/2}, \qquad (6.93)$$

$$\left(\int_{t-D}^{t}U^2(\tau)d\tau\right)^{1/2} \leq \left(|\vartheta(t-D)|^2 + \int_{t-D}^{t}U^2(\tau)d\tau\right)^{1/2}. \qquad (6.94)$$

By using (6.93) and (6.94), one has

$$\begin{aligned}
&|\vartheta(t-D)| + \sqrt{D}\left(\int_{t-D}^{t}U^2(\tau)d\tau\right)^{1/2} \\
\leq&(1+\sqrt{D})\left(|\vartheta(t-D)|^2 + \int_{t-D}^{t}U^2(\tau)d\tau\right)^{1/2}. \qquad (6.95)
\end{aligned}$$

From (6.92), it is straightforward to conclude that

$$\sup_{t-D\leq\sigma\leq t}|\vartheta(\sigma)| \leq (1+\sqrt{D})\left(|\vartheta(t-D)|^2 + \int_{t-D}^{t}U^2(\tau)d\tau\right)^{1/2}, \qquad (6.96)$$

and thus

$$|\vartheta(t)| \leq (1+\sqrt{D})\left(\left|\tilde{\theta}(t-D)\right|^2 + \int_{t-D}^{t}U^2(\tau)d\tau\right)^{1/2}. \qquad (6.97)$$

The above inequality (6.97) can be given in terms of the periodic solution $\vartheta^{\Pi}(t-D)$, $U^{\Pi}(\sigma)$, $\forall\sigma \in [t-D,t]$ as follows

$$|\vartheta(t)| \leq (1+\sqrt{D})\left(\left|\vartheta(t-D)-\vartheta^{\Pi}(t-D)+\vartheta^{\Pi}(t-D)\right|^2 \right. \\ \left. +\int_{t-D}^{t}\left[U(\tau)-U^{\Pi}(\tau)+U^{\Pi}(\tau)\right]^2 d\tau\right)^{1/2}. \tag{6.98}$$

Applying Young's inequality, the right-hand side of (6.98) and $|\vartheta(t)|$ can be majorized by

$$|\vartheta(t)| \leq \sqrt{2}\,(1+\sqrt{D})\left(\left|\vartheta(t-D)-\vartheta^{\Pi}(t-D)\right|^2+\left|\vartheta^{\Pi}(t-D)\right|^2 \right. \\ \left. +\int_{t-D}^{t}\left[U(\tau)-U^{\Pi}(\tau)\right]^2 d\tau+\int_{t-D}^{t}\left[U^{\Pi}(\tau)\right]^2 d\tau\right)^{1/2}. \tag{6.99}$$

From the averaging theorem [56], we have the exponential convergence

$$\vartheta(t-D)-\vartheta^{\Pi}(t-D) \to 0 \tag{6.100}$$

$$\int_{t-D}^{t}\left[U(\tau)-U^{\Pi}(\tau)\right]^2 d\tau \to 0 \tag{6.101}$$

Hence,

$$\limsup_{t\to+\infty}|\vartheta(t)| = \sqrt{2}\,(1+\sqrt{D}) \\ \times\left(\left|\vartheta^{\Pi}(t-D)\right|^2+\int_{t-D}^{t}[U^{\Pi}(\tau)]^2 d\tau\right)^{1/2}. \tag{6.102}$$

From (6.40) and (6.102), we can write

$$\limsup_{t\to+\infty}|\vartheta(t)| = \mathscr{O}(1/\omega). \tag{6.103}$$

From (6.24) and recalling that $\rho(t)=\hat{\rho}(t)+a\sin(\omega(t+D))$ and $\theta(t)=e(t-D)$, one has that

$$\rho(t)-\rho^{\star} = \vartheta(t)+a\sin(\omega(t+D)). \tag{6.104}$$

Since the first term in the right-hand side of (6.104) is ultimately of order $\mathscr{O}(1/\omega)$ and the second term is of order $\mathscr{O}(a)$, then

$$\limsup_{t\to+\infty} |\rho(t)-\rho^\star| = \mathscr{O}(a+1/\omega)\,. \tag{6.105}$$

Finally, from (6.22), we get (6.42) and the proof is complete. □

6.4 Simulation

In simulation, we choose Greenshield's model for equilibrium velocity-density relation. For clear section Zone C, the fundamental diagram of traffic flow-density relation is given by

$$Q(\rho) = -\frac{v_f}{\rho_m}\rho^2 + v_f\rho. \tag{6.106}$$

The maximum density is chosen to be

$$\rho_m = \frac{5 \text{ lanes}}{7.5 \text{ m}} = 0.8 \text{ vehicles/m}, \tag{6.107}$$

where the 7.5 m equals to the average vehicle length 5 m plus 50% safety distance. The maximum velocity is $v_f = 40\,\text{m/s} = 144\,\text{km/h}$. This $Q(\rho)$ is used in the nonlinear LWR PDE model simulation which describes the traffic dynamics upstream of bottleneck area. The maximum output flow also known as road capacity of Zone C is

$$q_c = \max_{0\le\rho\le\rho_m} Q(\rho) = 8 \text{ vehicles/s}. \tag{6.108}$$

The fundamental diagram in bottleneck area $Q_B(\rho)$, optimal/critical density $\rho^\star$ and maximum output flow $q^\star$ are unknown in practical implementation. The following function and parameters are chosen only for simulation purpose. For bottleneck section Zone B, we consider the situation that only 3 out of 5 lanes still function. As a result, the road capacity reduces and we define the capacity reduction rate as $C_d = 60\%$ compared with Zone C. Thus the following fundamental diagram is considered

$$Q_B(\rho) = C_d Q(\rho) = -\frac{v_f}{\rho_m}\rho^2 + v_f \rho, \tag{6.109}$$

where $\rho_m = 0.48$ vehicles/m is the maximum density for reduced lanes in the bottleneck area and the same maximum velocity $v_f = 40\,\mathrm{m/s} = 144\,\mathrm{km/h}$ is considered. The length of freeway segment is $L = 100\,m$. If we consider a linearized LWR for Zone C, the characteristic speed is

$$u = Q'(\rho)|_{\rho=\rho_r} = 20\,s. \tag{6.110}$$

The time delay for input is $D = \frac{L}{u} = 5\,s$. The outgoing flow $q_{\mathrm{out}}(t)$ of the bottleneck area is

$$\begin{aligned} q_{\mathrm{out}}(t) =& Q_B(\rho(L,t)) \\ =& q^\star + \frac{H}{2}\left(\rho\left(t-D\right) - \rho^\star\right)^2, \end{aligned} \tag{6.111}$$

where the optimal/critical density $\rho^\star$ and maximum output flow $q^\star$ are

$$\rho^\star = \frac{1}{2}\rho_m = 0.24\ \mathrm{vehicles/m}, \tag{6.112}$$

$$q^\star = C_d q_c = 4.8\ \mathrm{vehicles/s}. \tag{6.113}$$

The Hessian is obtained by taking second derivative of $Q_B(\rho)$

$$H = -\frac{2v_f}{\rho_m} = -166.7. \tag{6.114}$$

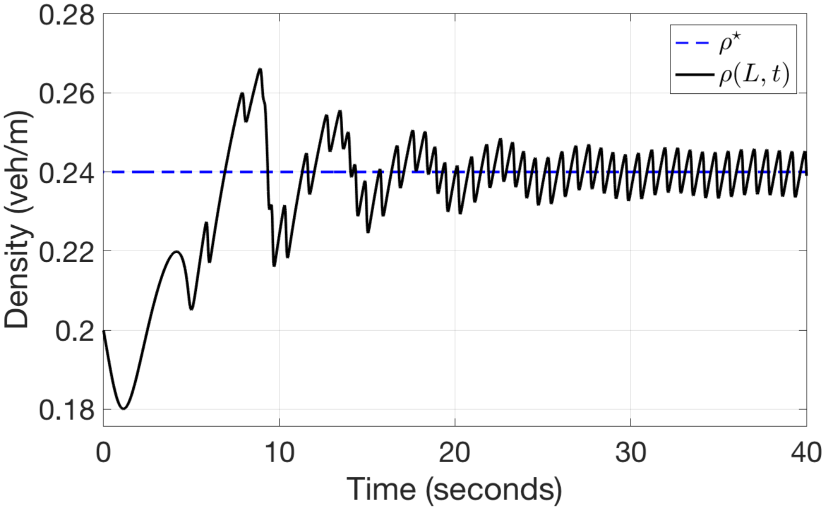

Figure 6.4: Traffic density $\rho(L,t)$ at the outlet of Zone C by nonlinear LWR model which is the input density for bottleneck area.

The Godnov scheme is employed for simulation of nonlinear LWR PDE model, which is commonly used in traffic flow application. The method is derived from the solution of local Riemann problems. The road segment is divided into spatial cell Δx and the solution is advanced in time step Δt, which satisfy the following CFL condition

$$u_{\max}\frac{\Delta t}{\Delta x} < 1, \tag{6.115}$$

where $u_{\max}$ is the maximum characteristic speed. We choose the spatial cell $\Delta x = 0.05$ m sufficiently small so that numerical errors are negligibly small relative to the errors of the model.

The simulation result of the closed-loop system with ES control is shown in Fig. 6.4, Fig. 6.5 and Fig. 6.6. The parameters of the sinusoidal input and the designed controller are chosen to be $\omega = 2.75\pi, a = 0.05, c = 50, K = 0.005$. One can observe that density in Fig. 6.4 converges to a neighborhood of the optimal value $\rho^\star = 0.24$ veh/m and the output flow of the bottleneck in Fig. 6.5 converges to a neighborhood of the extremum point $q^\star = 4.8$ veh/s. The

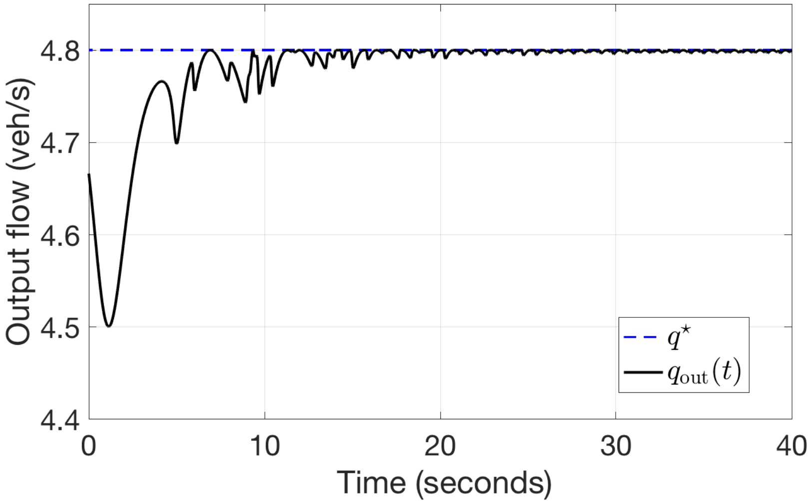

Figure 6.5: Outgoing traffic flow of the bottleneck area $q_{\text{out}}(t)$ which is also the output flow for bottleneck area and the optimal value of outgoing flow $q^\star$.

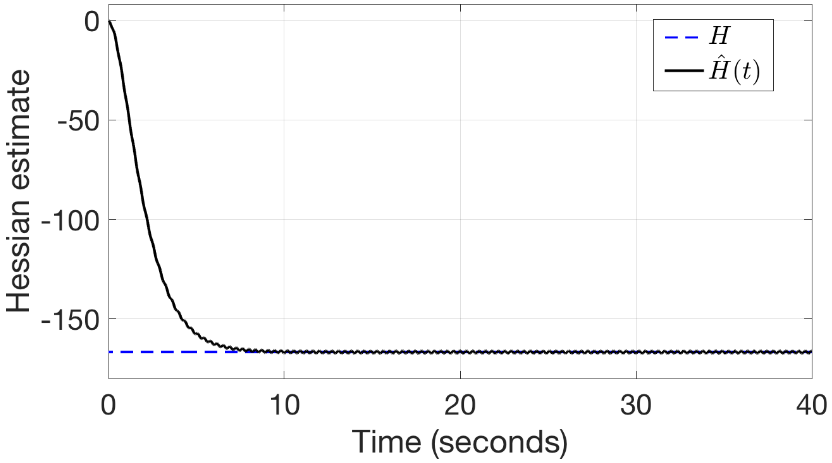

Figure 6.6: Hessian estimate $\hat{H}(t)$ of the ES control and prescribed Hessian value H.

Hessian estimate converges to the prescribed value -166.7. The convergence to optimal values is achieved in 40 s. In contrast, if we do not employ ES control for input density and the incoming flow depends only on upstream traffic. The open-loop system is shown in Fig. 6.7. The evolution of outgoing flow at the bottleneck area is run for 100 s. We can see that the outgoing flow of the bottleneck area keeps decreasing and therefore congestion at the bottleneck area is getting worse

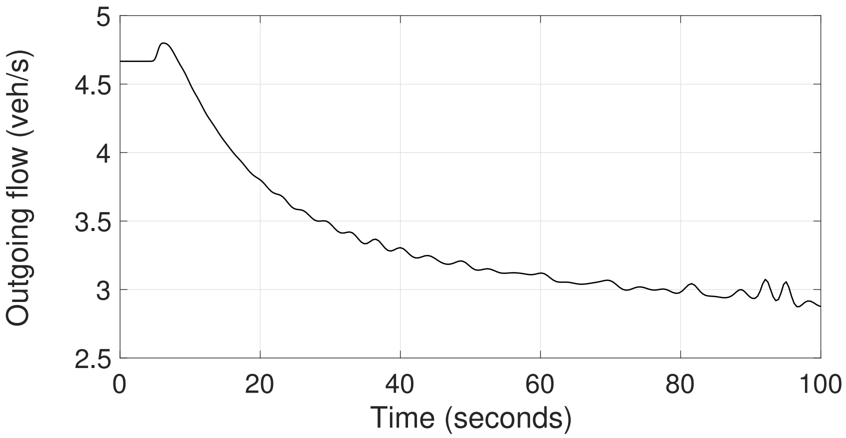

Figure 6.7: Output traffic flow of the bottleneck area without ES Control.

till a bumper-to-bumper jam.

6.5 Conclusion

In this chapter, we employ ES control to find a optimal density input for freeway traffic when there is a downstream bottleneck. To prevent traffic flow in bottleneck area overflowing the road capacity and furthermore causing congestion upstream in the freeway segment, the incoming traffic density at inlet of the freeway segment is regulated. The control design is achieved with delay compensation for ES control considering the upstream traffic is governed by the linearized LWR model. The optimal density and flow are achieved in the bottleneck area. The theoretical result is validated in simulation with the control design being applied on a nonlinear LWR PDE model along with an unknown fundamental diagram. Our future interest lies in conducting experimental validation of this problem. In a more sophisticated situation when there is multiple distant delays in presence of multi-lanes are going to be considered. It would also be interesting for authors to develop ES control with bounded update rates [98] under input delays exhibited through the LWR model and to develop a stochastic version of the algorithm presented in the paper by applying the results from [83] and [95].

Chapter 6 contains reprints and adaptations of the following paper: H. Yu, S. Koga, T. R. Oliveira, and M. Krstic, “Extremum seeking for traffic congestion control with a downstream bottleneck,” *IEEE Transactions on Control Systems Technology*, under review. The dissertation author is the primary investigator and author of this paper.

Chapter 7

Data Validation of Freeway Traffic State Estimation

Traffic state estimation plays an important role in traffic management. In order to mitigate freeway traffic congestion, various control algorithms are developed for ramp metering or variable speed limit. The effective implementation of control algorithms on traffic infrastructure relies on accurate information of traffic state. Due to the financial and technical limitations, traffic state on freeways is difficult to be measured everywhere at all times. Traffic state estimation refers to foresee of traffic state information with a model by accessing partially observed traffic data and some prior knowledge of the traffic. This topic has been extensively studied and gained an increasing attention in recent decades.

The comprehensive review of different models and approaches in traffic estimation problem by [97] proposes three categories including model-driven, data-driven and streaming data driven. Among them, the model driven approach is mostly widely used in traffic estimation problem which firstly develops traffic flow model to describe the traffic dynamics and then obtain state estimates based on the model and real-time data input. The physical model is calibrated with the historical data. In this section, we propose a model-driven approach by applying PDE backstepping technique for the second-order macroscopic ARZ traffic model.

Freeway traffic dynamics in spatial and temporal domain are usually described with macroscopic models of the aggregated values of traffic states, including traffic density, velocity and flux. The aggregated values average out the small-scale noises of the freeway traffic. Furthermore, a lot of field data use macroscopic quantiles which can be directly recorded by the stationary sensors like loop-detector.

Several studies have used the LWR model for traffic states estimation in [28] [29] [30] [68] due to its simplicity and efficiency in the model calibration and numerical simulation. However, LWR model fails to describe stop-and-go traffic, which represents the oscillatory behaviors of the congested traffic. The static equilibrium density-velocity relation of the LWR model is unable to reproduce the non-equilibrium relation appearing in the stop-and-go traffic. In addition to the density conservation equation, second-order models employ additional nonlinear hyperbolic PDE for traffic velocity to overcome the limitation of the LWR model. The deviations from the equilibrium traffic relation are allowed in the second-order model since the dynamics of velocity PDE is included.

The first well-known second-order PW model by [92] [114] predicts negative traffic velocity and information propagation faster than traffic which is physically unrealistic. Compared with the PW model, Aw-Rascle-Zhang model by [8] and [123] improves the second-order model by successfully addressing anisotropic behavior of traffic and correcting the PW model's prediction of traffic waves. For this reason, ARZ model has been studied intensively for the stop-and-go traffic over the recent years [18] [44] [45] [59] [67] [96]. In order to accurately estimate the non-equilibrium traffic states for congested traffic, this work considers the second-order ARZ model for observer design and data validation.

Traffic estimation by the particle filter in comparison with unscented Kalman filter is studied by [85] for a second-order extended cell-transmission model. The second-order PW model is used to develop an extended Kalman filter for state estimation in [112]. To author's best knowledge, state estimation problem of the nonlinear ARZ PDE model has never been studied before.

In dealing with the second-order coupled nonlinear hyperbolic system, PDE control of the ARZ model has been studied through many recent efforts including [18] [65] [117] [66] [121] [124] [125]. The previous work by authors [117] [121] firstly consider adopts the PDE backstepping methodology for control of the ARZ model. Boundary control and observer design using PDE backstepping method have been developed for 2×2 coupled hyperbolic systems [31] [116] and the theoretical result for the general hetero-directional hyperbolic systems developed in [7] [41] [80]. The applications of the theoretical results include open-channel flow, oil drilling, heat exchangers and multi-phase flow problems, but have never been considered in traffic problems. In [121], an observer design is proposed for the linearized ARZ model in an effort to construct an output feedback controller. In this paper, we generalize the previous observer design to address the freeway traffic estimation problem from a more practical perspective. In specific, the observer design is proposed for the nonlinear ARZ model. In addition, assumptions of boundary conditions are removed. The observer design accepts a general functional form of the equilibrium density-velocity relation, rather than the Greenshield's model.

In validation of the observer, vehicle trajectory data is used to obtain the aggregated values of traffic states. The ARZ model is calibrated with the historical field data. The model parameters are mostly obtained from historical data. The rest is determined from part of the dataset. Then the observer is constructed using the model parameters and real-time sensing of the data at boundaries. The performance of the PDE boundary observer is then evaluated with the field data in the temporal and spatial domain.

The contribution of this work: a systematic model-driven approach is developed for traffic state estimation. The PDE boundary observer based on the macroscopic ARZ traffic model is designed and validated. The theoretical observer design by backstepping method is generalized and adapted for the field-data validation. Vehicle trajectories data [48] and stationary loop detector data are used to construct and test the performance of the observer design. This result paves the way for implementing the PDE observer design in practice and give rise to a variety of opportunities to incorporate the PDE backstepping techniques in traffic estimation problem.

The outline of this chapter is as follows: in section 7.1, we firstly introduce the nonlinear ARZ modele with a general choice of velocity and density equilibrium function, and analyze the linearized ARZ model for distinguishing the free and congested traffic. Section 7.2 designs the boundary observer for the linearized ARZ model using the backstepping method and the nonlinear boundary observer is developed using the output injections obtained from the linearized model. In section 7.3, numerical simulations of the nonlinear ARZ PDE model and state estimation by the nonlinear boundary observer are conducted firstly from an ad-hoc choice of model parameters. In section 7.4, we calibrate the ARZ model with some field data and test the observer. The estimation errors are then analyzed.

7.1 Nonlinear ARZ Model

The nonlinear ARZ model for $(x,t) \in [0,L] \times [0,+\infty)$ is given

$$\partial_t \rho + \partial_x(\rho v) = 0, \tag{7.1}$$

$$\partial_t v + (v + \rho V(\rho))\partial_x v = \frac{V(\rho) - v}{\tau}. \tag{7.2}$$

The equilibrium velocity-density relationship $V(\rho)$ satisfy that the flux function $Q(\rho)$ is smooth, strictly concave $Q(\rho)'' < 0$ and a strictly decreasing velocity functional form $V'(\rho) < 0$. The equilibrium flux function $Q(\rho)$, also known as fundamental diagram, is defined as

$$Q(\rho) = \rho V(\rho). \tag{7.3}$$

Small deviations from the nominal profile are defined as

$$\tilde{q}(x,t) = q(x,t) - q^\star, \tag{7.4}$$

$$\tilde{v}(x,t) = v(x,t) - v^\star. \tag{7.5}$$

The steady density is given as $\rho^\star = q^\star/v^\star$ and setpoint density-velocity relation satisfy the equilibrium relation $V(\rho)$,

$$v^\star = V(\rho^\star). \tag{7.6}$$

The linearized ARZ model in $(\tilde{q}, \tilde{v})$ around the reference system $(q^\star, v^\star)$ with boundary conditions is given by

$$\begin{aligned} \tilde{q}_t + \lambda_1 \tilde{q}_x = & -\frac{q^\star}{v^\star}\left(v^\star + \frac{q^\star}{v^\star}V'\left(\frac{q^\star}{v^\star}\right)\right)\tilde{v}_x \\ & - q^\star \frac{(v^\star)^2 + q^\star V'\left(\frac{q^\star}{v^\star}\right)}{\tau (v^\star)^3}\tilde{v} + \frac{q^\star V'\left(\frac{q^\star}{v^\star}\right)}{\tau (v^\star)^2}\tilde{q}, \end{aligned} \tag{7.7}$$

$$\tilde{v}_t + \lambda_2 \tilde{v}_x = -\frac{(v^\star)^2 + q^\star V'\left(\frac{q^\star}{v^\star}\right)}{\tau (v^\star)^2}\tilde{v} + \frac{V'\left(\frac{q^\star}{v^\star}\right)}{\tau v^\star}\tilde{q}, \tag{7.8}$$

where the two characteristic speeds of the above linearized PDE model are

$$\lambda_1 = v^\star, \tag{7.9}$$

$$\lambda_2 = v^\star + \frac{q^\star}{v^\star}V'\left(\frac{q^\star}{v^\star}\right). \tag{7.10}$$

- Free-flow regime : $\lambda_1 > 0$, $\lambda_2 > 0$

  In the free-flow regime, both the disturbances of traffic flux and velocity travel downstream, at respective characteristic speeds λ_1 and λ_2. The linearized ARZ model in free-regime is a homo-directional hyperbolic system.

- Congested regime : $\lambda_1 > 0,\ \lambda_2 < 0$

  In the congested regime, the traffic density is greater than the critical value ρ_c that satisfies $Q(\rho)'|_{\rho_c} = 0$ and the second characteristic speed λ_2 becomes the negative value. Therefore, disturbances of the traffic speed travel upstream with λ_2 while the disturbances of the traffic flow flux are carried downstream with the characteristic speed λ_1. The hetero-directional propagations of disturbances force vehicles into the stop-and-go traffic.

In the free-flow regime, the linearized homo-directional hyperbolic PDEs can be solved explicitly by the inlet boundary values and therefore state estimates can be obtained by solving the hyperbolic PDEs. In this work, we focus on the congested regime with two hetero-directional hyperbolic PDEs. It is a more relevant and challenging problem for traffic states estimation.

7.2 Boundary Observer Design

In this section, boundary sensing is employed for the observer design. The state estimation of the nonlinear ARZ model is achieved using backstepping method. The output injection gains are designed for the linearized ARZ model and then adding to a copy of the nonlinear plant.

Boundary values of state variations from the steady states are defined as

$$Y_{q,in}(t) = \tilde{q}(0,t), \tag{7.11}$$

$$Y_{q,out}(t) = \tilde{q}(L,t), \tag{7.12}$$

$$Y_v(t) = \tilde{v}(L,t). \tag{7.13}$$

where the values of $\tilde{q}(0,t)$, $\tilde{q}(L,t)$ and $\tilde{v}(L,t)$ are obtained by subtracting setpoint values $(q^\star, v^\star)$ from the sensing of incoming traffic flux $q(0,t)$, outgoing flux $q(L,t)$ and outgoing velocity

$v(L,t)$,

$$y_q(t) = q(0,t), \tag{7.14}$$

$$y_{out}(t) = q(L,t), \tag{7.15}$$

$$y_v(t) = v(L,t). \tag{7.16}$$

Sensing of the aggregated values of the traffic flux and velocity can be obtained by high-speed camera or induction loop detectors. The induction loops are coils of wire embedded in the surface of the road to detect changes of inductance when vehicles pass. The high-speed cameras record the vehicle trajectories for a freeway segment.

7.2.1 Output injection for linearized ARZ model

We diagonalize the linearized equations and therefore write $(\tilde{q}, \tilde{v})$-system in the Riemann coordinates. The Riemann variables are defined as

$$\xi_1 = \frac{\rho^\star \lambda_2}{\lambda_1 - \lambda_2} \tilde{v} + \tilde{q}, \tag{7.17}$$

$$\xi_2 = \frac{q^\star}{\lambda_1 - \lambda_2} \tilde{v}. \tag{7.18}$$

The inverse transformation is given by

$$\tilde{v} = \frac{\lambda_1 - \lambda_2}{q^\star} \xi_2, \tag{7.19}$$

$$\tilde{q} = \xi_1 - \frac{\lambda_2}{\lambda_1} \xi_2. \tag{7.20}$$

The measurements are taken at boundaries lead to the following boundary conditions

$$\xi_1(0,t) = \frac{\lambda_2}{\lambda_1} \xi_2(0,t) + Y_q(t), \tag{7.21}$$

$$\xi_2(L,t) = \frac{q^\star}{\lambda_1 - \lambda_2} Y_v(t). \tag{7.22}$$

Therefore the linearized ARZ model in Riemann coordinates is obtained

$$\partial_t \xi_1 + \lambda_1 \partial_x \xi_1 = -\frac{1}{\tau}\xi_1, \tag{7.23}$$

$$\partial_t \xi_2 + \lambda_2 \partial_x \xi_2 = -\frac{1}{\tau}\xi_1, \tag{7.24}$$

$$\xi_1(0,t) = \frac{\lambda_2}{\lambda_1}\xi_2(0,t), \tag{7.25}$$

$$\xi_2(L,t) = \xi_1(L,t). \tag{7.26}$$

In order to diagonalize the right hand side to implement the backstepping method, we introduce a scaled state as follows:

$$\bar{w}(x,t) = \exp\left(\frac{x}{\tau\lambda_1}\right)\xi_1(x,t), \tag{7.27}$$

$$\bar{v}(x,t) = \xi_2(x,t). \tag{7.28}$$

The (ξ_1, ξ_2)-system is then transformed to a first-order 2×2 hyperbolic system

$$\bar{w}_t(x,t) + \lambda_1 \bar{w}_x(x,t) = 0, \tag{7.29}$$

$$\bar{v}_t(x,t) + \lambda_2 \bar{v}_x(x,t) = c(x)\bar{w}(x,t), \tag{7.30}$$

$$\bar{w}(0,t) = \frac{\lambda_2}{\lambda_1}\bar{v}(0,t) + Y_{q,in}(t), \tag{7.31}$$

$$\bar{v}(L,t) = \frac{q^\star}{\lambda_1 - \lambda_2} Y_v(t), \tag{7.32}$$

where the spatially varying parameter $c(x)$ is defined as

$$c(x) = -\frac{1}{\tau}\exp\left(-\frac{x}{\tau\lambda_1}\right), \tag{7.33}$$

Parameter $c(x)$ is a strictly increasing function and bounded by

$$-\frac{1}{\tau} \leq c(x) \leq -\frac{1}{\tau}\exp\left(-\frac{L}{\tau\lambda_1}\right). \tag{7.34}$$

Then we design a boundary observer for the linearized ARZ model to estimate $\bar{w}(x,t)$ and $\bar{v}(x,t)$ by constructing the following system

$$\hat{w}_t(x,t) + \lambda_1 \hat{w}_x(x,t) = r(x)(\bar{w}(L,t) - \hat{w}(L,t)), \tag{7.35}$$

$$\begin{aligned} \hat{v}_t(x,t) + \lambda_2 \hat{v}_x(x,t) =& c(x)\hat{w}(x,t) \\ &+ s(x)(\bar{w}(L,t) - \hat{w}(L,t)), \end{aligned} \tag{7.36}$$

$$\hat{w}(0,t) = \frac{\lambda_2}{\lambda_1}\hat{v}(0,t) + Y_{q,in}(t), \tag{7.37}$$

$$\hat{v}(L,t) = \frac{q^\star}{\lambda_1 - \lambda_2} Y_v(t), \tag{7.38}$$

where $\hat{w}(x,t)$ and $\hat{v}(x,t)$ are the estimates of the state variables $\bar{w}(x,t)$ and $\bar{v}(x,t)$. The value $\bar{w}(L,t)$ is obtained by plugging in the measured outgoing flow flux $Y_{q,out}(t)$ and velocity $Y_v(t)$ into (7.27),

$$\bar{w}(L,t) = \exp\left(\frac{L}{\tau\lambda_1}\right)\left(\frac{\rho^\star\lambda_2}{\lambda_1 - \lambda_2} Y_v(t) + Y_{q,out}(t)\right). \tag{7.39}$$

The term $r(x)$ and $s(x)$ are output injection gains to be designed. We denote estimation errors as

$$\check{w}(x,t) = \bar{w}(x,t) - \hat{w}(x,t), \tag{7.40}$$

$$\check{v}(x,t) = \bar{v}(x,t) - \hat{v}(x,t). \tag{7.41}$$

The error system is obtained by subtracting the estimates (7.35)-(7.38) from (7.29)-(7.32),

$$\begin{aligned} \check{w}_t(x,t)+\lambda_1\check{w}_x(x,t) =& r(x)\check{w}(L,t), \qquad (7.42) \\ \check{v}_t(x,t)+\lambda_2\check{v}_x(x,t) =& c(x)\check{w}(x,t)+s(x)\check{w}(L,t), \\ \check{w}(0,t) =& \frac{\lambda_2}{\lambda_1}\check{v}(0,t), \qquad (7.43) \\ \check{v}(L,t) =& 0. \qquad (7.44) \end{aligned}$$

The design of output injection gains $r(x)$ and $s(x)$ needs to guarantee that the error system $(\check{w},\check{v})$ decays to zero. Using the backstepping transformation, we transform the error system (7.42)-(7.44) into the following target system

$$\alpha_t(x,t)+\lambda_1\alpha_x(x,t) =0, \qquad (7.45)$$

$$\beta_t(x,t)+\lambda_2\beta_x(x,t) =0, \qquad (7.46)$$

$$\alpha(0,t) =\frac{\lambda_2}{\lambda_1}\beta(0,t), \qquad (7.47)$$

$$\beta(L,t) =0. \qquad (7.48)$$

The explicit solution to the target system (7.45)-(7.48) is easily found

$$\alpha(x,t) =\alpha\left(0,t-\frac{x}{\lambda_1}\right), \qquad t>\frac{L}{|\lambda_1|}, \qquad (7.49)$$

$$\beta(x,t) =\beta\left(L,t+\frac{L-x}{\lambda_2}\right), \qquad t>\frac{L}{|\lambda_2|}. \qquad (7.50)$$

Thus we have

$$\alpha(x,t)\equiv\beta(x,t)\equiv 0, \qquad (7.51)$$

after a finite time $t = t_f$ where

$$t_f = \frac{L}{|\lambda_1|} + \frac{L}{|\lambda_2|}. \tag{7.52}$$

It is straightforward to prove that the α, β system is L^2 exponentially stable.

The backstepping transformation is given in the form of spatial Volterra integral

$$\alpha(x,t) = \check{w}(x,t) - \int_x^L K(L+x-\xi)\check{w}(\xi,t)d\xi, \tag{7.53}$$

$$\beta(x,t) = \check{v}(x,t) - \int_x^L M(\lambda_1 x - \lambda_2 \xi)\check{w}(\xi,t)d\xi, \tag{7.54}$$

where the kernel variables $K(x)$ and $M(x)$ map the error system into the target system where the coupling term on the right hand-side is eliminated by the output injections. The kernel $M(x)$ is defined as

$$M(x) = -\frac{1}{\lambda_1 - \lambda_2} c\left(\frac{x}{\lambda_1 - \lambda_2}\right). \tag{7.55}$$

For boundary condition (7.47) to hold, the kernels $K(x)$ and $M(x)$ satisfy the relation

$$K(L-\xi) = M((\lambda_2 - \lambda_1)\xi). \tag{7.56}$$

The kernel K is then obtained

$$K(x) = -\frac{1}{\lambda_1 - \lambda_2} c\left(\frac{-\lambda_2}{\lambda_1 - \lambda_2}(L-x)\right). \tag{7.57}$$

According to the boundedness of $c(x)$ in (7.34), the kernels are bounded by

$$|K(x)| \leq \frac{1}{(\lambda_1 - \lambda_2)\tau}, \tag{7.58}$$

and therefore $M(x)$ is bounded. The output injection gain $r(x)$ and $s(x)$ are given by

$$r(x) = \lambda_1 K(x) = -\frac{\lambda_1}{\lambda_1 - \lambda_2} c\left(-\frac{\lambda_2}{\lambda_1 - \lambda_2}(L-x)\right), \tag{7.59}$$

$$\begin{aligned} s(x) =& -\lambda_1 M(\lambda_1 x - \lambda_2 L) \\ =& \frac{\lambda_1}{\lambda_1 - \lambda_2} c\left(x - \frac{\lambda_2}{\lambda_1 - \lambda_2}(L-x)\right). \end{aligned} \tag{7.60}$$

The backstepping transformation in (7.53) and (7.54) is invertible. Therefore, we study the stability of the error system through the target system (7.45)-(7.48). We arrive at the following theorem.

Theorem 7.1. *Consider system* (7.42)-(7.44) *with inital conditions* $\check{w}_0, \check{v}_0 \in L^2([0,L])$. *The equilibrium* $\check{w} \equiv \check{v} \equiv 0$ *is exponentially stable in the* L^2 *sense. It holds that*

$$||\bar{w}(\cdot,t) - \hat{w}(\cdot,t)|| \to 0 \tag{7.61}$$

$$||\bar{v}(\cdot,t) - \hat{v}(\cdot,t)|| \to 0 \tag{7.62}$$

and the convergence to the equilibrium is reached in the finite time $t = t_f$ *given in* (7.52).

7.2.2 Boundary observer design for Nonlinear ARZ model

For nonlinear boundary observer, we construct the system by keeping the output injections that are designed for the linearized ARZ model, then add them to the copy of the original nonlinear ARZ model.

We summarize the transformation from the linearized ARZ model in $(\tilde{q}, \tilde{v})$-system to $(\bar{w}, \bar{v})$-system,

$$\bar{w}(x,t) = \exp\left(\frac{x}{\tau\lambda_1}\right)\left(\frac{\rho^\star \lambda_2}{\lambda_1 - \lambda_2}\tilde{v}(x,t) + \tilde{q}(x,t)\right), \tag{7.63}$$

$$\bar{v}(x,t) = \frac{q^{\star}}{\lambda_1 - \lambda_2} \tilde{v}(x,t). \tag{7.64}$$

And the inverse transformation is given by

$$\tilde{q}(x,t) = \exp\left(-\frac{x}{\tau\lambda_1}\right) \bar{w}(x,t) - \frac{\lambda_2}{\lambda_1} \bar{v}(x,t), \tag{7.65}$$

$$\tilde{v}(x,t) = \frac{\lambda_1 - \lambda_2}{q^{\star}} \bar{v}(\xi,t). \tag{7.66}$$

Due to the equivalence of $(\check{w},\check{v})$ and $(\tilde{q},\tilde{v})$-system, we arrive at the following theorem for the linearized ARZ model.

Theorem 7.2. *Consider system* (7.7)-(7.8) *with inital conditions* $\tilde{q}_0, \tilde{v}_0 \in L^2([0,L])$. *The equilibrium* $\tilde{q} \equiv \tilde{v} \equiv 0$ *is exponentially stable in the* L^2 *sense. It holds that*

$$||q(\cdot,t) - q^{\star}|| \to 0 \tag{7.67}$$

$$||v(\cdot,t) - v^{\star}|| \to 0 \tag{7.68}$$

and the convergence to set points is reached in finite time $t = t_f$.

We denote the error injections designed for the linearized ARZ model (7.35)-(7.38) as

$$E_w(t) = r(x)(\bar{w}(L,t) - \hat{w}(L,t)), \tag{7.69}$$

$$E_v(t) = s(x)(\bar{w}(L,t) - \hat{w}(L,t)). \tag{7.70}$$

The output injection gains $r(x)$, $s(x)$ are designed in (7.59) and (7.60). According to (7.39), $\bar{w}(L,t)$ is obtained from the real-time measurement of the traffic boundary data in (7.11)-(7.13). Therefore, the values of output injections $E_w(t)$ and $E_v(t)$ are known.

The nonlinear observer for state estimation of density and velocity $(\hat{\rho}(x,t), \hat{v}(x,t))$ is obtained by combining the copy of the nonlinear ARZ model (ρ, v) given by (7.1), (7.2) and the

Table 7.1: Parameter choice for numerical simulation.

Parameter Name	**Value**
Maximum traffic density ρ_m	160 vehicles/km
Traffic pressure and coefficient γ	1
Maximum traffic velocity v_f	40 m/s
Relaxation time τ	60 s
Reference density $\rho^\star$	120 vehicles/km
Reference velocity $v^\star$	10 m/s
Freeway segment length L	400 m

above linear injection errors in original state variables density and velocity,

$$\partial_t \hat{\rho} + \partial_x(\hat{\rho}\hat{v}) = \frac{1}{v^\star}\left(\exp\left(-\frac{L}{\tau\lambda_1}\right)E_w - E_v\right), \tag{7.71}$$

$$\partial_t \hat{v} + (\hat{v} + \hat{\rho}V'(\hat{\rho}))\partial_x \hat{v} = \frac{V(\hat{\rho}) - \hat{v}}{\tau} + \frac{\lambda_1 - \lambda_2}{q^\star}E_v, \tag{7.72}$$

where the linear injection on the right hand side are obtained by transforming $(\hat{w},\hat{v})$ to (ρ,v) given in (7.65),(7.66). The boundary conditions are

$$\hat{\rho}(0,t) = \frac{y_q(t)}{\hat{v}(0,t)}, \tag{7.73}$$

$$\hat{v}(L,t) = y_v(t). \tag{7.74}$$

When the initial states of the system is close to the set points, the linearized part dominates the nonlinear estimation error system. Therefore L^2 exponential stability and finite-time convergence are achieved for the linearized ARZ model. The local H^2 exponential stability can be derived for the estimation error system of the nonlinear ARZ model, following approach in [31]. The estimation result is firstly validated in the following numerical simulation with an ad-hoc choice of parameters.

7.3 Numerical Simulation

For simulation of the nonlinear ARZ PDE model, we assume that the initial conditions are sinusoidal oscillations around the steady states $(\rho^\star, v^\star)$ which are in the congested regime. The initial conditions are assumed to be

$$\rho(x,0) = 0.1\sin\left(\frac{3\pi x}{L}\right)\rho^\star + \rho^\star, \tag{7.75}$$

$$v(x,0) = -0.1\sin\left(\frac{3\pi x}{L}\right)v^\star + v^\star. \tag{7.76}$$

Model parameters of a one-lane traffic in the congested regime is considered and chosen as shown in the table 1.

We consider a constant incoming flow and constant outgoing density for boundary conditions,

$$\tilde{q}(0,t) = 0, \tag{7.77}$$

$$\tilde{v}(L,t) = \frac{1}{\rho^\star}\tilde{q}(L,t). \tag{7.78}$$

In the next section, we validate the observer design with the traffic filed data, we do not prescribe any boundary conditions beforehand but directly take the measurement of the boundary data.

We use the finite volume method which is common in traffic flow applications. The numerical approach divides the freeway segment into cells and then approximates the cell values considering the balance of fluxes through the boundaries of the adjacent cells. In order to obtain the numerical fluxes, we write the ARZ model in the conservative variables, then apply two-stage Lax-Wendroff scheme to discretize the ARZ model in spatio-temporal domain. The scheme is second-order accurate in space and first-order in time. The spatial grid resolution is chosen to be smaller than the average vehicle size so that the numerical errors are smaller than the model errors. Therefore the numerical simulation is valid for this continuum model.

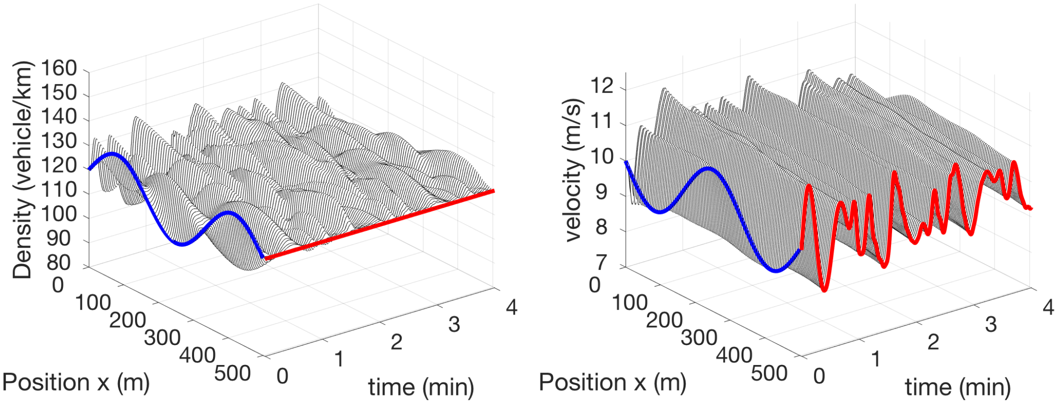

Figure 7.1: Density $\rho(x,t)$ and velocity $v(x,t)$ of nonlinear ARZ model.

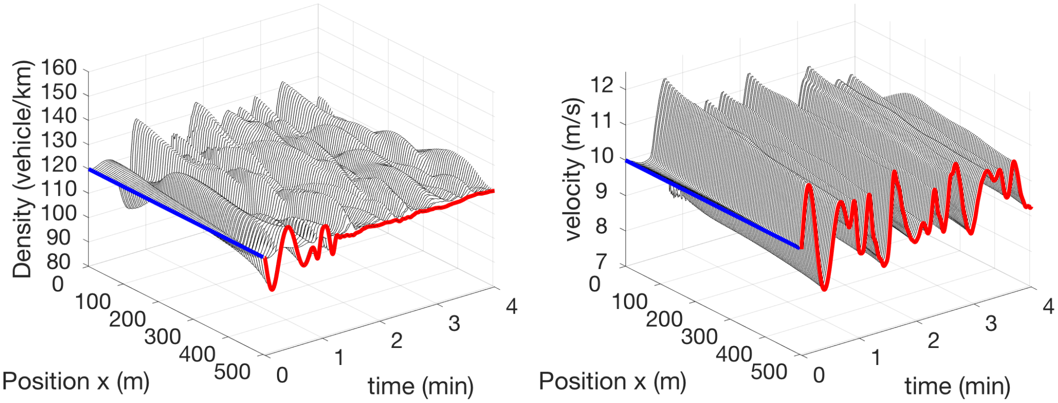

Figure 7.2: States estimates $\hat{\rho}(x,t)$ and $\hat{v}(x,t)$ of nonlinear boundary observer.

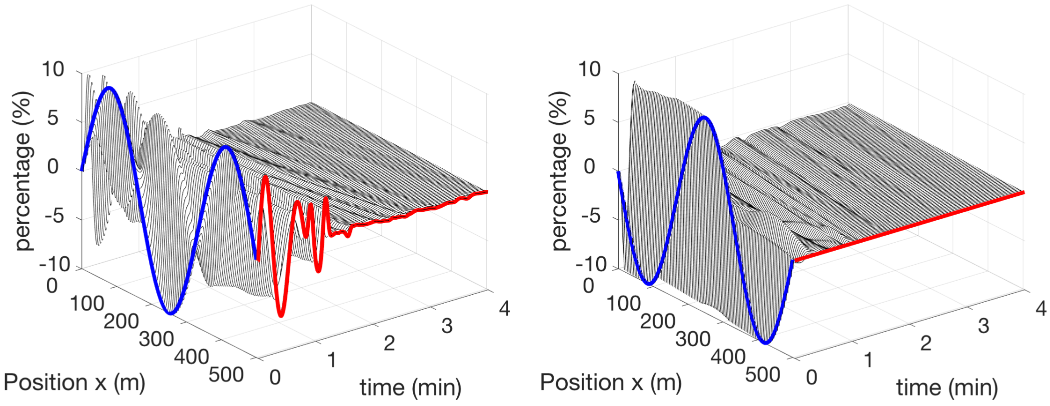

Figure 7.3: Estimation errors $\check{\rho}(x,t)$ and $\check{v}(x,t)$.

The inhomogeneous nonlinear ARZ model written in the conservative form is given by

$$\rho_t + (\rho v)_x = 0, \tag{7.79}$$
$$y_t + (yv)_x = -\frac{y}{\tau}, \tag{7.80}$$

where ρ and y are conservative variables, and y is defined as

$$y = \rho(v - V(\rho)). \tag{7.81}$$

The numerical fluxes are then obtained by

$$F_\rho = y + \rho V(\rho), \tag{7.82}$$
$$F_y = \frac{y^2}{\rho} + yV(\rho). \tag{7.83}$$

The Lax-wendroff numerical scheme is performed through two-stage update from $\left(\rho_j^n, y_j^n\right)$ to $\left(\rho_j^{n+1}, y_j^{n+1}\right)$.

At the first stage, the update law of $\left(\rho_j^n, y_j^n\right)$ to $\left(\rho_{j+\frac{1}{2}}^{n+\frac{1}{2}}, y_{j+\frac{1}{2}}^{n+\frac{1}{2}}\right)$ is given by

$$\rho_{j+\frac{1}{2}}^{n+\frac{1}{2}} = \frac{1}{2}\left(\rho_j^n + \rho_{j+1}^n\right) - \frac{\Delta t}{2\Delta x}\left((F_\rho)_{j+1}^n - (F_\rho)_j^n\right), \tag{7.84}$$
$$\begin{aligned} y_{j+\frac{1}{2}}^{n+\frac{1}{2}} =& \frac{1}{2}\left(y_j^n + y_{j+1}^n\right) - \frac{\Delta t}{2\Delta x}\left((F_y)_{j+1}^n - (F_y)_j^n\right) \\ & - \frac{\Delta t}{4\tau}\left(y_j^n + y_{j+1}^n\right), \end{aligned} \tag{7.85}$$

Then we calculate the numerical flux at the intermediate points of state variables and the obtain the final stage as

$$\rho_j^{n+1} = \rho_j^n - \frac{\Delta t}{\Delta x}\left((F_\rho)_{j+\frac{1}{2}}^{n+\frac{1}{2}} - (F_\rho)_{j-\frac{1}{2}}^{n+\frac{1}{2}}\right), \tag{7.86}$$

$$\begin{aligned} y_j^{n+1} =& y_j^n - \frac{\Delta t}{\Delta x}\left((F_y)_{j+\frac{1}{2}}^{n+\frac{1}{2}} - (F_y)_{j-\frac{1}{2}}^{n+\frac{1}{2}} \right) \\ & - \frac{\Delta t}{2\tau}\left(y_{j+\frac{1}{2}}^{n+\frac{1}{2}} + y_{j-\frac{1}{2}}^{n+\frac{1}{2}} \right). \end{aligned} \tag{7.87}$$

For the numerical stability of the Lax-Wendroff scheme, the spatial grid size Δx and time step Δt is chosen so that CFL condition is satisfied:

$$\max |\lambda_{1,2}| \leq \frac{\Delta x}{\Delta t}, \tag{7.88}$$

We specify state values at both $x = 0$ and $x = L$ boundaries. ARZ model will pick up some combination of ρ and v at each of the two boundaries, depending on the direction of characteristics at the boundary cells. We implement the boundary conditions in (7.77) and (7.78).

The numerical simulation result of the nonlinear ARZ, the nonlinear boundary observer estimation and the estimation errors are plotted in Fig. 1-3. Blue lines represent the initial conditions while the red lines represent the evolution of outlet state values in the temporal domain. The simulation is performed for a 500 m length of freeway segment and evolution of traffic states density and velocity are plotted for 4 min.

In Fig. 1, traffic density and velocity are slightly damped and keeps oscillating in the domain. It takes the initial disturbance-generated vehicles to leave the domain in 50 s but the oscillations sustain for more than 4 min which means the following incoming vehicles entering the acceleration-deceleration cycles under the influence of stop-and-go waves. The traffic states are chosen to be in the congested regime and the stop-and-go phenomenon is demonstrated in the simulation.

State estimation of traffic density and velocity by the nonlinear observer is shown in Fig. 2. The measurement is taken for the outgoing velocity and outgoing flow. The incoming flow is assumed to be at setpoint traffic flux. We do not assume any prior knowledge of the initial conditions and set the initial conditions to be at the setpoint density and velocity. We can see that state estimates converges to the values of plant after 75 s.

In Fig. 3, the evolution of estimation errors are shown. After 75 s, the estimation errors for density and velocity converge to value less than 1% of the setpoint value. There are still relatively very small estimation errors remain in the domain for two reasons. Our result only guarantees the convergence of estimates in the spatial L^2 norm. In addition, there could be nonlinearities of the error system not driven to zero by the linear output injections of the nonlinear boundary observer design.

7.4 Data Validation

In this section, we validate our boundary observer design with Next Generation Simulation (NGSIM) traffic data [48] which provides vehicle trajectories with great details and accuracy. The NGSIM trajectory data set is collected on April 13, 2005 by the Federal Highway Administration's project. The study area is a segment of Intestate 80 located at Emeryville, California. The dataset gathers trajectories of vehicles over a total of 45 minutes during rush hour: 4:00pm - 4:15pm, 5:00pm - 5:15pm, 5:15pm - 5:30pm.

Firstly, we calibrate the nonlinear ARZ model with part of the NGSIM data to obtain calibrated model parameters including the steady state values, the equilibrium velocity-density function $V(\rho)$ and the relaxation time τ. Then the rest datasets are used to test the observer design for the calibrated ARZ model. The estimation results of traffic states are compared with the NGSIM data. The boundary data is measured directly from the NGSIM data and traffic states are estimated for the considered domain. The result of reconstructed traffic data and boundary observer estimation of the traffic states are compared.

7.4.1 Model calibration with NGSIM data

Reconstruction from Data

We aim to calibrate the ARZ model which is a macroscopic model describing aggregated values. However, the NGSIM data set consists of microscopic measurements. The data was recorded with high-speed cameras for every 0.1 seconds. We need to process NGSIM trajectory data into macroscopic scale so that it can be used to calibrate the ARZ model.

The data was recorded on a 537-meter long freeway segment with six lanes for a time period of 15-minutes. Due to insufficient data collection at boundaries of segment, onset and offset of recording, the viable domain we choose to use in calibration and validation is 400-meter during a time period around 10-minutes. When we calibrate the parameters in ARZ model and fundamental diagram, we consider the freeway segment as a macroscopic general one-lane problem. That being said, six-lane densities need to be taken into account.

We will use the Edie's formula [43] to calculate aggregated traffic states $\rho(x,t)$, $v(x,t)$, $q(x,t)$ from the trajectory data of vehicles $x(t)$ with a resolution 0.1 s. At each time instance, positions of the multiple vehicles are collected. Consider a time-space domain $[0,T] \times [0,L]$, we divide it into $N \times M$ grids

$$[i\Delta t,(i+1)\Delta t] \ \times \ [j\Delta x,(j+1)\Delta x],$$

where $i \in 1,2,..,N$ and $j \in 1,2,..,M$. Within each cell, we consider $\rho_{i,j}, q_{i,j}, v_{i,j}$ to be constant. We use the following Edie's formula to map a set of vehicles' traces to speed, flow and density over the space-time grid. For each cells, suppose there are N_{ij} vehicle traces passing through the cell $[i\Delta t,(i+1)\Delta t] \ \times \ [j\Delta x,(j+1)\Delta x]$,

$$\rho_{i,j} = \frac{\Sigma_{k=1}^{N_{ij}} t_k}{\Delta x \Delta t}, \tag{7.89}$$

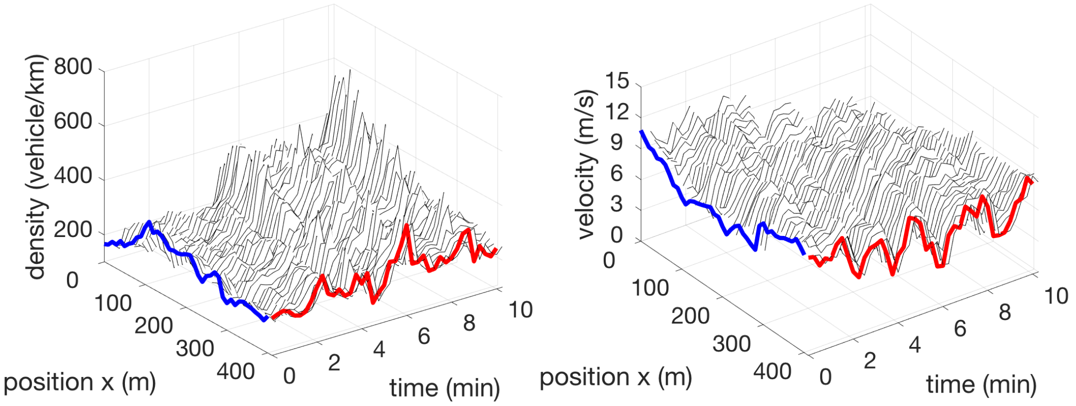

Figure 7.4: Density and velocity reconstructed from data of 4:00pm-4:15pm.

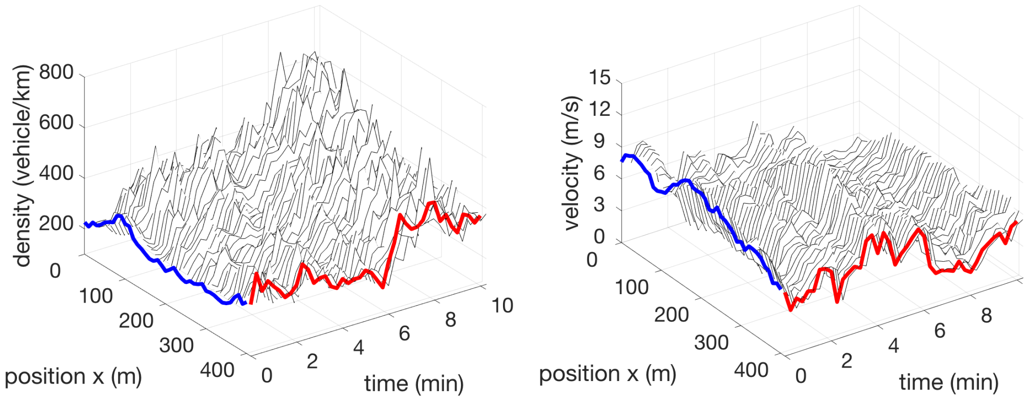

Figure 7.5: Density and velocity reconstructed from data of 5:00pm-5:15pm.

$$q_{i,j} = \frac{\Sigma_{k=1}^{N_{ij}} x_k}{\Delta x \Delta t}, \tag{7.90}$$

$$v_{i,j} = \frac{q_{i,j}}{\rho_{i,j}}. \tag{7.91}$$

After obtaining the cell values $\rho_{i,j}, q_{i,j}, v_{i,j}$, they can be later on compared with the observer estimates $\hat{\rho}_{i,j}, \hat{q}_{i,j}, \hat{v}_{i,j}$ with same griding. The number of cells are chosen such that in each cell, there are enough trajectory data. Otherwise, there could be cells that no trajectory has crossed. On the other hand, noises appear if a very fine discretization of grids is chosen. The following simulation is performed in a 41×41 grid.

Table 7.2: Averaged aggregate traffic data.

Data Set	**Density** (veh/km)	**Velocity** (km/h)	**Flow** (veh/h)
4:00 - 4:15pm	267	28.27	7548
5:00 - 5:15pm	353	20.23	7141
5:15 - 5:30pm	375	19.35	7256

We reconstruct the aggregated traffic states from all the three dataset. In Fig. 7.4 and Fig. 7.5, we show the surface plot of the density and velocity states for the dataset of 4:00pm - 4:15pm and the dataset of 5:00pm - 5:15pm. The initial conditions are highlighted with color red and the boundary conditions at outlet are highlighted with color blue. The congestion forms up as time goes by and propagates from the downstream to upstream. The most congested traffic appears at the inlet where the traffic density is relatively high and velocity is low.

We are mostly interested in the congested traffic where estimation of the traffic states becomes more relevant. The linearized ARZ model around the uniform reference is analyzed and employed for the observer design. By taking average of traffic aggregated values, we obtain the reference system $\rho^\star$, $v^\star$ and $q^\star$ of each dataset. Therefore, the average density, average velocity and average flow of each time period is calculated and shown in the Table 7.2. We observe that among the three data set, the traffic is most congested during 5:15pm - 5:30pm with largest averaged density and smallest velocity. Whether the traffic states are in congested or free regime need to be determined after we introduce the calibrated fundamental diagram.

Calibration of model parameters

For the ARZ model, the model parameters to be calibrated from the dataset is the equilibrium density-velocity relation $V(\rho)$ and relaxation time τ.

$$\partial_t \rho + \partial_x(\rho v) = 0, \tag{7.92}$$

$$\partial_t v + (v + \rho V'(\rho))\partial_x v = \frac{V(\rho) - v}{\tau}, \tag{7.93}$$

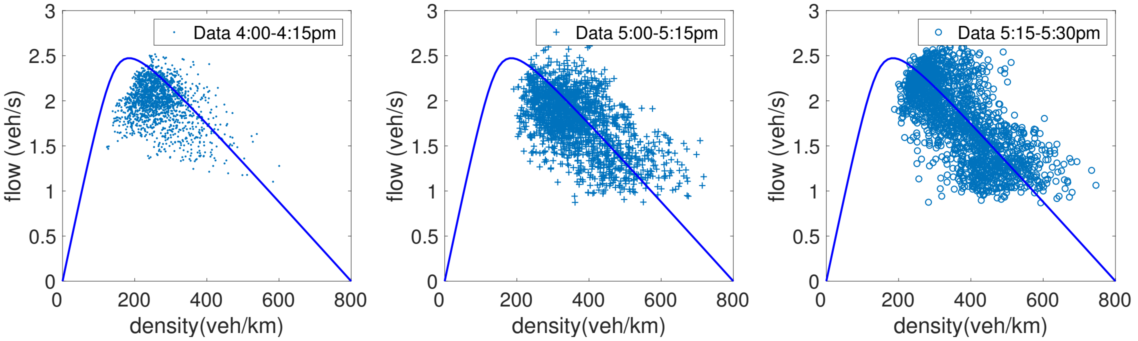

Figure 7.6: Density and flow from data of 4:00pm-4:15pm, 5:00pm-5:15pm and 5:15pm-5:30pm.

The fundamental diagram defined as $Q(\rho) = \rho V(\rho)$ describing the equilibrium density and flow rate relation is usually obtained by long-term measurements via loop-detectors. The loop-detector data set provides macroscopic density and flow rate data and its recording resolution is 30 s. In the previous section, we use Greenshield's model (6.3) for $V(\rho)$ as a simple choice for the boundary observer design. The Greenshield's fundamental diagram $Q(\rho)$ is given by

$$Q(\rho) = \rho v_f \left(1 - \left(\frac{\rho}{\rho_m}\right)^{\gamma}\right). \tag{7.94}$$

But Greenshield's model cannot accurately represent the fundamental diagram data. The critical density ρ_c satisfies $Q'(\rho)|_{\rho_c} = 0$ and thus segregates the free and congested regimes. The critical density ρ_c of the Greenshield's model $(\gamma = 1)$ occurs at $\rho_c = \frac{1}{2}\rho_m$. However, the critical density obtained from empirical traffic data usually shows up at $\rho_c = \frac{1}{4}\rho_m$. Hence, we need to consider a more realistic functional form for $Q(\rho)$. Here we employ a three-parameter fundamental diagram proposed by [45].

In [45], the following three-parameter (λ, p, α) fundamental diagram is calibrated with the NGSIM detector data set of the same freeway segement,

$$Q(\rho) = \alpha \left(a + (b-a)\frac{\rho}{\rho_m} - \sqrt{1 + \lambda^2 \left(\frac{\rho}{\rho_m} - p\right)^2}\right), \tag{7.95}$$

where a and b are denoted by

$$a = \sqrt{1+(\lambda p)^2}, \tag{7.96}$$

$$b = \sqrt{1+(\lambda(1-p))^2}. \tag{7.97}$$

The parameters (λ, p, α) do not have physical meaning but represent the shape of the functional form where λ represents the roundness, p tunes the critical density, α determines the maximum flow rate. The hyperbolicity $Q''(\rho) < 0, V'(\rho) < 0$ is guaranteed. The three parameters (λ, p, α) are determined using Least Square fitting with historical loop detector data.

Due to the lack of data near the maximum density, the value of ρ_m is prescribed according to the following equation

$$\rho_m = \frac{\text{number of lanes}}{\text{typical vehicle length} \times \text{safety distance factor}}. \tag{7.98}$$

The freeway segment in the dataset consists of 6 lanes and we consider the typical vehicle length to be 5-meter and the safety distance factor is 50% of vehicle length. Therefore, we have ρ_m for all lanes in our simulation

$$\rho_m = 800 \text{ veh/km}. \tag{7.99}$$

The calibrated fundamental diagram is plotted in Fig. 7.6. The traffic density and flow rate of the three dataset are plotted on the calibrated fundamental diagram. We can see that 4:00pm-4:15pm are in the transition region where the data points are partially in the free regime and partially in the congested regime. The traffic data of 5:00pm-5:15pm and 5:15pm-5:30pm are scattered in the congested regime of the fundamental diagram.

With the calibrated fundamental diagram $V(\rho)$, we choose the relaxation time τ from a range from $10s$ to $100s$ and calibrate it with the dataset of 5:00pm-5:15pm. The optimal

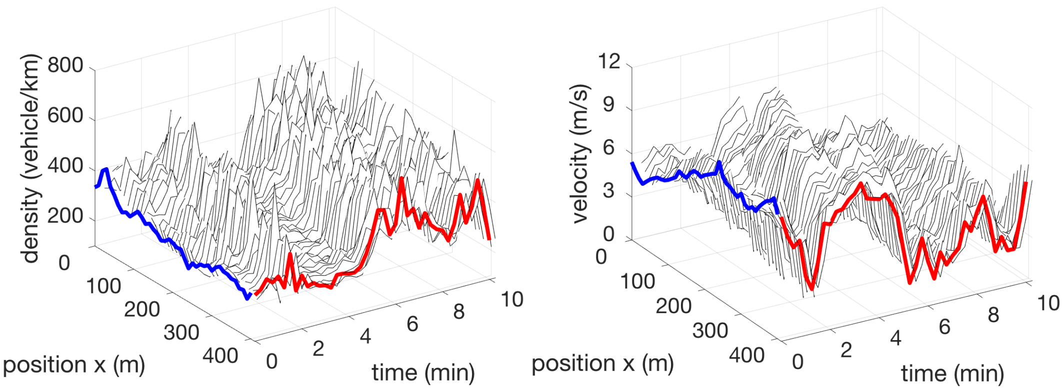

Figure 7.7: Density and velocity reconstructed from the data of 5:15pm-5:30pm.

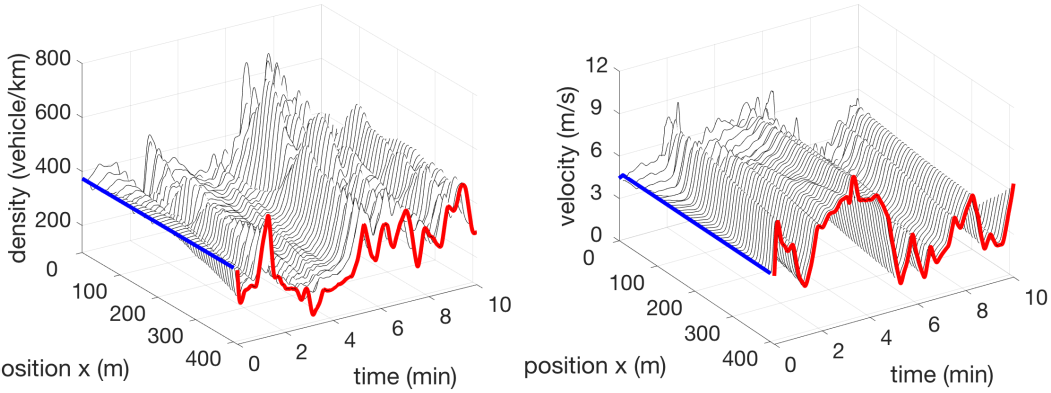

Figure 7.8: Estimates of density and velocity from the data of 5:15pm-5:30pm.

relaxation time is $\tau = 30s$ where the total error between the calibrated model and data is the lowest. In the next step, we use the calibrated fundamental diagram $V(\rho)$ and the relaxation time τ to construct the boundary observer.

7.4.2 Simulation for the nonlinear observer with calibrated parameters

We use the data of 5:15pm-5:30pm to test the boundary observer design. The reference system $(\rho^\star, v^\star, q^\star)$ is obtained from Table 7.2. Along with the calibrated parameters $V(\rho)$ and τ, the nonlinear observer is constructed with a copy of the nonlinear ARZ model with the output injection gains that drive the estimation errors to zero. The numerical solution of the nonlinear

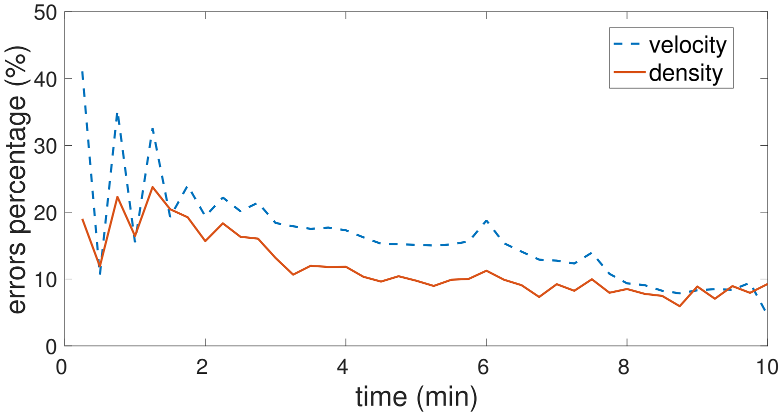

Figure 7.9: Density and velocity estimation errors for the data of 5:15pm-5:30pm.

PDEs are approximated with the Lax-Wendroff method. The boundary data is implemented with the ghost cell. The ARZ model collects the boundary values based both on flux of the computational domain and the boundary data of the ghost cells. Using the boundary measurements of the inlet and outlet of the freeway segment, the state estimation $(\hat{\rho}(x,t), \hat{v}(x,t))$ is generated without the knowledge of the initial condition. In Fig. 7.7, $(\rho(x,t), v(x,t))$ is obtained from the reconstruction of the data set of 5:15pm-5:30pm. In Fig. 7.8, it shows the evolution of the state estimates $(\hat{\rho}(x,t), \hat{v}(x,t))$. The initial condition, highlighted with color blue, is assumed to be the uniform reference system $(\rho^\star, v^\star, q^\star)$ which represents the averaged values of the dataset. The boundary conditions at outlet are highlighted with right color which gives the output injections in the observer. We notice that when density value is higher than 600 veh/km at inlet around 7 min, the estimation result is not satisfying at inlet. This could be related to the ARZ model's inaccuracy in predicting traffic states near maximum density since non-unique maximum densities exist for the ARZ model.

For the error analysis of the observer estimation, the estimation errors are considered in the L^2-norm, defined as

$$E_\rho(t) = \left[\frac{1}{L} \int_0^L \left(\frac{\rho(x,t) - \hat{\rho}(x,t)}{\rho^\star} \right)^2 dx \right]^{1/2}, \tag{7.100}$$

$$E_v(t) = \left[\frac{1}{L} \int_0^L \left(\frac{v(x,t) - \hat{v}(x,t)}{v^\star} \right)^2 dx \right]^{1/2}, \tag{7.101}$$

where $\rho^\star$ and $v^\star$ are the averaged state values of the data. We choose the L^2 of the estimation errors and average it over space. The convergence of the local stability in the L^2-sense for estimation errors to zero is guaranteed in Theorem 2. In addition, the spatial averaged errors can remove the influence of noises and outliers of the traffic data.

The temporal evolution of the space-averaged errors of density and velocity estimates in the L^2-sense is shown in Fig. 7.9. It reveals that at the initial time, density and velocity estimation errors start from 20% and 40% respectively. The finite convergence time is around $t_f = 3$ min. The estimation errors in the end converge at 10%. The linearization of output injections design, the data noise, the reconstruction errors and the numerical approximation errors could contribute to the remaining spatial averaged errors between the estimation and NGSIM traffic data after the convergence time.

7.5 Conclusion

In this chapter, we develop a nonlinear boundary observer for the second-order nonlinear hyperbolic PDEs, estimating traffic states of ARZ model and then validate the design with traffic field data. Analysis of the linearized ARZ model leads our main focus to the congested regime where stop-and-go happens. Using spatial transformation and PDE backstepping method, we construct a boundary observer with a copy of the nonlinear plant and output injection of measurement errors so that the exponential stability of estimation errors in the L^2 norm and finite-time convergence to zero are guaranteed. Simulations are performed for traffic estimation on a stretch of freeway. The nonlinear observer is tested with a calibrated ARZ model obtained from the NGSIM data.

For future work, observer design may be considered for a generalized ARZ model proposed by [44] to address the non-unique maximum density associated with ARZ model. The estimation accuracy in predicting the heterogeneous behaviors of drivers and spread of data for the congested regime could be improved. On the other hand, defining the fundamental diagram requires the calibration with the historical data. This assumption of using the historical data to determine model parameters may no hold when traffic becomes unpredictable in case of accidents. It is practically preferable if the model parameters could be estimated real-time. Therefore, it is of authors' interest to consider adaptive observer design for this problem.

Chapter 7 contains reprints and adaptations of the following paper: H. Yu, Q. Gan, A. M. Bayen and M. Krstic, "Boundary Observer Design and Validation for Freeway Traffic State Estimation via Aw-Rascle-Zhang model," *IEEE Transactions on Control Systems Technology*, under review. The dissertation author is the primary investigator and author of this paper.

Bibliography

[1] H. Anfinsen and O. M. Aamo, " Disturbance Rejection in the Interior Domain of Linear $2{\times}2$ Hyperbolic Systems," *IEEE Transactions on Automatic Control*, vol. 60, pp.186-191, 2014

[2] H. Anfinsen and O. M. Aamo, "Disturbance rejection in general heterodirectional 1-D linear hyperbolic systems using collocated sensing and control," *Automatica*, vol.76, pp.230-242, 2017.

[3] H. Anfinsen and O. M. Aamo, "Model Reference Adaptive Control of 2×2 Coupled Linear Hyperbolic PDEs," *IEEE Transactions on Automatic Control*, vol.63, pp.2405-2420, 2017.

[4] V. T. Arasan, and G. Dhivya, " Measuring heterogeneous traffic density", *In Proceedings of International Conference on Sustainable Urban Transport and Environment*, World Academy of Science, Engineering and technology, Bangkok, Vol. 36, pp. 342, 2018.

[5] K. B. Ariyur, and M. Krstic, *Real-Time Optimization by Extremum-Seeking Control.* John Wiley & Sons, 2003.

[6] P. Athol, " Interdependence of certain operational characteristics within a moving traffic stream", *Expressway Surveillance Project*, 1963.

[7] J. Auriol and F. Di Meglio, " Minimum time control of heterodirectional linear coupled hyperbolic PDEs," *Automatica*, vol.71, 300-307, 2016.

[8] A. Aw, and M. Rascle, " Resurrection of "second order" models of traffic flow," *SIAM journal on applied mathematics*, vol.60, no.3, pp.916-938, 2000.

[9] G. Bastin and J. M. Coron, "Stability and boundary stabilization of 1-d hyperbolic systems," Birkhuser, Switzerland, 2016.

[10] G. Bastin, J. M. Coron, A. Hayat and P. Shang. " Boundary feedback stabilization of hydraulic jumps". *IFAC Journal of Systems and Control*, 100026, 2019.

[11] N. Bekiaris-Liberis and M. Krstic. "Compensation of state-dependent input delay for nonlinear systems", *IEEE Transactions on Automatic Control*, vol.58, no.2, pp.275-289, 2012.

[12] N. Bekiaris-Liberis and M. Krstic. "Robustness of nonlinear predictor feedback laws to time-and state-dependent delay perturbations". *Automatica*, vol. 49, no. 6, pp.1576-1590, 2013.

[13] N. Bekiaris-Liberis and M. Krstic. "Compensation of state-dependent input delay for nonlinear systems". *IEEE Transactions on Automatic Control*, vol.58, no.2, pp.275-289, 2013.

[14] N. Bekiaris-Liberis and M. Krstic. "Predictor-feedback stabilization of multi-input nonlinear systems". *IEEE Transactions on Automatic Control*, vol.62, nol.2, pp.516531, 2017.

[15] N. Bekiaris-Liberis, and M. Krstic, "Compensation of transport actuator dynamics with input-dependent moving controlled boundary," *IEEE Transactions on Automatic Control*, vol.63, no.11, pp.3889-3896, 2018.

[16] N. Bekiaris-Liberis, and M. Krstic, "Compensation of actuator dynamics governed by quasilinear hyperbolic PDEs," *Automatica*, vol.92, pp.29-40, 2018.

[17] N. Bekiaris-Liberis and A. I. Delis, " PDE-Based Feedback Control of Freeway Traffic Flow via Time-Gap Manipulation of ACC-Equipped Vehicles," arXiv preprint arXiv:1812.08154,2018.

[18] F. Belletti, M. Huo, X. Litrico and A. M. Bayen, "Prediction of traffic convective instability with spectral analysis of the AwRascleZhang model," *Physics Letters A*, Vol.379(38), 2319-2330, 2015.

[19] M. Benosman, *Learning-Based Adaptive Control: An Extremum Seeking Approach–Theory and Applications,* Butterworth-Heinemann, 2016.

[20] S. Benzoni-Gavage and R. M. Colombo, "A \$n\$-populations model for traffic flow", *European Journal of Applied Mathematics,* vol.14(5), pp. 587-612, 2003.

[21] R. Borsche, R. M. Colombo and M. Garavello, " Mixed systems: ODEsbalance laws". *Journal of Differential equations*, 252(3), 2311-2338, 2012.

[22] M. Buisson-Fenet, S. Koga and M. Krstic. " Control of Piston Position in Inviscid Gas by Bilateral Boundary Actuation," *In 2018 IEEE Conference on Decision and Control (CDC)* (pp. 5622-5627). IEEE, 2018.

[23] R. Burger, P. Mulet and L.M. Villada, " A diffusively corrected multiclass Lighthill-Whitham-Richards traffic model with anticipation lengths and reaction times", *Advances in Applied Mathematics and Mechanics,* vol. 5(5), pp.728-758, 2013.

[24] X. Cai and M. Krstic. " Nonlinear control under wave actuator dynamics with timeand statedependent moving boundary". *International Journal of Robust and Nonlinear Control*, 25(2), 222-251, 2015.

[25] S. Chaniut and C. Buisson, “Macroscopic model and its numerical solution for two-flow mixed traffic with different speeds and lengths”, *Transportation research record,* vol. 1852(1), pp.209-219, 2003.

[26] M. D’Abbicco and M. Reissig, “ Semilinear structural damped waves”, *Mathematical Methods in the Applied Sciences*, vol.37, no.11, 1570-1592, 2014.

[27] M. J. Cassidy and J. R. Windover, “Methodology for assessing dynamics of freeway traffic flow”, *Transportation Research Record,* vol. 1484, pp. 73-79, 1995.

[28] C. G. Claudel and A. M. Bayen, “ Guaranteed bounds for traffic flow parameters estimation using mixed LagrangianEulerian sensing,” *46th Annual Allerton conference on communication, control, and computing* (pp. 636645), 2008.

[29] B. Coifman, “ Estimating travel times and vehicle trajectories on freeways using dual loop detectors,” *Transportation Research Part A: Policy and Practice*, vol. 36 (4), pp. 351364, 2002.

[30] B. Coifman, “Estimating density and lane inflow on a freeway segment,” *Transportation Research Part A: Policy and Practice*, vol.37 (8), 689701, 2003.

[31] J. M. Coron, R. Vazquez, M.Krstic and G. Bastin, “ Local exponential H_2 stabilization of a 2×2 quasilinear hyperbolic system using backstepping,” *SIAM Journal on Control and Optimization*, vol.51, pp.20052035, 2013.

[32] C.F. Daganzo, “ Requiem for second-order fluid approximations of traffic flow”, *Transportation Research Part B: Methodological*, vol. 29(4), pp.277-286, 1995.

[33] M. L. Delle Monache and P. Goatin. “ Scalar conservation laws with moving constraints arising in traffic flow modeling: an existence result”. *Journal of Differential equations*, 257(11), 4015-4029, 2014.

[34] J. Deutscher, “ Backstepping Design of Robust State Feedback Regulators for Linear 2×2 Hyperbolic Systems”, *IEEE Transactions on Automatic Control,* vol. 62(10), pp. 5240-5247, 2017

[35] J. Deutscher, “Finite-time output regulation for linear 2×2 hyperbolic systems using backstepping”, *Automatica,* vol. 75, pp. 54-62, 2017.

[36] J. Deutscher. “ Output regulation for general linear hetero-directional hyperbolic systems with spatially-varying coefficients,” *Automatica,* vol.85, pp.34-42, 2017.

[37] M. Diagne, N. Bekiaris-Liberis, & M. Krstic. “ Time and State Dependent Input Delay Compensated BangBang Control of a Screw Extruder for 3D Printing,” *International Journal of Robust and Nonlinear Control*, 27(17), 3727-3757, 2017.

[38] M. Diagne, N. Bekiaris-Liberis, A. Otto, & M. Krstic. "Control of transport PDE/nonlinear ODE cascades with state-dependent propagation speed". *IEEE Transactions on Automatic Control*, 62(12), 6278-6293, 2017.

[39] F. Di Meglio, G. O. Kaasa, N. Petit and V. Alstad, " Slugging in multiphase flow as a mixed initial-boundary value problem for a quasilinear hyperbolic system", In *Proceedings of the 2011 American Control Conference*, pp. 3589-3596. IEEE, 2011.

[40] F. Di Meglio, R. Vazquez, M. Krstic and N. Petit, " Backstepping stabilization of an underactuated 3×3 linear hyperbolic system of fluid flow equations", In *2012 American Control Conference (ACC)*, pp. 3365-3370, IEEE, 2012.

[41] F. Di Meglio, R. Vazquez and M. Krstic, "Stabilization of a system of $n+1$ coupled first-order hyperbolic linear PDEs with a single boundary input," *IEEE Transactions on Automatic Control*, vol.58(12), pp.3097-3111, 2013.

[42] F. Di Meglio, F.B. Argomedo, L. Hu and M. Krstic, " Stabilization of coupled linear heterodirectional hyperbolic PDEODE systems," *Automatica*, vol. 87, pp.281-289, 2018.

[43] L. C. Edie, " Discussion of Traffic Stream Measurements and Definitions," *Proc., 2nd International Symposium on the Theory of Road Traffic Flow*, Organisation for Economic Co-operation and Development, Paris, pp. 139154, 1965.

[44] M. R. Flynn, A. R. Kasimov, J. C. Nave, R. R. Rosales and B. Seibold, " Self-sustained nonlinear waves in traffic flow," *Physical Review E*, vol.79(5), 056113, 2009.

[45] S. Fan and B. Seibold, "Data-fitted first-order traffic models and their second-order generalizations: Comparison by trajectory and sensor data," *Transportation Research Record*, vol.2391(1), pp.32-43, 2013.

[46] S. Fan and D. B. Work, " A heterogeneous multiclass traffic flow model with creeping", *SIAM Journal on Applied Mathematics*, vol. 75(2), pp. 813-835, 2015.

[47] J. Feiling, S. Koga, M. Krstic, and T.R. Oliveira, "Gradient extremum seeking for static maps with actuation dynamics governed by diffusion PDEs," *Automatica*, vol.95, pp.197-206, 2018.

[48] FHWA, U.S. Department of Transportation. Next Generation Simulation (NGSIM). http://ops.fhwa.dot.gov/trafficanalysistools/ngsim.html.

[49] A. Ghaffari, M. Krstic, and D. Nesic, "Multivariable Newton-based extremum seeking," *Automatica*, vol.48, no.8, pp.1759-1767, 2012.

[50] A. Ghaffari, M. Krstic, and S. Seshagiri, "Power optimization and control in wind energy conversion systems using extremum seeking," *IEEE Transactions on Control Systems Technology*, vol.22, no.5, pp.1684-1695, 2014.

[51] A. Ghaffari, M. Krstic, and S. Seshagiri, “Power optimization for photovoltaic microconverters using multivariable newton-based extremum seeking,” *IEEE Transactions on Control Systems Technology*, vol.22, no.6, pp.2141-2149, 2014.

[52] B. D. Greenshields, W. Channing and H. Miller, “ A study of traffic capacity”, In *Highway research board proceedings*. National Research Council (USA), Highway Research Board, 1935.

[53] M. Guay, D. Dochain, and M. Perrier, “Adaptive extremum seeking control of continuous stirred tank bioreactors with unknown growth kinetics,” *Automatica*, vol.40, no.5, pp.881-888, 2004.

[54] M. Guay, and T. Zhang, “Adaptive extremum seeking control of nonlinear dynamic systems with parametric uncertainties,” *Automatica*, vol.39, no.7, pp.1283-1293, 2003.

[55] A. K. Gupta and V. K. Katiyar, “ A new multi-class continuum model for traffic flow”, *Transportmetrica*, vol. 3(1), pp. 73-85. 2017.

[56] J. K. Hale, and S.V. Lunel, “Averaging in infinite dimensions,” *The Journal of integral equations and applications*, pp.463-494, 1990.

[57] A. Hasan, O. M. Aamo and M. Krstic, “ Boundary observer design for hyperbolic PDE - ODE cascade systems”, *Automatica*, vol. 68, pp. 75-86, 2016.

[58] D. Helbing and A. Greiner, “ Modeling and simulation of multi-lane traffic flow,” *Physical Review E,* vol.55(5), pp.5498, 1997.

[59] D. Helbing and A. F. Johansson, “ On the controversy around Daganzos requiem for and Aw-Rascles resurrection of second-order traffic flow models,” *The European Physical Journal B*, vol. 69(4), pp. 549-562, 2009.

[60] M. Herty and A.Klar, “Modeling, simulation, and optimization of traffic flow networks,” *SIAM Journal on Scientific Computing,* vol.25(3), pp.1066-1087, 2003.

[61] R. Jiang and Q. S. Wu, “ Extended speed gradient model for mixed traffic”, *Transportation research record,* vol. 1883(1), pp. 78-84, 2014.

[62] S. Logghe, *Dynamic modeling of heterogeneous vehicular traffic*, Ph.D. thesis, Faculty of Applied Science, Katholieke Universiteit Leuven, Leuven, 2013.

[63] H. Y. Jin, and W.L. Jin, “Control of a lane-drop bottleneck through variable speed limits,” *Transportation Research Part C: Emerging Technologies,* vol.58, pp.568-584, 2015.

[64] Y. Kan, Y. Wang, M. Papageorgiou, and I. Papamichail, “Local ramp metering with distant downstream bottlenecks: A comparative study,” *Transportation Research Part C: Emerging Technologies,* vol.62, pp.149-170, 2016.

[65] I. Karafyllis, N. Bekiaris-Liberis and M. Papageorgiou, " Feedback Control of Nonlinear Hyperbolic PDE Systems Inspired by Traffic Flow Models," *IEEE Transactions on Automatic Control,* 2018.

[66] I. Karafyllis and M. Papageorgiou, "Feedback control of scalar conservation laws with application to density control in freeways by means of variable speed limits," *Automatica*, vol.105, pp. 228-236, 2019.

[67] B. S. Kerner, "Experimental features of self-organization in traffic flow," *Physical review letters*, vol. 81(17), pp. 3797, 1998.

[68] A. Kesting, & M. Treiber, "Online traffic state estimation based on floating car data," *Traffic and granular flow*, 2009.

[69] A. Klar and R. Wegener, " A hierarchy of models for multi-lane vehicular traffic I: Modeling," *SIAM Journal on Applied Mathematics,* vol.59(3), pp.983-1001, 1998.

[70] A. Klar, J. M. Greenberg and M. Rascle, " Congestion on multi-lane highways," *SIAM Journal on Applied Mathematics,* vol.63(3), pp.818-833, 2003.

[71] S. Koga, and M. Krstic, " Arctic sea ice temperature profile estimation via backstepping observer design", *In 2017 IEEE Conference on Control Technology and Applications (CCTA)*, (pp. 1722-1727), 2017.

[72] S. Koga, D. Straub, M. Diagne and M. Krstic, " Thermodynamic Modeling and Control of Screw Extruder for 3D Printing", *In 2018 Annual American Control Conference (ACC)*, pp. 2551-2556, 2018.

[73] S. Koga, M. Diagne and M. Krstic, " Control and state estimation of the one-phase Stefan problem via backstepping design", *IEEE Transactions on Automatic Control*, vol.64, no.2, pp.510-525, 2019.

[74] M. Krstic, "Performance improvement and limitations in extremum seeking control," *Systems & Control Letters*, vol.39, no.5, pp. 313-326, 2000.

[75] M. Krstic, and H-H. Wang, "Stability of extremum seeking feedback for general nonlinear dynamic systems," *Automatica,* vol.36, pp.595-601, 2000.

[76] M. Krstic, and A. Smyshlyaev, *Boundary Control of PDEs: A Course on Backstepping Designs*, Siam, 2008.

[77] M. Krstic, *Delay Compensation for Nonlinear, Adaptive, and PDE Systems*, Birkhuser Boston, 2009.

[78] C. Lattanzio, A. Maurizi and B. Piccoli. "Moving shockwaves in car traffic flow: a PDE-ODE coupled model". *SIAM Journal on Mathematical Analysis*, 43(1), 50-67, 2011.

[79] L. Hu and F. Di Meglio, " Finite-time backstepping boundary stabilization of $3x3$ hyperbolic systems", In *2015 European Control Conference (ECC)*, pp. 67-72, IEEE, 2015.

[80] L. Hu, F. Di Meglio, R.Vazquez and M. Krstic, " Control of homo-directional and general heterodirectional linear coupled hyperbolic PDEs," *IEEE Transactions on Automatic Control,* vol.61(11), pp.3301-3314,2016.

[81] M. J. Lighthill, & G. B. Whitham, "On kinematic waves. II. A theory of traffic flow on long crowded roads," *Proceedings of the Royal Society of London. Series A, Mathematical and Physical Sciences*, pp.317-345,1995.

[82] J. A. Laval and C. F. Daganzo, " Lane-changing in traffic streams," *Transportation Research Part B: Methodological,* vol.40(3), pp.251-264, 2006.

[83] S. J. Liu, and M. Krstic, "Stochastic averaging in continuous time and its applications to extremum seeking," *IEEE Transactions on Automatic Control,* vol.55, pp.2235-2250, 2010.

[84] S. J. Liu, and M. Krstic, *Stochastic Averaging and Stochastic Extremum Seeking*, Springer Science & Business Media, 2012.

[85] L. Mihaylova, R. Boel and A. Hegyi, "Freeway traffic estimation within particle filtering framework," *Automatica*, vol. 43(2), pp. 290-300, 2007.

[86] P. G. Michalopoulos, D. E. Beskos and Y.Yamauchi, "Multi-lane traffic flow dynamics: some macroscopic considerations," *Transportation Research Part B: Methodological,* vol.18(4-5), pp.377-395,1984.

[87] R. Mohan and G. Ramadurai, " Heterogeneous traffic flow modelling using second-order macroscopic continuum model", *Physics Letters A*, vol. 381(3), pp. 115-123, 2017.

[88] R. Nair, H. S. Mahmassani and E. Miller-Hooks, " A porous flow approach to modeling heterogeneous traffic in disordered systems", *Procedia-Social and Behavioral Sciences*, vol. 17, pp. 611-627, 2011.

[89] D. Ngoduy, and R. Liu, "Multiclass first-order simulation model to explain non-linear traffic phenomena", *Physica A: Statistical Mechanics and its Applications*, vol. 385 (2), pp. 667-682, 2007.

[90] T. R. Oliveira, M. Krstic, and D. Tsubakino, "Extremum seeking for static maps with delays," *IEEE Transactions on Automatic Control*, vol.62, no.4, pp.1911-1926, 2017.

[91] M. Papageorgiou, H. Hadj-Salem, and J.M. Blosseville, "ALINEA: A local feedback control law for on-ramp metering," *Transportation Research Record*, 1320(1), 58-67, 1991.

[92] H. J. Payne, "Models of freeway traffic and control", *Mathematical Models of Public Systems*, 1971.

[93] P. Paz, T. R. Oliveira, A. V. Pino, and A. P. Fontana, "Model-Free Neuromuscular Electrical Stimulation by Stochastic Extremum Seeking," *IEEE Transactions on Control Systems Technology*, already on IEEE Xplore, https://doi.org/10.1109/TCST.2019.2892924, 2019.

[94] P. I. Richards, "Shock waves on the highway," *Operations research*, vol. 4(1), pp. 42-51, 1956.

[95] D. Rušiti, G. Evangelisti, T.R. Oliveira, M. Gerdts, and M. Krstic, "Stochastic extremum seeking for dynamic maps with delays," *IEEE Control Systems Letters,* vol.3, no.1, pp.61-66, 2019.

[96] B. Seibold, M. R. Flynn, A. R. Kasimov, R. R. Rosales, "Constructing set-valued fundamental diagrams from jamiton solutions in second order traffic models," arXiv preprint arXiv:1204.5510,2012.

[97] T. Seo, A. M. Bayen, T. Kusakabe, & Y. Asakura, "Traffic state estimation on highway: A comprehensive survey," *Annual Reviews in Control*, vol. 43, pp. 128-151, 2017.

[98] A. Scheinker, and M. Krstic, 2014. "Extremum seeking with bounded update rates," *Systems & Control Letters,* vol.63, pp.25-31, 2014.

[99] E. Smaragdis, M. Papageorgiou, and E. Kosmatopoulos, "A flow-maximizing adaptive local ramp metering strategy," *Transportation Research Part B: Methodological*, vol.38, no.3, pp.251-270, 2004.

[100] A. Smyshlyaev and M. Krstic, "Adaptive control of parabolic PDEs," *Princeton University Press*, 2010.

[101] Y. Tan, D. Nešić, and I. Mareels, "On non-local stability properties of extremum seeking control," *Automatica*, vol.42, no.6, pp.889-903, 2006.

[102] Y. Tan, D. Nešić, I. Mareels, and A. Astolfi, "On global extremum seeking in the presence of local extrema," *Automatica*, vol.45, no.1, pp.245-251, 2009.

[103] C. F. Tang, R. Jiang, Q. S. Wu, B. Wiwatanapataphee and Y. H. Wu, " Mixed traffic flow in anisotropic continuum model", *Transportation Research Record*, vol. 1999(1), pp. 13-22, 2007.

[104] T. Q. Tang, H. J. Huang, S. G. Zhao and H. Y. Shang, " A new dynamic model for heterogeneous traffic flow", *Physics Letters A*, vol. 373(29), pp. 2461-2466, 2009.

[105] M. Treiber and A. Kesting. "Traffic flow dynamics: data, models and simulation". *Physics Today*, 67(3), 54, 2014.

[106] D. Tsubakino, M. Krstic and T. R. Oliveira, "Exact predictor feedbacks for multi-input LTI systems with distinct input delays". *Automatica*, 71, 143-150, 2016.

[107] J. W. C. Van Lint, S. P. Hoogendoorn and M. Schreuder, “Fastlane: New multiclass first-order traffic flow model”, *Transportation Research Record*, vol. 2088(1), pp. 177-187, 2008.

[108] R. Vazquez, M. Krstic and J. M. Coron, “ Backstepping boundary stabilization and state estimation of a 2×2 linear hyperbolic system”, In *2011 50th IEEE Conference on Decision and Control and European Control Conference*, pp. 4937-4942, IEEE, 2011.

[109] S. Villa, P. Goatin and C. Chalons. “ Moving bottlenecks for the Aw-Rascle-Zhang traffic flow model”. *Discrete and Continuous Dynamical Systems-Series B*, 22(10), 3921-3952, 2016.

[110] J. Wang, S. Koga, Y.Pi and M. Krstic. “ Axial Vibration Suppression in a Partial Differential Equation Model of Ascending Mining Cable Elevator”. *Journal of Dynamic Systems, Measurement, and Control*, 140(11), 111003, 2018.

[111] H. H. Wang, S. Yeung, and M. Krstic, “Experimental application of extremum seeking on an axial-flow compressor,” *IEEE Transactions on Control Systems Technology*, vol.8, no.2, pp.300-309, 2000.

[112] Y. Wang and M. Papageorgiou, “Real-time freeway traffic state estimation based on extended Kalman filter: A general approach,” *Transportation Research Part B: Methodological*, vol. 39 (2), pp. 141167, 2005.

[113] Y. Wang, E.B. Kosmatopoulos, M. Papageorgiou, and I. Papamichail, “Local ramp metering in the presence of a distant downstream bottleneck: Theoretical analysis and simulation study,” *IEEE Transactions on Intelligent Transportation Systems,* vol.15, no.5, pp.2024-2039, 2014.

[114] G. B. Whitham, *Linear and nonlinear waves*, Vol. 42, John Wiley & Sons, 2011

[115] G. C. K. Wong and S.C. Wong, “ A multi-class traffic flow model - an extension of LWR model with heterogeneous drivers”, *Transportation Research Part A: Policy and Practice*, vol. 36(9), pp. 827-841, 2002.

[116] H. Yu, R. Vazquez and M. Krstic, “ Adaptive output feedback for hyperbolic PDE pairs with non-local coupling, *In American Control Conference (ACC),* pp. 487-492, IEEE, 2017.

[117] H. Yu, and M. Krstic, “ Varying Speed Limit Control of Aw-Rascle-Zhang Traffic Model,” *In 2018 21st IEEE International Conference on Intelligent Transportation Systems(ITSC),* pp. 1846-1851, IEEE, 2018.

[118] H. Yu, and M. Krstic. “Traffic congestion control on Aw-Rascle-Zhang model: Full-state feedback,” *In 2018 Annual American Control Conference (ACC),* (pp. 943-948). IEEE, 2018.

[119] H. Yu, and M. Krstic. " Adaptive Output Feedback for Aw-Rascle-Zhang Traffic Model in Congested Regime," *In 2018 Annual American Control Conference (ACC),* (pp. 3281-3286). IEEE.

[120] H. Yu, S. Koga and M. Krstic. " Stabilization of Traffic Flow With a Leading Autonomous Vehicle," *In ASME 2018 Dynamic Systems and Control Conference,* (pp. V002T22A006-V002T22A006). American Society of Mechanical Engineers, 2018.

[121] H. Yu, and M. Krstic, "Traffic congestion control for Aw-Rascle-Zhang model," *Automatica,* vol.100, pp.38-51, 2019.

[122] H. Yu, and M. Krstic, "Traffic Congestion Control on Two-lane Aw-Rascle-Zhang Model," In *2018 IEEE Conference on Decision and Control*, pp. 2144-2149, IEEE, 2018.

[123] H. M. Zhang, "A non-equilibrium traffic model devoid of gas-like behavior," *Transportation Research Part B: Methodological,* vol.36, no.3, pp.275-290, 2002.

[124] L. Zhang and C. Prieur, " Necessary and Sufficient Conditions on the Exponential Stability of Positive Hyperbolic Systems", *IEEE Transactions on Automatic Control*, vol.62(7), pp.3610-3617, 2017.

[125] L. Zhang, C. Prieur and J. Qiao. " Local Exponential Stabilization of Semi-Linear Hyperbolic Systems by Means of a Boundary Feedback Control", *IEEE Control Systems Letters*, 2(1), 55-60, 2018.

[126] L. Zhang, C. Prieur and J. Qiao. " PI boundary control of linear hyperbolic balance laws with stabilization of ARZ traffic flow models". *Systems & Control Letters*, 123, 85-91, 2019.

[127] P. Zhang, R. X. Liu, S. C. Wong and S. Q. Dai, " Hyperbolicity and kinematic waves of a class of multi-population partial differential equations", *European Journal of Applied Mathematics*, vol. 17(2), pp. 171-200, 2006.